AD-A201 621

NAVAL POSTGRADUATE SCHOOL
Monterey, California

THESIS

THE MODELING OF VISCOELASTIC
CIRCULAR PLATES FOR USE AS
WAVEGUIDE ABSORBERS

by

Charles D. Hettema

September 1988

Thesis Advisor:　　　　　　Young S. Shin

Approved for public release; distribution is unlimited

88　12　27　162

REPORT DOCUMENTATION PAGE

1a REPORT SECURITY CLASSIFICATION UNCLASSIFIED		1b RESTRICTIVE MARKINGS			
2a SECURITY CLASSIFICATION AUTHORITY		3 DISTRIBUTION AVAILABILITY OF REPORT Approved for Public Release; Distribution is Unlimited			
2b DECLASSIFICATION DOWNGRADING SCHEDULE					
4 PERFORMING ORGANIZATION REPORT NUMBER(S)		5 MONITORING ORGANIZATION REPORT NUMBER(S)			
6a NAME OF PERFORMING ORGANIZATION Naval Postgraduate School	6b OFFICE SYMBOL (If applicable) 62	7a NAME OF MONITORING ORGANIZATION Naval Postgraduate School			
6c ADDRESS (City, State, and ZIP Code) Monterey, CA 93943-5000		7b ADDRESS (City, State, and ZIP Code) Monterey, CA 93943-5000			
8a NAME OF FUNDING SPONSORING ORGANIZATION	8b OFFICE SYMBOL (If applicable)	9 PROCUREMENT INSTRUMENT IDENTIFICATION NUMBER			
8c ADDRESS (City, State, and ZIP Code)		10 SOURCE OF FUNDING NUMBERS			
		PROGRAM ELEMENT NO	PROJECT NO	TASK NO	WORK UNIT ACCESSION NC

11 TITLE (Include Security Classification)
THE MODELING OF VISCOELASTIC CIRCULAR PLATES FOR USE AS WAVEGUIDE ABSORBERS

12 PERSONAL AUTHOR(S)
Hettema, Charles Dean

13a TYPE OF REPORT Master's Thesis	13b TIME COVERED FROM ____ TO ____	14 DATE OF REPORT (Year, Month, Day) September 1988	15 PAGE COUNT 211

16 SUPPLEMENTARY NOTATION
The views expressed in this thesis are those of the author and do not reflect the official policy or position of the Department of Defense or the U.S. Government.

17 COSATI CODES			18 SUBJECT TERMS (Continue on reverse if necessary and identify by block number)
FIELD	GROUP	SUB-GROUP	waveguide absorber, viscoelastic, plate, Mindlin thin
			plate theory

19 ABSTRACT (Continue on reverse if necessary and identify by block number)

A long standing concern of the Navy has been the need to reduce structural vibrations in plates, such as ship's hulls. Recently, it was proposed to use waveguide absorbers as a means to reduce structural vibrations. A waveguide absorber is a device which is made from damping material but mounted to the structure at a point rather than the full surface. A waveguide absorber removes and then dissipates vibrational energy from the structure through traveling waves. The performance of a waveguide absorber is determined from the driving point impedance, the ratio of force to velocity a the attachment point. This study has determined the theoretical driving point impedance for viscoelastic circular plates.

20 DISTRIBUTION/AVAILABILITY OF ABSTRACT ☒ UNCLASSIFIED/UNLIMITED ☐ SAME AS RPT ☐ DTIC USERS	21 ABSTRACT SECURITY CLASSIFICATION Unclassified	
22a NAME OF RESPONSIBLE INDIVIDUAL Y.S. Shin	22b TELEPHONE (Include Area Code) (408)373-2341	22c OFFICE SYMBOL 69Sg

DD FORM 1473, 84 MAR   83 APR edition may be used until exhausted
All other editions are obsolete

Unclassified

Block 19 Continued from page i

The constitutive relations for viscoelastic material were evaluated and it was proven that a complex Young's modulus and shear modulus can be used to represent the viscoelastic material. Mindlin's theory for elastic isotropic plates, with complex moduli, was used to solve for the driving point impedance. The solutions are in terms Bessel functions. Poisson's boundary conditions were used at the free edge of the circular plate, and clamped boundary conditions were used at the attachment point, which is at the center of the plate. A non-numeric language, REDUCE, was used to solve for the driving point impedance given the appropriate equations of motion and boundary conditions. The complex Bessel functions, needed for the results of the REDUCE program, were generated by a FORTRAN program. To validate the results of this study, elastic and viscoelastic plates were tested to determine their driving point impedance. A comparison of the theoretical results and the experimental results shows that there is agreement for all cases studied.

THE MODELING OF VISCOELASTIC CIRCULAR PLATES FOR USE AS WAVEGUIDE ABSORBERS

by

Charles Dean Hettema
Lieutenant Commander, United States Navy
B.S.E.E., Tulane University, 1976

Submitted in partial fulfillment of the
requirements for the degree of

MASTER OF SCIENCE IN MECHANICAL ENGINEERING

from the

NAVAL POSTGRADUATE SCHOOL
September 1988

Author: _____
Charles Dean Hettema

Approved by: _____
Y.S. Shin, Thesis Advisor

_____
K.S. Kim, Second Reader

_____
A.J. Healey, Chairman,
Department of Mechanical Engineering

_____
Gordon E. Schacher,
Dean of Science and Engineering

ABSTRACT

A long standing concern of the Navy has been the need to reduce structural vibrations in plates, such as ship's hulls. Recently, it was proposed to use waveguide absorbers as a means to reduce structural vibrations. A waveguide absorber is a device which is made from damping material but mounted to the structure at a point rather than the full surface. A waveguide absorber removes and then dissipates vibrational energy from the structure through traveling waves. The performance of a waveguide absorber is determined from the driving point impedance, the ratio of force to velocity at the attachment point. This study has determined the theoretical driving point impedance for viscoelastic circular plates.

The constitutive relations for viscoelastic material were evaluated and it was proven that a complex Young's modulus and shear modulus can be used to represent the viscoelastic material. Mindlin's theory for elastic isotropic plates, with complex moduli, was used to solve for the driving point impedance. The solutions are in terms of Bessel functions. Poisson's boundary conditions were used at the free edge of the circular plate, and clamped boundary conditions were used at the attachment point, which is at the center of the plate. A non-numeric language, REDUCE, was used to solve for the driving point impedance given the appropriate equations of motion and boundary conditions. The complex Bessel functions, needed for the results of the REDUCE program, were generated by a FORTRAN program. To validate the results of this study, elastic and

viscoelastic plates were tested to determine their driving point impedance. A comparison of the theoretical results and the experimental results shows that there is agreement for all cases studied.

TABLE OF CONTENTS

LIST OF TABLES

LIST OF FIGURES

xix

ACKNOWLEDGMENTS

I. INTRODUCTION

A. BACKGROUND

The reduction of structural vibration in ships and submarines has been a long standing concern of the Navy. Reducing structural vibrations can increase the life of equipment as well as decrease the amount radiated noise into the water. One of the most widely used methods of passive structural vibration reduction has been the addition of damping material directly to the surface of the structure[Ref. 1 : pp. 312 -362]. Recently Ungar and Kurzweil [Ref. 2] have proposed the use of a waveguide absorber to reduce structural vibrations. A waveguide absorber is a damping device that is attached indirectly to the structure through a mount, at a point, rather than directly to the surface. The purpose of the waveguide absorber is to remove energy from the structure and then dissipate the energy as traveling waves. The waveguide absorber is expected to remove more energy per unit mass of damping material than a surface damping treatment can.

Past studies of waveguide absorbers have been by Ungar and Kurzweil [Ref. 3] , by Ungar and Williams [Ref.4], and by Lee [Ref. 5] . These studies show that a waveguide absorber is able to reduce the magnitude of the vibrations in a structure. The theoretical results are based upon the driving point impedance, the ratio of force to velocity at the attachment point. There has not been good agreement between the experimental results and the theoretical results in these studies. However,

1

in the study by Lee [Ref. 5] of viscoelastic beams, it was determined that using an underlining theory that included the shear deformation and rotatory inertia, i.e. the Timoshenko beam theory, produced better results than those theories which did not include them, i.e., the Euler beam theory.

B.   PURPOSE

Based upon the experimental success of beam waveguide absorbers to reduce structural vibrations, there is reason to believe that a two dimensional geometry may provide increased damping per unit mass of damping material than the one dimensional beam does. The purpose of this study is to investigate the feasibility of using viscoelastic circular plates as waveguide absorbers, by determining the driving point impedance of the plate. The driving point impedance will be evaluated over a frequency range of 10 to 2000 Hz. This range of frequencies was chosen because data gathering techniques and material information are not reliable below five to ten hertz, and the distance that vibrations or noise can travel in water above 2000 Hz is very small and normally ignored. It is the goal of this study that the driving point impedance be presented an easy to use equation, or an easy to use computer program. The driving point impedance should be able to be calculated with a limited number of inputs.

C.   FORMAT

This study has been broken down into four sections even though the actions occurred at the same time. The sections are theoretical results, experimental results, a comparison of the theoretical and experimental

results, with conclusions, and recommendations for future studies. The body of this study was written based upon all of the plates used, but only shows, in the figures, the results for one plate size. The figures for the other plate sizes are found in Appendix C. This was done so as to keep the body of this study as small as possible.

II. THEORY

A.   VISCOELASTIC MATERIAL MODELING

In the past study by Bailey and Chen [Ref. 6], it was shown that one of the best methods of modeling viscoelastic material is by separating the elastic and viscoelastic parts. The elastic portion is not time dependent, where as the viscoelastic portion is time dependent. The model of viscoelastic material can be created by using a resistive element as shown in Figure 1 and a damping element as shown in Figure 2, where σ is the stress, ε is the strain, E is the Young's modulus, and C is the damping of the material. These models are based upon electrical impedance where strain is the equivalent of voltage, stress the equivalent of current, and the inverse of the characteristics is the equivalent of impedance.
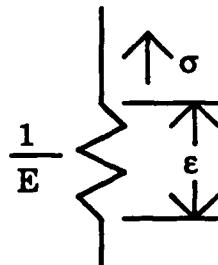
Figure 1. Resistive Element Model.
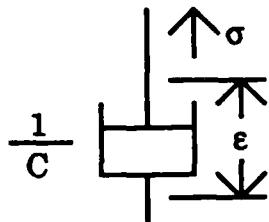
Figure 2. Damping Element Model.

The stress versus strain relationship for the resistance elements is:

$$\varepsilon = \frac{\sigma}{E} \qquad (2.1)$$

and for the damping element is:

$$\varepsilon = \int \frac{\sigma}{C} dt \qquad (2.2)$$

The combination of a resistive element and a damping element is known as the Maxwell model [Ref. 7]. The model shown in Figure 3 is based on a two element Maxwell model, where the full element, with damping, represents the viscoelastic portion and the degenerate element, no damping, represents the elastic portion of the material. The notation used is, E_e is the elastic Young's modulus, E_V is the viscoelastic Young's modulus, C_V is the viscoelastic damping, σ_e is the elastic stress, σ_V is the viscoelastic stress, σ is the total stress, and ε is the total strain in the material.

5
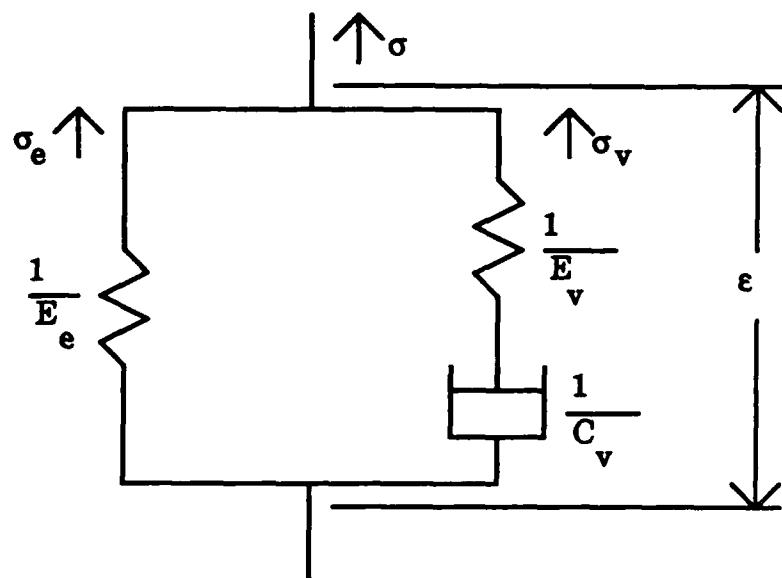
Figure 3. Viscoelastic Material Model.

The total stress,σ, of the material is:

$$\sigma = \sigma_e + \sigma_v \tag{2.3}$$

The strain versus stress relationship for the elastic portion of the material is:

$$\varepsilon = \frac{\sigma_e}{E_e} \tag{2.4a}$$

or in a more familiar form:

$$\sigma_e = E_e \varepsilon \tag{2.4b}$$

6

For the viscoelastic portion the strain verse stress relationship is:

$$\varepsilon = \frac{\sigma_v}{E_v} + \int \frac{\sigma_v}{C_v} dt \qquad (2.5a)$$

or taking the time derivative of equation (2.5a) gives:

$$\dot{\varepsilon} = \frac{\dot{\sigma}_v}{E_v} + \frac{\sigma_v}{C_v} \qquad (2.5b)$$

It is concluded that the total stress of equation (2.3) can be rewritten as:

$$\sigma = E_e \varepsilon + \sigma_v \qquad (2.6)$$

where the viscoelastic stress must obey the relationship of equation (2.5b). The stress versus strain relationship can be characterized as the normal elastic relationship plus an added term that incorporates the viscoelastic effects.

For reference purposes the coordinate system of Figure 4 is used for the discussion that follows.
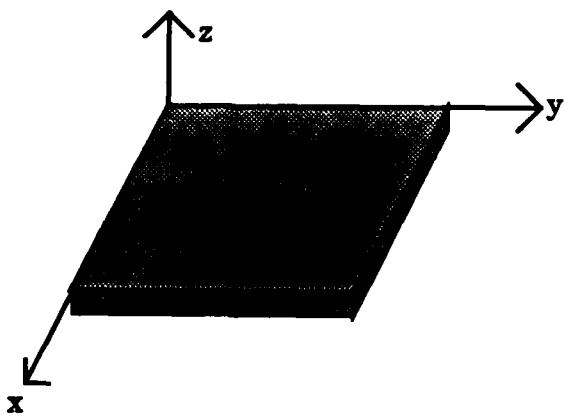
Figure 4. Rectangular Coordinate System for a Plate.

7

For thin plates, it is normal to assume that the plate undergoes a biaxial stress state [Ref. 8], but for this study triaxial stress is used with the modification that the strain in the z direction is zero and that the stress in the z direction is very small and can be ignored. This assumption will allow the inclusions of the shear deformation and rotatory inertia later. The stresses acting a small piece of material are shown in Figure 5, where σ_i, or σ_{ii}, is the normal stress on the i face in the i direction, τ_{ij} is the shear stress on the i face in the j direction, which is equal to τ_{ji}.
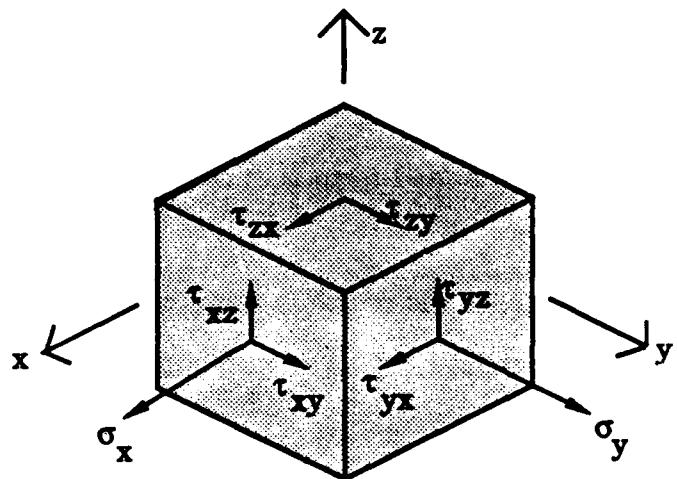
Figure 5. Stresses in a Cube of Material.

Based upon the model in Figure 3 with resultant equation (2.6), the three dimensional stress versus strain relationships for isotropic material become:

$$\varepsilon_z = 0 \tag{2.7a}$$

$$\sigma_x = \frac{E_e}{1 - v_e^2}(\varepsilon_x + v_e \varepsilon_y) + \sigma_{x_v} \tag{2.7b}$$

$$\sigma_y = \frac{E_e}{1 - v_e^2}(\varepsilon_y + v_e \varepsilon_x) + \sigma_{y_v} \tag{2.7c}$$

$$\tau_{xy} = \frac{E_e}{2(1 + v_e)}\gamma_{xy} + \tau_{xy_v} \tag{2.7d}$$

$$\tau_{xz} = \frac{E_e}{2(1 + v_e)}\gamma_{xz} + \tau_{xz_v} \tag{2.7e}$$

$$\tau_{yz} = \frac{E_e}{2(1 + v_e)}\gamma_{yz} + \tau_{yz_v} \tag{2.7f}$$

where ε_i is the strain in the i direction, γ_{ij} is the rotation in the i-j plane, which is equal to γ_{ji}, and the sub-sub-script of v is for the viscoelastic portion. The viscoelastic terms must also meet the following conditions:

$$\frac{\dot{\sigma}_{x_v}}{E_v} + \frac{\sigma_{x_v}}{C_v} = \frac{1}{1 - v_v^2}(\dot{\varepsilon}_x + v_v \dot{\varepsilon}_y) \tag{2.8a}$$

$$\frac{\dot{\sigma}_{y_v}}{E_v} + \frac{\sigma_{y_v}}{C_v} = \frac{1}{1 - v_v^2}(\dot{\varepsilon}_y + v_v \dot{\varepsilon}_x) \tag{2.8b}$$

$$\frac{\dot{\tau}_{xy_v}}{E_v} + \frac{\tau_{xy_v}}{C_v} = \frac{1}{2(1 + v_v)}\dot{\gamma}_{xy} \tag{2.8c}$$

$$\frac{\dot{\tau}_{xz_v}}{E_v} + \frac{\tau_{xz_v}}{C_v} = \frac{1}{2(1 + v_v)}\dot{\gamma}_{xz} \tag{2.8d}$$

$$\frac{\dot{\tau}_{yz_v}}{E_v} + \frac{\tau_{yz_v}}{C_v} = \frac{1}{2(1 + v_v)}\dot{\gamma}_{yz} \tag{2.8e}$$

9

The use of these constitutive relations proves to be quite cumbersome in all but the most simplest of problems. This is because simultaneous differential equations must be solved to relate the stresses to strains. By the use of a complex model, where the time dependent terms are replaced by complex terms, some of these problems can be overcome. Figure 6 shows the Laplace Transform [Ref. 9], of the model shown in Figure 3.
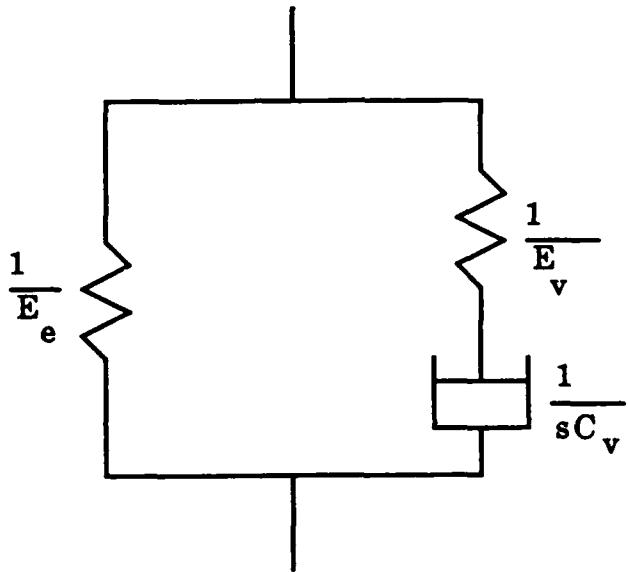
Figure 6. Laplace Transform of Viscoelastic Material Model

By applying circuit analysis methods to the model shown in Figure 6, an equivalent model, shown in Figure 7, with a complex Young's modulus, E^*, can be determined. The viscoelastic elements are in series with each other and together are in parallel with the elastic element. Solving for E^* yields:

$$\frac{1}{\frac{1}{E^*}} = \frac{1}{\frac{1}{E_e}} + \frac{1}{\left(\frac{1}{E_v} + \frac{1}{sC_v}\right)} \tag{2.9}$$

Rearranging terms and substituting $j\omega$ for s, where $j = \sqrt{-1}$ and ω is the rotational frequency in rads/sec, in equation (2.9) yields:

$$E^* = \frac{E_e E_v^2 + \omega^2 C_v^2 E_v + \omega^2 C_v^2 E_e}{E_v^2 + \omega^2 C_v^2} + j\frac{\omega C_v E_v^2}{E_v^2 + \omega^2 C_v^2} \tag{2.10}$$

The resultant complex model is shown in Figure 7.
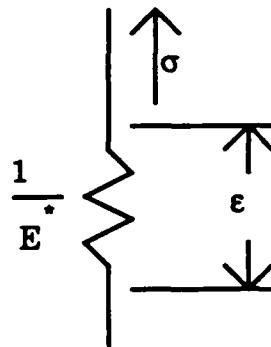
Figure 7. Complex Viscoelastic Material Model.

The complex model not only allows the use all of the elastic theory, with its well defined mathematics, but has the added benefit that most of the manufactures of viscoelastic material provide material data in this form [Ref. 1, pp. 363-440]. Instead of leaving the complex Young's modulus in terms of the elastic and viscoelastic parameters, as in equation (2.10), three new terms are defined and used. The real part, E', is defined as:

$$E' = \frac{E_e E_v^2 + \omega^2 C_v^2 E_v + \omega^2 C_v^2 E_e}{E_v^2 + \omega^2 C_v^2} \tag{2.11}$$

11

The imaginary part, E", by:

$$E'' = \frac{\omega C_v E_v^2}{E_v^2 + \omega^2 C_v^2} \qquad (2.12)$$

The ratio of the imaginary part to the real part is known as the loss damping factor, η, and defined as:

$$\eta = \frac{E''}{E'} \qquad (2.13)$$

The complex Young's modulus may now be written as:

$$E^* = E' + jE'' \qquad (2.14)$$

or as:

$$E^* = E'(1 + j\eta) \qquad (2.15)$$

It is normal to assume that the Poisson's ratio,ν , for the viscoelastic material is the same for the elastic and viscoelastic portions, which leads to the result that the shear modulus is also a complex parameter, G^*, and is related to the complex Young's modulus by:

$$G^* = \frac{E^*}{2(1 + \nu)} = G' + jG'' \qquad (2.16)$$

The real and imaginary parts, respectively, of the Young's modulus and shear modulus are related in identical manner. The loss factor is the same for both moduli.

12

Elastic theory can now be used to analyze structures using viscoelastic material when Young's modulus and shear modulus are replaced by the viscoelastic's complex moduli. This is a great benefit in the analysis of structures with viscoelastic plates because a separate and new governing theory does not have to be created.

B. ELASTIC SOLUTION

For this study an elastic thin plate theory that includes the effects of shear deformation and rotatory inertia was needed to determine the driving point impedance of the viscoelastic plate. The use of such a theory, for beams, in the study by Lee [Ref. 5] provided better agreement between theoretical and experimental results than did theories which did not incorporate these effects. Mindlin [Ref. 10] has presented such a theory for isotropic thin plates. This work showed that isotropic elastic thin plates can be described by a set of three simultaneous partial differential equations. It is based upon assuming that the displacements in the x direction, u, and in the y direction, v, of Figure 4, vary linearly in the z direction and the displacement in the z direction, w, is not a function of z, or written in equation form:

$$u = z \cdot \psi_x(x, y, t) \qquad (2.17a)$$

$$v = z \cdot \psi_y(x, y, t) \qquad (2.17b)$$

$$w = W(x, y, t) \qquad (2.17c)$$

where ψ_x and ψ_y are potential functions to be determined. This implies that the displacements in the x and y directions, u and v, vary as shown in Figure 8.
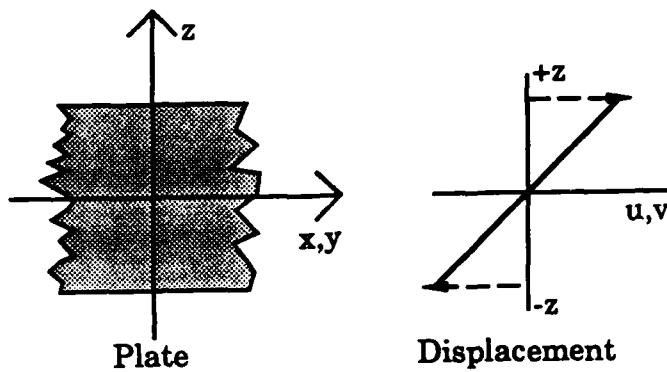
Figure 8. Variations in x and y displacements as a function of z for the Mindlin Plate Theory.

Mindlin's original work was in a rectangular coordinate system, but was adapted to cylindrical coordinate system by Mindlin and Deresiewicz [Ref. 11] and then updated by Irie, Yamada, and Aomura [Ref.12], and to curvilinear by Callahan [Ref.13]. The notation of Irie, Yamada, and Aomura [Ref. 12] is used in this study owing to studying circular plates and their use of dimensionless parameters. The reference directions of the cylindrical coordinate system are shown in Figure 9.
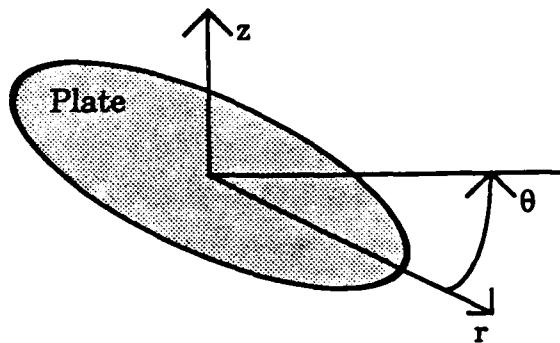
Figure 9. Cylindrical Coordinate System for a Plate.

The displacements, in terms of cylindrical coordinates, which are equivalent to those of equation (2.17) are the radial displacement, u_r, the angular displacement, u_θ, and the displacement in the z direction, w. They are expressed mathematically as:

$$u_r = z \cdot \psi_{rt}(r, \theta, t) \tag{2.18a}$$

$$u_\theta = z \cdot \psi_{\theta t}(r, \theta, t) \tag{2.18b}$$

$$w = W_t(r, \theta, t) \tag{2.18c}$$

where ψ_{rt} and $\psi_{\theta t}$ are potential functions that are to be determined. The moments and shears in a plate are shown in Figure 10 and defined in equation (2.19) [Ref. 10] for the case of cylindrical coordinate system.

15
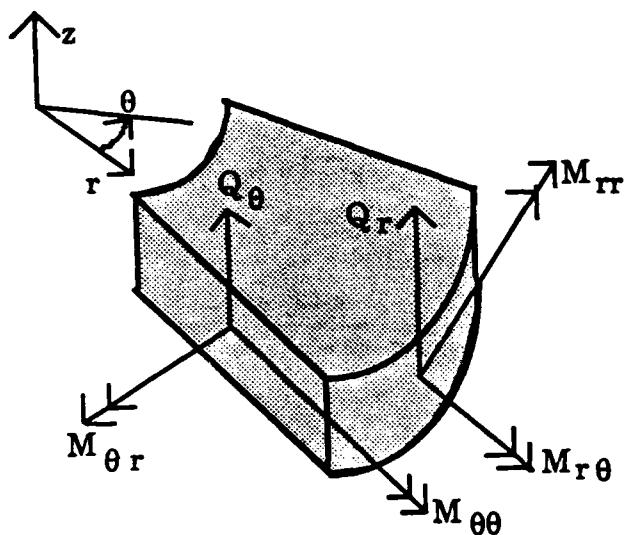
Figure 10. Moments and Shears in a Plate for Cylindrical Coordinates.

$$M_{ii} = \int\limits_{-\frac{h}{2}}^{\frac{h}{2}} z\sigma_{ii} dz \qquad (2.19a)$$

$$M_{ij} = \int\limits_{-\frac{h}{2}}^{\frac{h}{2}} z\tau_{ij} dz \qquad (2.19b)$$

$$Q_i = \int\limits_{-\frac{h}{2}}^{\frac{h}{2}} \tau_{ij} dz \qquad (2.19c)$$

16

where M_{ii}, or M_i, is the bending moment on the i face per unit of length in the r-θ plane, M_{ij}, which is equal to M_{ji}, is the twisting moment on the i face per unit of length in the r-θ plane, and Q_i, is the shear on the i face per unit of length in the r-θ plane . The plate geometry is shown in Figure 8 and Figure 9.
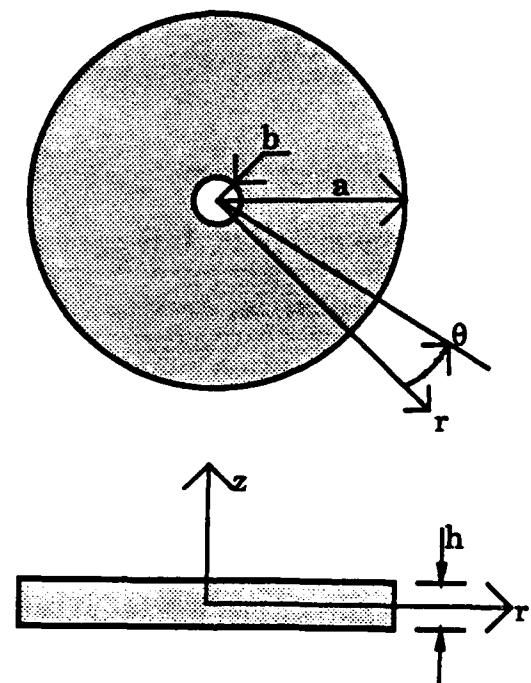
Figure 11. Plan and Side View of Plate Showing Geometry.

For the case of an isotropic plate in cylindrical coordinates, the Mindlin governing equations are [Ref.11]:

$$\frac{\partial M_{rr}}{\partial r} + \frac{1}{r}\frac{\partial M_{r\theta}}{\partial \theta} + \frac{M_{rr} - M_{\theta\theta}}{r} - Q_r = \frac{\rho h^3}{12}\frac{\partial^2 \psi_r}{\partial t^2} \qquad (2.20a)$$

$$\frac{\partial M_{r\theta}}{\partial r} + \frac{1}{r}\frac{\partial M_{\theta\theta}}{\partial \theta} + \frac{2M_{r\theta}}{r} - Q_\theta = \frac{\rho h^3}{12}\frac{\partial^2 \psi_\theta}{\partial t^2} \qquad (2.20b)$$

$$\frac{\partial Q_r}{\partial r} + \frac{1}{r}\frac{\partial Q_\theta}{\partial \theta} + \frac{Q_r}{r} = \rho h\frac{\partial^2 w}{\partial t^2} \qquad (2.20c)$$

where ρ is the density of the material. It is not desirable to solve equations (2.20) in the present form, because of the simultaneous differential equations, but rather in a simpler form. Mindlin [Ref. 10] showed that the three simultaneous second order partial differential equations, can be combined to produce a single fourth order partial differential equation, in terms of w. The only drawback of using this single equation is that it can not handle the full number of geometric boundary conditions. Another suggestion by Mindlin [Ref. 10] was to assume that the displacements were all periodic functions of time of the type exp(ωt). By doing this, the three simultaneous equations can be converted into three independent second order partial differential equations, which are much easier to solve, but still use of all the geometric boundary conditions.

For this study, it was desired to use the geometric boundary conditions directly, in order to improve the agreement between the

theoretical and experimental results, and since most shipboard structural vibrations are from rotating equipment, periodic in nature, the final suggestion by Mindlin will be used. As such, the displacements are assumed to be periodic of the form exp(ωt), and expressed as:

$$u_r = z \cdot \psi_r(r, \theta)e^{j\omega t} \tag{2.21a}$$

$$u_\theta = z \cdot \psi_\theta(r, \theta)e^{j\omega t} \tag{2.21b}$$

$$w = W(r, \theta)e^{j\omega t} \tag{2.21c}$$

where the unknowns are ψ_r, ψ_θ, and W. It is convenient to define the following dimensionless parameters that are based upon the plate geometry and the frequency [Ref. 12]:

$$R = \frac{\left(\frac{h}{a}\right)^2}{12} \tag{2.22a}$$

$$S = \frac{D}{\kappa^2 G a^2 h} = \frac{1}{6(1-v)\kappa^2}\left(\frac{h}{a}\right)^2 \tag{2.22b}$$

$$\lambda^4 = \frac{\rho h a^4 \omega^2}{D} \tag{2.22c}$$

$$\delta_1^2 = \frac{1}{2}\lambda^4 \cdot \left[R + S + \left\{ (R-S)^2 + \frac{4}{\lambda^4} \right\}^{\frac{1}{2}} \right] \qquad (2.22d)$$

$$\delta_2^2 = \frac{1}{2}\lambda^4 \cdot \left[R + S - \left\{ (R-S)^2 + \frac{4}{\lambda^4} \right\}^{\frac{1}{2}} \right] \qquad (2.22e)$$

$$\delta_3^2 = \frac{2\left(R\lambda^4 - \frac{1}{S} \right)}{1 - \nu} \qquad (2.22f)$$

$$\sigma_1 = \frac{\delta_2^2}{R\lambda^4 - \frac{1}{S}} \qquad (2.22g)$$

$$\sigma_2 = \frac{\delta_1^2}{R\lambda^4 - \frac{1}{S}} \qquad (2.22h)$$

where D is the flexural rigidity expressed by:

$$D = \frac{Eh^3}{12(1 - \nu^2)} \qquad (2.23)$$

and κ is the shear coefficient taken from Mindlin [Ref.10]. The shear coefficient is used to take into account that the shear is not a constant value as assumed, but varies across the thickness of the plate. For elastic plates the shear coefficient is normally set equal to:

20

$$\kappa^2 = \frac{\pi^2}{12} \tag{2.24}$$

For the presently assumed case of periodic motion of isotropic plates, the governing partial differential equations become [Ref. 12]:

$$\left(\nabla^2 + \delta_1^2\right)w_1 = 0 \tag{2.25a}$$

$$\left(\nabla^2 + \delta_2^2\right)w_2 = 0 \tag{2.25b}$$

$$\left(\nabla^2 + \delta_3^2\right)w_3 = 0 \tag{2.25c}$$

where ∇^2 is the Laplacian operator and the variable w_1, w_2, and w_3 are dummy variables which are related to the unknowns, ψ_r, ψ_θ, and W by the following relationships [Ref. 12]:

$$\psi_r = \left(\sigma_1 - 1\right)\frac{\partial w_1}{\partial r} + \left(\sigma_2 - 1\right)\frac{\partial w_2}{\partial r} + \frac{1}{r}\frac{\partial w_3}{\partial \theta} \tag{2.26a}$$

$$\psi_\theta = \left(\sigma_1 - 1\right)\frac{1}{r}\frac{\partial w_1}{\partial \theta} + \left(\sigma_2 - 1\right)\frac{1}{r}\frac{\partial w_2}{\partial \theta} - \frac{\partial w_3}{\partial r} \tag{2.26b}$$

$$W = w_1 + w_2 \tag{2.26c}$$

It is much easier to work with the governing equations as shown in Equation (2.25) than those of Equation (2.20). The problem has been reduced from having to solve simultaneous partial differential equations, to solving three independent partial differential equations. Equation (2.25) is a form of Bessel's partial differential equation which has a solution in terms of Bessel functions [Ref. 14] [Ref.15, pp. 22-26]. For this study the solution to equation (2.25) is assumed to be:

$$w_1 = \left[A_1 J_n\left(\delta_1 \frac{r}{a} \right) + A_4 Y_n\left(\delta_1 \frac{r}{a} \right) \right] \cos(n\theta) \qquad (2.27a)$$

$$w_2 = \left[A_2 J_n\left(\delta_2 \frac{r}{a} \right) + A_5 Y_n\left(\delta_2 \frac{r}{a} \right) \right] \cos(n\theta) \qquad (2.27b)$$

$$w_3 = \left[A_3 J_n\left(\delta_3 \frac{r}{a} \right) + A_6 Y_n\left(\delta_3 \frac{r}{a} \right) \right] \sin(n\theta) \qquad (2.27c)$$

where A_i are constants to be set by the boundary conditions, $J_n(x)$ is the Bessel function of the first kind of order n, and $Y_n(x)$ is the Bessel function of the second kind of order n. The Bessel function of the second kind of order n, has been added to the solution of Irie, Yamada, and Aomura [Ref.12] because of the hole in the center of the plates being used in this study.

Six boundary conditions are needed to completely establish the solution to this plate problem. For the plates under study, three boundary conditions are at the center of the plate, at r=b, and three boundary conditions are at the edge of the plate, at r=a. The boundary conditions are given in terms of displacements and the stress in the plate. At the center,

r=b, for a plate being used as a waveguide absorber, it must be mounted to a fixture. It has been assumed that the fixture is rigid, has a radius of b, and clamps the plate such that there is no twisting and that the displacement in the z direction at r=b is the same for the fixture as the plate. In mathematical terms, the boundary conditions at the plate's center are:

$$\psi_r(b, \theta) = 0 \qquad (2.28a)$$

$$\psi_\theta(b, \theta) = 0 \qquad (2.28b)$$

$$W(b, \theta) = w_0 \qquad (2.28c)$$

If the plate was not attached to the fixture, or if b=0, then the constants A_4, A_5, and A_6 would have to be set to zero to insure that the solution remained bounded, as the Bessel functions of the second kind are unbounded as the argument approaches zero.

At the free edge of the plate, r=a, the boundary conditions are no bending moments, twisting moments, or shearing on the free edge, or in mathematical terms:

$$M_{rr}(a, \theta) = 0 \qquad (2.29a)$$

$$M_{r\theta}(a, \theta) = 0 \qquad (2.29b)$$

$$Q_r(a, \theta) = 0 \qquad (2.29c)$$

These are known as Poisson's boundary conditions [Ref.16]. Poisson's boundary conditions can be used because the governing differential equations were not reduced to form a single differential equation which ignores, or reduces the effects of the shear deformation and rotary inertia. Had a reduced differential equation been used, then Kirchoff's boundary [Ref. 16] [Ref.17] conditions would have to be used. Kirchoff's boundary conditions for the free edge are:

$$M_r(a, \theta) = 0 \qquad (2.30a)$$

$$\left[Q_r(r, \theta) + \frac{1}{r} \frac{\partial M_{r\theta}(r, \theta)}{\partial \theta} \right]_{r = a} = 0 \qquad (2.30b)$$

Kirchoff's boundary conditions are an attempt to include the three geometric boundary conditions of Poisson that exists at the free edge into two equations. The necessity for this arose from a plate theory, equivalent to the Euler beam theory, which could not incorporate three edge boundary conditions but only two. The present theory, Mindlin's, does not give up boundary conditions for simplicity. The use of a reduced theory and Kirchoff's boundary condition can lead to a large disparity between the theoretical and the experimental displacements [Ref. 18] when r approaches the free edge at a.

All that is left to allow analyzing the plate is to relate the displacements, or potential functions, to the moments and shears. The equations below accomplish this [Ref. 12] :

$$M_{rr} = D\left\{\frac{\partial\psi_r}{\partial r} + \frac{v}{r}\left(\psi_r + \frac{\partial\psi_\theta}{\partial\theta}\right)\right\} \qquad (2.31a)$$

$$M_{\theta\theta} = D\left\{\frac{1}{r}\left(\psi_r + \frac{\partial\psi_\theta}{\partial\theta}\right) + v\frac{\partial\psi_r}{\partial r}\right\} \qquad (2.31b)$$

$$M_{r\theta} = \frac{D}{2}(1-v)\left\{\frac{1}{r}\left(\frac{\partial\psi_r}{\partial\theta} - \psi_\theta\right) + \frac{\partial\psi_\theta}{\partial r}\right\} \qquad (2.31c)$$

$$Q_r = \kappa^2 Gh\left(\psi_r + \frac{\partial W}{\partial r}\right) \qquad (2.31d)$$

$$Q_\theta = \kappa^2 Gh\left(\psi_\theta + \frac{1}{r}\frac{\partial W}{\partial\theta}\right) \qquad (2.31e)$$

Finding the constants A_1 to A_6, is a straight forward matter of combining equation (2.27) into equation (2.26), and then into equation (2.31) from which the boundary conditions of equations (2.28) and (2.29) can be satisfied. Once the constants A_1 to A_6 are known, the potential functions,ψ_r and ψ_θ, the displacements,u_r, u_θ, and w, and the moments and shears, M_{rr}, $M_{\theta\theta}$, $M_{r\theta}$, Q_r, and Q_θ, are known anywhere in the plate. With this information the driving point impedance can be calculated.

Mechanical impedance, Z, is defined as:

$$Z = \frac{F}{V} \tag{2.32}$$

where F is the force at the point of interest and V is the velocity at the point of interest. For this study, the point of interest is the the driving point where the fixture mounts to the plate. Based upon the assumption made about the fixture and nature of the displacements, the force, F, at the driving point can be calculated by:

$$F = \int_0^{2\pi} r Q_r(b, \theta) e^{j\omega t} \partial \theta \tag{2.33}$$

and the velocity, V, is related to the displacement at the driving point by:

$$V = \frac{\partial \left(W(b, \theta) e^{j\omega t} \right)}{\partial t} = j\omega W(b, \theta) e^{j\omega t} = j\omega w_0 e^{j\omega t} \tag{2.34}$$

Combining equations (2.33) and (2.34) into equation (2.32) yields:

$$Z = \frac{\displaystyle\int_0^{2\pi} r Q_r(b, \theta) \partial \theta}{j\omega w_0} \tag{2.35}$$

Equation (2.35) is the driving point impedance.

26

The steps necessary to solve for the driving point impedance have now been laid out. The only difficulty lies in determining the constants A_1 to A_6 for any plate geometry (a,b,h) and material (ρ,E^*,ν). The work necessary to determine these constants is beyond the capability of normal hand written calculations. Assuming that the driving point impedance can be derived, the driving point impedance must be calculated over and over for different frequencies, material, and geometry. The only way to solve for the driving point impedance is with the aid of a computer. The use of the computer was split into two parts. The first was to use a symbolic language to algebraically determine the driving point impedance, and the second was to use a numerical language to calculate the driving point impedance for a given set of conditions.

C. COMPUTER IMPLEMENTATION

Figure 12 shows the flow path used in the symbolic program to determine the driving point impedance. One of the primary considerations in the selection of a non numerical language, which will be used to determine the driving point impedance, was the ease of differentiating Bessel functions. The language of REDUCE [Ref. 19] has the capability to be easily taught how differentiate functions, so was used in this study.

```
                          ↓↓
          ┌─────────────────────────────────┐
          │  Methods for Differentiation    │
          │     of Bessel Functions         │
          └─────────────────────────────────┘
                          ↓↓
             ┌──────────────────────────┐
             │   Assumed Solution       │
             │      Eq (2.27)           │
             └──────────────────────────┘
                          ↓↓
              ┌─────────────────────────┐
              │  Determine Potential    │
              │   Functions and w       │
              │      Eq (2.26)          │
              └─────────────────────────┘
                          ↓↓
              ┌─────────────────────────┐
              │   Determine Moments     │
              │      and Shears         │
              │      Eq (2.31)          │
              └─────────────────────────┘
                          ↓↓
              ┌─────────────────────────┐
              │  Determine Boundary     │
              │  Condition Equations    │
              │  Eq (2.28) and (2.29)   │
              └─────────────────────────┘
                          ↓
              ┌─────────────────────────┐
              │   Solve for A1 to A6    │
              └─────────────────────────┘
                          ↓↓
              ┌─────────────────────────┐
              │   Determine Driving     │
              │   Point Impedance, Z    │
              │      Eq (2.35)          │
              └─────────────────────────┘
                          ↓↓
              ┌─────────────────────────┐
              │   Write Z in FORTRAN    │
              │    Type Statements      │
              └─────────────────────────┘
```
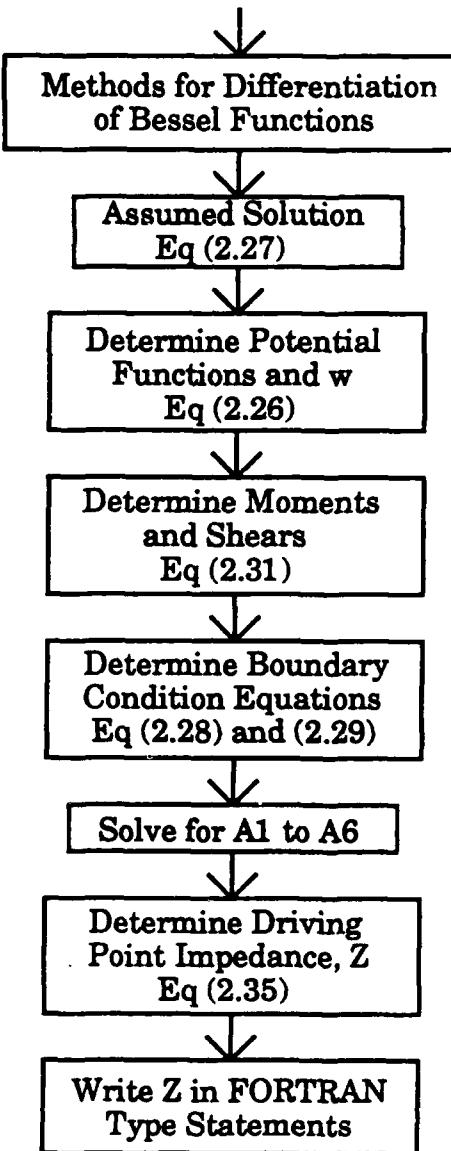
Figure 12. Symbolic Language Program Flow Chart.

The REDUCE program did the differentiation of the Bessel functions
and substitutions as required very well. The program showed that the
resultant motion was symmetric with n equal to zero. This agrees with the
boundary conditions imposed at the center of the plate, motion only in the z

direction with no twisting. It was only at the point of trying to determine the constants A_1 to A_6 did REDUCE have trouble. In effect, the REDUCE program was solving a linear six by six symbolic matrix. In the present implementation of REDUCE on the Naval Postgraduate School's IBM 3033 computer there was insufficient storage to to find all six constants directly. In order to alleviate this problem, the program was broken up into two parts, one part to set up the necessary equations to be solved, and the other to solve the simultaneous linear equations. Cramer's rule of linear matrix solution [Ref. 20] was employed to solve the simultaneous linear equations through the use of dummy variables. Even using this approach there was insufficient memory to solve the system of equations. The symmetry of the problem was then taken advantage of, A_3 and A_6 do not need to be solved because $\sin(n\theta)$ is zero. The result was, that the REDUCE program only had to solve a four by four matrix for A_1, A_2, A_4, and A_5, which it was able to do. Once these constants were found then the magnitude of the force, F, magnitude of the velocity, V, and the driving point impedance, Z, were found. The driving point impedance is in terms of Bessel functions evaluated at the center, r=b, and free edge, r=a, of the circular plate. As a final step in the REDUCE program the driving point impedance was written in FORTRAN type statements to allow a simpler generation of a FORTRAN program. The REDUCE programs used in this study are in Appendix A.

The flow chart for the numerical program used to calculate the driving point impedance is shown in Figure 13. The numerical language of FORTRAN was used in this study.
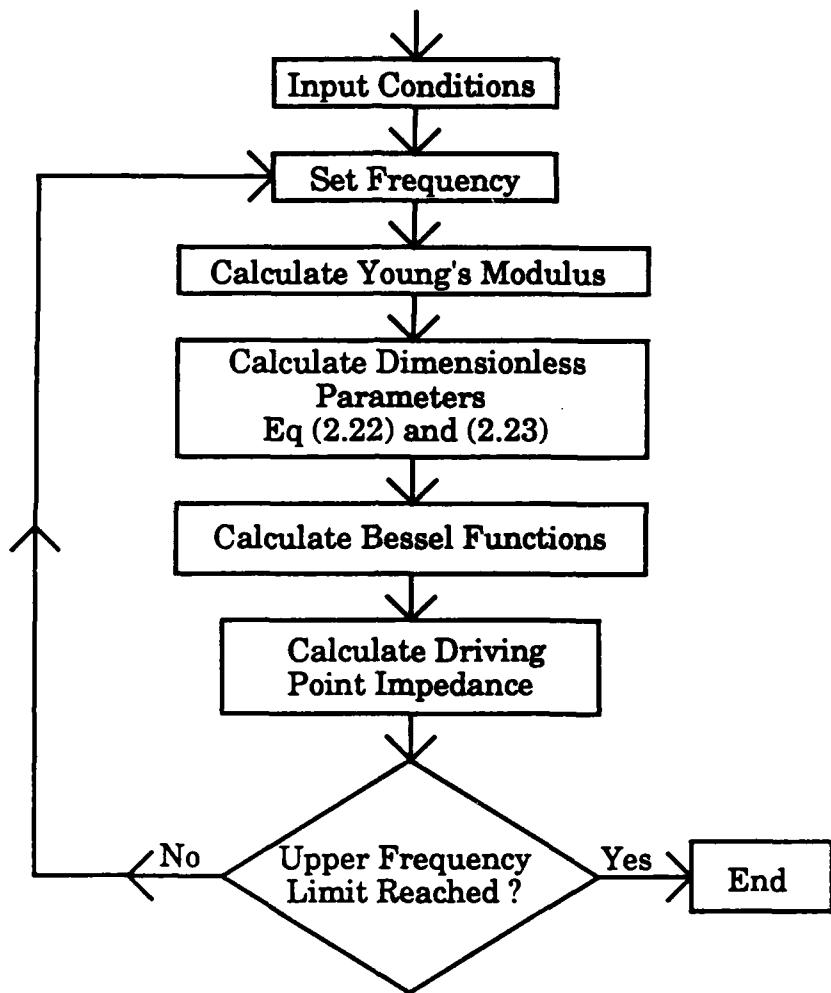
Figure 13. Flow Chart for FORTRAN Program.

The FORTRAN program was written to so as to minimize the number of inputs required in order to calculate the driving point impedance over a range of frequencies. It was decided that the inputs would be the type of material, geometry, and temperature of the plate, and the upper and

lower frequency bounds of interest. The remaining information needed to calculate the driving point impedance would either be calculated or stored in table faction.

As was noted by Irie, Yamada, and Aomura [Ref.12], the parameters $\delta_2{}^2$ and $\delta_3{}^2$ can become negative such that the argument of the Bessel function is a complex value. In their study, to get around this, whenever $\delta_2{}^2$ or $\delta_3{}^2$ become negative, the assumed solution went from the Bessel function of the first kind to the modified Bessel function of the first kind and the argument of the Bessel function was made into a real quantity. When dealing with viscoelastic plates, where the argument of the Bessel functions is always complex, this strategy was not acceptable. It was pointed out by McLachlan [Ref. 15, p. 27] that the Bessel functions of the first and second kind are still solutions to the Bessel's partial differential equation even with complex arguments. This means that the solution can be calculated if the Bessel functions are in complex notation. All of the Bessel function algorithms found on the Naval Postgraduate School's IBM 3033 are written for real valued arguments, not complex arguments, so could not be used. A computer algorithm had to be written to find the values of the Bessel function of the first kind, second kind, and their first and second derivatives. It was decided that the simplest method, and most straight forward, though not the most elegant, would be to write the algorithm with the Taylor series expansion of the functions. It must also be pointed out that this algorithm was written for the special case of Bessel function order, n, being zero. The Taylor series expansions used to calculate the Bessel functions and their first and second derivatives are [Ref 21]:

$$J_0(x) = 1 - \frac{x^2}{2^2} + \frac{x^4}{2^2 \cdot 4^2} - \frac{x^6}{2^2 \cdot 4^2 \cdot 6^2} + \frac{x^8}{2^2 \cdot 4^2 \cdot 6^2 \cdot 8^2} - \cdots \qquad (2.36a)$$

$$J_0'(x) = -\frac{x}{2} + \frac{x^3}{2^2 \cdot 4} - \frac{x^5}{2^2 \cdot 4^2 \cdot 6} + \frac{x^7}{2^2 \cdot 4^2 \cdot 6^2 \cdot 8} - \cdots \qquad (2.36b)$$

$$J_0''(x) = -\frac{1}{2} + \frac{3x^2}{2^2 \cdot 4} - \frac{5x^4}{2^2 \cdot 4^2 \cdot 6} + \frac{7x^6}{2^2 \cdot 4^2 \cdot 6^2 \cdot 8} - \cdots \qquad (2.36c)$$

$$Y_0(x) = \frac{2}{\pi}\left\{\ln\left(\frac{x}{2}\right) + \gamma\right\}J_0(x)$$
$$+ \frac{2}{\pi}\left\{\frac{x^2}{2^2} - \frac{x^4}{2^2 \cdot 4^2}\left(1 + \frac{1}{2}\right) + \frac{x^6}{2^2 \cdot 4^2 \cdot 6^2}\left(1 + \frac{1}{2} + \frac{1}{3}\right) - \cdots\right\} \qquad (2.36d)$$

$$Y_0'(x) = \frac{2}{\pi}\left[\left\{\ln\left(\frac{x}{2}\right) + \gamma\right\}J_0'(x) + \frac{1}{x}J_0(x)\right]$$
$$+ \frac{2}{\pi}\left\{\frac{x}{2} - \frac{x^3}{2^2 \cdot 4}\left(1 + \frac{1}{2}\right) + \frac{x^5}{2^2 \cdot 4^2 \cdot 6}\left(1 + \frac{1}{2} + \frac{1}{3}\right) - \cdots\right\} \qquad (2.36e)$$

$$Y_0''(x) = \frac{2}{\pi}\left[\left\{\ln\left(\frac{x}{2}\right) + \gamma\right\}J_0''(x) + \frac{2}{x}J_0'(x) - \frac{1}{x^2}J_0(x)\right]$$
$$+ \frac{2}{\pi}\left\{\frac{1}{2} - \frac{3x^2}{2^2 \cdot 4}\left(1 + \frac{1}{2}\right) + \frac{5x^4}{2^2 \cdot 4^2 \cdot 6}\left(1 + \frac{1}{2} + \frac{1}{3}\right) - \cdots\right\} \qquad (2.36f)$$

where x is a dummy variable and γ is Euler's number which is equal to:

$$\gamma = \lim_{n \to \infty}\left(1 + \frac{1}{2} + \frac{1}{3} + \cdots + \frac{1}{n} - \ln(n)\right) \qquad (2.37)$$

For this study Euler's number was approximated by:

$$\gamma \approx 0.5772156649015328606065 \qquad (2.38)$$

The code used to calculate the Bessel functions was written in quadruple precision complex FORTRAN, which is an extension of FORTRAN 77 found on the Naval Postgraduate School's IBM 3033 computer. Using this precision of code for the Taylor series expansion insured that the resultant values had an accuracy of at least six significant places.

In order to validate the programs written for this study, the driving point impedance of elastic plates would also be calculated and compared experimentally. This did not present any problems in the use of the programs, because an elastic material's Young' modulus and shear modulus can be represented by complex values with zero imaginary part. The only addition required to the programs is the elastic material's characteristics. For the elastic material aluminum was chosen, and for the viscoelastic material LD-400 was chosen.

It has been pointed out by Mindlin [Ref.10] ,and Reismann and Pawlik [Ref. 22] that the value of shear coefficient, κ in equation (2.24), is not fixed but depends on the material's Poisson's ratio and the frequency of the first antisymmetric mode of thickness-shear vibration. Equation (2.24) is based upon only the first antisymmetric mode of thickness-shear vibration and corresponds to a Poisson's ratio of $\nu = 0.176$. For both the elastic material and viscoelastic material under study the Poisson's ratio is greater than this. It was decided that two values of the shear coefficient

33

will be used for each type of material being studied. The values used are shown in Table 1.

The material Young's modulus, or shear modulus, and the Poisson's ratio must also be supplied. For the aluminum plate this information was taken from Timoshenko [Ref. 23]. For the viscoelastic plates, the information was taken from Lee [Ref. 5] , which was based upon data from Nashif, Jones, and Henderson [Ref. 1, pp. 390-392], and from material data sheet supplied by the manufacture, United McGill [Ref. 24]. Only the data from United McGill [Ref. 24] was temperature compensated in the program written for this study. The information from United McGill [Ref. 24] was provided on a log-log scale chart which allowed determination of complex Young's modulus at three different temperatures, 68, 86, and 104 degrees Fahrenheit. For each temperature the complex Young's modulus was determined at four frequencies, 10, 100, 1000, and 10,000 Hz. The information was taken in terms of the log of the value, so that the data was better conditioned for use in the numerical calculations. A four point, third order polynomial curve fit [Ref. 25] was applied at each of the above temperatures to allow calculating the modulus at other frequencies. At plate temperatures between those taken, a linear interpolation was used. The polynomial equations used are shown below. For a temperature of 68 degrees Fahrenheit:

$$D_{E'} = 2.025 - 0.06250 f_{log} + 0.1000 f_{log}^2 - 0.01250 f_{log}^3 \quad (2.39a)$$

$$D_{E''} = 1.775 - 0.07084 f_{log} + 0.1125 f_{log}^2 - 0.01667 f_{log}^3 \quad (2.39b)$$

For a temperature of 86 degrees Fahrenheit:

$$D_{E'} = 1.000 + 0.6125 f_{log} - 0.1875 f_{log}^2 + 0.02500 f_{log}^3 \quad (2.40a)$$

$$D_{E''} = 1.050 + 0.3875 f_{log} - 0.1000 f_{log}^2 + 0.01250 f_{log}^3 \quad (2.40b)$$

For a temperature of 104 degrees Fahrenheit:

$$D_{E'} = 0.9000 + 0.08750 f_{log} + 0.01250 f_{log}^2 + 0.0000001590 f_{log}^3 \quad (2.41a)$$

$$D_{E''} = 0.8000 + 0.2542 f_{log} - 0.06250 f_{log}^2 + 0.008333 f_{log}^3 \quad (2.41b)$$

where f_{log} is related to the frequency by:

$$f_{log} = \log (f) \qquad (2.42)$$

$D_{E'}$ and $D_{E''}$ are dummy variables which are related to the real part, E',
and the imaginary part, E", of the complex modulus by:

$$E' = 10^{\left(D_{E'}\right)} \cdot 1450.5 \qquad (2.43a)$$

$$E'' = 10^{\left(D_{E''}\right)} \cdot 1450.5 \qquad (2.43b)$$

where E' and E" are in the units of pounds per square inch. The material characteristics for the three reference temperatures are shown in Figures 14 to 16. The linear temperature interpolation was done in terms of $D_{E'}$ and $D_{E''}$ and then converted into E' and E" by equation (2.43). It was felt that aluminum would be insensitive to temperature changes and the data from Nashif, Jones, and Henderson [Ref. 1, pp. 390-392] was too coarse to allow accurate calculations other than at room temperature, 75 degrees Fahrenheit. The shear modulus and loss factor equations are repeated here for the data from Nashif, Jones, and Henderson [Ref. 1, pp. 390-392]:

$$G' = 0.00002503 \cdot f^3 - 0.1752 \cdot f^2 + 457.5883 \cdot f + 29280 \qquad (2.44a)$$

$$\eta = 0.65 e^{\left[-0.52732\left|\log\left(\frac{f}{62}\right)\right|^{1.956}\right]} \qquad (2.44b)$$

The moduli and loss factor for the viscoelastic material, from both sources are shown in Figures 17 to 19 for a temperature of 75 degrees Fahrenheit. This shows for the same material, there is little agreement on the material characteristics by different sources.
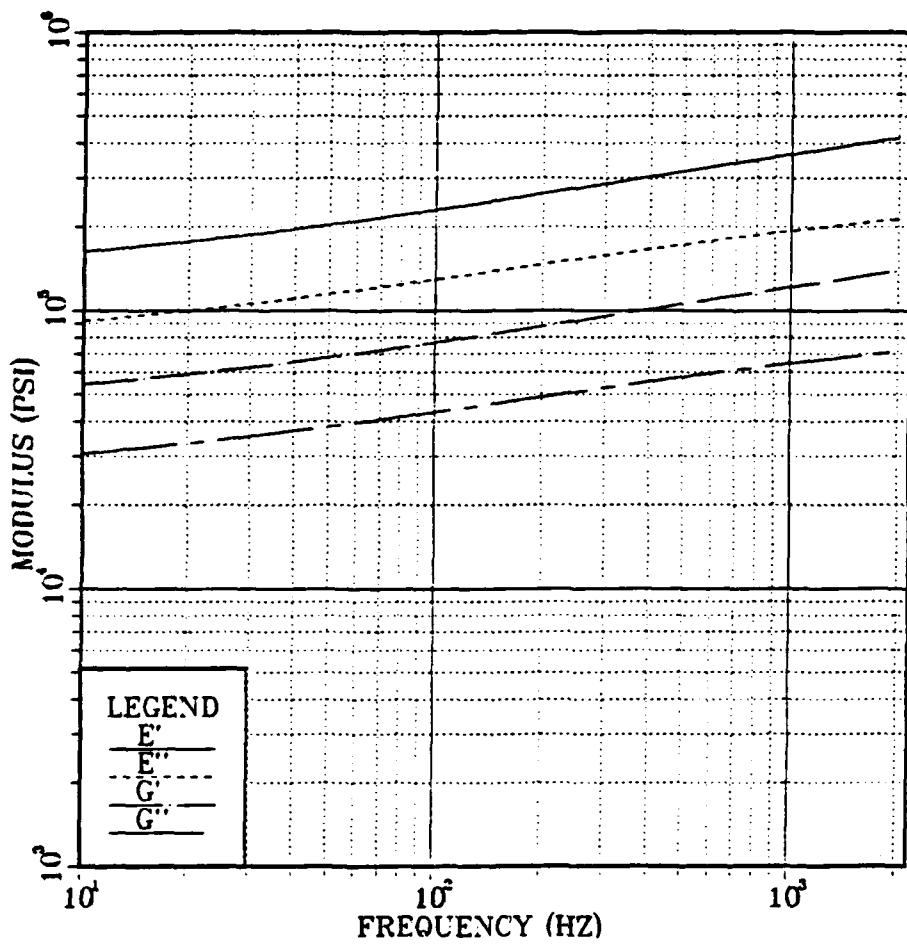
Figure 14. Viscoelastic Material Characteristics from
United McGill [Ref. 24] at 68 Degrees Fahrenheit.
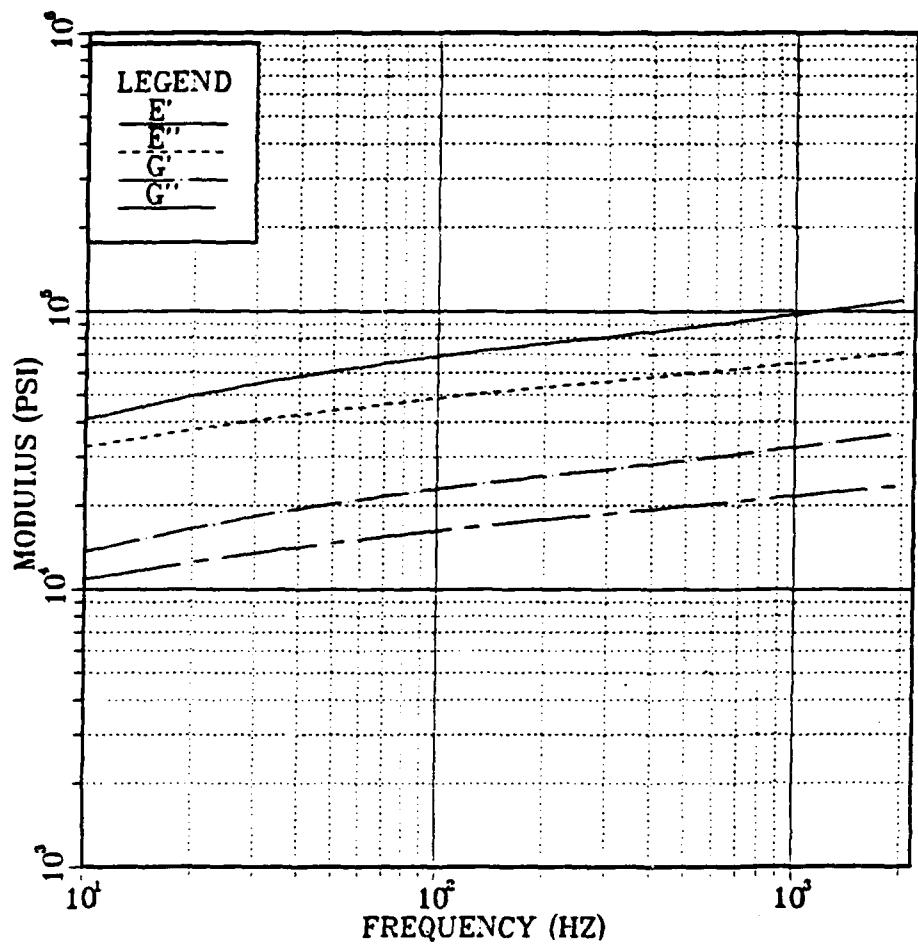
Figure 15. Viscoelastic Material Characteristics from United McGill [Ref. 24] at 86 Degrees Fahrenheit.
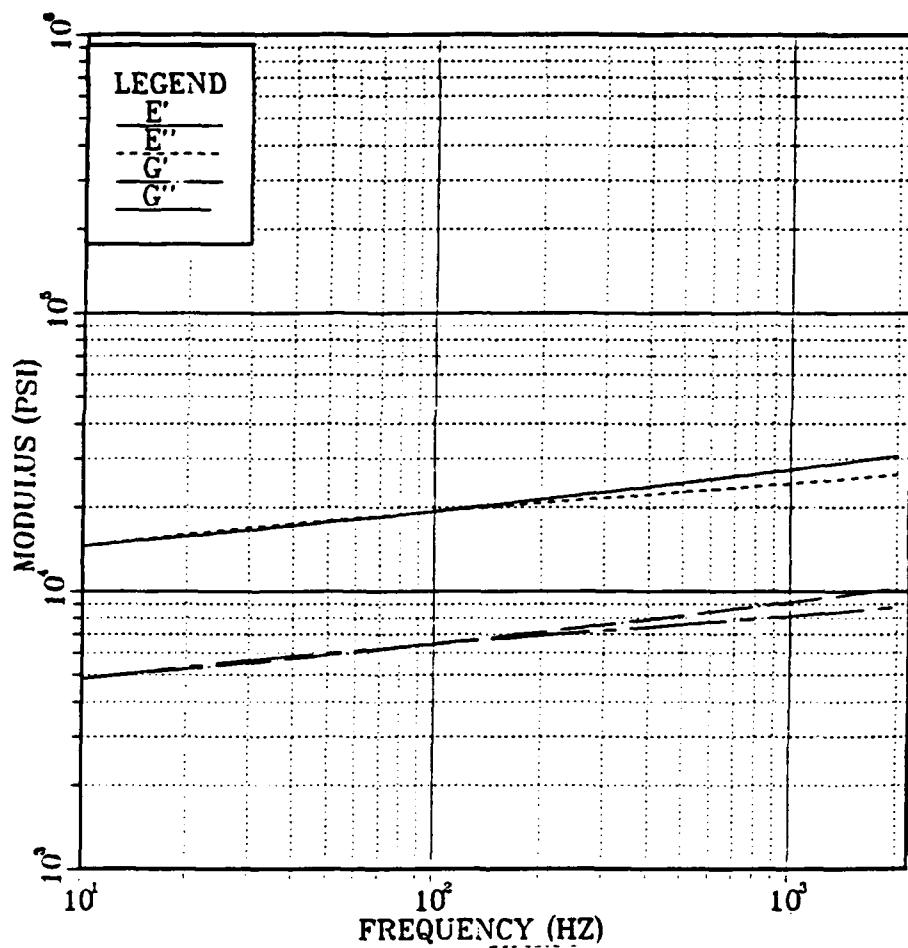
Figure 16. Viscoelastic Material Characteristics from
United McGill [Ref. 24] at 104 Degrees Fahrenheit.

39
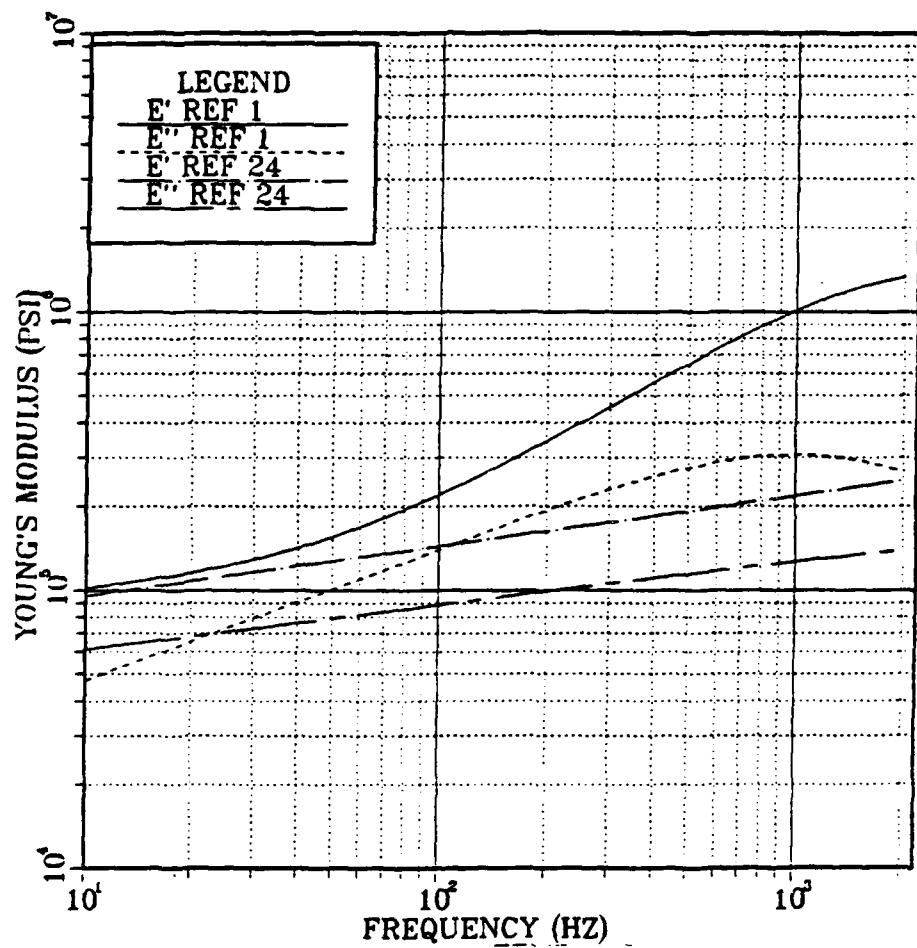
Figure 17. Comparison of Viscoelastic Material Young's Modulus
from Nashif, Jones, Henderson [Ref. 1, pp. 390-392] and
United McGill [Ref. 24].

40
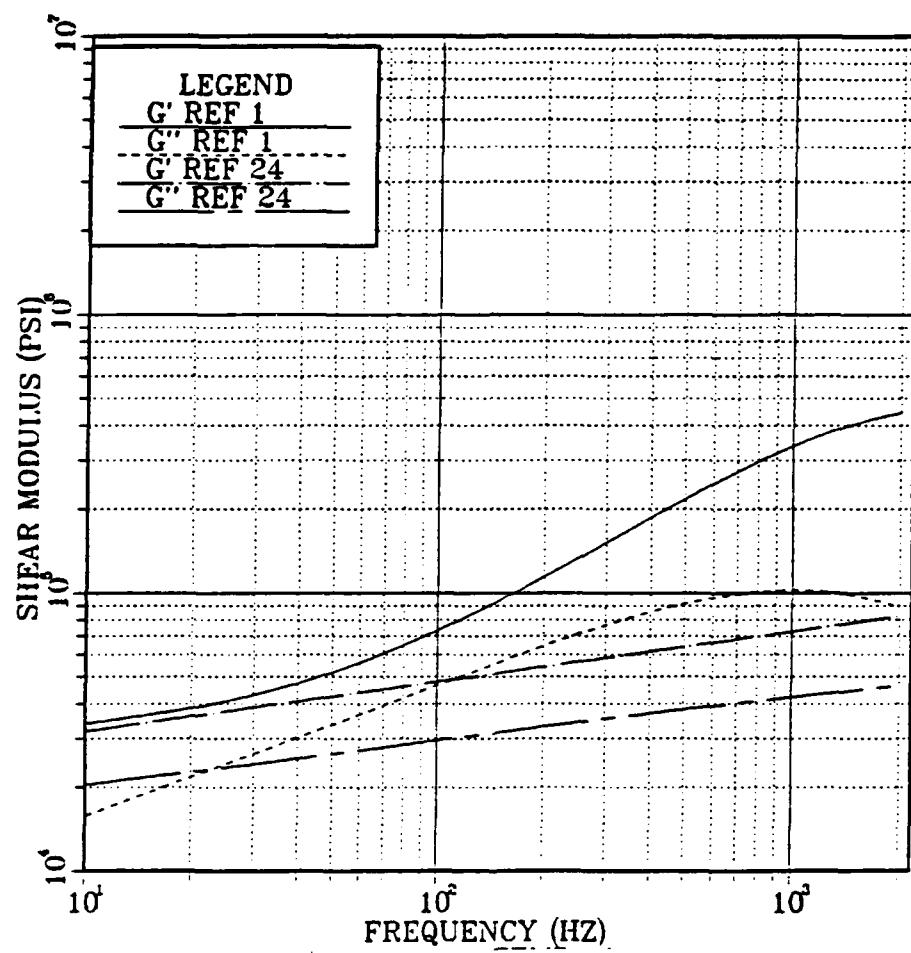
Figure 18. Comparison of Viscoelastic Material Shear Modulus from
Nashif, Jones, Henderson [Ref. 1, pp. 390-392] and
United McGill [Ref. 24].

41
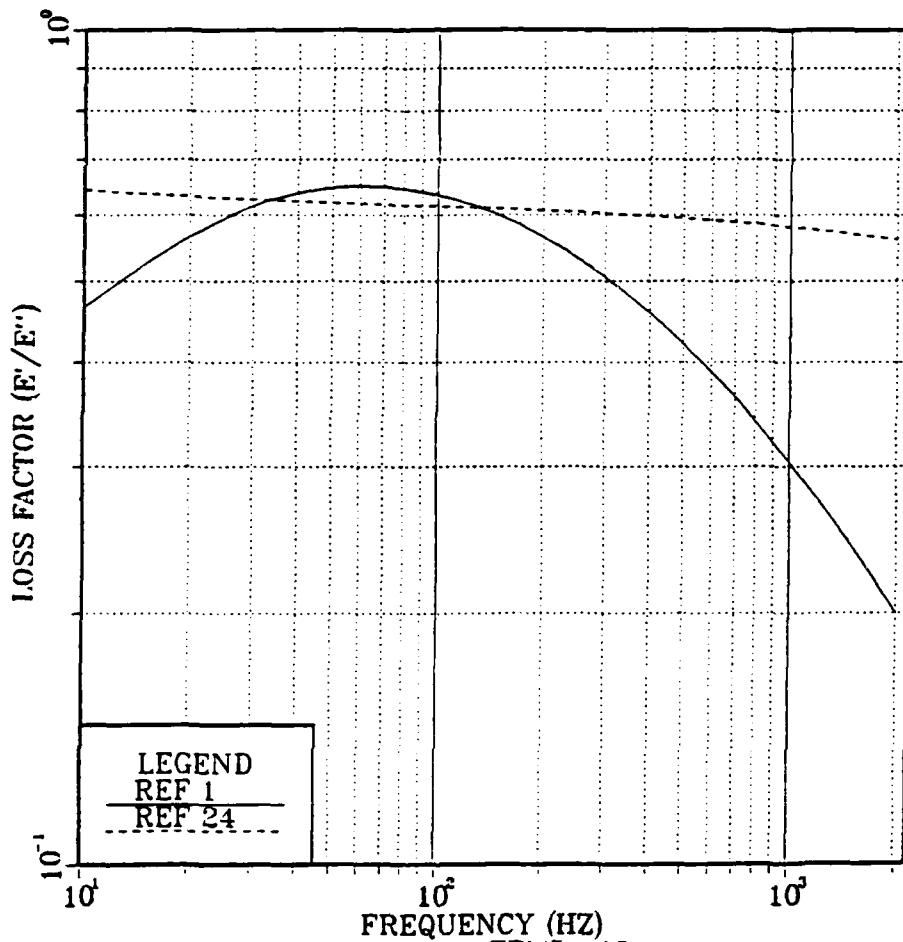
Figure 19. Comparison of Viscoelastic Material Loss Factor from
Nashif, Jones, Henderson [Ref. 1, pp. 390-392] and
United McGill [Ref. 24].

42

Other inputs to the FORTRAN program are the density and the temperature of the plate. The summary of the constants used are listed in Table 1. A copy of the FORTRAN programs used can be found in Appendix B. The driving point impedance was calculated at 100 point across the frequency range of interest. For the case of the elastic plate, the theoretical impedance at a mode will tend to infinity. However, for the frequency range of interest, 100 to 2000 Hz, the chances of having the frequency of interest being the same frequency as a mode are very small, and an overflow of the computer is unlikely. The results, for all materials, are shown in the real and imaginary parts of the driving point impedance due to the waveguide predictions being based upon the real part of the impedance. In an effort to check the calibration of the experimental portion of this study, the driving point impedance was calculated in the range of 10 to 105 Hz. The lower limit, 10 Hz, was set by the material characteristics of United McGill [Ref. 24] not going less than this, while the upper limit corresponded to the lower limit of the normal frequency range with a 5 Hz overlap.

TABLE 1. DIMENSIONS AND PROPERTIES OF MATERIALS UNDER STUDY.

	ELASTIC	VISCOELASTIC	
MATERIAL	AL	LD- 400	—DM- 375
Reference	Ref. 23	Ref. 1	Ref. 24
h (in)	$\frac{3}{8}$		
a (in)	4, 5, and 6		
b (in)	$\frac{5}{8}$		
E (psi)	11.0 M		
E' (psi)			Equations (2.39) to (2.43)
E" (psi)			
G' (psi)		Equation (2.44)	
η			
ν	0.33	0.5	
κ^2	$\frac{\pi^2}{12}$ and 0.8600	$\frac{\pi^2}{12}$ and 0.9128	
$\rho \; \frac{slugs}{in^3}$	3.06713×10^{-3}	1.71101×10^{-3}	1.70736×10^{-3}

44

The results for the elastic plates, shown in Figures 20 and 21, show that the plate is acting as a lumped mass in the low frequency range of 10 to 105 Hz. A lumped mass has no real part to the impedance, and the imaginary increases at a linear rate, which is what is happening here. The results for the high frequency range, 100 to 2000 Hz, do not provide much information, except the frequency of the first mode, as shown in Figures 22 and 23.

The results for the viscoelastic plates, shown in Figures 24 to 27, show that there is a significant difference in the driving point impedance due to the material characteristics used, either Nashif, Jones, and Henderson [Ref. 1, pp. 390-392] or United McGill [Ref. 24]. It also shows that at very low frequencies the viscoelastic material is behaving as a lumped mass, with little real part and a linearly increasing imaginary part. The effect of the temperature compensation of the material characteristics supplied by United McGill [Ref. 24] is demonstrated by the results shown in Figures 28 and 29. This shows that the impedance decreases and becomes smother with increases in temperature.

In all cases the effect of a different shear coefficient, κ, is insignificant and a shear coefficient of $\kappa^2 = \pi^2/12$ ($\kappa = 0.9069$) will be used for the remainder of this study.

The dominant factors for the viscoelastic plates which effect the calculated driving point impedance, are the source of material characteristics and plate temperature for a fixed plate geometry, and the geometry of the plate. Figures 74 to 77 and Figures 96 to 99, in Appendix C, show the results for the five and four inch plates.
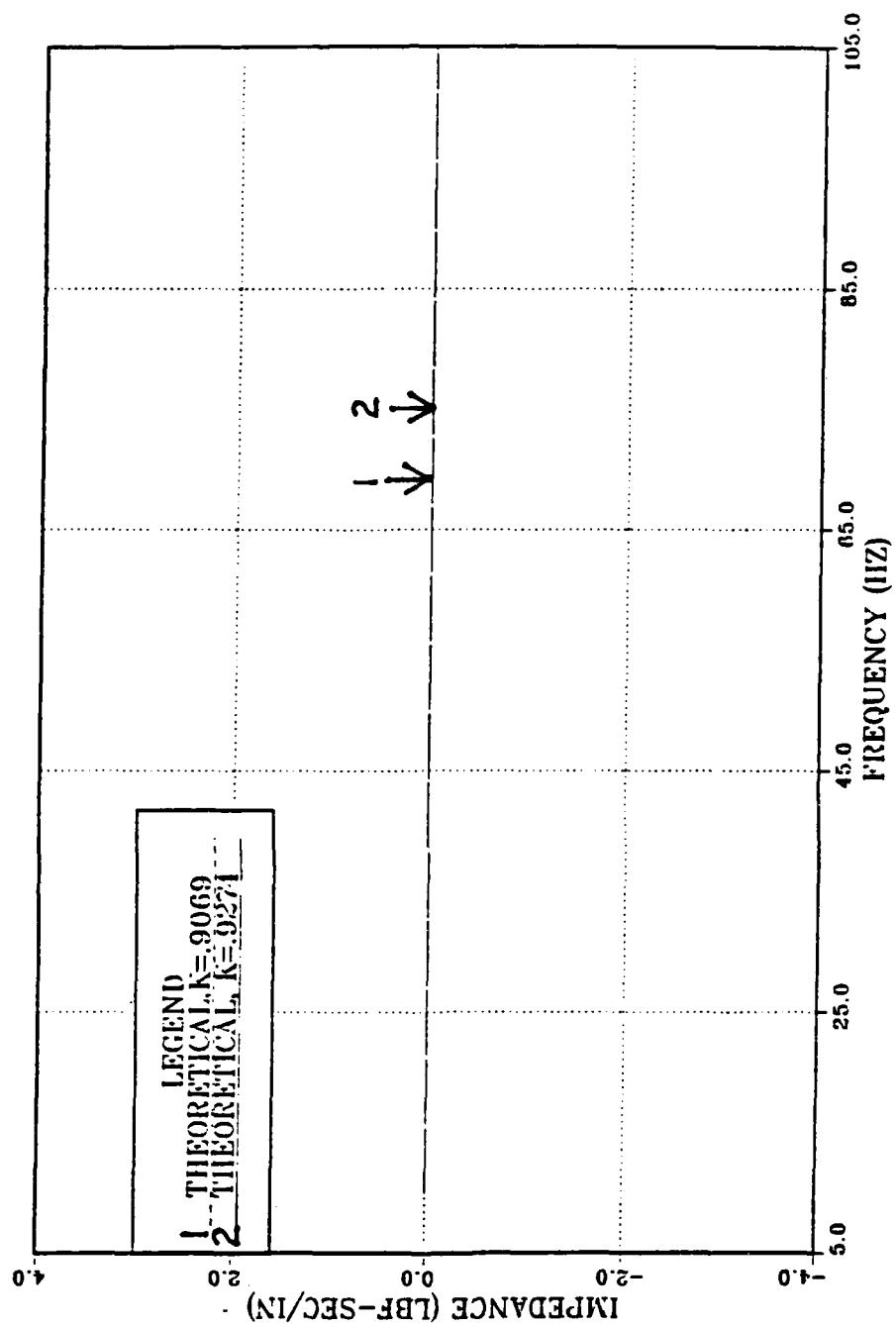
Figure 20. Effect of Shear Coefficient on the Theoretical Real Part of the Driving Point Impedance for a 6 in Radius Elastic Plate in the Frequency Range of 10 to 105 Hz.
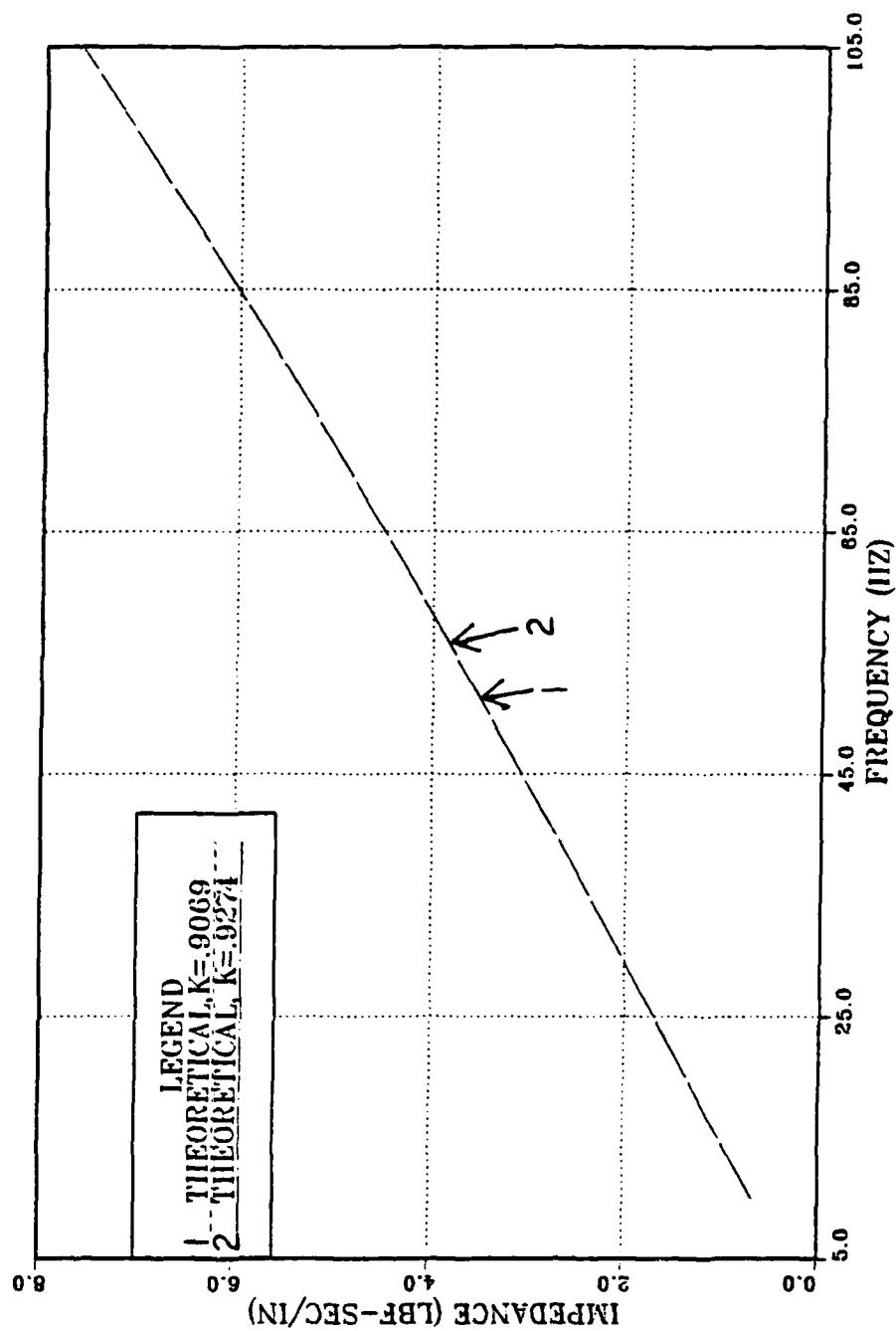
Figure 21. Effect of Shear Coefficient on the Theoretical Imaginary Part of the Driving Point Impedance for a 6 in Radius Elastic Plate in the Frequency Range of 10 to 105 Hz.

48
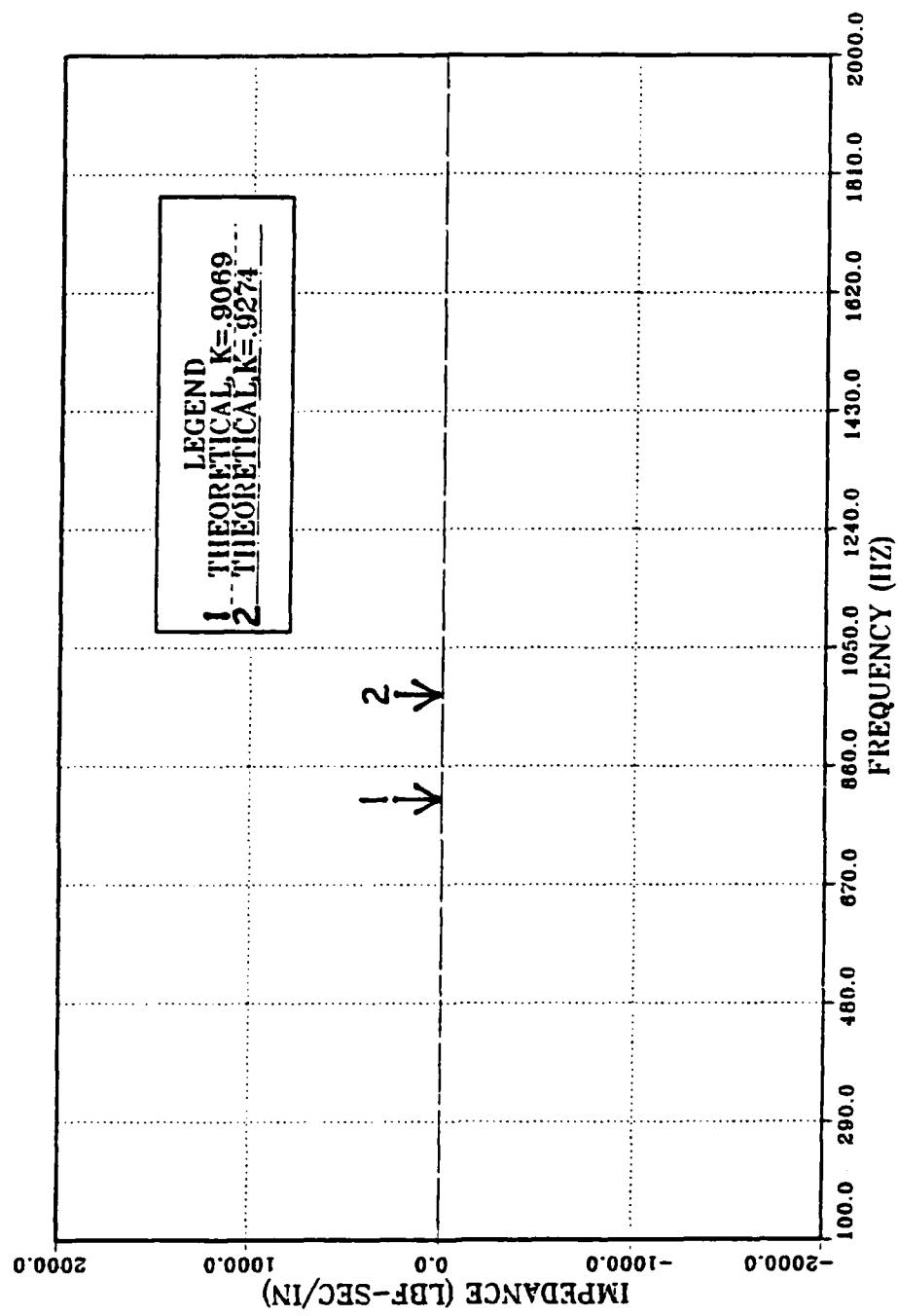
Figure 22. Effect of Shear Coefficient on the Theoretical Real Part of the Driving Point Impedance for a 6 in Radius Elastic Plate in the Frequency Range of 100 to 2000 Hz.
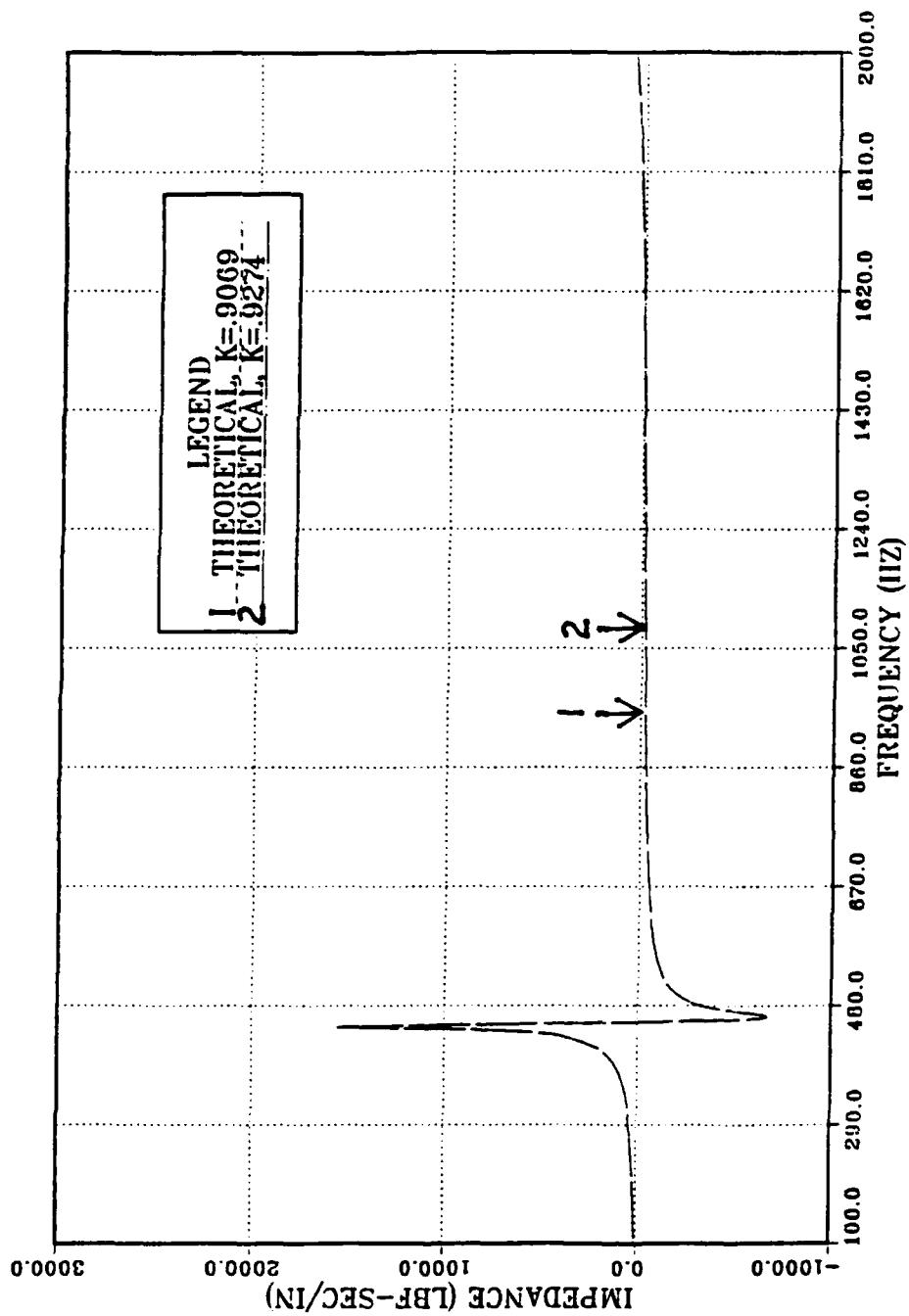
Figure 23. Effect of Shear Coefficient on the Theoretical Imaginary Part of the Driving Point Impedance for a 6 in Radius Elastic Plate in the Frequency Range of 100 to 2000 Hz.

50
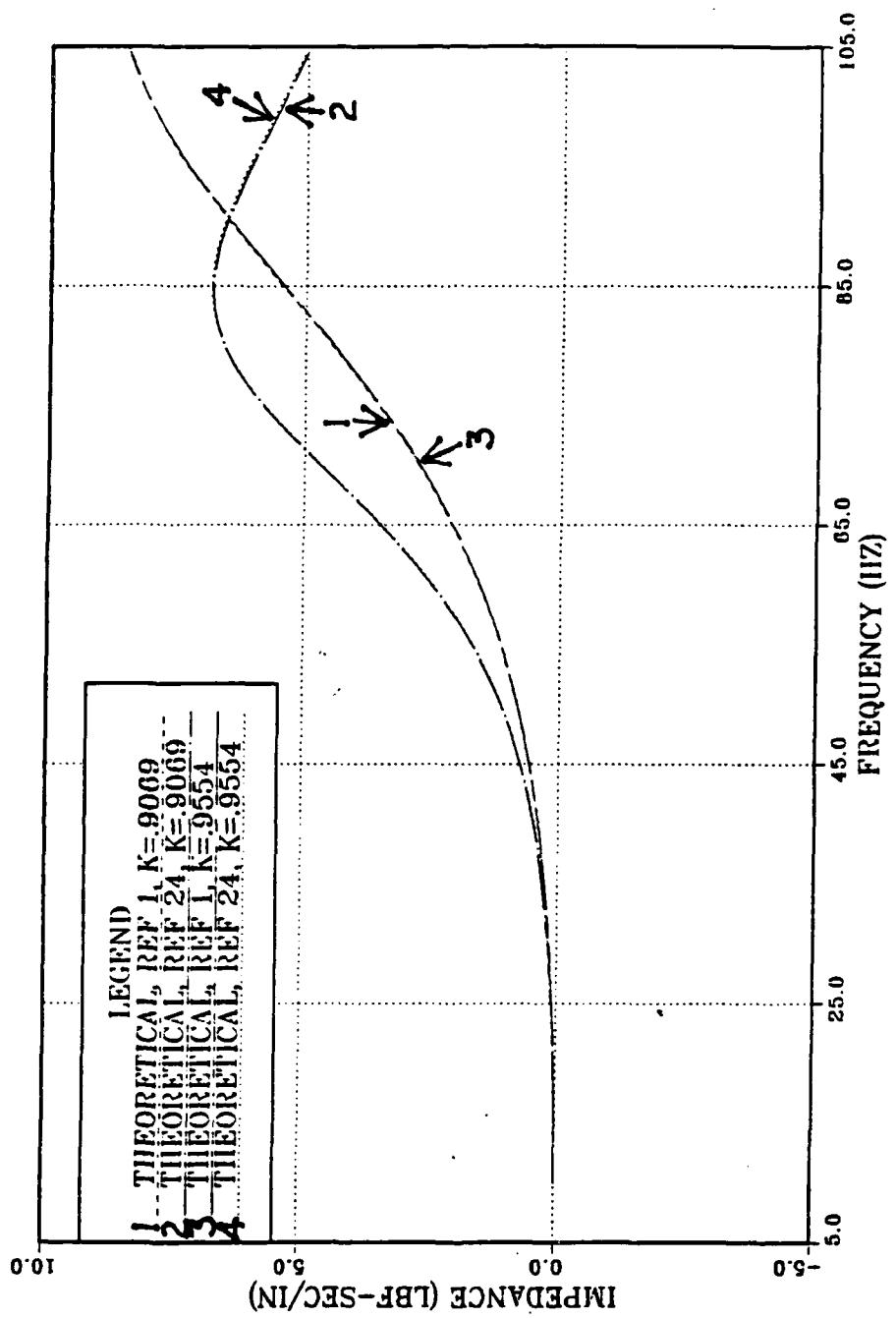
Figure 24. Effect of Shear Coefficient and Material Characteristics on the Theoretical Real Part of the Driving Point Impedance for a 6 in Radius Viscoelastic Plate in the Frequency Range of 10 to 105 Hz at a Temperature of 75.0 Deg. F.

51
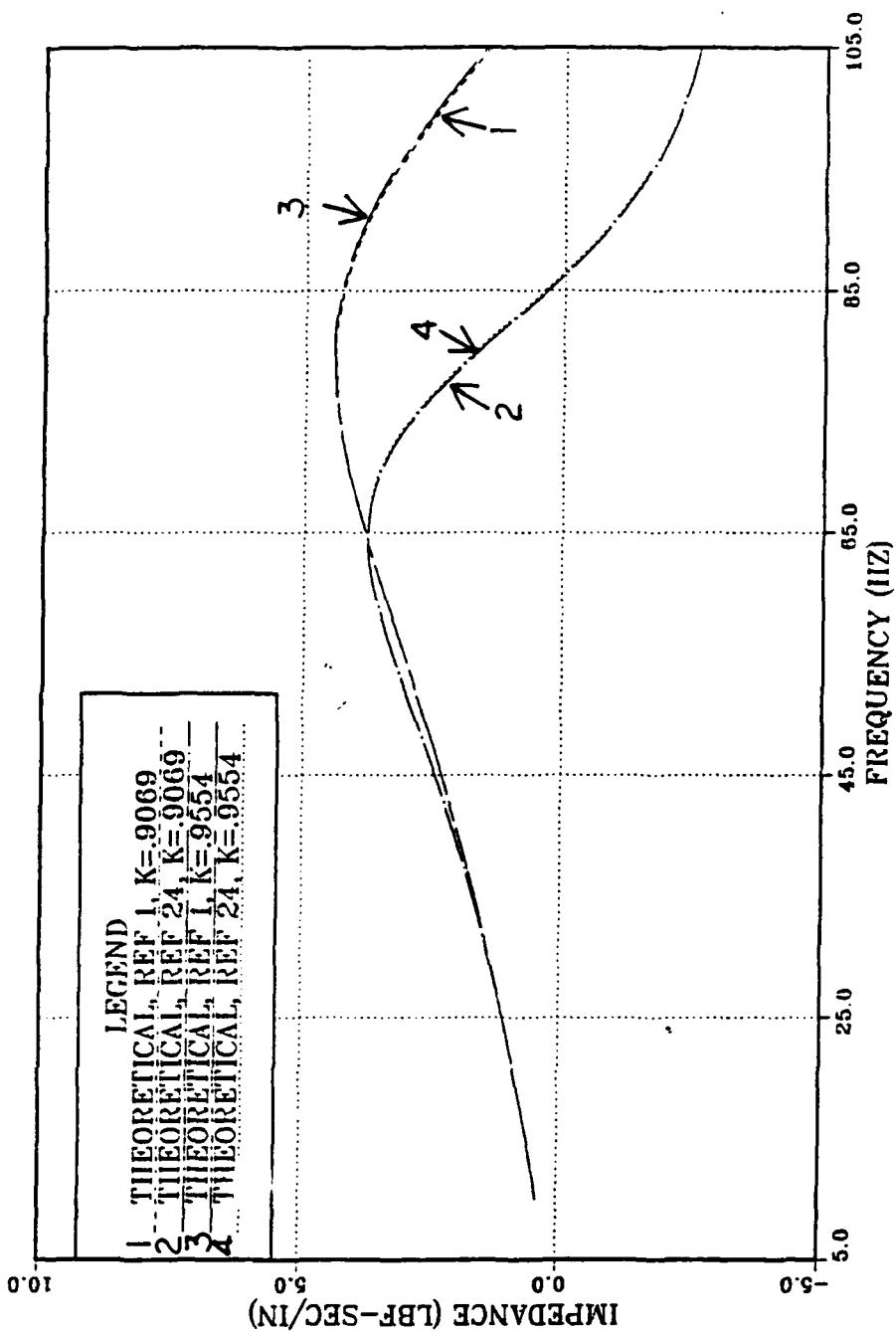
Figure 25. Effect of Shear Coefficient and Material Characteristics on the Theoretical Imaginary Part of the Driving Point Impedance for a 6 in Radius Viscoelastic Plate in the Frequency Range of 10 to 105 Hz at a Temperature of 75.0 Deg. F.

52
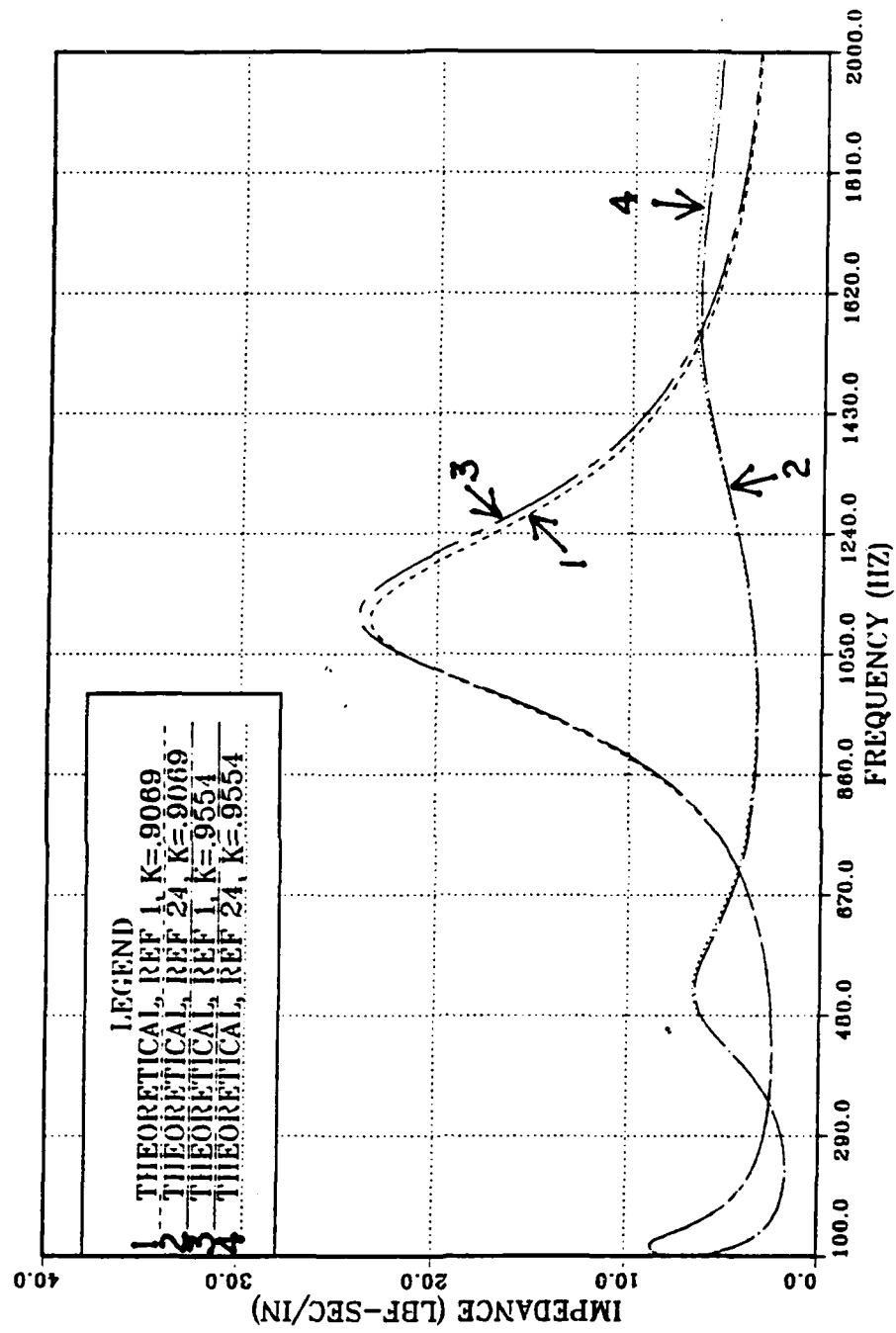
Figure 26. Effect of Shear Coefficient and Material Characteristics on
the Theoretical Real Part of the Driving Point Impedance
for a 6 in Radius Viscoelastic Plate in the Frequency
Range of 100 to 2000 Hz at a Temperature of 74.5 Deg. F.

53
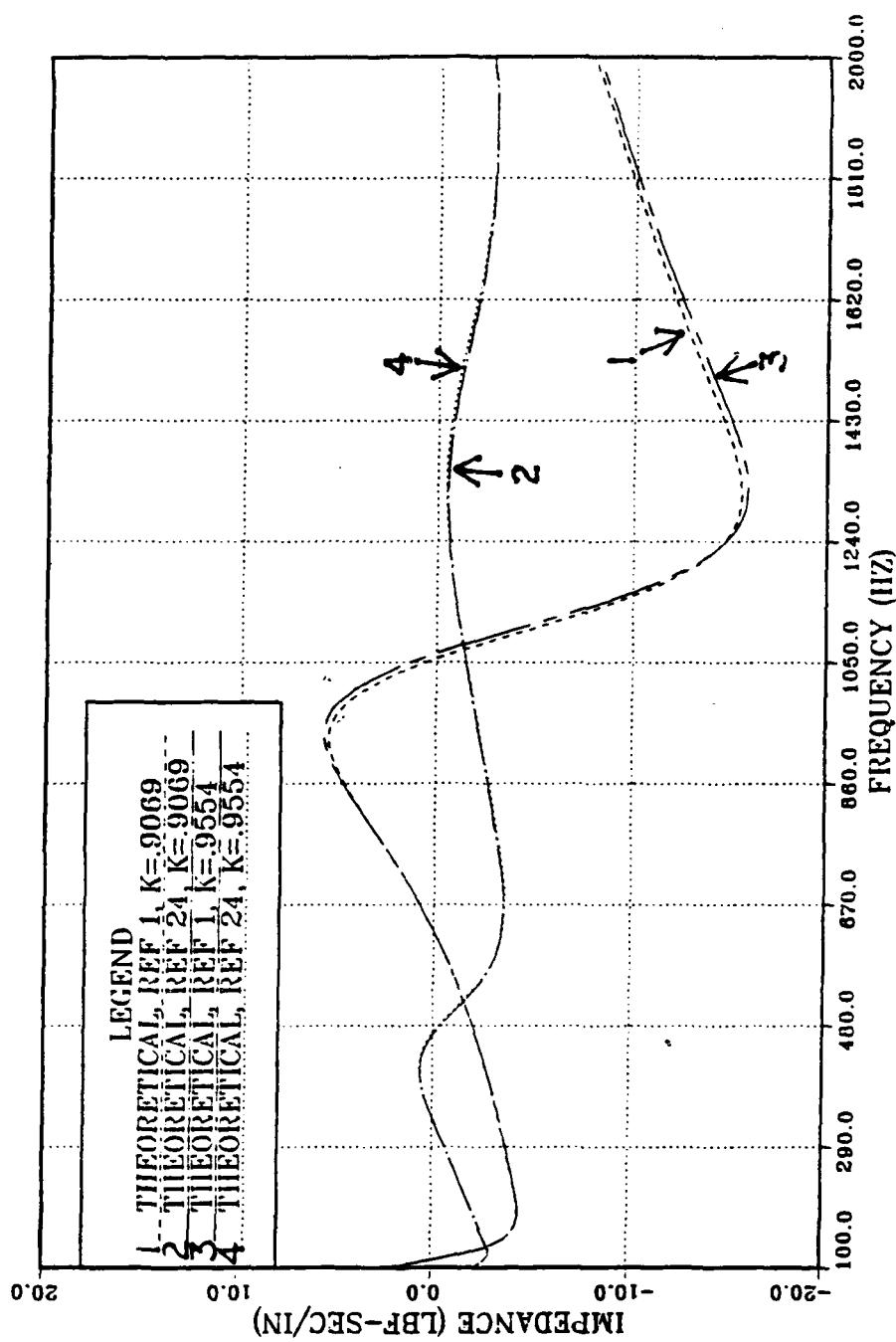
Figure 27. Effect of Shear Coefficient and Material Characteristics on the Theoretical Imaginary Part of the Driving Point Impedance for a 6 in Radius Viscoelastic Plate in the Frequency Range of 100 to 2000 Hz at a Temperature of 74.5 Deg. F.

54
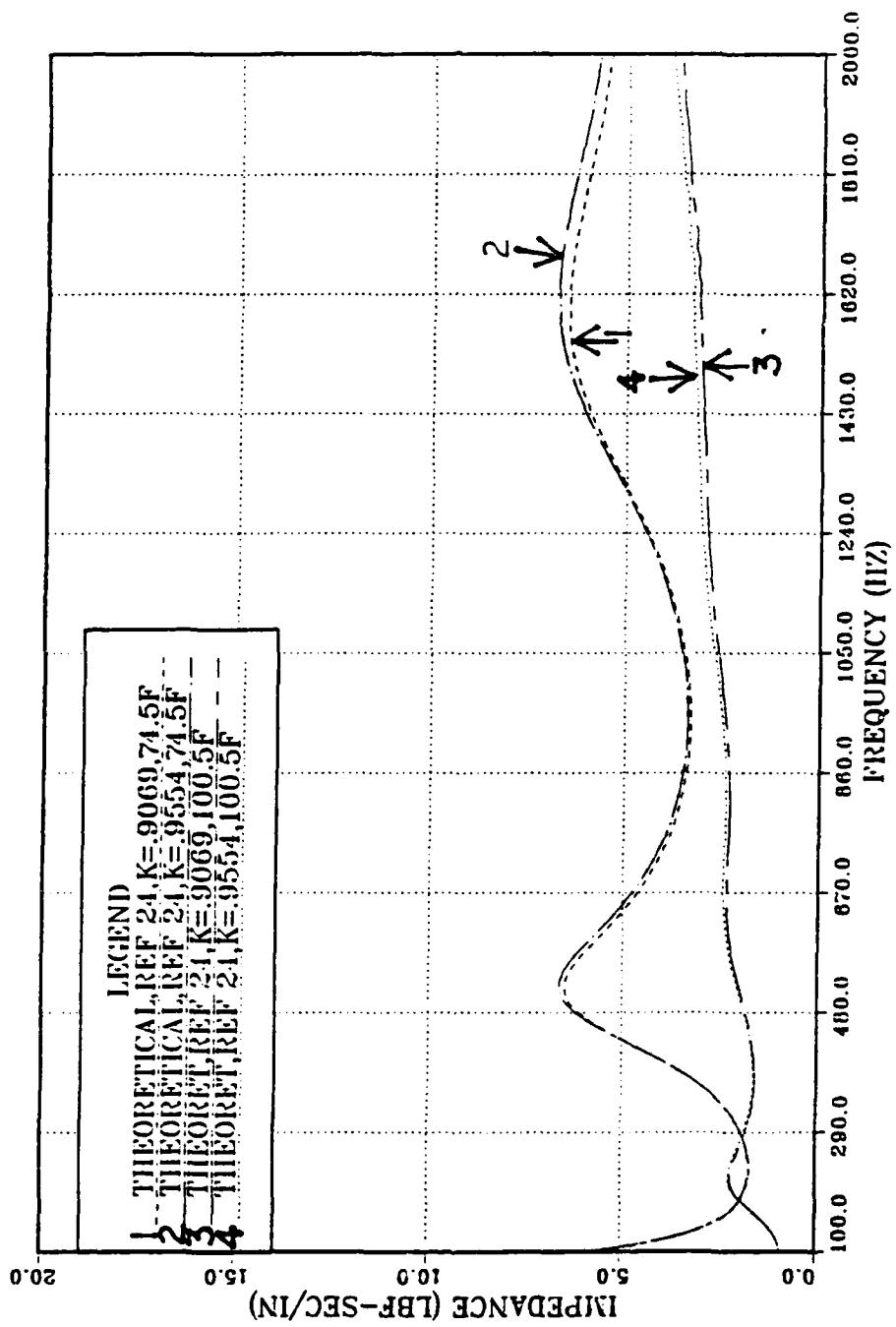
Figure 28. Effect of Shear Coefficient, Material Characteristics, and Temperature on the Theoretical Real Part of the Driving Point Impedance for a 6 in Radius Viscoelastic Plate in the Frequency Range of 100 to 2000 Hz.

55
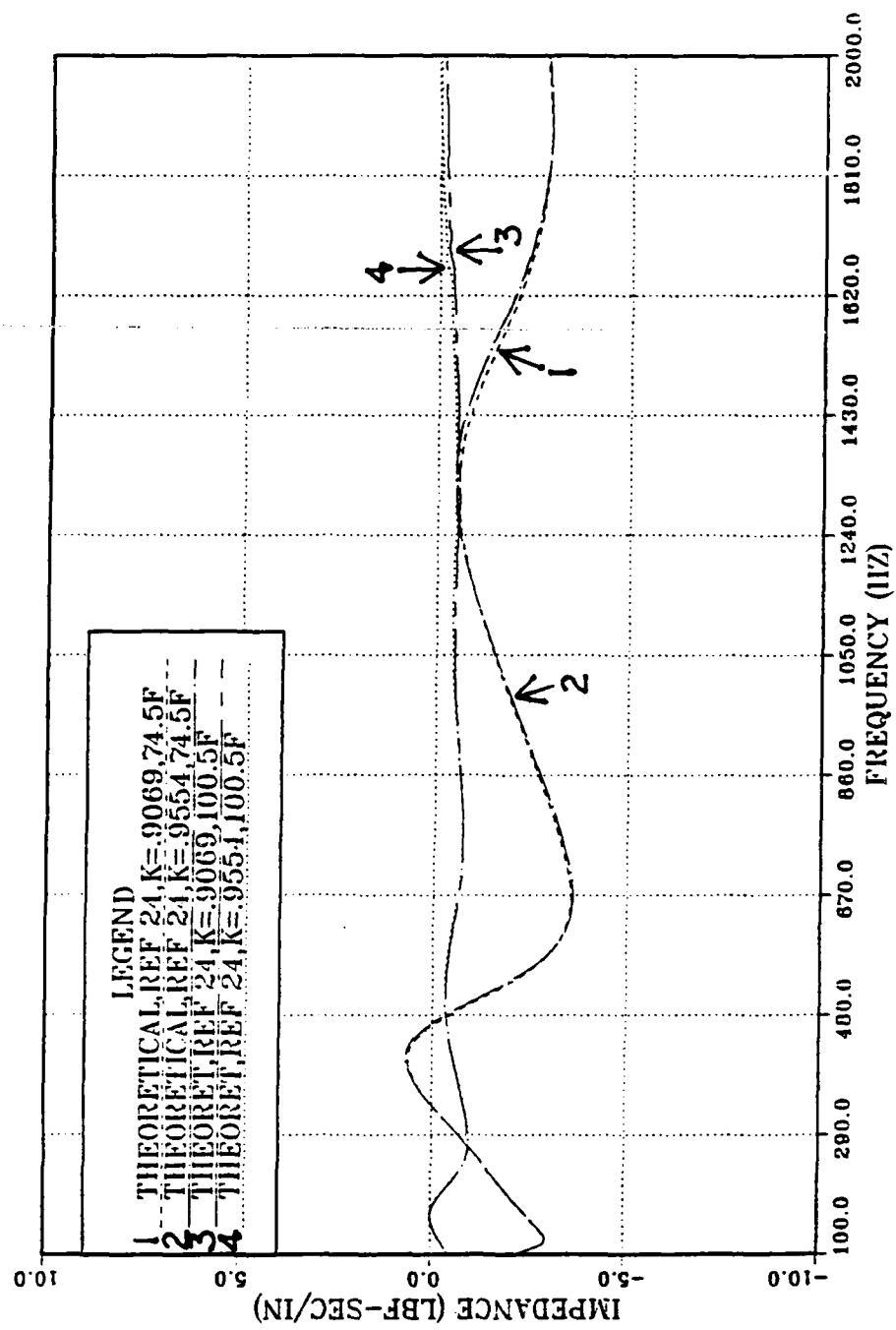
Figure 29. Effect of Shear Coefficient, Material Characteristics, and Temperature on the Theoretical Imaginary Part of the Driving Point Impedance for a 6 in Radius Viscoelastic Plate in the Frequency Range of 100 to 2000 Hz.

56

III. EXPERIMENT

A.   EXPERIMENT SET UP

A total of 6 plates were tested during this study. Three were made
out of aluminum, an elastic material, and three were made out of LD-400
material, a viscoelastic material. All were 3/8 of an inch thick with a plate
from each material at a radius of four, five, and six inches as listed in
Table 1. The viscoelastic plates where made from twelve inch square tiles
that are 3/8 inch thick, this limited the maximum plate size to a six inch
radius. The other two plates were chosen so that there would be a definite
change in characteristics for a change in geometry and so that the ratio of
thickness to radius did not become too large and deviate from thin plate
theory. To determine the driving point impedance of the plates, the
equipment and configuration of Figure 30 was used.
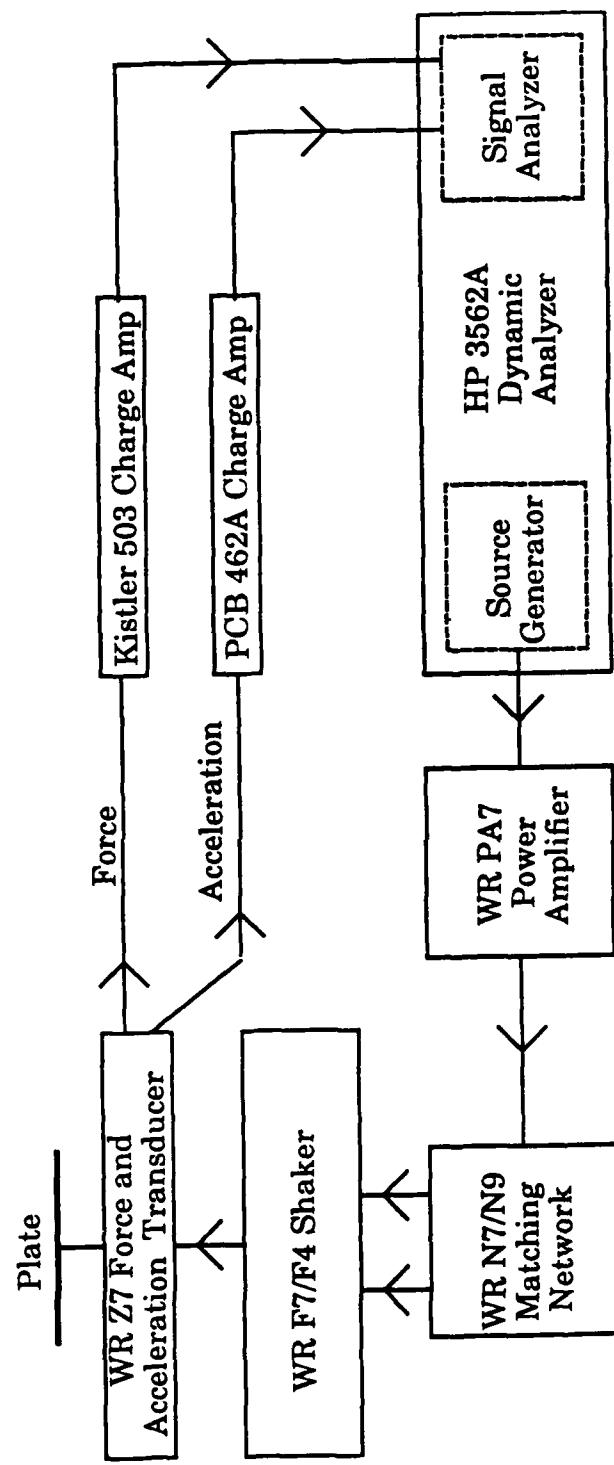
Figure 30. Experiment Set Up.

58

In Figure 30, WR is for Wilcoxon Research and HP for Hewlett Packard. The Wilcoxon Research F4/F7 shaker and Z7 measurement head are an integral unit that was mounted on a stand for the impedance measurements. The driving signal to the shaker is provided by the Hewlett Packard HP-3562A dynamic signal analyzer via the Wilcoxon Research PA7 power amplifier and N7/N9 matching network. The force and acceleration measurements of the plate were provided by the Wilcoxon Research Z7 impedance head mounting base, and then amplified by a Kistler 503 charge amplifier, for the force signal, or by a PCB 462A charge amplifier, for the acceleration signal, before going to the HP-3562A dynamic signal analyzer. The HP-3562A dynamic signal analyzer was operated in the swept sine mode for all of the tests to insure that the coherence of the data was at, or almost at, one. A minimum of 400 sample points were taken when the frequency range of interest was 100 to 2000 Hz, and a minimum of 160 sample points were taken when the frequency range of interest was 5 to 105 Hz. These were only a minimum as the analyzer was set to provide auto frequency resolution, or take more sample points, when the incoming data showed a large change from the previous data point. The analyzer was also set up to control the amount of power going to the shaker so that the incoming signals were of a quality that would keep the coherence at one. In the frequency range of less than 2000 Hz, the data was taken with the F7 piezoelectric vibration generator electrically secured and all data gathered with the F4 electromagnetic vibration generator. This was done because the F7 was producing considerable ring in the force and acceleration signals, which was degenerating the quality of the signal

going to the analyzer. The F7 is normally used for the high frequency measurements and the F4 for the low frequency measurements [Ref.26]. A photograph of the four inch radius plate mounted on the shaker is shown in Figure 31.
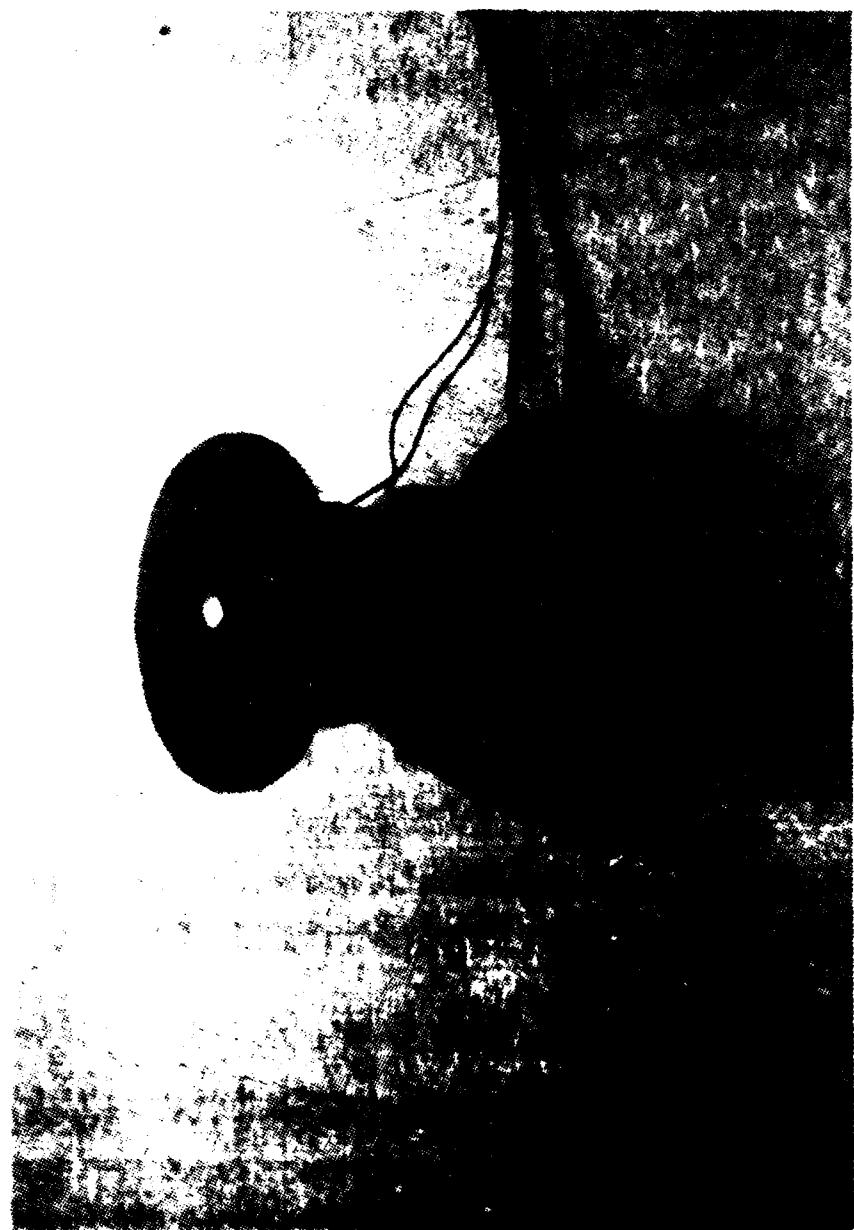
Figure 31. Photograph of Four Inch Plate Mounted on Shaker.

The easiest method of determining the driving point impedance of the plate from the information, force and acceleration, being provided to the analyzer, is to start with the plate's frequency response and then mathematically convert this information into the driving point impedance by math functions built into the analyzer. The frequency response, H(f) , as measured by the analyzer, is:

$$H(f) = \frac{G_{FA}(f)}{G_{FF}(f)} \tag{3.1}$$

where $G_{FA}(f)$ is the cross spectrum between the force signal, F, and the acceleration signal, A, and $G_{FF}(f)$ is the power spectrum of the force signal [Ref. 27]. The transfer function, H(f), is the ratio of acceleration to force or:

$$H(f) = \frac{A}{F} \tag{3.2}$$

The acceleration is related to the velocity by:

$$A = \frac{\partial V}{\partial t} = j\omega V \tag{3.3}$$

By combining equations (3.3) and (3.2) and rearranging the resultant equation the driving point impedance becomes:

62

$$Z = \frac{j\omega}{H(f)} \qquad\qquad (3.4)$$

In the analyzer the frequency response, H(f), was first multiplied by $(j\omega)^{-1}$ and then the reciprocal of the resultant function was taken to be the driving point impedance, Z.

B.   PLATE MOUNTING DESIGN

Some way of attaching the plate to the shaker must be designed and used. For use as a waveguide absorber, the plate will have a hole drilled at the center of the plate for a bolt or screw. This idea was used as the starting point for the design of the plate to shaker mount. A mount was manufactured from steel rod two inches long with 3/8 inch threads on one end, the shaker end, and 1/4 inch threads on the other end, the plate end. The plate was held between two 1/4 inch nuts and washers and a lock washer as shown in Figure 32.
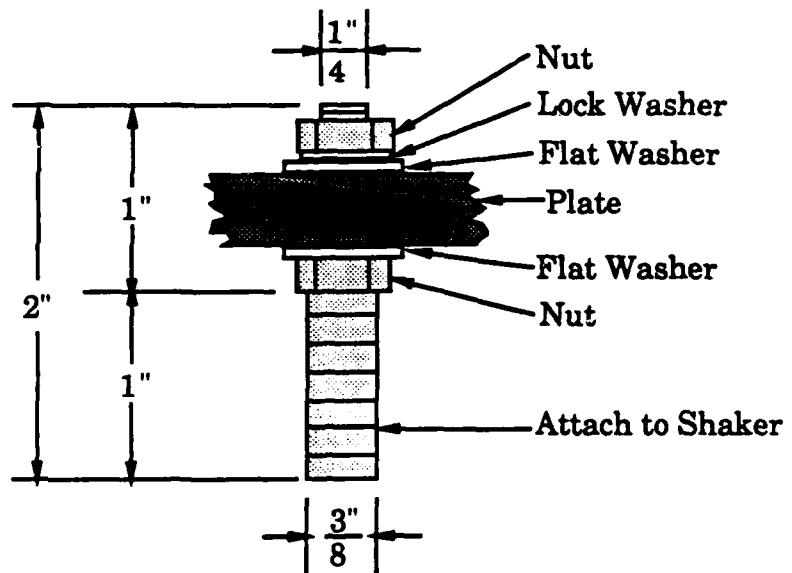
Figure 32. Steel Plate to Shaker Mount.

This mount proved to be unsatisfactory in operation. Its weight and size were totally against it. It resonated right in the middle, from about 700 to 1200 Hz, of the frequency range of interest, 100 to 2000 Hz. The data taken, when using this mount, was useless. A new mounting system was designed, using aluminum, to minimize the weight and size of the mount and is shown in Figure 33.
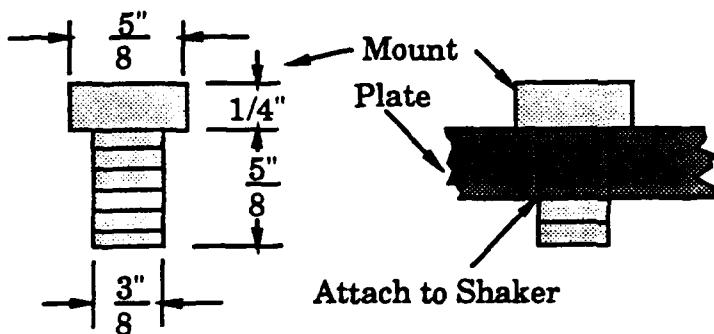
Figure 33. Aluminum Plate to Shaker Mount.

This mount was extremely light weight and has almost no effect on the plate data. There was sufficient friction produced in the attachment to the shaker, that the plate and mount did not vibrate lose during the data runs, and a lock washer was not required. As a means of checking the effectiveness of this mount, the driving point impedance of the shaker and mount, with no plate, were determined over the same frequency range as with the plate. For these runs, the analyzer had the same configuration as with plates except that the auto frequency resolution was turned off. If the auto frequency resolution were left on, the data runs would have taken too long, greater than 2 hours. The results of these runs showed that the shaker and mount were acting as if a pure mass of 1.48656 mslugs. The shaker and mount mass is much less than the mass of the smallest plate

65

under study, so its effects are ignored. A 3/8 inch hole was drilled in the center of each plate to allow mounting. The plate sat on a 5/8 inch outside diameter boss on the shaker, and then was clamped down by the aluminum mount. Both the shaker and mount have an outside diameter of 5/8 inch which was used in all of the theoretical calculations for the value of inner radius, b.

C. VERIFICATION OF IMPEDANCE SCALE

In all of the data runs, the calibrated output from the force and acceleration transducer, plus the gain of the charge amplifiers, was inputted into the analyzer to insure that the results of the analyzer were of the proper scale. As a means of checking the scale of these inputs, the driving point impedance of an elastic plate can be compared experimentally and theoretically at a certain frequency. At frequencies less than the first mode, the elastic plate can be considered as a lumped mass as shown in Figure 34.
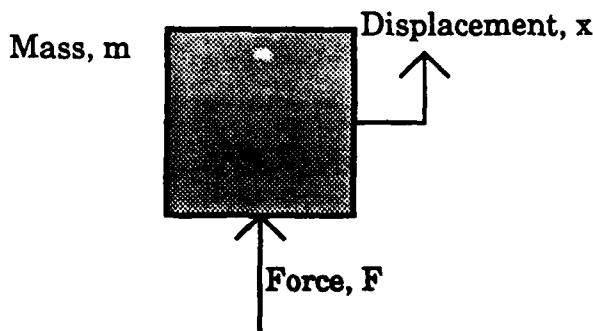
Figure 34. Lumped Mass Model of Elastic Plate.

Summing the forces on the mass, results in the equation of motion:

$$F - ma = F - m\ddot{x} = 0 \qquad (3.5)$$

The acceleration, a, in terms of velocity, V, is:

$$a = \frac{\partial V}{\partial t} = j\omega V \qquad (3.6)$$

The force, F, in terms of the velocity, V, is:

$$F = j\omega mV \qquad (3.7)$$

The *impedance*, Z, then becomes:

$$Z = \frac{F}{V} = j\omega m \qquad (3.8)$$

This allows calculating the impedance of the plate, based upon its weight, or mass, and the frequency of interest. A frequency of 100 Hz was chosen for this comparison on the elastic plates under study. The 100 Hz frequency is less than the lowest mode of the plates under study. The results of this comparison as shown in Table 2. Only the imaginary parts of the impedance are looked at, as the model shows there is no real part, only an imaginary part.

67

TABLE 2. IMAGINARY PART OF IMPEDANCE FOR ELASTIC PLATES.

		Data Run	
Plate Radius	Calculated	5-105 Hz	100-2K Hz
	Impedance, Imaginary Part, lbf-sec/in		
4 in	3.1178	2.77836	2.79759
5 in	4.8973	4.22329	4.45218
6 in	7.0535	6.79937	6.9406

The results of this comparison show that the analyzer and the associated equipment have the proper impedance scale.

D. DATA RUNS

Each of the six plates used in this study, were subjected to two different frequency ranges at room temperature. One data run was from 5 to 105 Hz, for the purpose of checking the operation and calibration of the equipment, and the other from 100 to 2000 Hz, the frequency range of interest. As an added measure both of the six inch, elastic and viscoelastic, plates were run from 100 to 2000 Hz at an elevated temperature of about 100

degrees Fahrenheit to check the effect of temperature on Young' modulus. The surface temperature of the plate was measured with an Omega 871 digital thermometer with a type K surface temperature probe. A number of points on the plate were measured before and after the data run. It was observed that the shaker was adding heat to the plates during the data run. This resulted in a temperature gradient of about five degrees Fahrenheit from the center of the plate to the outer edge. The temperature of the plate was taken as the average of all of the readings.

On all data runs the coherence remained at one for every sample point taken. The repeatability of the data was tested on six inch radius elastic and viscoelastic plates by repeating the data runs after being removed from the shaker and then reinstalled, and by running the swept sine run in the decreasing mode instead of the increasing mode. There was almost no difference in the driving point impedance for these runs and the normal data run. It is concluded that the data is repeatable.

E.   EFFECT OF THE SHAKER ON THE IMPEDANCE MEASUREMENTS

The shaker and the mount have mass which contributes to the data measurements. The effect of this mass can be taken into account by considering the model of the measurement system shown in Figure 35.
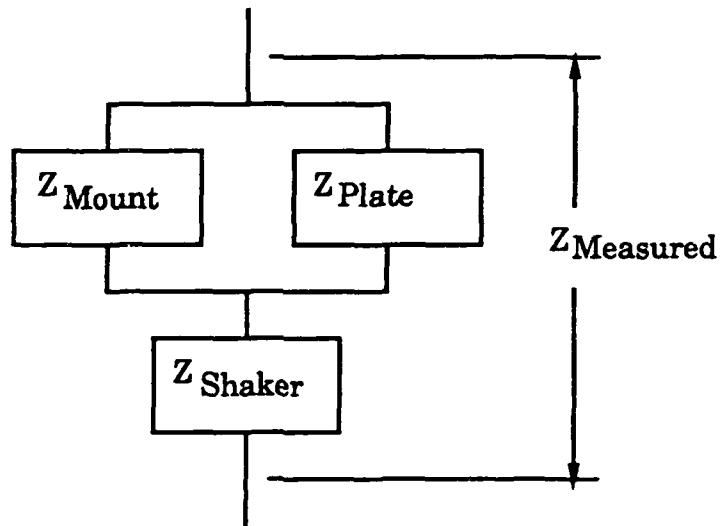
Figure 35. Impedance Measurement Model.

The measured impedance for this model is:

$$Z_{Measured} = Z_{Shaker} + \frac{Z_{Mount} \cdot Z_{Plate}}{Z_{Mount} + Z_{Plate}} \qquad (3.9)$$

If the impedance of the mount can be ignored, then the plate impedance becomes the measured impedance minus the shaker impedance or:

$$Z_{Plate} = Z_{Measured} - Z_{Shaker} \qquad (3.10)$$

This calculation can be accomplished in the analyzer very easily. In order to determine the impedance of the shaker and the mount, data runs were taken of the shaker and mount together, and with the shaker alone. The results of these data runs, Figures 36 to 39, show that the shaker and mount are effectively a lumped mass with little real impedance and a linearly increasing imaginary impedance with frequency. This occurred over both frequency ranges, 5 to 105 Hz and 100 to 2000 Hz, tested. The mass of the mount was measured to be 0.34946 mslugs, while the mass of the shaker, from $m=Z/\omega$, is 1.0374 mslugs. The mass of the lightest plate is 30.0123 mslugs, which is almost 100 times greater than the mount mass and 30 times greater than the shaker mass. As such the mass effect of the mount has been ignored and the plate impedance found by equation (3.10). It was noted that the data below about 15 Hz was very hard to accurately get without the mass of a plate being present. The data in this region has a fair amount of scatter.
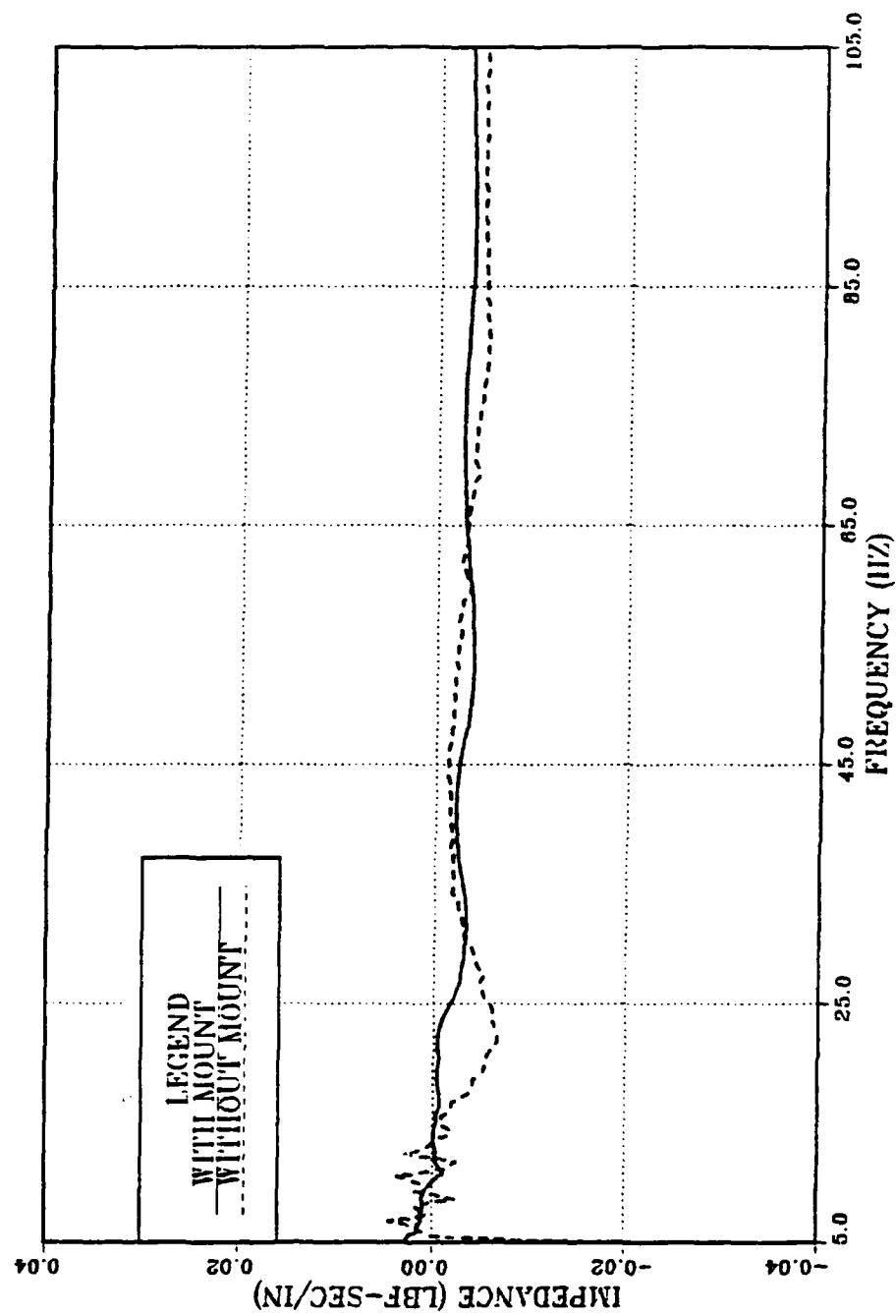
Figure 36. **Experimental Real Part of the Impedance of Shaker, With and Without Mount, in the Frequency Range of 5 to 105 Hz.**

72
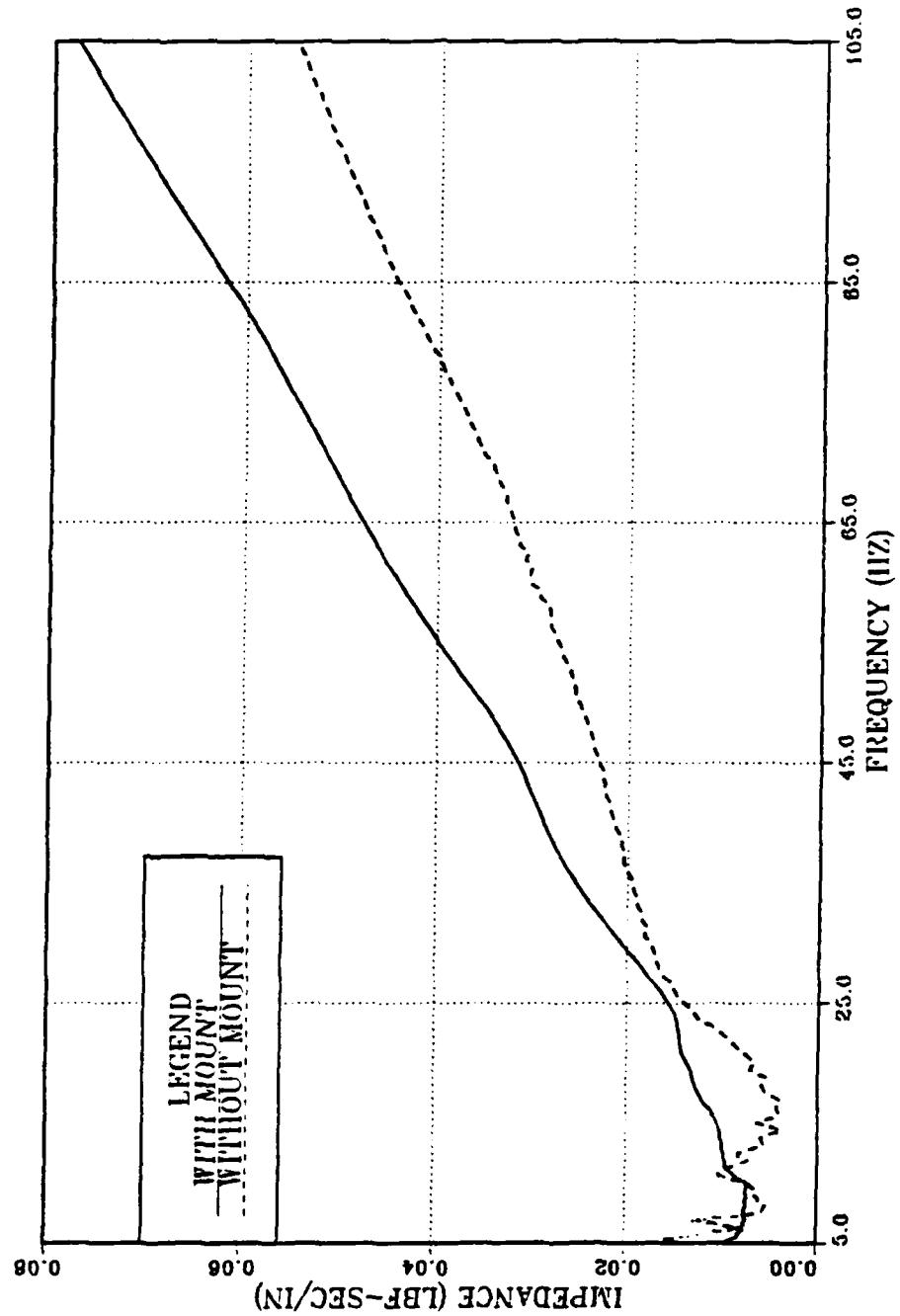
Figure 37. Experimental Imaginary Part of the Impedance of Shaker, With and Without Mount, in the Frequency Range of 5 to 105 Hz.
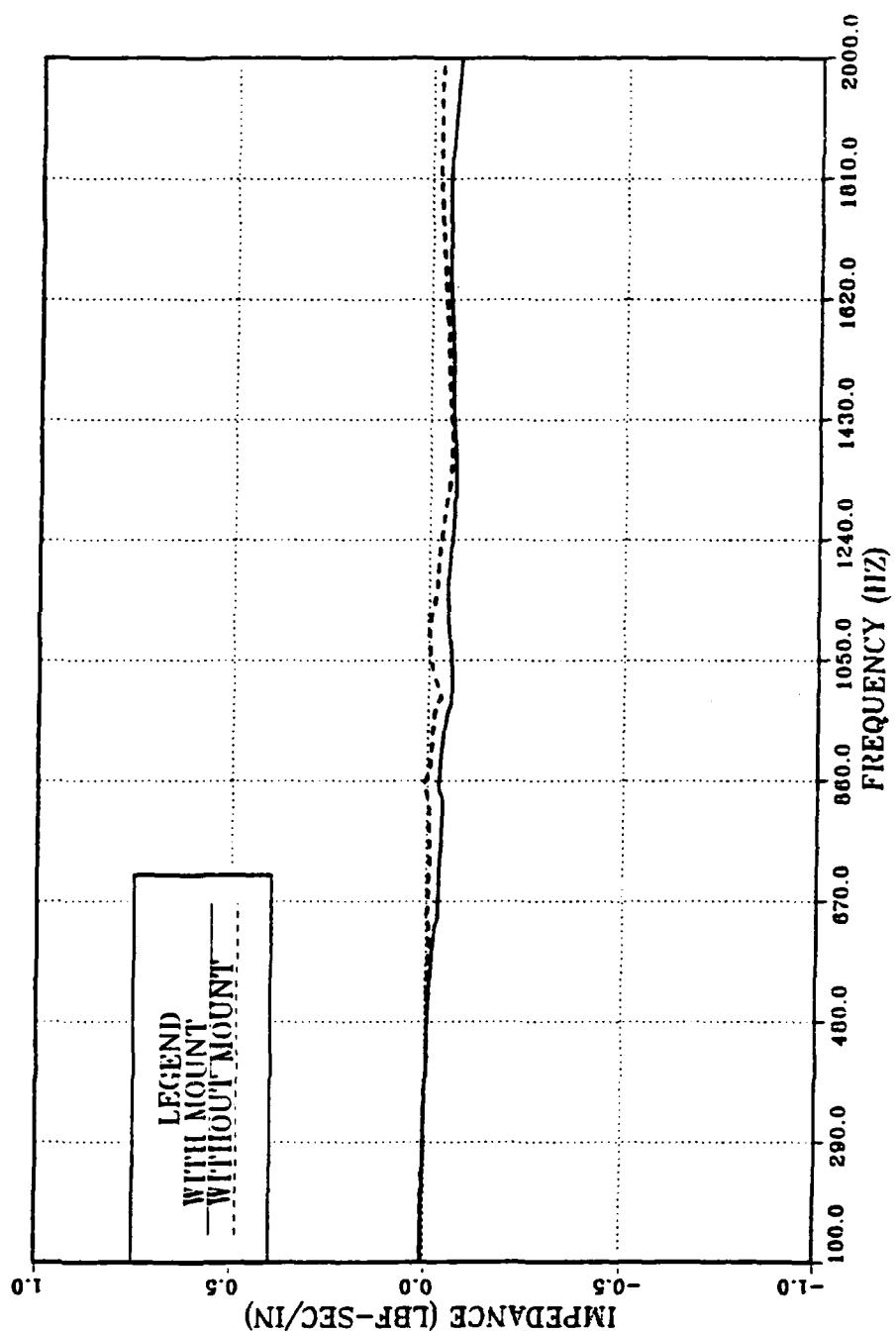
Figure 38. Experimental Real Part of the Impedance of Shaker, With and Without Mount, in the Frequency Range of 100 to 2000 Hz.

74
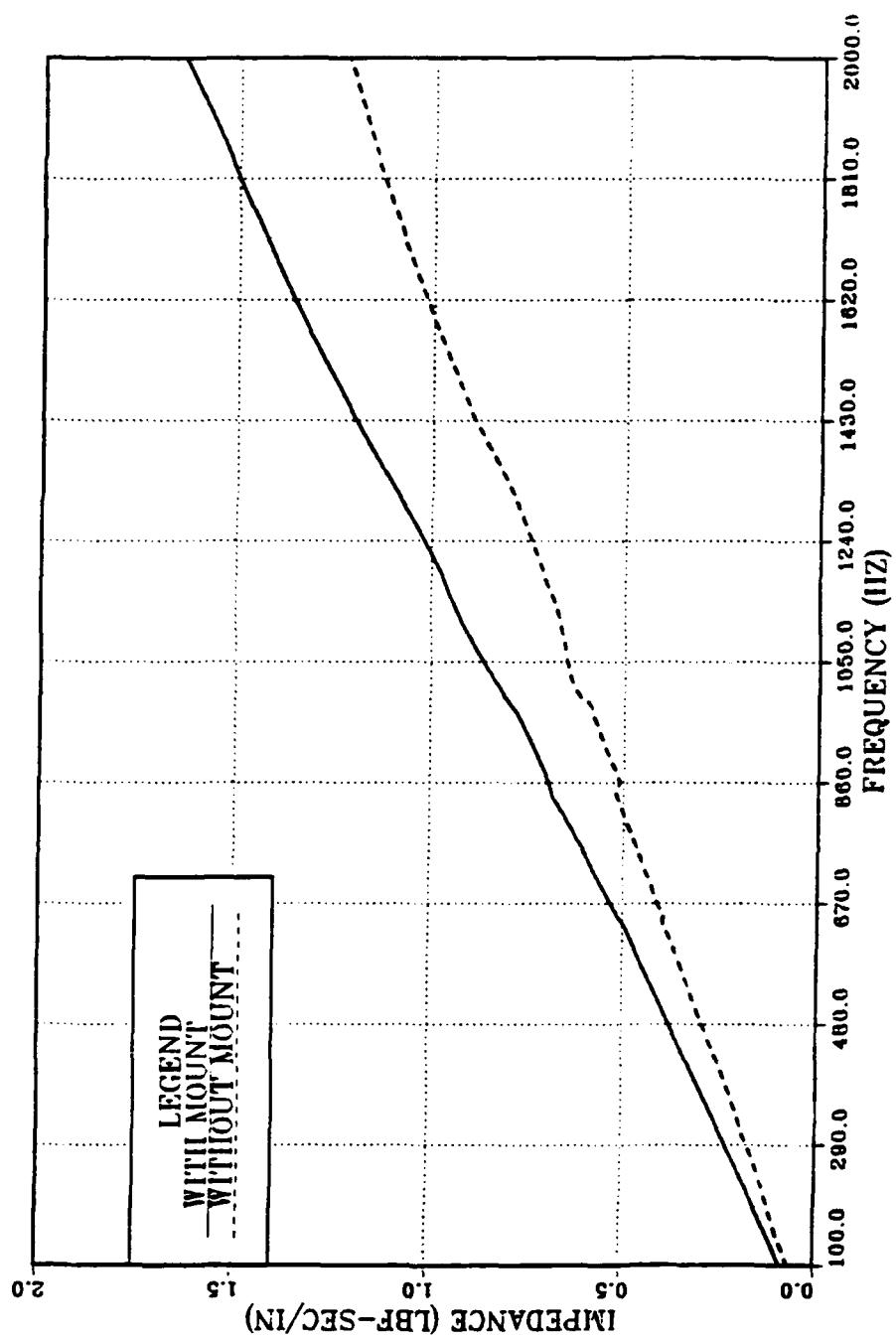
Figure 39. Experimental Imaginary Part of the Impedance of Shaker, With and Without Mount, in the Frequency Range of 100 to 2000 Hz.

In Figures 40 to 43 the difference between the measured and corrected plate impedance is shown. There is some small difference in the case of imaginary impedance and no difference for the real impedance, the shaker appears as a lumped mass. However the difference between the measured and corrected impedance is not considered to be significant to the conclusions of this study, and as such, the data will be in the uncorrected form for the rest of this study.
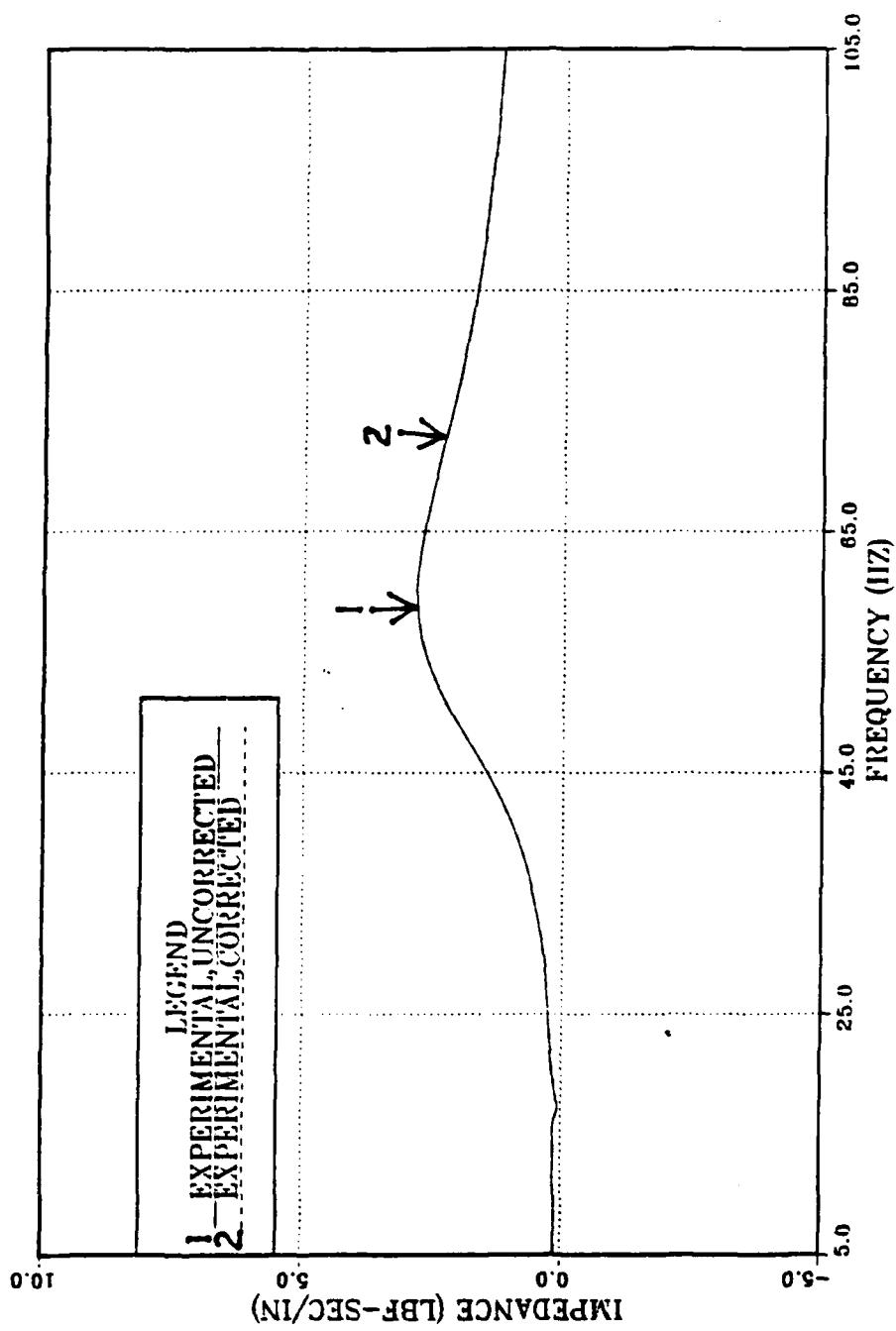
Figure 40. Experimental Real Part of the Driving Point Impedance of a 6 in Radius Viscoelastic Plate, With and Without Shaker and Mount Correction, in the Frequency Range of 5 to 105 Hz at a Temperature of 75.0 Deg. F.
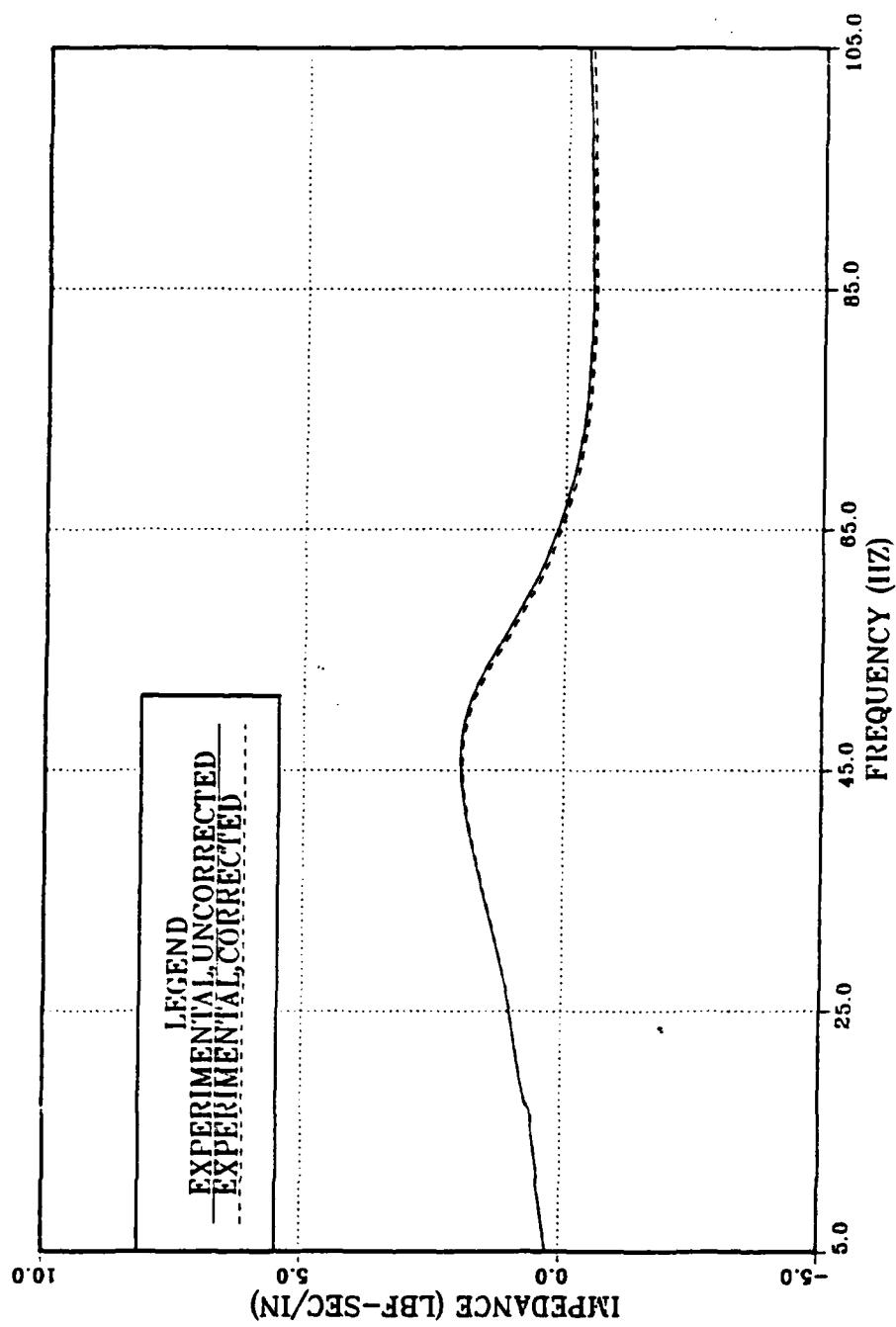
Figure 41. Experimental Imaginary Part of the Driving Point Impedance of a 6 in Radius Viscoelastic Plate, With and Without Shaker and Mount Correction, in the Frequency Range of 5 to 105 Hz at a Temperature of 75.0 Deg. F.
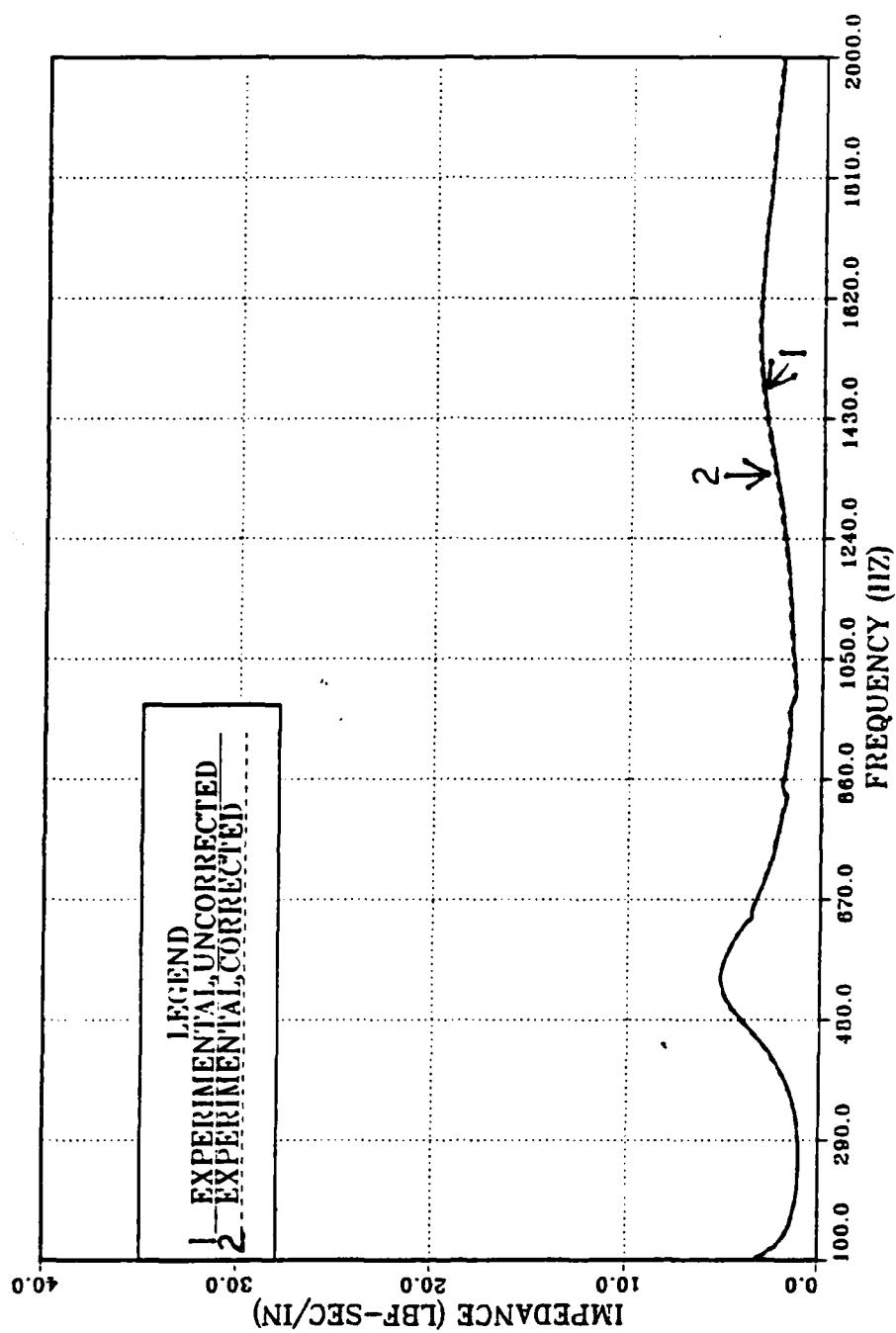
Figure 42. Experimental Real Part of the Driving Point Impedance of a 6 in Radius Viscoelastic Plate, With and Without Shaker and Mount Correction, in the Frequency Range of 100 to 2000 Hz at a Temperature of 74.5 Deg. F.

79
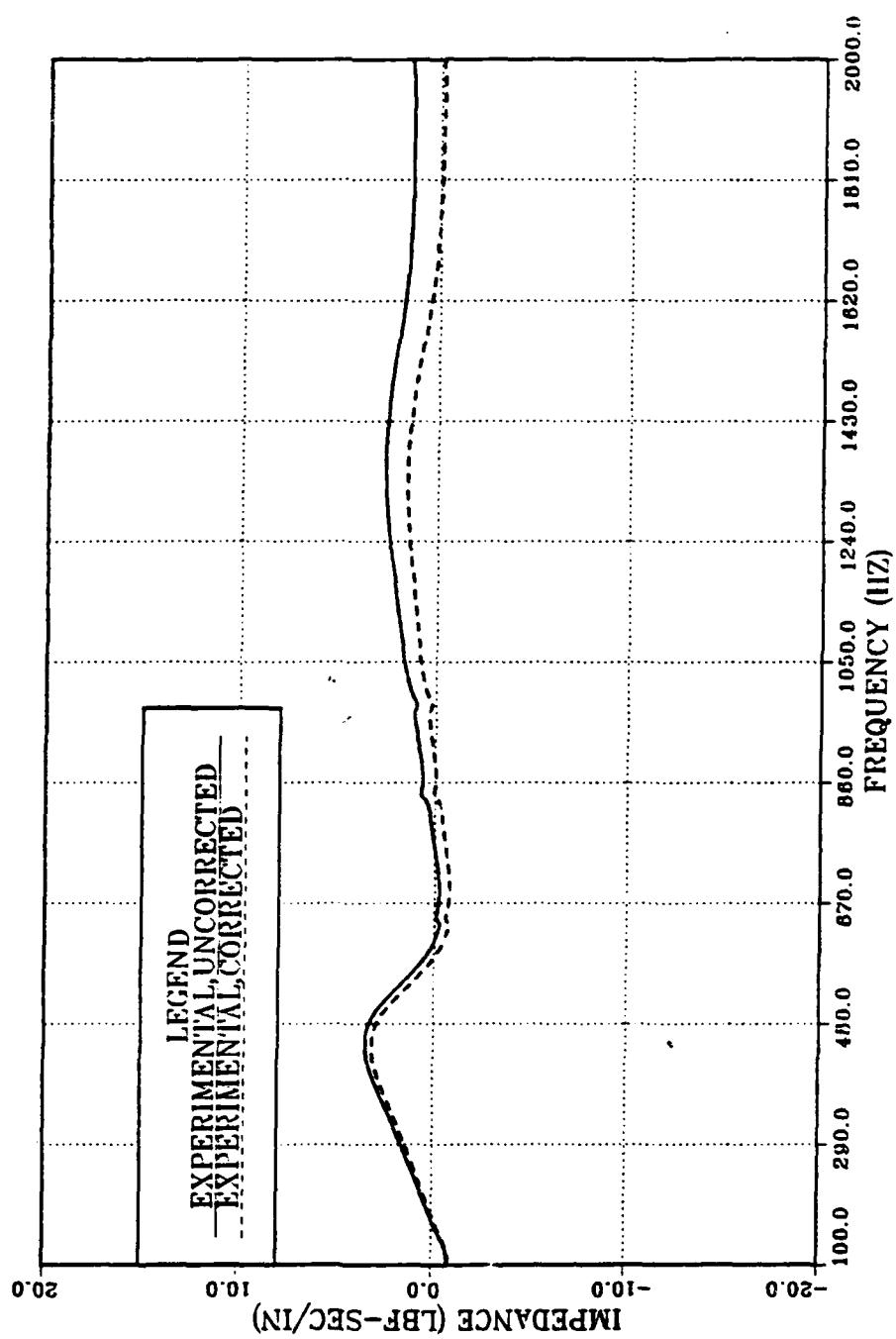
Figure 43. Experimental Imaginary Part of the Driving Point
Impedance of a 6 in Radius Viscoelastic Plate, With and
Without Shaker and Mount Correction, in the Frequency
Range of 100 to 2000 Hz at a Temperature of 74.5 Deg. F.

80

F. RESULTS OF DATA RUNS

For the elastic plates in the low frequency range of 5 to 105 Hz, shown in Figures 44 and 45, the plates appear to lumped mass as expected, with a small real part and a linearly increasing imaginary part with frequency. In the normal frequency range, 100 to 2000 Hz, the results, Figures 46 and 47, for the elastic plates hold little information, only showing the location of the first mode, as was the case in the theoretical portion. There was almost no difference in the driving point impedance for the six inch elastic plate when data was taken at room temperature and when taken at an elevated temperature, as shown in Figures 48 and 49. This confirms that Young's and shear moduli for the aluminum plate need not be temperature compensated.
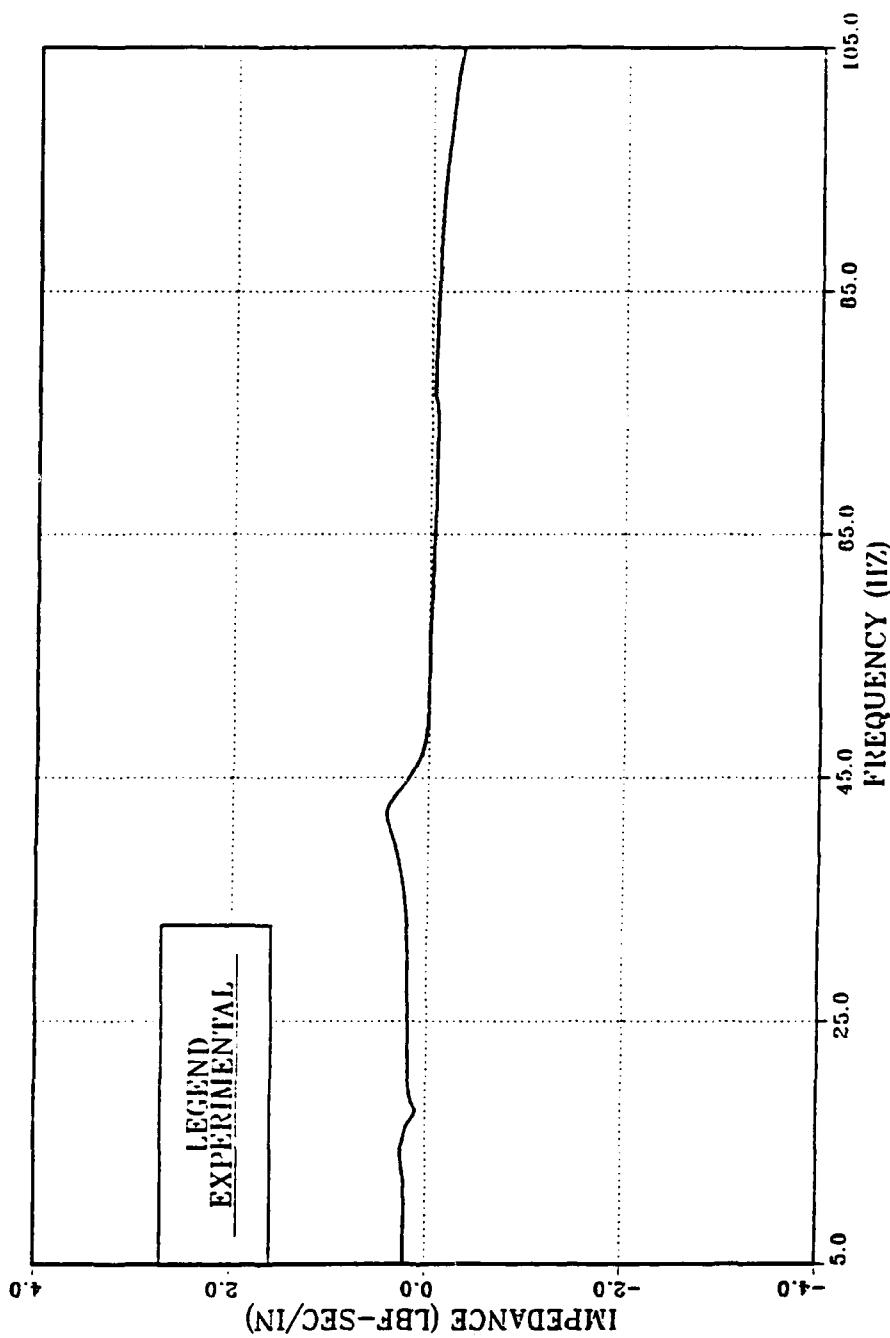
Figure 44. Experimental Real Part of the Driving Point Impedance of a 6 in Radius Elastic Plate in the Frequency Range of 5 to 105 Hz.

82
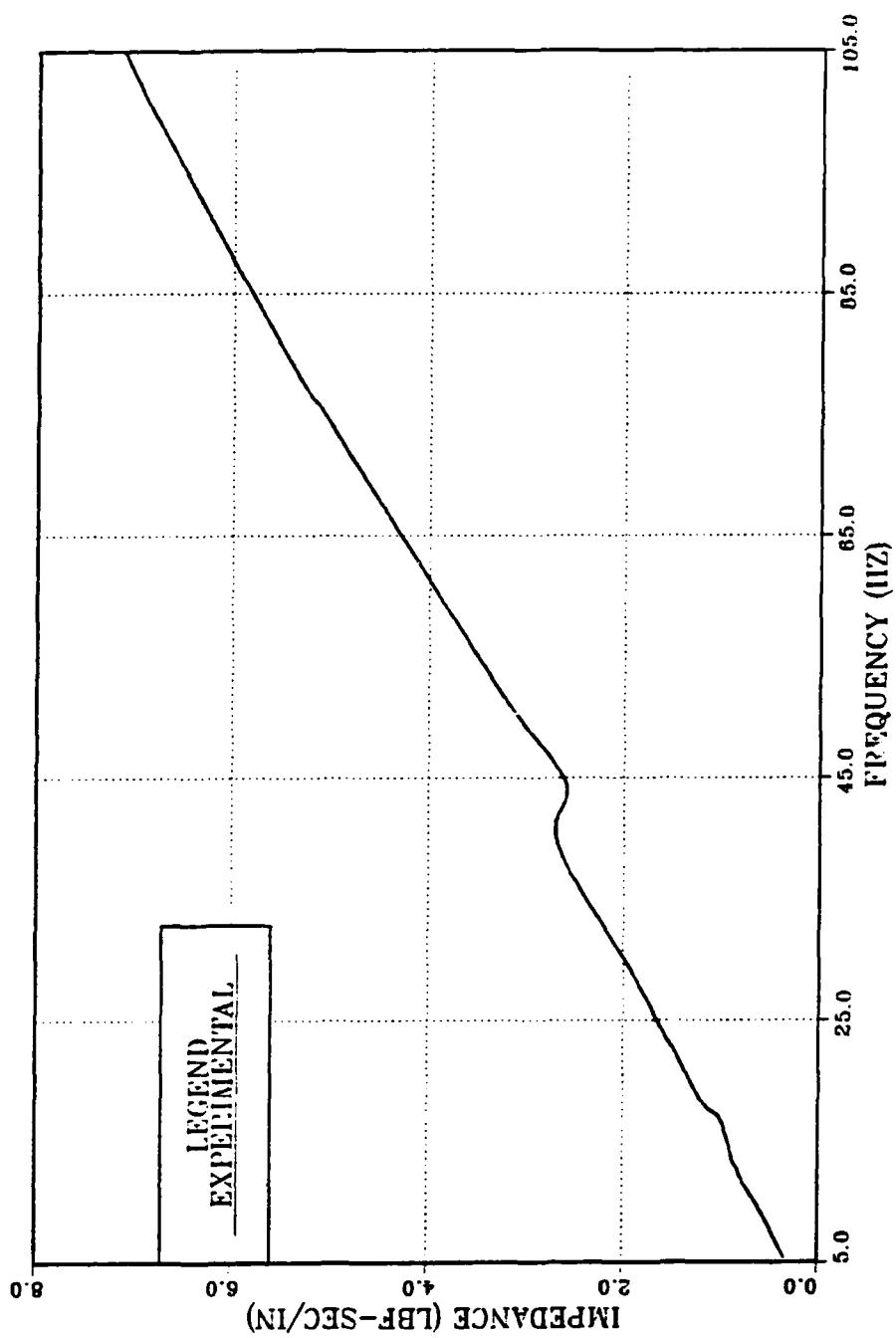
Figure 45. Experimental Imaginary Part of the Driving Point Impedance of a 6 in Radius Elastic Plate in the Frequency Range of 5 to 105 Hz.

83
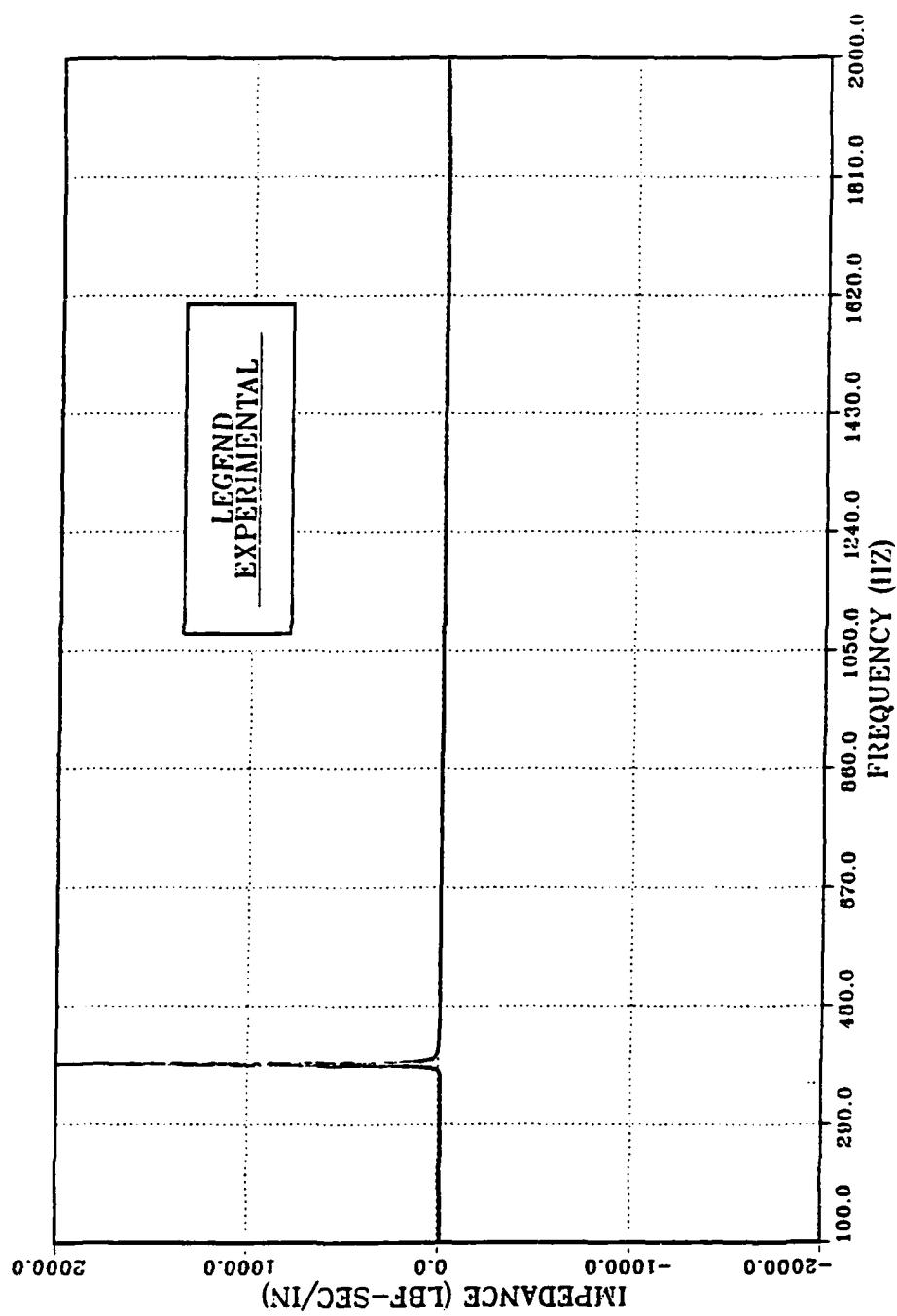
Figure 46. Experimental Real Part of the Driving Point Impedance of a 6 in Radius Elastic Plate in the Frequency Range of 100 to 2000 Hz.

84
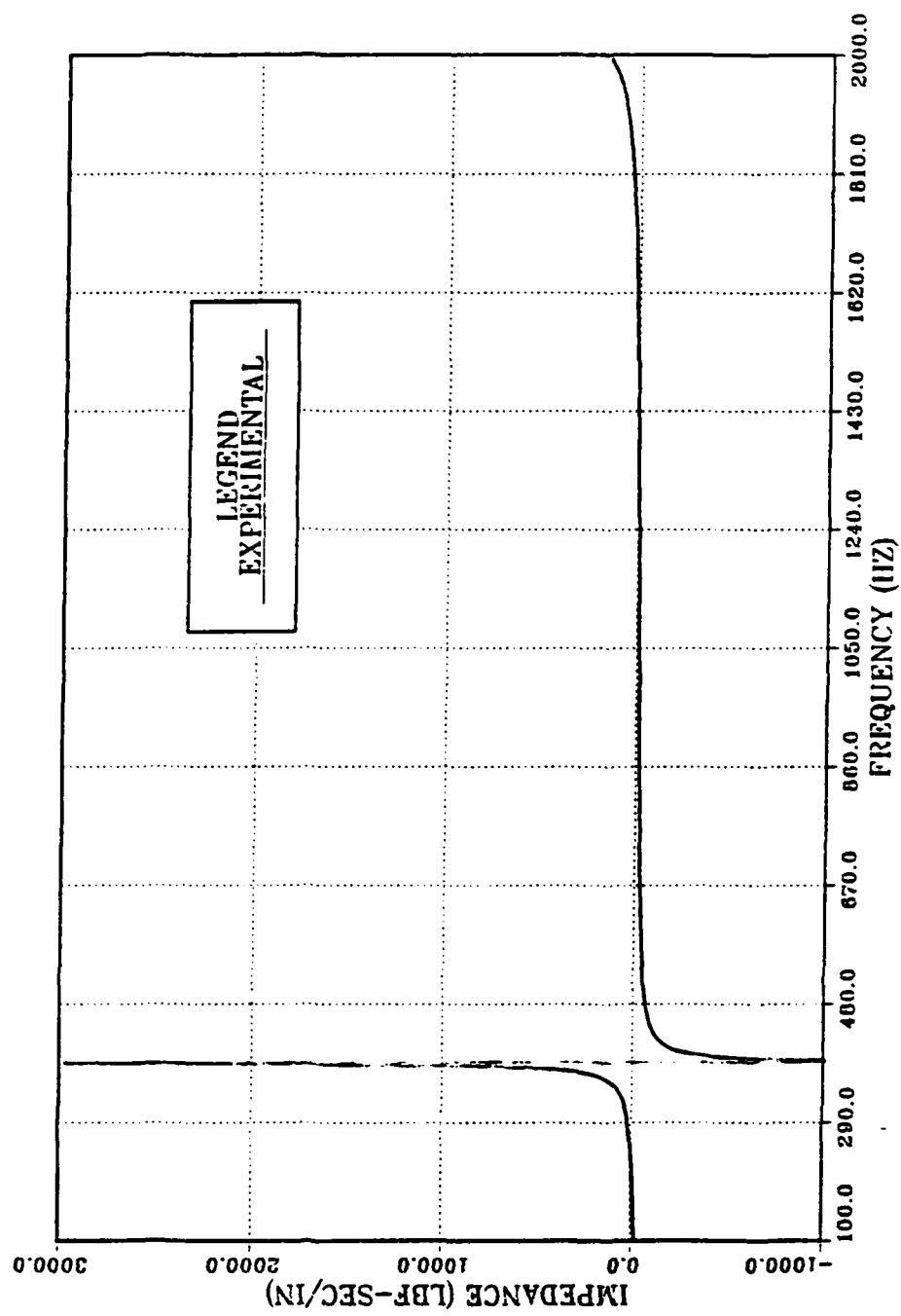
Figure 47. Experimental Imaginary Part of the Driving Point
Impedance of a 6 in Radius Elastic Plate in the Frequency
Range of 100 to 2000 Hz.

85
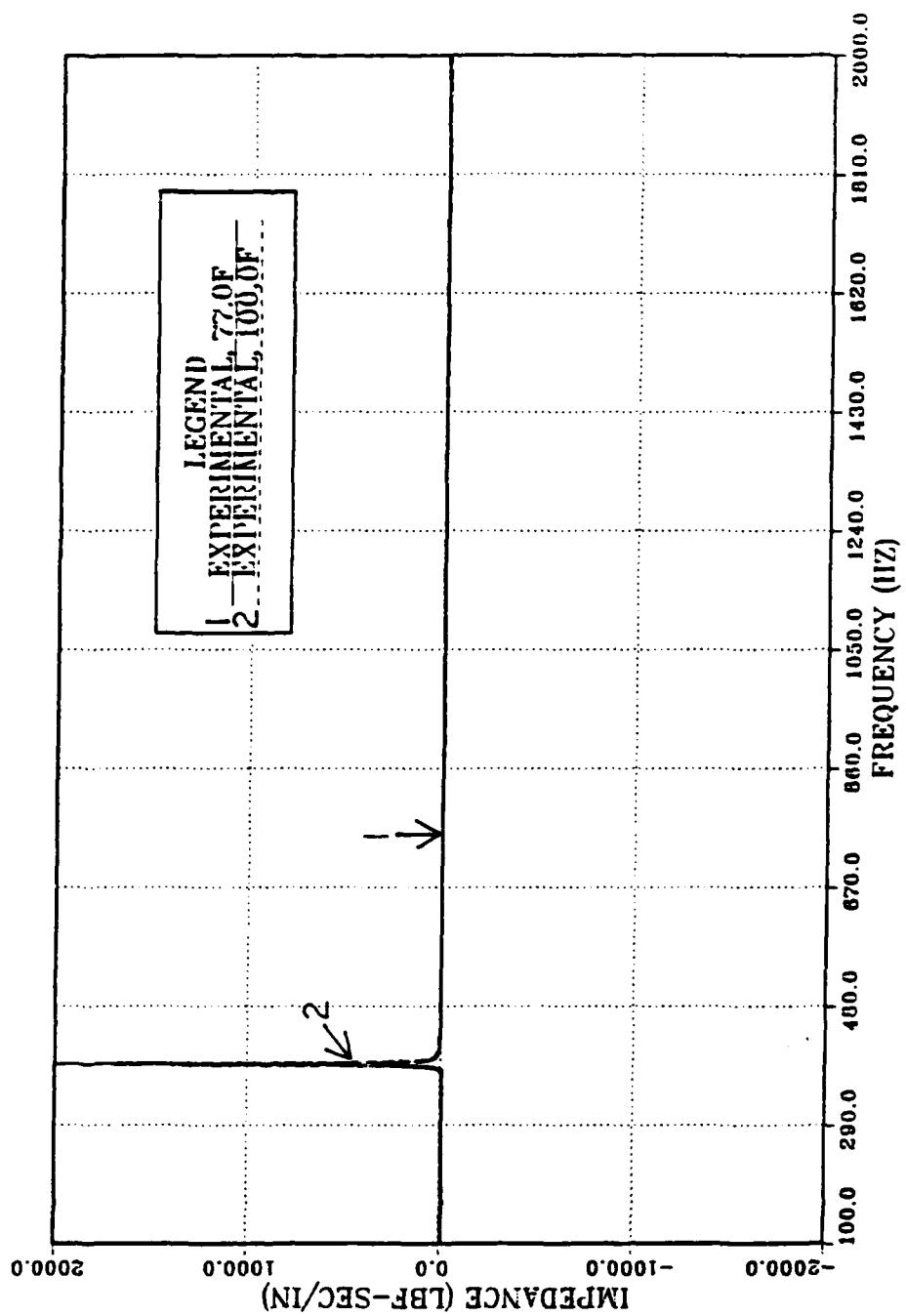
Figure 48. Effect of Temperature on the Experimental Real Part of
the Driving Point Impedance for a 6 in Radius Elastic
Plate in the Frequency Range of 100 to 2000 Hz.

86
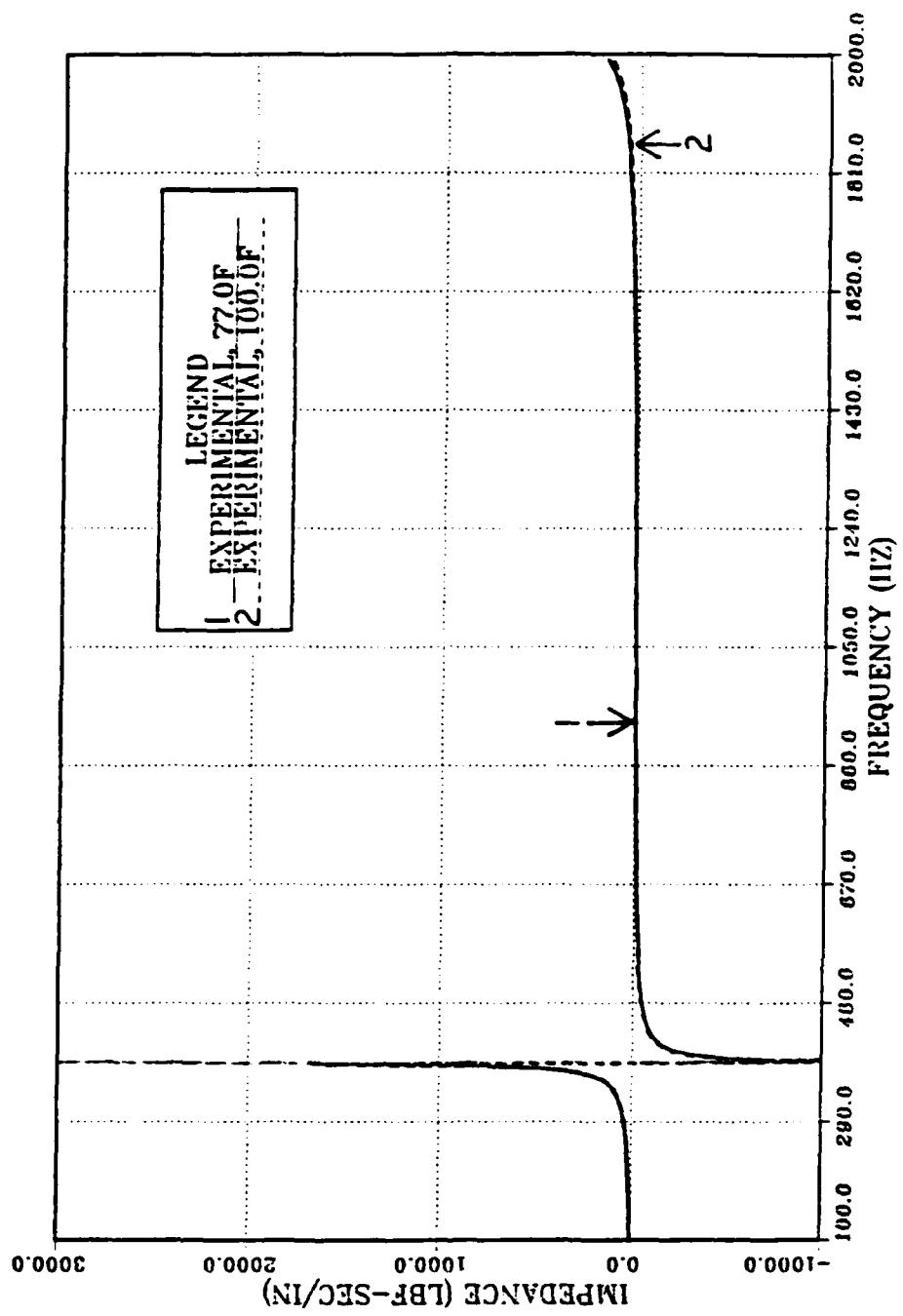
Figure 49. Effect of Temperature on the Experimental Imaginary Part of the Driving Point Impedance for a 6 in Radius Elastic Plate in the Frequency Range of 100 to 2000 Hz.

87

The driving point impedance for the viscoelastic plate in the low frequency range of 5 to 105 Hz is shown in Figures 50 and 51. The results for the normal frequency rage of 100 to 2000 Hz are shown in Figures 52 and 53. There is a major effect on the driving point impedance by the temperature of the plate, as was shown in the theoretical calculations. This is shown in Figures 54 and 55.

Although the accuracy of the data is effected by such things as the calibration of equipment and the actual plate geometry, it is dominated by the material characteristics used. The material characteristics are a design specification provided by the vendor and the material may have a significant statistical variation in the material properties. The plate temperature also effects the material conditions for a fixed plate geometry and a different temperature measurement technique may provide a slight increase in the accuracy.
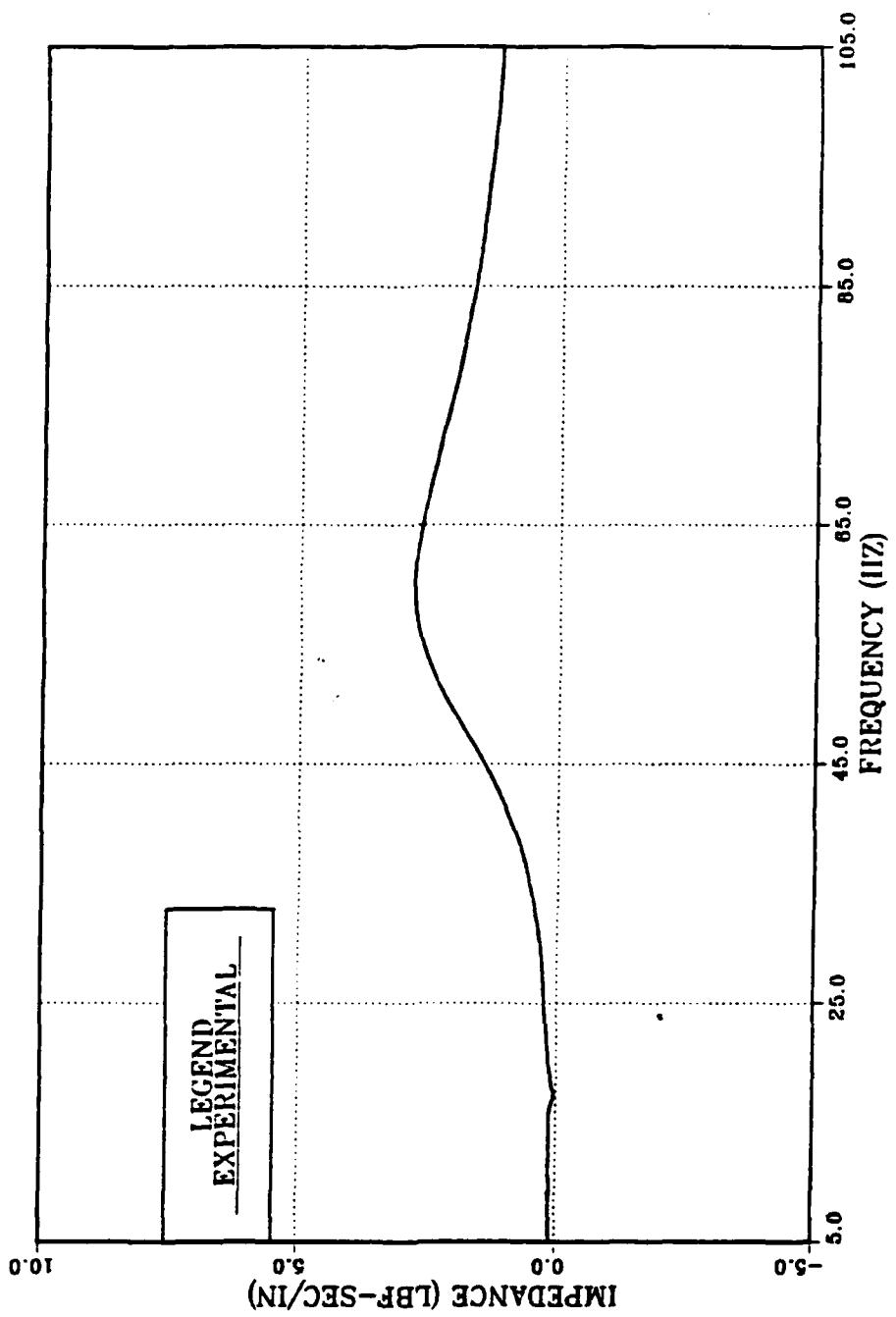
Figure 50. Experimental Real Part of the Driving Point Impedance for a 6 in Radius Viscoelastic Plate in the Frequency Range of 10 to 105 Hz at a Temperature of 75.0 Deg. F.
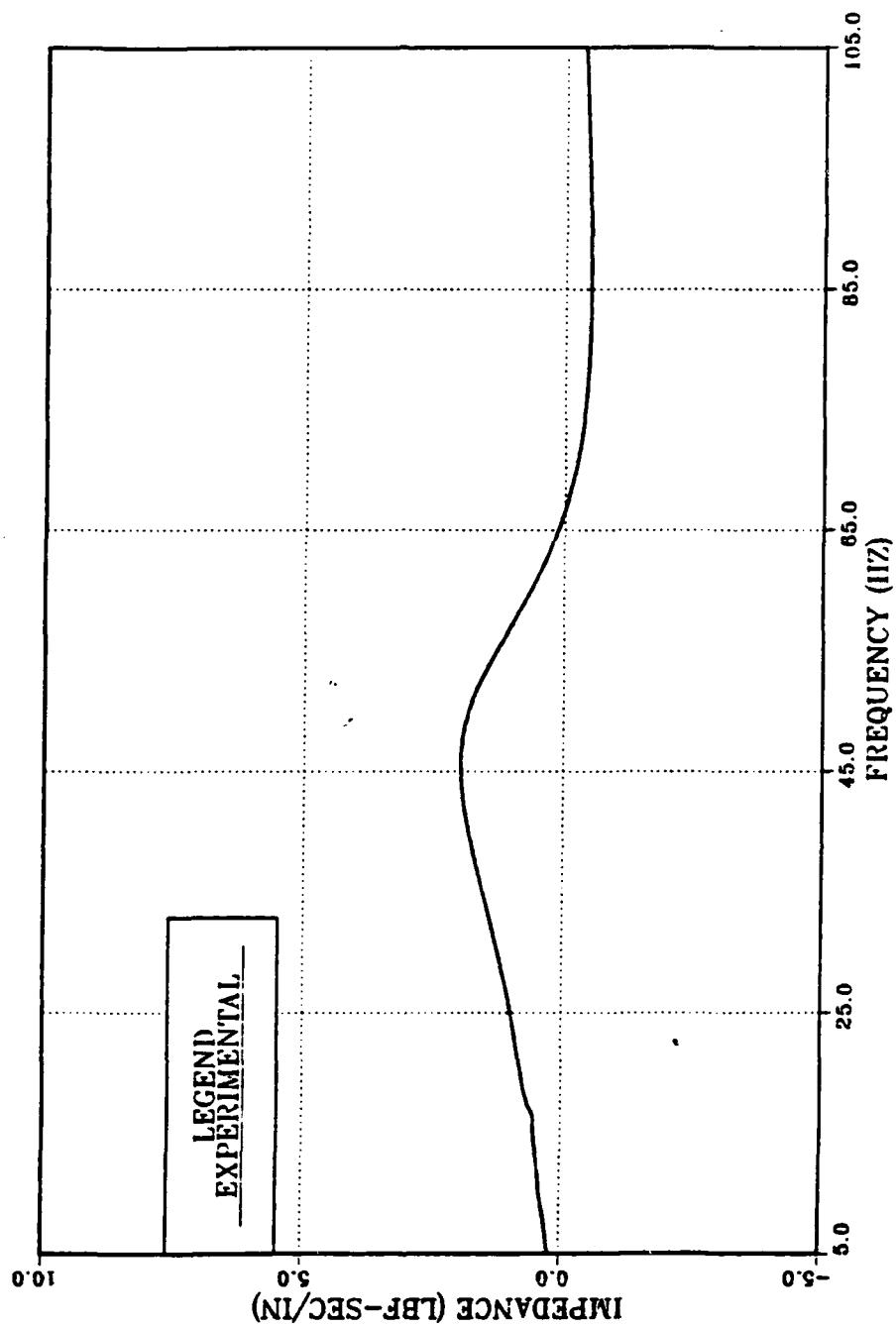
Figure 51. Experimental Imaginary Part of the Driving Point
Impedance for a 6 in Radius Viscoelastic Plate in the
Frequency Range of 10 to 105 Hz at a Temperature of 75.0
Deg. F.

90
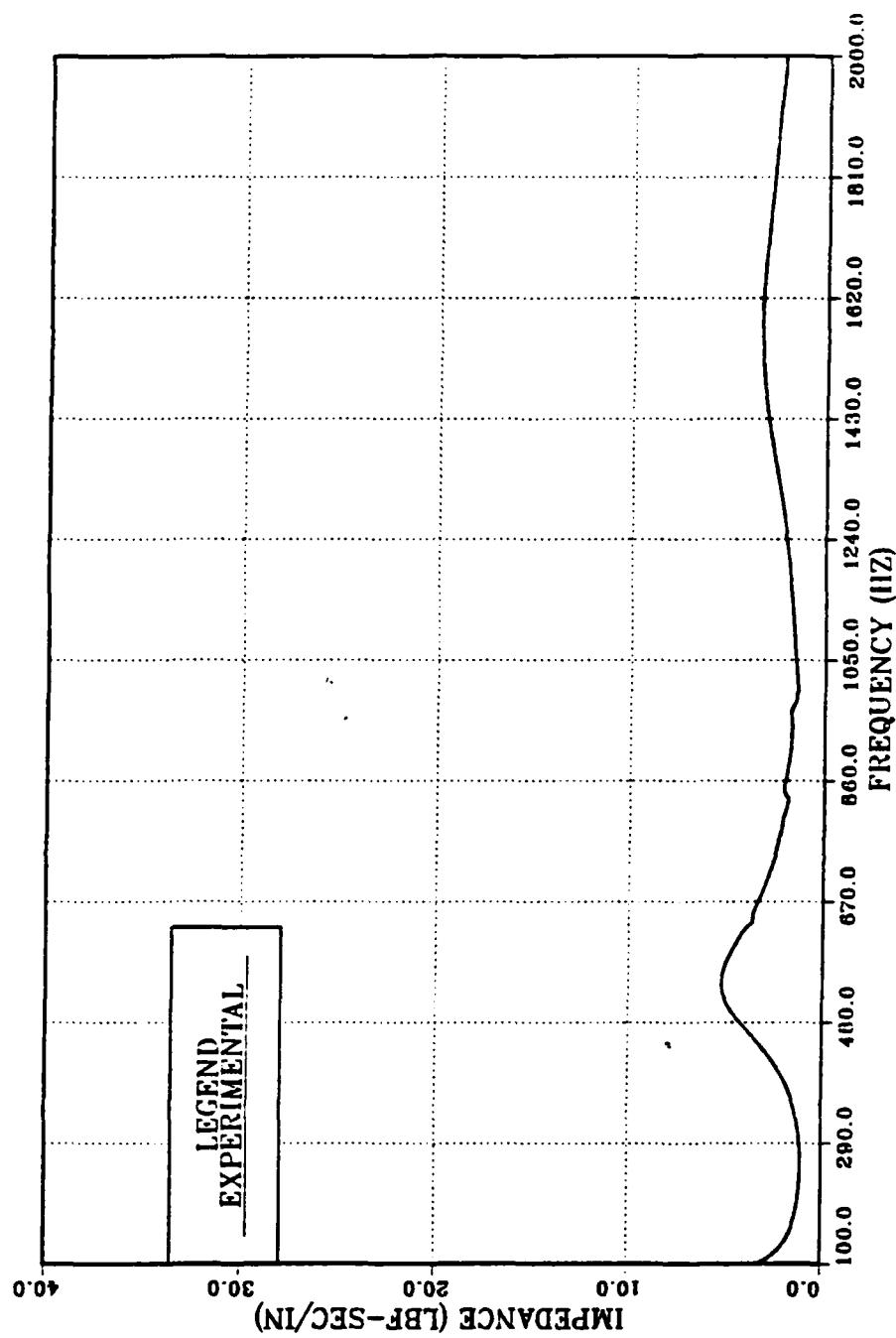
Figure 52. Experimental Real Part of the Driving Point Impedance
for a 6 in Radius Viscoelastic Plate in the Frequency
Range of 100 to 2000 Hz at a Temperature of 74.5 Deg. F.
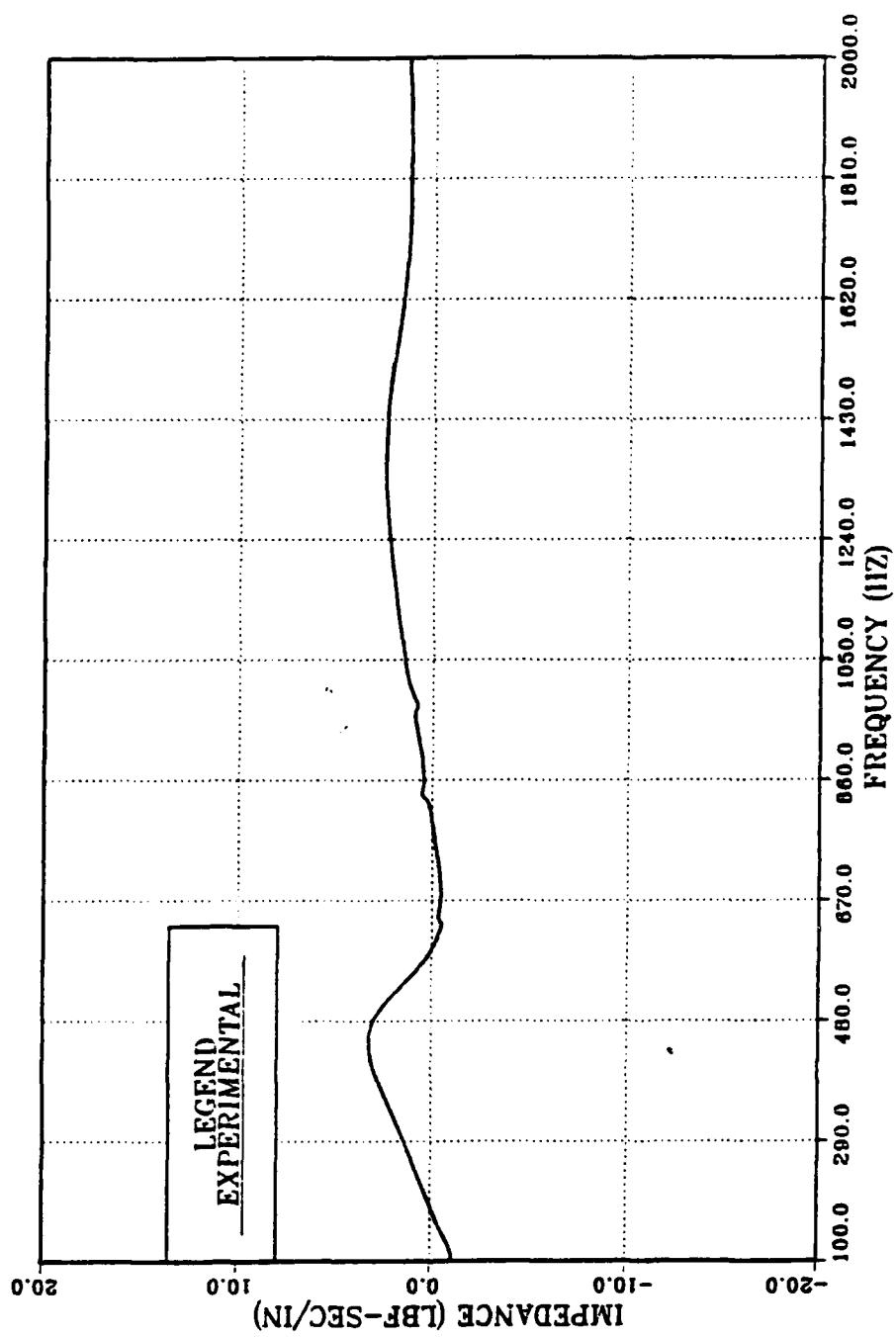
Figure 53. Experimental Imaginary Part of the Driving Point
Impedance for a 6 in Radius Viscoelastic Plate in the
Frequency Range of 100 to 2000 Hz at a Temperature of
74.5 Deg. F.

92
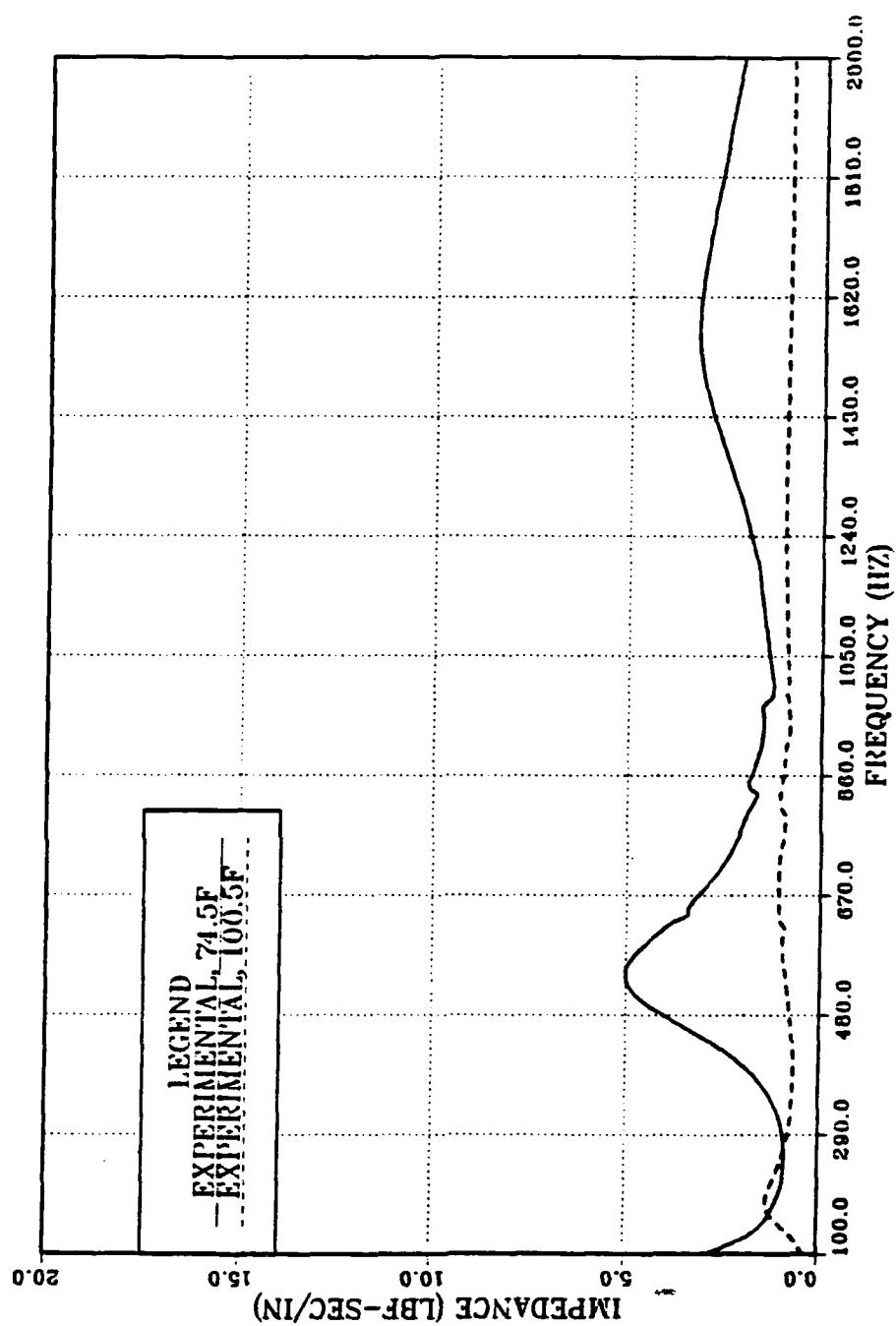
Figure 54. Effect of Temperature on the Experimental Real Part of the Driving Point Impedance for a 6 in Radius Viscoelastic Plate in the Frequency Range of 100 to 2000 Hz.

93
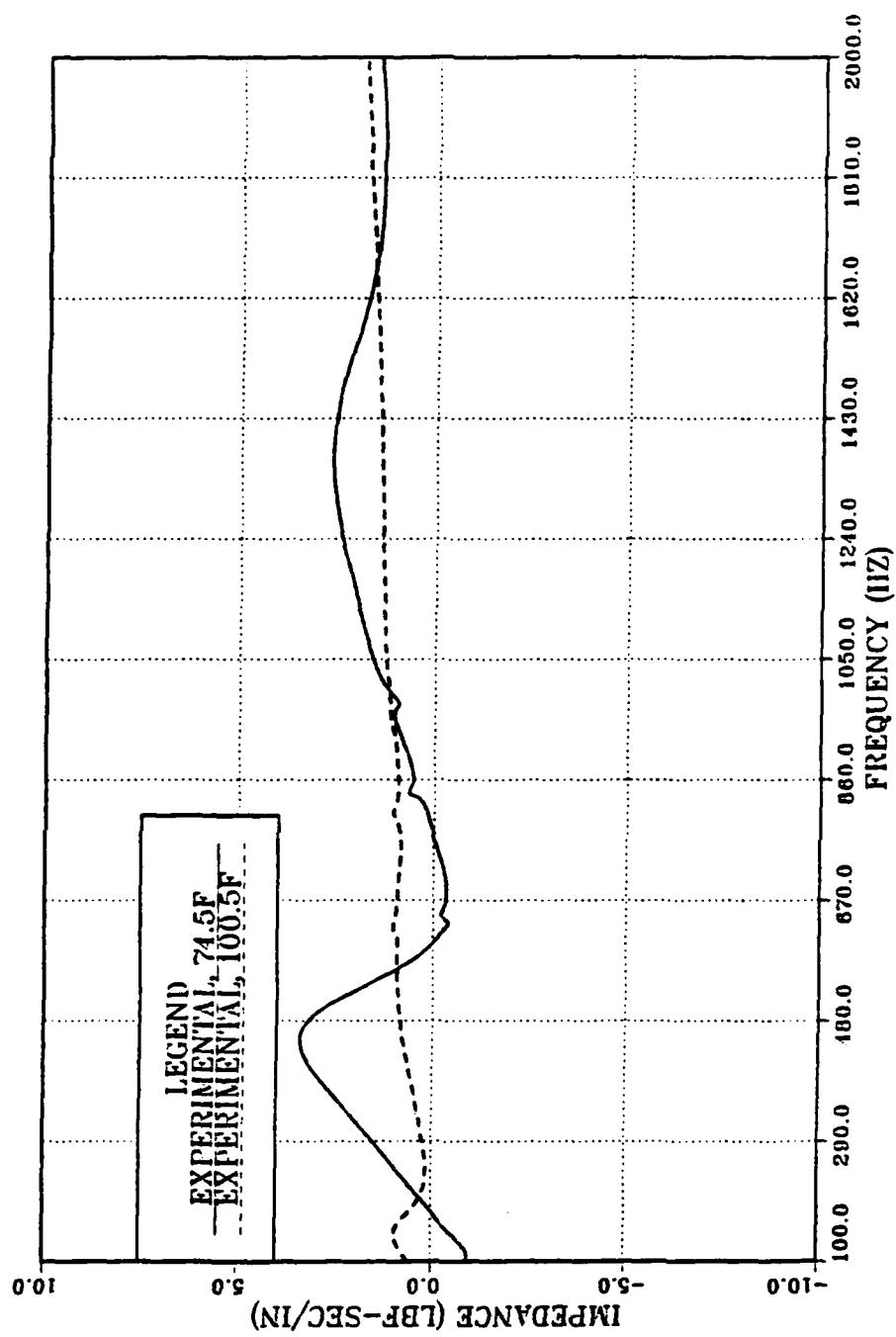
Figure 55. Effect of Temperature on the Experimental Imaginary Part of the Driving Point Impedance for a 6 in Radius Viscoelastic Plate in the Frequency Range of 100 to 2000 Hz.

94

IV. COMPARISON

A.   ELASTIC PLATES

For the elastic plates in the frequency range of 10 to 105 Hz the agreement between the theoretical results and the experimental results is very good as shown by Figures 56 and 57. In the frequency range of 100 to 2000 Hz the only thing that can be compared is the location, in frequency, of the impedance peak, as shown in Figures 58 and 59. For the three elastic plates studied the experimental peak occurred at a lower frequency, by about 100 Hz, than the theoretical peak. In the high frequency range, the theoretical calculations entirely missed the spike in the real portion of the driving point impedance, due to the frequency resolution used in the calculations.

It is concluded that the ideas and programs used in this study have been validated to be correct by these results.
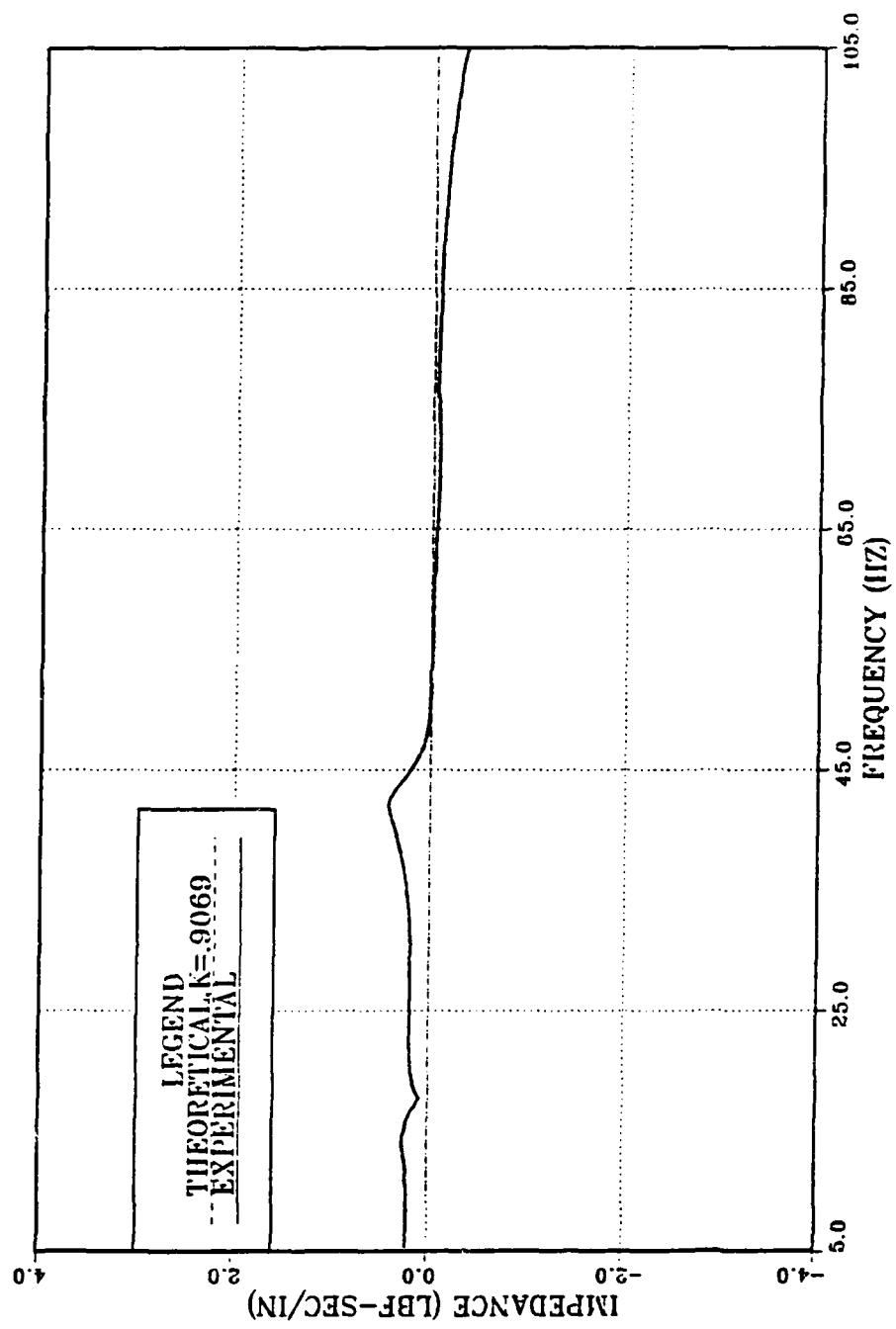
Figure 56. Theoretical and Experimental Comparison of the Real Part
of the Driving Point Impedance for a 6 in Radius Elastic
Plate in the Frequency Range of 5 to 105 Hz.

96
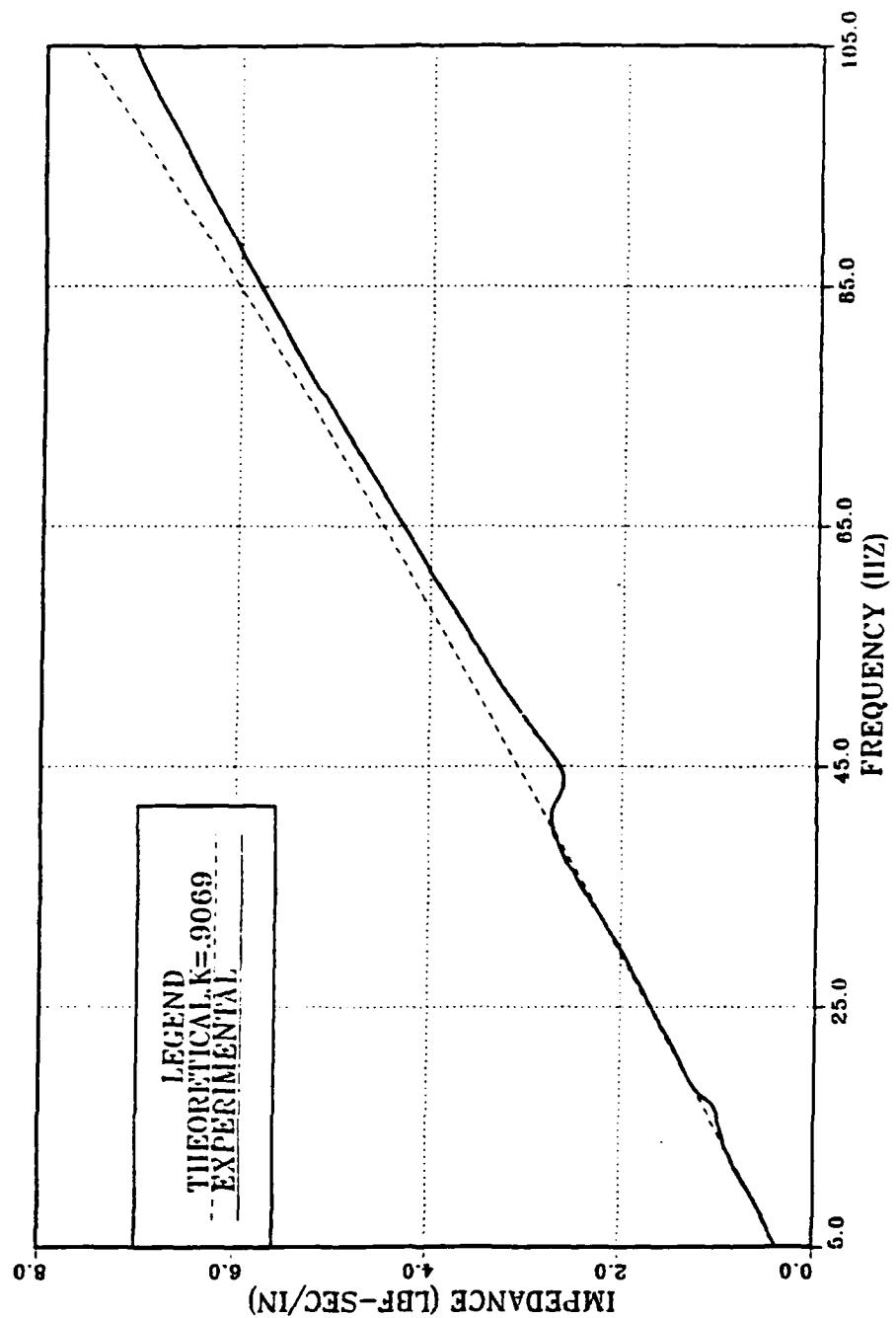
Figure 57. Theoretical and Experimental Comparison of the Imaginary Part of the Driving Point Impedance for a 6 in Radius Elastic Plate in the Frequency Range of 5 to 105 Hz.
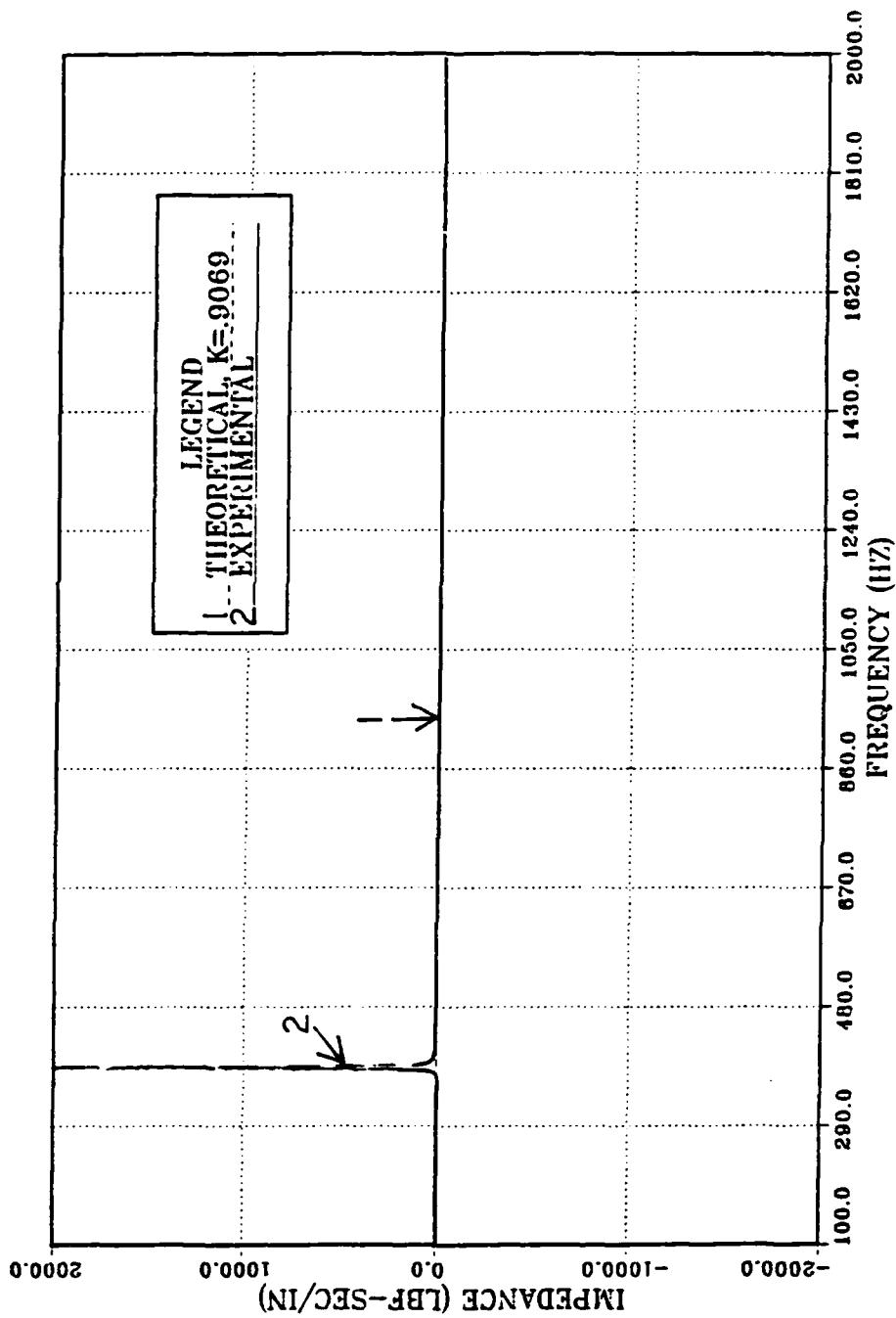
Figure 58. Theoretical and Experimental Comparison of the Real Part of the Driving Point Impedance for a 6 in Radius Elastic Plate in the Frequency Range of 100 to 2000 Hz.

98
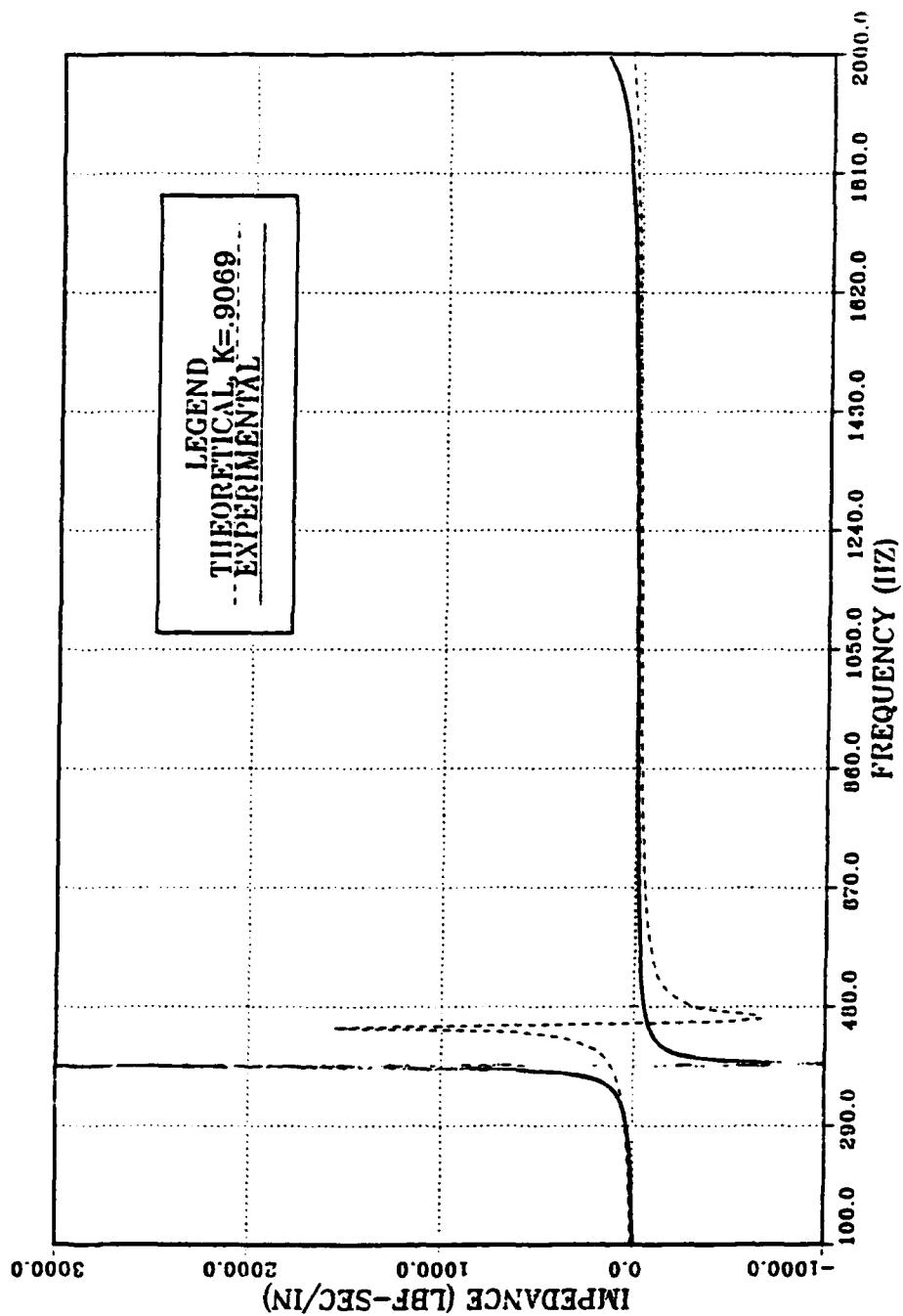
Figure 59. Theoretical and Experimental Comparison of the Imaginary Part of the Driving Point Impedance for a 6 in Radius Elastic Plate in the Frequency Range of 100 to 2000 Hz.

99

B.   VISCOELASTIC PLATES

In all cases there was almost no agreement between the experimental results and the theoretical results when the material characteristics of Nashif, Jones, and Henderson [Ref. 1, pp. 390-392] were used. But, as shown by Figures 60 to 63, there is agreement between the experimental results and the theoretical results when the material characteristics of United McGill [Ref. 24] are used.

The remaining discussion deals with theoretical results with material characteristics supplied by United McGill [Ref.24]. In the low frequency range the experimental results would break or change at a lower frequency than the theoretical results would. This effect is similar to the experimental first mode for the elastic plates being lower than the theoretical. In the high frequency range the experimental real part of the driving point impedance was always lower than the theoretical, while the experimental imaginary part of the driving point impedance was always higher than the theoretical. It is as if the theoretical calculations are a few degrees in phase off from the experimental results. Figures 64 and 65 show the importance of including the temperature in the determination of the material characteristics. The theoretical and experimental results have the same shape but are shifted by a small amount. It is felt that this shift is due to the uncertainty in the material characteristics used in the theoretical calculations.
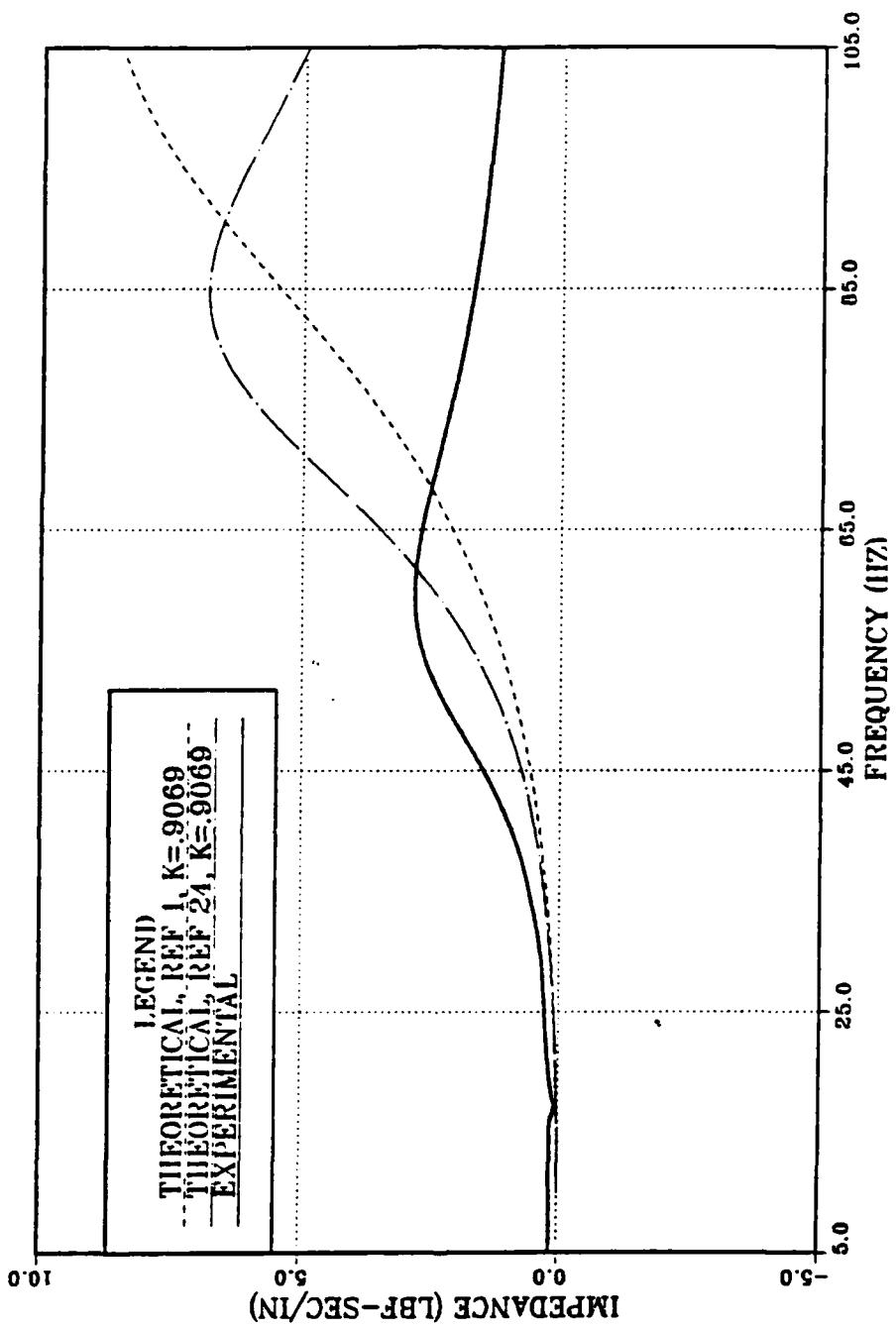
Figure 60. Theoretical and Experimental Comparison of the Real Part
of the Driving Point Impedance for a 6 in Radius
Viscoelastic Plate in the Frequency Range of 5 to 105 Hz at
a Temperature of 75.0 Deg. F.
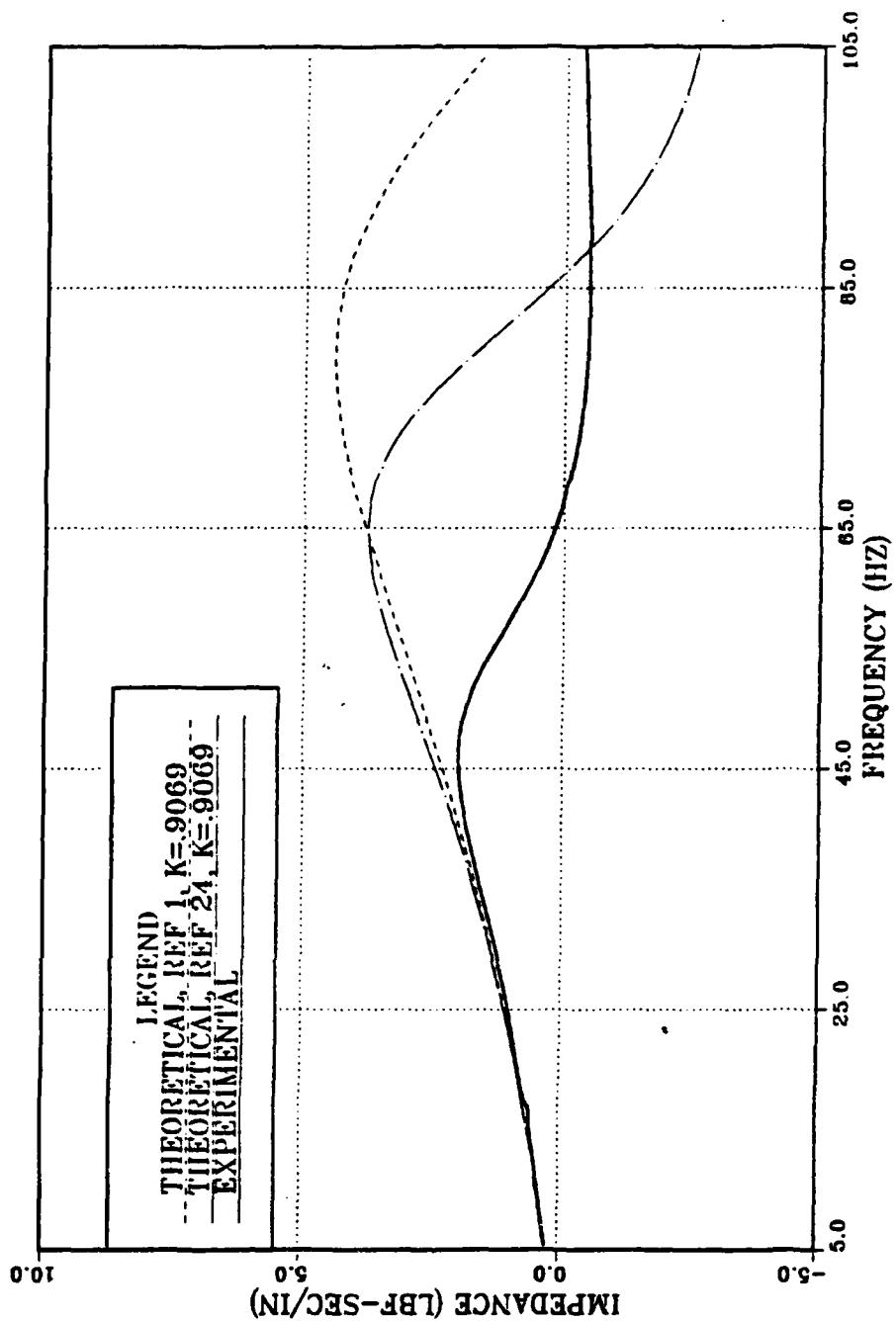
Figure 61. Theoretical and Experimental Comparison of the Imaginary Part of the Driving Point Impedance for a 6 in Radius Viscoelastic Plate in the Frequency Range of 5 to 105 Hz at a Temperature of 75.0 Deg. F.

102
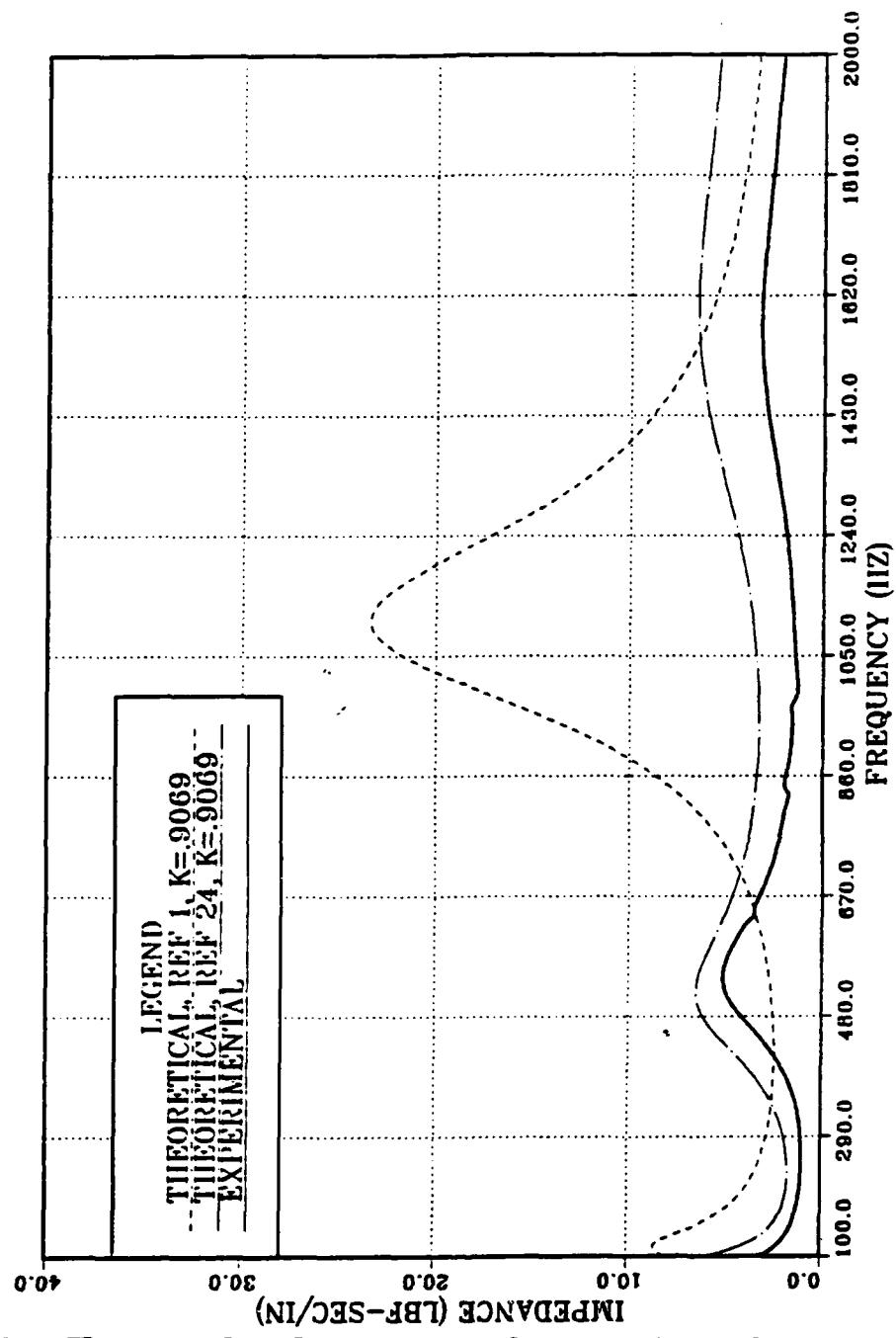
Figure 62. Theoretical and Experimental Comparison of the Real Part of the Driving Point Impedance for a 6 in Radius Viscoelastic Plate in the Frequency Range of 100 to 2000 Hz at a Temperature of 74.5 Deg. F.

103
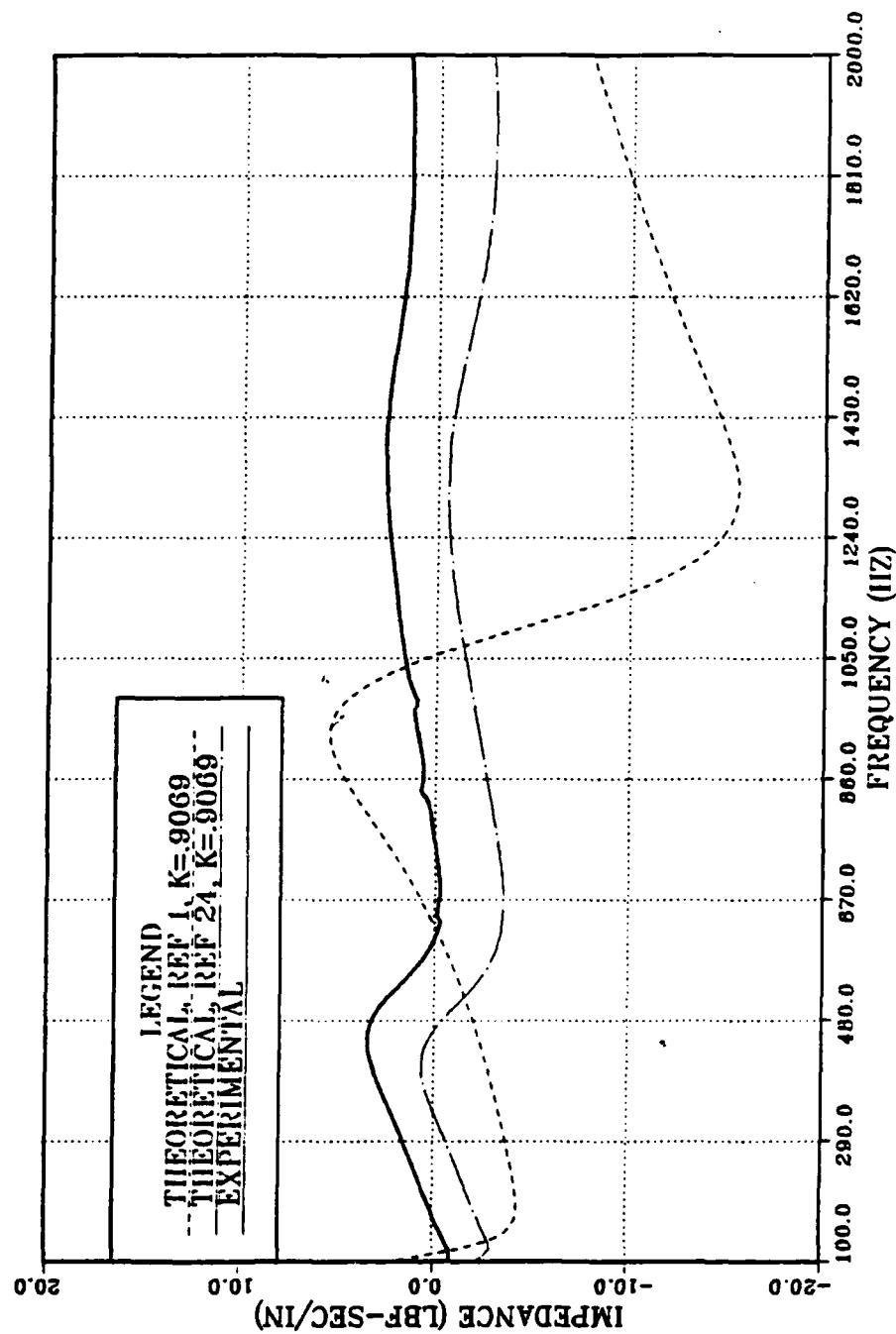
Figure 63. Theoretical and Experimental Comparison of the Imaginary Part of the Driving Point Impedance for a 6 in Radius Viscoelastic Plate in the Frequency Range of 100 to 2000 Hz at a Temperature of 74.5 Deg. F.

104
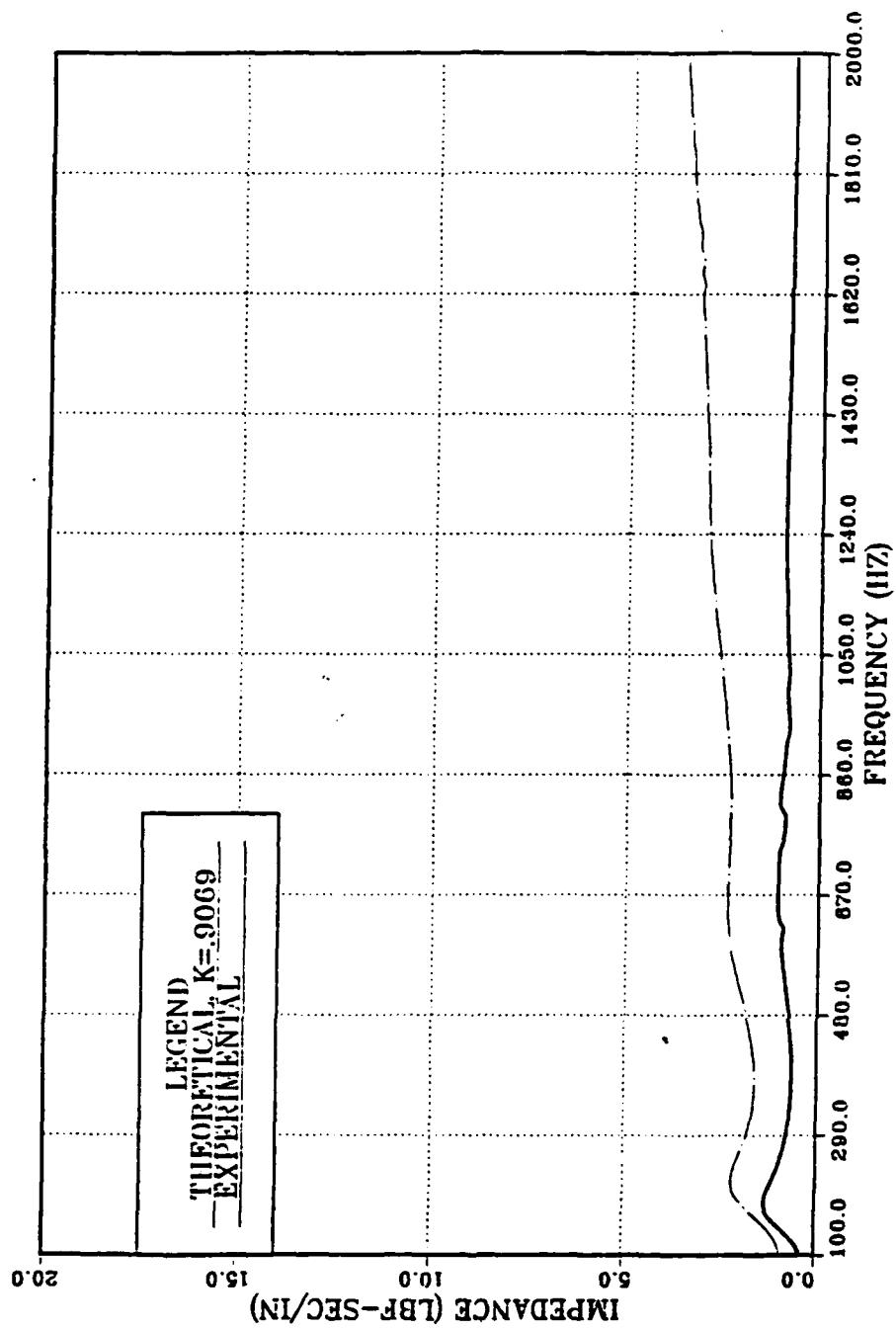
**Figure 64. Theoretical and Experimental Comparison of the Real Part
of the Driving Point Impedance for a 6 in Radius
Viscoelastic Plate in the Frequency Range of 100 to 2000 Hz
at a Temperature of 100.5 Deg. F.**

105
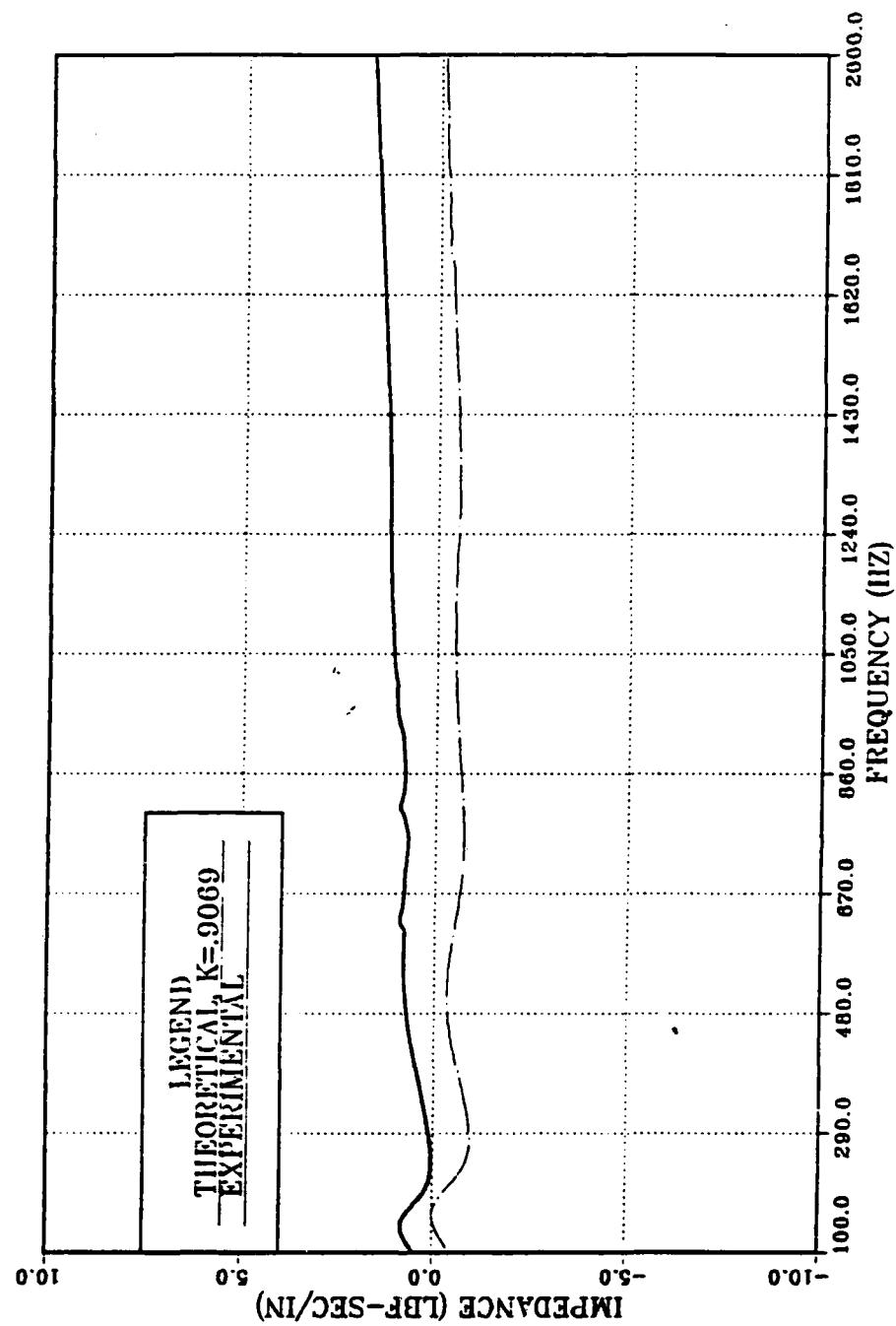
Figure 65. Theoretical and Experimental Comparison of the Imaginary Part of the Driving Point Impedance for a 6 in Radius Viscoelastic Plate in the Frequency Range of 100 to 2000 Hz at a Temperature of 100.5 Deg. F.

106

C. CONCLUSIONS

1.   The driving point impedance of a circular viscoelastic plate can be predicted by the programs developed by this study by knowing the plate's geometry and the material characteristics. The shape of the theoretical and experimental results is the same, but are shifted a small amount due to the material conditions used.

2.   The effect of differing shear coefficients on the driving point impedance is immaterial and can be ignored.

3.   The driving point impedance of a viscoelastic plate is controlled by the plate geometry and material conditions. The material conditions are greatly effected by the temperature of the plate.

4.   For viscoelastic plates, the magnitude of the real and imaginary part of the driving point impedance at a mode are about the same.

V. RECOMMENDATIONS

Based upon the results of this study the following recommendations are made for studies continuing in this area.

1. Investigate the effect of twisting of the waveguide absorber mount on the driving point impedance.

2. In the past study by Lee [Ref. 5] a constrained layer beam waveguide absorber was used with some success. A constrained layer circular plate can be used as a waveguide absorber and its characteristics need to be studied.

3. The effectiveness of the present viscoelastic circular waveguide absorbers on vibration control need to be studied and compared to a surface damping treatment and a point mass, all of the same weight. Investigate whether the circular plate waveguide absorbers can provide more energy dissipation per unit mass or volume of damping device than other forms of vibration control?

4. This study has shown that plate geometry and plate temperature effect the driving point impedance. A sensitivity study should be undertaken to further investigate this dependance of the driving point impedance to changes in plate geometry and plate temperature.

5. Investigate the ability to design a circular waveguide absorber to remove a set amount of energy, at a point on the structure, at a certain frequency band. The design should be based upon the driving point impedance of the waveguide absorber and driving point impedance of the structure at the attachment point.

6. Investigate the ability to design and use multiple waveguide absorbers to dampen over a wide frequency range or temperature range.

APPENDIX A.

A.   REDUCE PROGRAM TO SOLVE A FOUR BY FOUR MATRIX.

```
%    THIS PROGRAM IS DESIGNED TO SOLVE A 4 BY 4 MATRIX;
%    MATRIX METHOD;
%      PROGRAM TCA4A;
OFF NAT$
OUT TT1H$
LINELENGTH (72);
D1:=DET MAT((B11,B22,B33,B44),(C21,C22,C23,C24),
            (C31,C32,C33,C34),(C41,C42,C43,C44);
D2:=DET MAT((C11,C12,C13,C14),(B11,B22,B33,B44),
            (C31,C32,C33,C34),(C41,C42,C43,C44);
D3:=DET MAT((C11,C12,C13,C14),(C21,C22,C23,C24),
            (B11,B22,B33,B44),(C41,C42,C43,C44);
D4:=DET MAT((C11,C12,C13,C14),(C21,C22,C23,C24),
            (C31,C32,C33,C34),(B11,B22,B33,B44);
D:=DET MAT((C11,C12,C13,C14),(C21,C22,C23,C24),
            (C31,C32,C33,C34),(C41,C42,C43,C44);
SHUT TT1H$
BYE;
```

110

B. REDUCE PROGRAM TO DETERMINE THE DRIVING POINT IMPEDANCE.

```
%***********************************************************;
%       PROGRAM TA6C;
%       SPECIAL CASE OF N=0;
OFF NAT$
OUT TT1F$
%    THIS PROGRAM ATTEMPTS TO FIND THE SIX(6) FACTORS REQUIRED TO;
%    DESCRIBE THE WAVE MOTION OF A PLATE WITH FREE EDGES AT R=A, AND;
%    A DRIVEN CLAMPED CONDITION AT THE CENTER R=B.;
%       SPECIAL CASE OF N=0;
%    LINE SIZE TO ALLOW FILE STORAGE;
LINELENGTH (72);
% ADDED DIFFERENTIATION RULES FOR THE BESSEL FUNCTIONS;
%    JN OF DELTA1;
OPERATOR JN1,JN1DF1,JN1DF2,JN1DF3;
FOR ALL R LET DF(JN1(R),R)=DELTA1*JN1DF1(R)/A;
FOR ALL R LET DF(JN1DF1(R),R)=DELTA1*JN1DF2(R)/A;
FOR ALL R LET DF(JN1DF2(R),R)=DELTA1*JN1DF3(R)/A;
%    YN OF DELTA1;
OPERATOR YN1,YN1DF1,YN1DF2,YN1DF3;
FOR ALL R LET DF(YN1(R),R)=DELTA1*YN1DF1(R)/A;
FOR ALL R LET DF(YN1DF1(R),R)=DELTA1*YN1DF2(R)/A;
FOR ALL R LET DF(YN1DF2(R),R)=DELTA1*YN1DF3(R)/A;
%    JN OF DELTA2;
OPERATOR JN2,JN2DF1,JN2DF2,JN2DF3;
FOR ALL R LET DF(JN2(R),R)=DELTA2*JN2DF1(R)/A;
FOR ALL R LET DF(JN2DF1(R),R)=DELTA2*JN2DF2(R)/A;
FOR ALL R LET DF(JN2DF2(R),R)=DELTA2*JN2DF3(R)/A;
%    YN OF DELTA2;
OPERATOR YN2,YN2DF1,YN2DF2,YN2DF3;
FOR ALL R LET DF(YN2(R),R)=DELTA2*YN2DF1(R)/A;
FOR ALL R LET DF(YN2DF1(R),R)=DELTA2*YN2DF2(R)/A;
FOR ALL R LET DF(YN2DF2(R),R)=DELTA2*YN2DF3(R)/A;
%    JN OF DELTA3;
OPERATOR JN3,JN3DF1,JN3DF2,JN3DF3;
FOR ALL R LET DF(JN3(R),R)=DELTA3*JN3DF1(R)/A;
FOR ALL R LET DF(JN3DF1(R),R)=DELTA3*JN3DF2(R)/A;
FOR ALL R LET DF(JN3DF2(R),R)=DELTA3*JN3DF3(R)/A;
%    YN OF DELTA3;
OPERATOR YN3,YN3DF1,YN3DF2,YN3DF3;
FOR ALL R LET DF(YN3(R),R)=DELTA3*YN3DF1(R)/A;
FOR ALL R LET DF(YN3DF1(R),R)=DELTA3*YN3DF2(R)/A;
FOR ALL R LET DF(YN3DF2(R),R)=DELTA3*YN3DF3(R)/A;
%  SPECIAL CASE;
N:=0;
%    ASSUMED SOLUTION WITH THE BESSEL FUNCTION OF SECOND KIND;
W1:= (A1*JN1(R) + A4*YN1(R))*COS(N*THETA);
W2:= (A2*JN2(R) + A5*YN2(R))*COS(N*THETA);
W3:= (A3*JN3(R) + A6*YN3(R))*SIN(N*THETA);
%    POTENTIAL FUNCTIONS;
KSIR:= (SIGMA1-1)*DF(W1,R) + (SIGMA2-1)*DF(W2,R) + DF(W3,THETA)/R;
```

```
KSIT:= (SIGMA1-1)*DF(W1,THETA)/R + (SIGMA2-1)*DF(W2,THETA)/R -
       DF(W3,R);
W:= W1 + W2;
%    MOMENTS AND SHEARS;
MR:= D*(DF(KSIR,R) + (MU/R)*(KSIR + DF(KSIT,THETA)));
MT:= D*((KSIR + DF(KSIT,THETA))/R + MU*DF(KSIR,R));
MRT:= (D*(1-MU)/2)*((DF(KSIR,THETA) - KSIT)/R + DF(KSIT,R));
QR:= K**2*G*H*(KSIR + DF(W,R));
QT:= K**2*G*H*(KSIT + DF(W,THETA)/R);
%    BOUNDRY CONDITIONS;
%    R = A, MR=0,MRT=0, AND QR=0;
MRBCA:= SUB(R=A,MR);
MRTBCA:= SUB(R=A,MRT);
QRBCA:= SUB(R=A,QR);
%    R = B AT THE CENTER,KSIR=0,KSIT=0, W = WT0;
%    WT0 IS THE DRIVING POINT DISPLACEMENT;
B:=0;
KSIRBCB:= SUB(R=B,KSIR);
KSITBCB:= SUB(R=B,KSIT);
WBCB:= SUB(R=B,W) - WT0;
%    SOLVE FOR THE CONSTANTS A1 TO A6;
        AA1:= ( - B4*C34*C23*C12 + B4*C34*C22*C13 + B4*C33*C24*C12
  - B4*C33*C22*C14 - B4*C32*C24*C13 + B4*C32*C23*C14
  + C44*B3*C23*C12 - C44*B3*C22*C13 - C44*C33*B2*C12
  + C44*C33*C22*B1 + C44*C32*B2*C13 - C44*C32*C23*B1
  - C43*B3*C24*C12 + C43*B3*C22*C14 + C43*C34*B2*C12
  - C43*C34*C22*B1 - C43*C32*B2*C14 + C43*C32*C24*B1
  + C42*B3*C24*C13 + C42*B3*C23*C14 - C42*C34*B2*C13
  + C42*C34*C23*B1 + C42*C33*B2*C14 - C42*C33*C24*B1)/
(C44*C33*C22*C11 - C44*C33*C21*C12 - C44*C32*C23*C11 + C44*C32*C21*
C13 + C44*C31*C23*C12 - C44*C31*C22*C13 - C43*C34*C22*C11 + C43*
C34*C21*C12 + C43*C32*C24*C11 - C43*C32*C21*C14 - C43*C31*C24*C12
 + C43*C31*C22*C14 + C42*C34*C23*C11 - C42*C34*C21*C13 - C42*C33*
C24*C11 + C42*C33*C21*C14 + C42*C31*C24*C13 - C42*C31*C23*C14 -
C41*C34*C23*C12 + C41*C34*C22*C13 + C41*C33*C24*C12 - C41*C33*C22*
C14 - C41*C32*C24*C13 + C41*C32*C23*C14);
        AA2:= (B4*C34*C23*C11 - B4*C34*C21*C13 - B4*C33*C24*C11 + B4
*C33*C21*C14 + B4*C31*C24*C13 - B4*C31*C23*C14 - C44*
B3*C23*C11 + C44*B3*C21*C13 + C44*C33*B2*C11 - C44*
C33*C21*B1 - C44*C31*B2*C13 + C44*C31*C23*B1 + C43*B3
*C24*C11 - C43*B3*C21*C14 - C43*C34*B2*C11 + C43*C34*
C21*B1 + C43*C31*B2*C14 - C43*C31*C24*B1 - C41*B3*C24
*C13 + C41*B3*C23*C14 + C41*C34*B2*C13 - C41*C34*C23*
B1 - C41*C33*B2*C14 + C41*C33*C24*B1)/(C44*C33*C22*
C11 - C44*C33*C21*C12 - C44*C32*C23*C11 + C44*C32*C21*C13 + C44*
C31*C23*C12 - C44*C31*C22*C13 - C43*C34*C22*C11 + C43*C34*C21*
C12 + C43*C32*C24*C11 - C43*C32*C21*C14 - C43*C31*C24*C12 + C43*
C31*C22*C14 + C42*C34*C23*C11 - C42*C34*C21*C13 - C42*C33*C24*
C11 + C42*C33*C21*C14 + C42*C31*C24*C13 - C42*C31*C23*C14 - C41*
C34*C23*C12 + C41*C34*C22*C13 + C41*C33*C24*C12 - C41*C33*C22*
C14 - C41*C32*C24*C13 + C41*C32*C23*C14);
        AA4:= ( - B4*C34*C22*C11 + B4*C34*C21*C12 + B4*C32*C24*C11
  - B4*C32*C21*C14 - B4*C31*C24*C12 + B4*C31*C22*C14
  + C44*B3*C22*C11 - C44*B3*C21*C12 - C44*C32*B2*C11
  + C44*C32*C21*B1 + C44*C31*B2*C12 - C44*C31*C22*B1
  - C42*B3*C24*C11 + C42*B3*C21*C14 + C42*C34*B2*C11
  - C42*C34*C21*B1 - C42*C31*B2*C14 + C42*C31*C24*B1
  + C41*B3*C24*C12 - C41*B3*C22*C14 - C41*C34*B2*C12
  + C41*C34*C22*B1 + C41*C32*B2*C14 - C41*C32*C24*B1)/
(C44*C33*C22*C11 - C44*C33*C21*C12 - C44*C32*C23*C11 + C44*C32*C21*
```

112

```
     C13 + C44*C31*C23*C12 - C44*C31*C22*C13 - C43*C34*C22*C11 + C43*
   C34*C21*C12 + C43*C32*C24*C11 - C43*C32*C21*C14 - C43*C31*C24*C12
    + C43*C31*C22*C14 + C42*C34*C23*C11 - C42*C34*C21*C13 - C42*C33*
   C24*C11 + C42*C33*C21*C14 + C42*C31*C24*C13 - C42*C31*C23*C14 -
   C41*C34*C23*C12 + C41*C34*C22*C13 + C41*C33*C24*C12 - C41*C33*C22*
   C14 - C41*C32*C24*C13 + C41*C32*C23*C14);
         AA5:= (B4*C33*C22*C11 - B4*C33*C21*C12 - B4*C32*C23*C11 + B4
   *C32*C21*C13 + B4*C31*C23*C12 - B4*C31*C22*C13 - C43*
   B3*C22*C11 + C43*B3*C21*C12 + C43*C32*B2*C11 - C43*
   C32*C21*B1 - C43*C31*B2*C12 + C43*C31*C22*B1 + C42*B3
   *C23*C11 - C42*B3*C21*C13 - C42*C33*B2*C11 + C42*C33*
   C21*B1 + C42*C31*B2*C13 - C42*C31*C23*B1 - C41*B3*C23
   *C12 + C41*B3*C22*C13 + C41*C33*B2*C12 - C41*C33*C22*
   B1 - C41*C32*B2*C13 + C41*C32*C23*B1)/(C44*C32*C22*
   C11 - C44*C33*C21*C12 - C44*C32*C23*C11 + C44*C32*C21*C13 + C44*
   C31*C23*C12 - C44*C31*C22*C13 - C43*C34*C22*C11 + C43*C34*C21*
   C12 + C43*C32*C24*C11 - C43*C32*C21*C14 - C43*C31*C24*C12 + C43*
   C31*C22*C14 + C42*C34*C23*C11 - C42*C34*C21*C13 - C42*C33*C24*
   C11 + C42*C33*C21*C14 + C42*C31*C24*C13 - C42*C31*C23*C14 - C41*
   C34*C23*C12 + C41*C34*C22*C13 + C41*C33*C24*C12 - C41*C33*C22*
   C14 - C41*C32*C24*C13 + C41*C32*C23*C14);
   A3:= AA3;
   A6:= AA6;
   %    DERIVATION OF C11 TO C44 AND B1 TO B4;
   C11:= SUB(A1=1,A2=0,A4=0,A5=0,MRBCA);
   C12:= SUB(A1=0,A2=1,A4=0,A5=0,MRBCA);
   C13:= SUB(A1=0,A2=0,A4=1,A5=0,MRBCA);
   C14:= SUB(A1=0,A2=0,A4=0,A5=1,MRBCA);
   C21:= SUB(A1=1,A2=0,A4=0,A5=0,QRBCA);
   C22:= SUB(A1=0,A2=1,A4=0,A5=0,QRBCA);
   C23:= SUB(A1=0,A2=0,A4=1,A5=0,QRBCA);
   C24:= SUB(A1=0,A2=0,A4=0,A5=1,QRBCA);
   C31:= SUB(A1=1,A2=0,A4=0,A5=0,KSIRBCB);
   C32:= SUB(A1=0,A2=1,A4=0,A5=0,KSIRBCB);
   C33:= SUB(A1=0,A2=0,A4=1,A5=0,KSIRBCB);
   C34:= SUB(A1=0,A2=0,A4=0,A5=1,KSIRBCB);
   C41:= SUB(A1=1,A2=0,A4=0,A5=0,WT0=0,WBCB);
   C42:= SUB(A1=0,A2=1,A4=0,A5=0,WT0=0,WBCB);
   C43:= SUB(A1=0,A2=0,A4=1,A5=0,WT0=0,WBCB);
   C44:= SUB(A1=0,A2=0,A4=0,A5=1,WT0=0,WBCB);
   B1:= 0;
   B2:= 0;
   B3:= 0;
   B4:= WT0;
   A1:= AA1;
   A2:= AA2;
   A4:= AA4;
   A5:= AA5;
   FOFT2:= INT(R*QR,THETA);
   FOFT1:= SUB(R=B,FOFT2);
   FOFT:= SUB(THETA=2*PI,FOFT1) - SUB(THETA=0,FOFT1);
   Z:= FOFT/(OMEGA*WT0);
   %  SPECIAL CASE OF N = 0;
   ON FORT;
   WRITE Z;
   OFF FORT;
   SHUT TT1F$
   BYE;
```

APPENDIX B.

FORTRAN PROGRAM TO CALCULATE THE DRIVING POINT

IMPEDANCE

```
      PROGRAM THESIS
C******************************************************************
C*    THE PURPOSE OF THIS PROGRAM IS TO GENERATE THE DATA WHICH IS   *
C*    NECESSARY TO CALCULATE THE DRIVING POINT IMPEDANCE VS FREQUENCY *
C******************************************************************
C*    LIST OF VARIABLES                                              *
C*    FL              LOWER FREQUENCY OF INTEREST, HZ                 *
C*    FH              UPPER FREQUNECY OF INTEREST, HZ                 *
C*    F               FREQUENCY OF INTEREST, HZ                       *
C*    OMEGA           ANGULAR FREQUENCY OF INTEREST, =2PI*F, RAD/SEC  *
C*    A               RADIUS OF OUTER EDGE OF PLATE, IN               *
C*    B               RADIUS OF WAVE GUIDE ATTACHMENT, IN             *
C*    H               THICKNESS OF PLATE, IN                          *
C*    TEMP            AVERAGE PLATE TEMP IN DEGREES F                 *
C*    IMAT            TYPE OF MATERIAL                                *
C*                    = 0, ELASTIC                                    *
C*                    = 1, VISCOELASTIC WITH DATA FROM G.G.LEE        *
C*                    = 2, VISCOELASTIC WITH DATA FROM UNITED MCGILL  *
C*    RHO             DENSITY OF PLATE, SLUGS/IN**3                   *
C*    E               YOUNG'S MODULUS, PSI                            *
C*    G               SHEAR MODULUS,PSI                               *
C*    MU              POISSON'S RATIO                                 *
C*    JXY             BESSEL FUNCTION OF THE FIRST KIND, EVALUATED AT *
C*                    DELTAX*Y/A                                      *
C*    YXY             BESSEL FUNCTION OF THE SECOND KIND, EVALUATED AT*
C*                    DELTAX*Y/A                                      *
C*    JXDF1Y          FIRST DERIVATIVE OF THE BESSEL FUNCTION OF THE  *
C*                    FIRST KIND, EVALUATED AT DELTAX*Y/A             *
C*    YXDF1Y          FIRST DERIVATIVE OF THE BESSEL FUNCTION OF THE  *
C*                    SECOND KIND, EVALUATED AT DELTAX*Y/A            *
C*    JXDF2Y          SECOND DERIVATIVE OF THE BESSEL FUNCTION OF THE *
C*                    FIRST KIND, EVALUATED AT DELTAX*Y/A             *
C*    YXDF2Y          SECOND DERIVATIVE OF THE BESSEL FUNCTION OF THE *
C*                    SECOND KIND, EVALUATED AT DELTAX*Y/A            *
C*    DELTA1          DEMENSIONLESS PARAMETER                         *
C*    DELTA2          DEMENSIONLESS PARAMETER                         *
C*    DELTA3          DEMENSIONLESS PARAMETER                         *
C*    SIGMA1          DEMENSIONLESS PARAMETER                         *
C*    SIGMA2          DEMENSIONLESS PARAMETER                         *
C*                    DRIVING POINT IMPEDANCE                         *
C*    ZZ              COMPLEX IMPEDANCE, LBF-SEC/IN                   *
C*    Z               MAGNITUDE OF ZZ, LBF-SEC/IN                     *
C*    ZR              REAL PART OF ZZ, LBF-SEC/IN                     *
C*    ZI              IMAGINARY PART OF ZZ, LBF-SEC/IN                *
C*    ZDB             Z IN DB,                                        *
C*    K               SHEAR COEFFICEINT                              *
C*    PI              3.14....                                        *
C*    X               DUMMY ARGUMENT FOR BESSEL FUNCTION EVALUATION   *
C******************************************************************
      IMPLICIT COMPLEX*8 (A,D,J,S,Y)
```

```fortran
        COMPLEX*8 E,X,G
        REAL MU,A,K
        CHARACTER ANS*1, NAME*6
        COMMON/BESS1A/J1A,J1DF1A,J1DF2A,Y1A,Y1DF1A,Y1DF2A
        COMMON/BESS1B/J1B,J1DF1B,J1DF2B,Y1B,Y1DF1B,Y1DF2B
        COMMON/BESS2A/J2A,J2DF1A,J2DF2A,Y2A,Y2DF1A,Y2DF2A
        COMMON/BESS2B/J2B,J2DF1B,J2DF2B,Y2B,Y2DF1B,Y2DF2B
        COMMON/BESS3A/J3A,J3DF1A,J3DF2A,Y3A,Y3DF1A,Y3DF2A
        COMMON/BESS3B/J3B,J3DF1B,J3DF2B,Y3B,Y3DF1B,Y3DF2B
        COMMON/GEOMTY/A,B,H,K
        COMMON/MAT/IMAT,E,G,MU,RHO,TEMP
        COMMON/CONST1/DELTA1,DELTA2,DELTA3,SIGMA1,SIGMA2
        PI= ARCOS(-1.0)
C       WRITE(6,*)' PI =',PI
C
C       INPUT OF MATERIAL TYPE
C
   5    CONTINUE
        CALL FRTCMS ('CLRSCRN ')
        WRITE(6,*)' THE FOLLOWING MATERIALS ARE SUPPORTED'
        WRITE(6,*)' '
        WRITE(6,*)'  TYPE              NAME            CHARACTERISTICS FROM
       1'
        WRITE(6,*)' '
        WRITE(6,*)'  ELASTIC(E)        ALUMINUM        GERE-TIMOSHENKO'
        WRITE(6,*)' '
        WRITE(6,*)'  VISCOELASTIC(V)   LD-400          VIBRATION DAMPING'
        WRITE(6,*)'  VISCOELASTIC(M)   C-2204          UNITED MCGILL '
        WRITE(6,*)' '
        WRITE(6,*)' WHAT TYPE OF MATERIAL IS UNDER STUDY?'
        WRITE(6,*)' TYPE E, V, OR M.'
        READ(5,'(A1)') ANS
        WRITE(6,*)' ',ANS
        IF ( ANS .NE. 'E' .AND. ANS .NE. 'V' .AND. ANS .NE. 'M' ) GO TO 5
        IMAT = 0
        IF ( ANS .EQ. 'V' ) IMAT = 1
        IF ( ANS .EQ. 'M' ) IMAT = 2
        WRITE(6,*)' IMAT=',IMAT
C
C       INPUT OF PLATE TEPERATURE
C
   6    WRITE(6,*)' WHAT IS THE AVERAGE TEMPERATURE OF THE PLATE IN DEGREE
       1 F?(TEMP)'
        READ(5,*) TEMP
        WRITE(6,*)' TEMP=',TEMP,' F'
        IF ( TEMP .LT. 63.0 .OR. TEMP .GT. 104.0 ) GO TO 6
C
C       INPUT OF PLATE GEOMETRY
C
        WRITE(6,*)' WHAT IS THE RADIUS OF THE PLATE IN INCHS?(A)'
        READ(5,*) A
        WRITE(6,*)' A=',A,' IN'
        IF ( A .LE. 0.0 ) GO TO 5
   7    CONTINUE
C       WRITE(6,*)' WHAT IS THE MOUNT RADIUS IN INCHS?(B)'
C       READ(5,*) B
        B = 0.3125
        WRITE(6,*)' B=',B,' IN'
        IF ( B .LE. 0.0 ) GO TO 7
   8    CONTINUE
```

```
C       WRITE(6,*)' WHAT IS THE THICKNESS OF THE PLATE IN INCHS?(H)'
C       READ(5,*) H
        H = 3.0/8.0
        WRITE(6,*)' H=',H,' IN'
        IF ( H .LE. 0.0 ) GO TO 8
C
C       INPUT OF FREQUENCY RANGE
C
  10    WRITE(6,*)' WHAT IS THE LOW FREQUENCY OF INTEREST, IN HZ?(FL)'
        READ(5,*) FL
        WRITE(6,*)' FL=',FL,' HZ'
        IF ( FL .LE. 0.0 ) GO TO 10
  15    WRITE(6,*)' WHAT IS THE HIGH FREQUENCY OF INTEREST, IN HZ?(FH)'
        READ(5,*) FH
        WRITE(6,*)' FH=',FH,' HZ'
        IF ( FH .LE. FL ) GO TO 15
C
C       INPUT OF LOCATION TO WRITE RESULTS
C
        WRITE(6,*) ' WHAT IS THE FILE NAME? '
        READ(6,'(A)') NAME
        OPEN(UNIT=15,FILE= NAME, FORM= 'FORMATTED',ACCESS= 'SEQUENTIAL',ST
       1ATUS= 'NEW' )
        IF ( IMAT .EQ. 0 ) IPOINT = 99
        IF ( IMAT .EQ. 1 .OR. IMAT .EQ. 2 ) IPOINT = 99
C
C       START OF CALCULATIONS
C
        DO 90 I=0,IPOINT
C
C       FREQUENCY OF INTEREST
C
        F = FL + (FH - FL)*FLOAT(I)/FLOAT(IPOINT)
        OMEGA = 2.0*PI*F
C       WRITE(6,*)' I=',I,'  F=',F,'HZ  OMEGA=',OMEGA,'RAD/SEC'
C
C       GENERATION OF DIMENSIONLESS PARAMETERS
C
        CALL CONST(OMEGA,F)
C
C       GENERATION OF BESSEL FUNCTIONS
C
C       BESSEL FUNCTIONS FOR DELTA1 AND RADIUS A
        X = DELTA1
C       WRITE(6,*)' X=',X
        CALL BESSEL(X,J1A,J1DF1A,J1DF2A,Y1A,Y1DF1A,Y1DF2A)
C       BESSEL FUNCTIONS FOR DELTA1 AND RADIUS B
        X = DELTA1*B/A
C       WRITE(6,*)' X=',X
        CALL BESSEL(X,J1B,J1DF1B,J1DF2B,Y1B,Y1DF1B,Y1DF2B)
C       BESSEL FUNCTIONS FOR DELTA2 AND RADIUS A
        X = DELTA2
C       WRITE(6,*)' X=',X
        CALL BESSEL(X,J2A,J2DF1A,J2DF2A,Y2A,Y2DF1A,Y2DF2A)
C       BESSEL FUNCTIONS FOR DELTA2 AND RADIUS B
        X = DELTA2*B/A
C       WRITE(6,*)' X=',X
        CALL BESSEL(X,J2B,J2DF1B,J2DF2B,Y2B,Y2DF1B,Y2DF2B)
C       BESSEL FUNCTIONS FOR DELTA3 AND RADIUS A
        X = DELTA3
```

116

```
C       WRITE(6,*)' X=',X
        CALL BESSEL(X,J3A,J3DF1A,J3DF2A,Y3A,Y3DF1A,Y3DF2A)
C       BESSEL FUNCTIONS FOR DELTA3 AND RADIUS B
        X = DELTA3*B/A
C       WRITE(6,*)' X=',X
        CALL BESSEL(X,J3B,J3DF1B,J3DF2B,Y3B,Y3DF1B,Y3DF2B)
C
C       IMPERANCE CALCULATIONS
C
        CALL IMPEDO(OMEGA,Z,ZR,ZI,ZDB)
        WRITE(15,20) F,Z,ZR,ZI,ZDB
 90     CONTINUE
        WRITE(6,*)' DO YOU WANT TO CONTINUE?(Y/N).'
        READ(5,'(A)') ANS
        CALL FRTCMS ('CLRSCRN ')
        IF ( ANS .EQ. 'Y' ) GO TO 5
 20     FORMAT(1X,5(G15.7,1X))
        END
        SUBROUTINE CONST(OMEGA,F)
C*******************************************************************
C*      THE PUPOSE OF THIS PROGRAM IS TO DETERMINE THE DIMENSIONLESS    *
C*      PARAMETERS AND YOUNG'S AND SHEAR MODULUS FOR THE                *
C*      VISCOELASTIC MATERIAL                                           *
C*******************************************************************
C*      LIST OF VARIABLE                                                *
C*      A              PLATE RADIUS, IN                                 *
C*      B              WAVEGUIDE ATTACHMENT RADIUS, IN                  *
C*      H              PLATE THICKNESS, IN                              *
C*      TEMP           AVERAGE PLATE TEMP IN DEGREES F                  *
C*      IMAT           TYPE OF MATERIAL                                 *
C*                     = 0, ELASTIC MATERIAL                            *
C*                     = 1, VISCOELASTIC WITH DATA FROM G.G.LEE         *
C*                     = 2, VISCOELASTIC WITH DATA FROM UNITED MCGILL   *
C*      E              YOUNG'S MODULUS, PSI                             *
C*      G              SHEAR MODULUS, PSI                               *
C*      ETHA           VISCOELASTIC LOSS FACTOR                         *
C*      GMAG           VISCOELASTIC SHEAR MODULUS                       *
C*      D              FLEXURAL RIGIDITY, PSI-IN                        *
C*      MU             POISSON'S RATIO                                  *
C*      RHO            MASS DENSITY OF PLATE, SLUGS/IN**3               *
C*      K              SHEAR MODULUS                                    *
C*      OMEGA          CIRCULAR FREQUENCY OF INTEREST, RAD/SEC          *
C*      F              FREQUENCY OF INTEREST, HZ                        *
C*      DELTA1         DEMENSIONLESS PARAMETER                          *
C*      DELTA2         DEMENSIONLESS PARAMETER                          *
C*      DELTA3         DEMENSIONLESS PARAMETER                          *
C*      SIGMA1         DEMENSIONLESS PARAMETER                          *
C*      SIGMA2         DEMENSIONLESS PARAMETER                          *
C*      DELT12         DELTA1**2                                        *
C*      DELT22         DELTA2**2                                        *
C*      DELT32         DELTA3**2                                        *
C*      RR             DEMENSIONLESS PARAMETER                          *
C*      S              DEMENSIONLESS PARAMETER                          *
C*      L4             DEMENSIONLESS PARAMETER                          *
C*      PI             3.14....                                         *
C*******************************************************************
        COMPLEX*8 DELTA1,DELTA2,DELTA3,SIGMA1,SIGMA2,L4,D,E,G,DELT12,
       1DELT22,DELT32
        REAL MU,K
        COMMON/GEOMTY/A,B,H,K
```

117

```
          COMMON/MAT/IMAT,E,G,MU,RHO,TEMP
          COMMON/CONST1/DELTA1,DELTA2,DELTA3,SIGMA1,SIGMA2
          PI=ACOS(-1.0)
C         WRITE(*,*)' PI =',PI
C
C         CALCULATION OF THE MATERIAL CHARACTERISTICS
C
          CALL YOUNGS(F)
C
C         CALCULATION OF FLEXURAL RIGIDITY
C
          D = E*H**3/(12.0*(1.0-MU**2))
C
C         SHEAR COEFFICIENT
C
C         K = SQRT(PI**2/12.0)
C         K = 0.95541
          K = 0.92736
C         WRITE(6,*)' K=',K
C         WRITE(6,*)' D=',D
C         WRITE(6,*)' G=',G
C         WRITE(6,*)' RHO',RHO
C
C         DIMENSIONLESS PARAMETERS
C
          RR = (H/A)**2/12.0
C         WRITE(6,*)' RR=',RR
          S = (1.0/(6.0*K**2*(1.0-MU)))*(H/A)**2
C         WRITE(6,*)' S=',S
          L4 = RHO*H*A**4*OMEGA**2/(12.0*D)
C         WRITE(6,*)' L4=',L4
          DELT12 =  (L4*(RR+S+SQRT((RR-S)**2+4.0/L4))/2.0)
C         WRITE(6,*)' DELT12=',DELT12
          DELT22 =  (L4*(RR+S-SQRT((RR-S)**2+4.0/L4))/2.0)
C         WRITE(6,*)' DELT22=',DELT22
          DELT32 =  (2.0*(RR*L4-1.0/S)/(1.0-MU))
C         WRITE(6,*)' DELT32=',DELT32
          SIGMA1 = DELT22 /(RR*L4-1.0/S)
C         WRITE(6,*)' SIGMA1=',SIGMA1
          SIGMA2 = DELT12/(RR*L4-1.0/S)
C         WRITE(6,*)' SIGMA2=',SIGMA2
          DELTA1 = SQRT(DELT12)
C         WRITE(6,*)' DELTA1=',DELTA1
          DELTA2 = SQRT(DELT22)
C         WRITE(6,*)' DELTA2=',DELTA2
          DELTA3 = SQRT(DELT32)
C         WRITE(6,*)' DELTA3=',DELTA3
C         GO TO 10
  999     CONTINUE
          RETURN
          END
          SUBROUTINE YOUNGS(F)
C***********************************************************************
C*    THE MATERIAL CHARACTERISTICS                                    *
C*    THE PURPOSE OF THIS PROGRAM IS TO GENERATE YOUNG'S MODULUS      *
C*    AND SHEAR MODULUS FOR THE MATERIAL UNDER STUDY                  *
C*                       C.D.HETTEMA              4 AUG 88            *
C***********************************************************************
C*    LIST OF VARIABLES                                               *
C*    F                 FREQUENCY OF INTEREST, HZ                     *
```

118

```
C*      FLOG            LOG10(F)                                                 *
C*      TEMP            AVERAGE PLATE TEMP IN DEGREES F                          *
C*      IMAT            TYPE OF MATERIAL                                         *
C*                      = 0, ELASTIC                                            *
C*                      = 1, VISCOELASTIC WITH DATA FROM G.G.LEE               *
C*                      = 2, VISCOELASTIC WITH DATA FROM UNITED MCGILL          *
C*      RHO             DENSITY OF PLATE, SLUGS/IN**3                           *
C*      E               YOUNG'S MODULUS, PSI                                    *
C*      G               SHEAR MODULUS,PSI                                       *
C*      ETHA            LOSS FACTOR                                             *
C*      EP              REAL PART OF COMPLEX YOUNG'S MODULUS                     *
C*      EDP             COMPLEX PART OF COMPLEX YOUNG'S MODULUS                  *
C*      EPX             REAL PART OF COMPLEX YOUNG'S MODULUS AT TEMP X           *
C*      EDPX            COMPLEX PART OF COMPLEX YOUNG'S MODULUS AT TEMP X        *
C*      DEP             DUMMY VARIABLE FOR EP                                    *
C*      DEDP            DUMMY VARIABLE FOR EDP                                   *
C*      DEPX            DUMMY VARIABLE FOR EPX                                   *
C*      DEDPX           DUMMY VARIABLE FOR EDPX                                  *
C*      MU              POISSON'S RATIO                                         *
C*      PI              3.14....                                                *
C***********************************************************************************
        COMPLEX*8 E,G
        REAL MU
        CHARACTER ANS*1
        COMMON/MAT/IMAT,E,G,MU,RHO,TEMP
C
C       FOR USE IN UNITED MCGILL DATA
C
        FLOG = LOG10(F)
C***********************************************************************************
C
C       ELASTIC MATERIAL DATA
C
        IF ( IMAT .EQ. 0 ) THEN
        E = (11.0E6,0.0)
        MU = 0.33
        G = E/(2.0*(1.0+MU))
        RHO = 3.06713E-3
C***********************************************************************************
C
C       VISCOELASTIC MATERIAL CHARACTERISTICS FROM NASHIF, JONES, AND
C       HENDERSON
C
        ELSE IF ( IMAT .EQ. 1 ) THEN
        ETHA = 0.65*EXP(-0.52732*((ABS(LOG10(F/62)))**1.956))
        GMAG = 0.00002503*F**3 - 0.1752*F**2 + 457.5883*F + 29280
        G = GMAG*((1.0,0.0) + (0.0,1.0)*ETHA)
        MU = 0.5
        E = G*(2.0*(1.0+MU))
        RHO = 1.71101E-3
C***********************************************************************************
C
C       VISCOELASTIC MATERIAL CHARACTERISTICS FROM UNITED MCGILL
C
        ELSE IF ( IMAT .EQ. 2 ) THEN
C
C       FOUR POINT, THIRD ORDER CURVE FITS FOR A SET TEMP
C
C
C       TEMP OF 68 F
```

119

```
C
C     DEP FOR T=68F
        A3=-0.124999657E-01
        A2= 0.999998450E-01
        A1=-0.625001788E-01
        A0=  2.02499962
        DEPA = A0 + A1*FLOG + A2*FLOG**2 + A3*FLOG**3
C     DEDP FOR T=68F
        A3=-0.166667290E-01
        A2= 0.112500608
        A1=-0.708351135E-01
        A0=  1.77500057
        DEDPA = A0 + A1*FLOG + A2*FLOG**2 + A3*FLOG**3
C
C        TEMP OF 86 F
C
C     DEP FOR T=86F
        A3= 0.250002518E-01
        A2=-0.187501848
        A1= 0.612504184
        A0= 0.999996543
        DEPB = A0 + A1*FLOG + A2*FLOG**2 + A3*FLOG**3
C     DEDP FOR T=86F
        A3= 0.124999657E-01
        A2=-0.999993682E-01
        A1= 0.387497604
        A0=  1.05000114
        DEDPB = A0 + A1*FLOG + A2*FLOG**2 + A3*FLOG**3
C
C        TEMP OF 104 F
C
C     DEP FOR T=104F
        A3= 0.158945682E-06
        A2= 0.124988556E-01
        A1= 0.875023007E-01
        A0= 0.899998665
        DEPC = A0 + A1*FLOG + A2*FLOG**2 + A3*FLOG**3
C     DEDP FOR T=104F
        A3= 0.833320618E-02
        A2=-0.624990463E-01
        A1= 0.254164696
        A0= 0.800001144
        DEDPC = A0 + A1*FLOG + A2*FLOG**2 + A3*FLOG**3
C
C     LINEAR FIT FOR SET FREQUENCY
C
      IF ( TEMP .GE. 68.0 .AND. TEMP .LT. 86.0 ) THEN
      DEP = (DEPB-DEPA)*(TEMP-68.0)/18.0 + DEPA
      DEDP = (DEDPB-DEDPA)*(TEMP-68.0)/18.0 + DEDPA
      ELSE IF ( TEMP .GE. 86.0 .AND. TEMP .LE. 104.0 ) THEN
      DEP = (DEPC-DEPB)*(TEMP-86.0)/18.0 + DEPB
      DEDP = (DEDPC-DEDPB)*(TEMP-86.0)/18.0 + DEDPB
      END IF
C
C     CONVERSION OF DATA TO PSI UNITS
C
      EP = 1.0E8*10**DEP*1.45047E-5
      EDP = 1.0E8*10**DEDP*1.45047E-5
      E = EP*(1.0,0.0) + EDP*(0.0,1.0)
      ETHA = EDP/EP
```

120

```
          MU = 0.5
          G = E/(2.0*(1.0+MU))
          RHO = 1.70736E-3
          END IF
          RETURN
          END
          SUBROUTINE BESSEL(XX,J0,JODF1,JODF2,Y0,YODF1,YODF2)
C*******************************************************************
C*    THIS PROGRAM CALCULATES THE BESSEL FUNCTION OF THE FIRST AND *
C*    SECOND KIND ALONG WITH THE FIRST AND SECOND DERIVATIVE OF EACH *
C*    THIS WILL BE BY TAYLOR SERIES EXPANTION                      *
C*    N = 0                                                        *
C*******************************************************************
C*    LIST OF VARIABLES                                           *
C*    M             COUNTER                                       *
C*    M1            COUNTER FOR DERIVATIVES, M1=M+1               *
C*    ZM            DOUBLE PRECISION M                            *
C*    ZM1           DOUBLE PRECISION M1                           *
C*    ZMI           SUM OF THE INVERSE OF M                       *
C*    X             ARGUMENT OF THE FUNCTION                      *
C*    XXXD          DOUBLE PRECISION VALUE OF XXX                 *
C*    J0            BESSEL FUNCTION, FIRST KIND                   *
C*    JODF1         FIRST DERIVATIVE OF J0                        *
C*    JODF2         SECOND DERIVATIVE OF J0                       *
C*    J0A           CHANGE IN J0 EACH STEP                        *
C*    JDF1A         CHANGE IN JODF1 EACH STEP                     *
C*    JDF2A         CHANGE IN JODF2 EACH STEP                     *
C*    J01           ABS OF J0A                                    *
C*    JDF11         ABS OF JDF1A                                  *
C*    JDF21         ABS OF JDF2A                                  *
C*    Y0            BESSEL FUNCTION, SECOND KIND                  *
C*    YODF1         FIRST DERIVATIVE OF Y0                        *
C*    YODF2         SECOND DERIVATIVE OF Y0                       *
C*    Y0A           CHANGE IN Y0 EACH STEP                        *
C*    YDF1A         CHANGE IN YODF1 EACH STEP                     *
C*    YDF2A         CHANGE IN YODF2 EACH STEP                     *
C*    Y01           ABS OF Y0A                                    *
C*    YDF11         ABS OF YDF1A                                  *
C*    YDF21         ABS OF YDF2A                                  *
C*    GAMMA         EULER'S CONSTANT                              *
C*    ERRORM        MAXIMUM ALLOWED ERROR                        *
C*    ZZZMAX        MAXIMUM SIZE NUMBER ALLOWED                   *
C*    MC1,MC2,MC3   COUNTERS                                      *
C*    D             DUMMY VARIABLE                                *
C*******************************************************************
C
C     QUAD COMPLEX
C
      IMPLICIT REAL*16 (A-H,O-Z)
C
C     DOUBLE COMPLEX
C
C     IMPLICIT COMPLEX*16 (A-H,O-Z)
      COMPLEX*32 J0D,JODF1D,JODF2D,J0AD,JDF1AD,JDF2AD,J01D,JDF11D,JDF21d
      COMPLEX*32 Y0D,YODF1D,YODF2D,Y0AD,YDF1AD,YDF2AD,Y01D,YDF11D,YDF21D
      COMPLEX*32 X
      COMPLEX*8 J0,JODF1,JODF2
      COMPLEX*8 Y0,YODF1,YODF2
      COMPLEX*8 XX
      CHARACTER ANS*1
```

```fortran
      ZERO = 0.0D0
      ONE = 1.0D0
      TWO = 2.0D0
      PI = DARCOS(-ONE)
C
C     MAXIMUM ERROR ALLOWED
C
      ERRORM = 1.0D-15
C
C     MAXIMUM SIZE NUMBER ALLOWED
C
      ZZZMAX = 1.0D30
      GAMMA = 0.5772156649015328606065120D0
5     CONTINUE
C     J0 = ZERO
C
C     CONVERSION OF X TO QUAD PERCISION
C
      X = XX * ONE
C
C     CHECK TO PREVENT Y0 FROM BEING UNBOUNDED
C
      D =  ABS(X)
      IF ( D .LT. 1.0D-3 ) THEN
      WRITE(6,*)'  **** X IS TOO SMALL ****'
      GO TO 50
      END IF
      M = 0
60    CONTINUE
C
C     J0 CALCULATIONS
C
      M1 = M + 1
      ZM = DBLE(M)
      ZM1 = DBLE(M1)
C
C     SET UP OF TAYLOR SERIES
C
      IF ( M .EQ. 0 ) THEN
      J0D = ONE
      J0AD = ZERO
      J01D = ONE
      J0DF1D = -ONE*X/TWO
      JDF1AD = ZERO
      JDF11D = ONE*X/TWO
      J0DF2D = -ONE/TWO
      JDF2AD = ZERO
      JDF21D = ONE/TWO
      MLAST = 0
      MC1 = 1
      MC2 = 1
      MC3 = 1
C
C     EXPANSION OF TAYLOR SERIES
C
      ELSE IF ( M .GT. 0 ) THEN
      M2 = M/2
C
C     FOR J0
C
```

```
          DA = ABS(J01D)
          IF ( D .GT. ERRORM ) THEN
          J01D = J01D*((X/(TWO*ZM))**2)
          JOAD = J01D
          IF ( M2 .EQ. MLAST ) JOAD = -J01D
          JOD = JOD + JOAD
          MC1 = MC1 + 1
          END IF
C
C         FOR JODF
C
          DB = ABS(JDF11D)
          IF ( D .GT. ERRORM ) THEN
          JDF11D = JDF11D*X**2/((TWO*(ZM1-ONE))*(TWO*ZM1))
          JDF1AD = - JDF11D
          IF ( M2 .EQ. MLAST ) JDF1AD = JDF11D
          JODF1D = JODF1D + JDF1AD
          MC2 = MC2 + 1
          END IF
C
C         FOR JODF2
C
          DC = ABS(JDF21D)
          IF ( D .GT. ERRORM ) THEN
          JDF21D = JDF21D*X**2*(TWO*ZM1-ONE)/((TWO*(ZM1-ONE))*(TWO*ZM1
         1)*(TWO*(ZM1-ONE) - ONE))
          JDF2AD = - JDF21D
          IF ( M2 .EQ. MLAST ) JDF2AD = JDF21D
          JODF2D = JODF2D + JDF2AD
          MC3 = MC3 + 1
          END IF
          MLAST = M2
          END IF
C
C         CHECK IF SERIES CONVERGED
C
          D = ABS(JOD)
          D1 = ABS(JODF1D)
          D2 = ABS(JODF2D)
          IF ( M .GT. 300 .OR. D .GT. ZZZMAX   .OR. DA .GT. ZZZMAX .OR.
         1D1 .GT. ZZZMAX   .OR. DB .GT. ZZZMAX .OR.
         2D2 .GT. ZZZMAX   .OR. DC .GT. ZZZMAX ) THEN
          WRITE(6,*)'  ****   FUNCTION HAS NOT CONVERGED ****'
          GO TO 50
          END IF
          IF ( DA .LE. ERRORM .AND. M .GT. 0 .AND.
         1DB .LE. ERRORM .AND. DC .LE. ERRORM ) GO TO 20
          M = M + 1
          GO TO 60
   20     CONTINUE
C
C         CONVERSION FROM QUAD TO SINGLE PERCISION
C
          JO = JOD*1.0
          JODF1 = JODF1D*1.0
          JODF2 = JODF2D*1.0
C
C         YO CALCULATIONS
C
          M = 0
```

```
C
C      SET UP OF TAYLOR SERIES
C
       YOD = (TWO/PI)*(LOG(X/TWO)+GAMMA)*JOD
       YODF1D = (TWO/PI)*((LOG(X/TWO)+GAMMA)*JODF1D + JOD/X) + X/PI
       YODF2D = (TWO/PI)*((LOG(X/TWO)+GAMMA)*JODF2D + TWO*JODF1D/X -
      1JO/(X**2)) + ONE/PI
       YO1D = ONE
       YDF11D = X/TWO
       YDF21D = ONE/TWO
       ZMI = ZERO
       MLAST = 0
       MC1 = 0
       MC2 = 1
       MC3 = 1
C
C      EXPANSION OF TAYLOR SERIES
C
  30   M = M + 1
       ZM = DBLE(M)
       ZMI = ZMI + ONE/ZM
       M2 = M/2
C
C      FOR YO
C
       DA = ABS(YO1D)
       IF ( DA .GT. ERRORM ) THEN
       YO1D = YO1D*((X/(TWO*ZM))**2)
       YOAD = -YO1D
       IF ( M2 .EQ. MLAST ) YOAD = YO1D
       YOD = YOD + TWO*YOAD*ZMI/PI
       MC1 = MC1 + 1
       END IF
C
C      FOR YODF
C
       DB = ABS(YDF11D)
       IF ( DB .GT. ERRORM .AND. M .GT. 1 ) THEN
       YDF11D = YDF11D*X**2/((TWO*(ZM-ONE))*(TWO*ZM))
       YDF1AD = -YDF11D
       IF ( M2 .EQ. MLAST ) YDF1AD = YDF11D
       YODF1D = YODF1D + YDF1AD*TWO*ZMI/PI
       MC2 = MC2 + 1
       END IF
C
C      FOR YODF2
C
       DC = ABS(YDF21D)
       IF ( DC .GT. ERRORM .AND. M .GT. 1 ) THEN
       YDF21D = YDF21D*X**2*(TWO*ZM-ONE)/((TWO*(ZM-ONE))*(TWO*ZM)
      1*(TWO*(ZM-ONE) - ONE))
       YDF2AD = -YDF21D
       IF ( M2 .EQ. MLAST ) YDF2AD = YDF21D
       YODF2D = YODF2D + YDF2AD*TWO*ZMI/PI
       MC3 = MC3 + 1
       END IF
C
C      CHECK IF SERIES CONVERGED
C
       MLAST = M2
```

```
       D = ABS(YOD)
       D1 = ABS(YODF1D)
       D2 = ABS(YODF2D)
       IF ( M .GT. 300 .OR. D .GT. ZZZMAX  .OR. DA .GT. ZZZMAX .OR.
      1D1 .GT. ZZZMAX  .OR. DB .GT. ZZZMAX .OR.
      2D2 .GT. ZZZMAX  .OR. DC .GT. ZZZMAX ) THEN
       WRITE(6,*)' **** FUNCTION HAS NOT CONVERGED ****'
       GO TO 40
       END IF
       IF ( DA .LE. ERRORM .AND. M .GT. 0 .AND.
      1DB .LE. ERRORM .AND. DC .LE. ERRORM ) GO TO 40
       GO TO 30
  40   CONTINUE
C
C      CONVERSION FROM QUAD TO SINGLE PERCISION
C
       YO = YOD*1.0
       YODF1 = YODF1D*1.0
       YODF2 = YODF2D*1.0
  50   CONTINUE
       RETURN
       SUBROUTINE IMPED0(OMEGA,Z,ZR,ZI,ZDB)
C******************************************************************
C*     THE PURPOSE OF THIS SUBROUTINE IS TO CALCULATE THE IMPEDANCE, *
C*     AT THE DRIVING POINT, OF A CIRCULAR DISK BASED UPON BESSEL    *
C*     FUNCTIONS, DISK GEOMETRY, AND DRIVING FREQUENCY.              *
C*     **** SPECIAL CASE OF N=0 ****                                 *
C******************************************************************
C*     LIST OF VARIABLE                                              *
C*     ZZ             COMPLEX IMPEDANCE, LBF-SEC/IN                   *
C*     Z              MAGNITUDE OF ZZ, LBF-SEC/IN                     *
C*     ZR             REAL PART OF ZZ, LBF-SEC/IN                     *
C*     ZI             IMAGINARY PART OF ZZ, LBF-SEC/IN                *
C*     ZDB            Z IN DB,                                        *
C*     A              PLATE RADIUS, IN                                *
C*     B              WAVEGUIDE ATTACHMENT RADIUS, IN                 *
C*     H              PLATE THICKNESS, IN                             *
C*     IMAT           TYPE OF MATERIAL                                *
C*     E              YOUNG'S MODULUS, PSI                            *
C*     G              SHEAR MODULUS, PSI                              *
C*     D              FLEXURAL RIGIDITY, PSI-IN                       *
C*     MU             POISSON'S RATIO                                 *
C*     RHO            MASS DENSITY OF PLATE, SLUGS/IN**3              *
C*     K              SHEAR COEFFICIENT                               *
C*     OMEGA          CIRCULAR FREQUENCY OF INTEREST, RAD/SEC         *
C*     DELTA1         DEMENSIONLESS PARAMETER                         *
C*     DELTA2         DEMENSIONLESS PARAMETER                         *
C*     DELTA3         DEMENSIONLESS PARAMETER                         *
C*     SIGMA1         DEMENSIONLESS PARAMETER                         *
C*     SIGMA2         DEMENSIONLESS PARAMETER                         *
C*     RR             DEMENSIONLESS PARAMETER                         *
C*     S              DEMENSIONLESS PARAMETER                         *
C*     L4             DEMENSIONLESS PARAMETER                         *
C*     PI             3.14....                                        *
C*     ANSX           INTERMEDIATE STEP  X ANSWERS                    *
C******************************************************************
       IMPLICIT COMPLEX*8 (A,D,J,S,Y)
       COMPLEX*8 ZZ,E,G
       REAL MU,A,K
       COMMON/BESS1A/J1A,J1DF1A,J1DF2A,Y1A,Y1DF1A,Y1DF2A
```

```
      COMMON/BESS1B/J1B,J1DF1B,J1DF2B,Y1B,Y1DF1B,Y1DF2B
      COMMON/BESS2A/J2A,J2DF1A,J2DF2A,Y2A,Y2DF1A,Y2DF2A
      COMMON/BESS2B/J2B,J2DF1B,J2DF2B,Y2B,Y2DF1B,Y2DF2B
      COMMON/BESS3A/J3A,J3DF1A,J3DF2A,Y3A,Y3DF1A,Y3DF2A
      COMMON/BESS3B/J3B,J3DF1B,J3DF2B,Y3B,Y3DF1B,Y3DF2B
      COMMON/GEOMTY/A,B,H,K
      COMMON/MAT/IMAT,E,G,MU,RHO,TEMP
      COMMON/CONST1/DELTA1,DELTA2,DELTA3,SIGMA1,SIGMA2
      PI=ACOS(-1.0)
C
C
C     IMPEDANCE CALCULATION, FROM REDUCE PROGRAM
C
      ANS4=Y2DF1B*J2DF1A*Y1DF1A*J1DF1B*MU*SIGMA2**2-
    . 2.*Y2DF1B*J2DF1A*Y1DF1A*J1DF1B*MU*SIGMA2*
    . SIGMA1+Y2DF1B*J2DF1A*Y1DF1A*J1DF1B*MU*SIGMA1
    . **2+Y2DF1B*J2DF1A*Y1DF1B*J1DF1A*SIGMA2**2*
    . SIGMA1*DELTA1-Y2DF1B*J2DF1A*Y1DF1B*J1DF1A*
    . SIGMA2**2*DELTA1-Y2DF1B*J2DF1A*Y1DF1B*J1DF1A*
    . SIGMA2*SIGMA1**2*DELTA1+Y2DF1B*J2DF1A*Y1DF1B*
    . J1DF1A*SIGMA2*SIGMA1*DELTA1-Y2DF1B*J2DF1A*Y1DF1B
    . *J1DF1A*MU*SIGMA2**2+2.*Y2DF1B*J2DF1A*Y1DF1B
    . *J1DF1A*MU*SIGMA2*SIGMA1-Y2DF1B*J2DF1A*Y1DF1B
    . *J1DF1A*MU*SIGMA1**2
      ANS3=Y2DF1A*J2DF1B*Y1DF1B*J1DF1A*SIGMA2*SIGMA1
    . **2*DELTA1-Y2DF1A*J2DF1B*Y1DF1B*J1DF1A*SIGMA2
    . *SIGMA1*DELTA1+Y2DF1A*J2DF1B*Y1DF1B*J1DF1A*MU
    . *SIGMA2**2-2.*Y2DF1A*J2DF1B*Y1DF1B*J1DF1A*MU*
    . SIGMA2*SIGMA1+Y2DF1A*J2DF1B*Y1DF1B*J1DF1A*MU*
    . SIGMA1**2+Y2DF1B*J2DF2A*Y1DF1A*J1DF1B*SIGMA2
    . **2*SIGMA1*DELTA2-Y2DF1B*J2DF2A*Y1DF1A*J1DF1B
    . *SIGMA2*SIGMA1**2*DELTA2-Y2DF1B*J2DF2A*Y1DF1A*
    . J1DF1B*SIGMA2*SIGMA1*DELTA2+Y2DF1B*J2DF2A*Y1DF1A
    . *J1DF1B*SIGMA1**2*DELTA2-Y2DF1B*J2DF2A*Y1DF1B
    . *J1DF1A*SIGMA2**2*SIGMA1*DELTA2+Y2DF1B*J2DF2A
    . *Y1DF1B*J1DF1A*SIGMA2*SIGMA1**2*DELTA2+Y2DF1B*
    . J2DF2A*Y1DF1B*J1DF1A*SIGMA2*SIGMA1*DELTA2-Y2DF1B
    . *J2DF2A*Y1DF1B*J1DF1A*SIGMA1**2*DELTA2-Y2DF1B
    . *J2DF1A*Y1DF2A*J1DF1B*SIGMA2**2*SIGMA1*DELTA1
    . +Y2DF1B*J2DF1A*Y1DF2A*J1DF1B*SIGMA2**2*DELTA1
    . +Y2DF1B*J2DF1A*Y1DF2A*J1DF1B*SIGMA2*SIGMA1**2
    . *DELTA1-Y2DF1B*J2DF1A*Y1DF2A*J1DF1B*SIGMA2*
    . SIGMA1*DELTA1+ANS4
      ANS2=-Y2DF2A*J2DF1B*Y1DF1A*J1DF1B*SIGMA2**2*
    . SIGMA1*DELTA2+Y2DF2A*J2DF1B*Y1DF1A*J1DF1B*
    . SIGMA2*SIGMA1**2*DELTA2+Y2DF2A*J2DF1B*Y1DF1A*
    . J1DF1B*SIGMA2*SIGMA1*DELTA2-Y2DF2A*J2DF1B*Y1DF1A
    . *J1DF1B*SIGMA1**2*DELTA2+Y2DF2A*J2DF1B*Y1DF1B
    . *J1DF1A*SIGMA2**2*SIGMA1*DELTA2-Y2DF2A*J2DF1B
    . *Y1DF1B*J1DF1A*SIGMA2*SIGMA1**2*DELTA2-Y2DF2A*
    . J2DF1B*Y1DF1B*J1DF1A*SIGMA2*SIGMA1*DELTA2+Y2DF2A
    . *J2DF1B*Y1DF1B*J1DF1A*SIGMA1**2*DELTA2+Y2DF1A
    . *J2DF1B*Y1DF2A*J1DF1B*SIGMA2**2*SIGMA1*DELTA1
    . -Y2DF1A*J2DF1B*Y1DF2A*J1DF1B*SIGMA2**2*DELTA1
    . -Y2DF1A*J2DF1B*Y1DF2A*J1DF1B*SIGMA2*SIGMA1**2
    . *DELTA1+Y2DF1A*J2DF1B*Y1DF2A*J1DF1B*SIGMA2*
    . SIGMA1*DELTA1-Y2DF1A*J2DF1B*Y1DF1A*J1DF1B*MU*
    . SIGMA2**2+2.*Y2DF1A*J2DF1B*Y1DF1A*J1DF1B*MU*
    . SIGMA2*SIGMA1-Y2DF1A*J2DF1B*Y1DF1A*J1DF1B*MU*
    . SIGMA1**2-Y2DF1A*J2DF1B*Y1DF1B*J1DF1A*SIGMA2
    . **2*SIGMA1*DELTA1+Y2DF1A*J2DF1B*Y1DF1B*J1DF1A
```

```
  .  *SIGMA2**2*DELTA1+ANS3
ANS1=2.*B*G*H*K**2*PI*DELTA2*DELTA1*ANS2
ANS13=Y2B*J2DF1B*Y1DF1A*J1DF1A*SIGMA2*SIGMA1**
  .  2*DELTA1**2-Y2B*J2DF1B*Y1DF1A*J1DF1A*SIGMA2*
  .  SIGMA1*DELTA1**2-Y2B*J2DF1B*Y1DF1A*J1DF1A*
  .  SIGMA1**2*DELTA1**2+Y2B*J2DF1B*Y1DF1A*J1DF1A*
  .  SIGMA1*DELTA1**2
ANS12=-2.*Y2B*J2DF1A*Y1DF2A*J1DF1B*SIGMA2*
  .  SIGMA1*DELTA1**2+Y2B*J2DF1A*Y1DF2A*J1DF1B*
  .  SIGMA2*DELTA1**2-Y2B*J2DF1A*Y1DF1A*J1DF1B*MU*
  .  SIGMA2*SIGMA1*DELTA1+Y2B*J2DF1A*Y1DF1A*J1DF1B
  .  *MU*SIGMA2*DELTA1+Y2B*J2DF1A*Y1DF1A*J1DF1B*MU
  .  *SIGMA1**2*DELTA1-Y2B*J2DF1A*Y1DF1A*J1DF1B*MU
  .  *SIGMA1*DELTA1-Y2B*J2DF1A*Y1DF1B*J1DF1A*
  .  SIGMA2*SIGMA1**2*DELTA1**2+2.*Y2B*J2DF1A*Y1DF1B*
  .  J1DF1A*SIGMA2*SIGMA1*DELTA1**2-Y2B*J2DF1A*Y1DF1B
  .  *J1DF1A*SIGMA2*DELTA1**2+Y2B*J2DF1A*Y1DF1B
  .  *J1DF1A*MU*SIGMA2*SIGMA1*DELTA1-Y2B*J2DF1A*
  .  Y1DF1B*J1DF1A*MU*SIGMA2*DELTA1-Y2B*J2DF1A*
  .  Y1DF1B*J1DF1A*MU*SIGMA1**2*DELTA1+Y2B*J2DF1A*
  .  Y1DF1B*J1DF1A*MU*SIGMA1*DELTA1-Y2B*J2DF1B*
  .  Y1DF2A*J1DF1A*SIGMA2*SIGMA1**2*DELTA1**2+Y2B*
  .  J2DF1B*Y1DF2A*J1DF1A*SIGMA2*SIGMA1*DELTA1**2+Y2B
  .  *J2DF1B*Y1DF2A*J1DF1A*SIGMA1**2*DELTA1**2-Y2B
  .  *J2DF1B*Y1DF2A*J1DF1A*SIGMA1*DELTA1**2+ANS13
ANS11=-Y2DF1B*J2B*Y1DF2A*J1DF1A*SIGMA2*SIGMA1*
  .  DELTA1**2-Y2DF1B*J2B*Y1DF2A*J1DF1A*SIGMA1**2*
  .  DELTA1**2+Y2DF1B*J2B*Y1DF2A*J1DF1A*SIGMA1*
  .  DELTA1**2-Y2DF1B*J2B*Y1DF1A*J1DF1A*SIGMA2*
  .  SIGMA1**2*DELTA1**2+Y2DF1B*J2B*Y1DF1A*J1DF1A*
  .  SIGMA2*SIGMA1*DELTA1**2+Y2DF1B*J2B*Y1DF1A*J1DF1A
  .  *SIGMA1**2*DELTA1**2-Y2DF1B*J2B*Y1DF1A*J1DF1A
  .  *SIGMA1*DELTA1**2-Y2B*J2DF2A*Y1DF1A*J1DF1B
  .  *SIGMA2*SIGMA1**2*DELTA2*DELTA1+Y2B*J2DF2A*Y1DF1A
  .  *J1DF1B*SIGMA2*SIGMA1*DELTA2*DELTA1+Y2B*J2DF2A*
  .  Y1DF1A*J1DF1B*SIGMA1**2*DELTA2*DELTA1-Y2B*J2DF2A
  .  *Y1DF1A*J1DF1B*SIGMA1*DELTA2*DELTA1+Y2B*
  .  J2DF2A*Y1DF1B*J1DF1A*SIGMA2*SIGMA1**2*DELTA2*
  .  DELTA1-Y2B*J2DF2A*Y1DF1B*J1DF1A*SIGMA2*SIGMA1
  .  *DELTA2*DELTA1-Y2B*J2DF2A*Y1DF1B*J1DF1A*
  .  SIGMA1**2*DELTA2*DELTA1+Y2B*J2DF2A*Y1DF1B*J1DF1A
  .  *SIGMA1*DELTA2*DELTA1+Y2B*J2DF1A*Y1DF2A*
  .  J1DF1B*SIGMA2*SIGMA1**2*DELTA1**2+ANS12
ANS10=-Y2DF1B*J2DF1A*Y1DF2A*J1B*SIGMA2**2*
  .  SIGMA1*DELTA2*DELTA1+Y2DF1B*J2DF1A*Y1DF2A*J1B
  .  *SIGMA2**2*DELTA2*DELTA1+Y2DF1B*J2DF1A*Y1DF2A*
  .  J1B*SIGMA2*SIGMA1*DELTA2*DELTA1-Y2DF1B*J2DF1A*
  .  Y1DF2A*J1B*SIGMA2*DELTA2*DELTA1+Y2DF1B*J2DF1A
  .  *Y1DF1A*J1B*MU*SIGMA2**2*DELTA2-Y2DF1B*J2DF1A
  .  *Y1DF1A*J1B*MU*SIGMA2*SIGMA1*DELTA2-Y2DF1B*
  .  J2DF1A*Y1DF1A*J1B*MU*SIGMA2*DELTA2+Y2DF1B*
  .  J2DF1A*Y1DF1A*J1B*MU*SIGMA1*DELTA2+Y2DF1B*
  .  J2DF1A*Y1B*J1DF1A*SIGMA2**2*SIGMA1*DELTA2*DELTA1
  .  -Y2DF1B*J2DF1A*Y1B*J1DF1A*SIGMA2**2*DELTA2*
  .  DELTA1-Y2DF1B*J2DF1A*Y1B*J1DF1A*SIGMA2*SIGMA1
  .  *DELTA2*DELTA1+Y2DF1B*J2DF1A*Y1B*J1DF1A*
  .  SIGMA2*DELTA2*DELTA1-Y2DF1B*J2DF1A*Y1B*J1DF1A
  .  *MU*SIGMA2**2*DELTA2+Y2DF1B*J2DF1A*Y1B*J1DF1A
  .  *MU*SIGMA2*SIGMA1*DELTA2+Y2DF1B*J2DF1A*Y1B*
  .  J1DF1A*MU*SIGMA2*DELTA2-Y2DF1B*J2DF1A*Y1B*
```

```
. J1DF1A*MU*SIGMA1*DELTA2+Y2DF1B*J2B*Y1DF2A*
. J1DF1A*SIGMA2*SIGMA1**2*DELTA1**2+ANS11
 ANS9=Y2DF1A*J2B*Y1DF1A*J1DF1B*MU*SIGMA2*SIGMA1
. *DELTA1-Y2DF1A*J2B*Y1DF1A*J1DF1B*MU*SIGMA2*
. DELTA1-Y2DF1A*J2B*Y1DF1A*J1DF1B*MU*SIGMA1**2*
. DELTA1+Y2DF1A*J2B*Y1DF1A*J1DF1B*MU*SIGMA1**2*
. DELTA1+Y2DF1A*J2B*Y1DF1B*J1DF1A*SIGMA2*SIGMA1
. **2*DELTA1**2-2.*Y2DF1A*J2B*Y1DF1B*J1DF1A*
. SIGMA2*SIGMA1*DELTA1**2+Y2DF1A*J2B*Y1DF1B*J1DF1A
. *SIGMA2*DELTA1**2-Y2DF1A*J2B*Y1DF1B*J1DF1A
. *MU*SIGMA2*SIGMA1*DELTA1+Y2DF1A*J2B*Y1DF1B*
. J1DF1A*MU*SIGMA2*DELTA1+Y2DF1A*J2B*Y1DF1B*
. J1DF1A*MU*SIGMA1**2*DELTA1-Y2DF1A*J2B*Y1DF1B*
. J1DF1A*MU*SIGMA1*DELTA1+Y2DF1B*J2DF2A*Y1DF1A*
. J1B*SIGMA2**2*SIGMA1*DELTA2**2-2.*Y2DF1B*J2DF2A*
. Y1DF1A*J1B*SIGMA2*SIGMA1*DELTA2**2+Y2DF1B*J2DF2A
. *Y1DF1A*J1B*SIGMA1*DELTA2**2-Y2DF1B*J2DF2A
. *Y1B*J1DF1A*SIGMA2**2*SIGMA1*DELTA2**2+2.*Y2DF1B
. *J2DF2A*Y1B*J1DF1A*SIGMA2*SIGMA1*DELTA2**2-
. Y2DF1B*J2DF2A*Y1B*J1DF1A*SIGMA1*DELTA2**2+
. ANS10
 ANS8=-Y2DF1A*J2DF1B*Y1DF2A*J1B*SIGMA2*SIGMA1*
. DELTA2*DELTA1+Y2DF1A*J2DF1B*Y1DF2A*J1B*SIGMA2
. *DELTA2*DELTA1-Y2DF1A*J2DF1B*Y1DF1A*J1B*MU*
. SIGMA2**2*DELTA2+Y2DF1A*J2DF1B*Y1DF1A*J1B*MU*
. SIGMA2*SIGMA1*DELTA2+Y2DF1A*J2DF1B*Y1DF1A*J1B
. *MU*SIGMA2*DELTA2-Y2DF1A*J2DF1B*Y1DF1A*J1B*MU
. *SIGMA1*DELTA2-Y2DF1A*J2DF1B*Y1B*J1DF1A*
. SIGMA2**2*SIGMA1*DELTA2*DELTA1+Y2DF1A*J2DF1B*Y1B
. *J1DF1A*SIGMA2**2*DELTA2*DELTA1+Y2DF1A*J2DF1B*
. Y1B*J1DF1A*SIGMA2*SIGMA1*DELTA2*DELTA1-Y2DF1A*
. J2DF1B*Y1B*J1DF1A*SIGMA2*DELTA2*DELTA1+Y2DF1A
. *J2DF1B*Y1B*J1DF1A*MU*SIGMA2**2*DELTA2-Y2DF1A
. *J2DF1B*Y1B*J1DF1A*MU*SIGMA2*SIGMA1*DELTA2-
. Y2DF1A*J2DF1B*Y1B*J1DF1A*MU*SIGMA2*DELTA2+
. Y2DF1A*J2DF1B*Y1B*J1DF1A*MU*SIGMA1*DELTA2-
. Y2DF1A*J2B*Y1DF2A*J1DF1B*SIGMA2*SIGMA1**2*
. DELTA1**2+2.*Y2DF1A*J2B*Y1DF2A*J1DF1B*SIGMA2*
. SIGMA1*DELTA1**2-Y2DF1A*J2B*Y1DF2A*J1DF1B*
. SIGMA2*DELTA1**2+ANS9
 ANS7=-Y2DF2A*J2B*Y1DF1A*J1DF1B*SIGMA1**2*
. DELTA2*DELTA1+Y2DF2A*J2B*Y1DF1A*J1DF1B*SIGMA1
. *DELTA2*DELTA1-Y2DF2A*J2B*Y1DF1B*J1DF1A*
. SIGMA2*SIGMA1**2*DELTA2*DELTA1+Y2DF2A*J2B*Y1DF1B
. *J1DF1A*SIGMA2*SIGMA1*DELTA2*DELTA1+Y2DF2A*J2B*
. Y1DF1B*J1DF1A*SIGMA1**2*DELTA2*DELTA1-Y2DF2A*J2B
. *Y1DF1B*J1DF1A*SIGMA1*DELTA2*DELTA1-Y2DF1A*
. J2DF2A*Y1DF1B*J1B*SIGMA2**2*SIGMA1*DELTA2**2+
. Y2DF1A*J2DF2A*Y1DF1B*J1B*SIGMA2**2*DELTA2**2+
. Y2DF1A*J2DF2A*Y1DF1B*J1B*SIGMA2*SIGMA1*DELTA2
. **2-Y2DF1A*J2DF2A*Y1DF1B*J1B*SIGMA2*DELTA2**2
. +Y2DF1A*J2DF2A*Y1B*J1DF1B*SIGMA2**2*SIGMA1*
. DELTA2**2-Y2DF1A*J2DF2A*Y1B*J1DF1B*SIGMA2**2*
. DELTA2**2-Y2DF1A*J2DF2A*Y1B*J1DF1B*SIGMA2*
. SIGMA1*DELTA2**2+Y2DF1A*J2DF2A*Y1B*J1DF1B*
. SIGMA2*DELTA2**2+Y2DF1A*J2DF1B*Y1DF2A*J1B*
. SIGMA2**2*SIGMA1*DELTA2*DELTA1-Y2DF1A*J2DF1B*Y1DF2A
. *J1B*SIGMA2**2*DELTA2*DELTA1+ANS8
 ANS6=Y2DF2A*J2DF1A*Y1DF1B*J1B*SIGMA2**2*SIGMA1
. *DELTA2**2-Y2DF2A*J2DF1A*Y1DF1B*J1B*SIGMA2**2
```

```
       .  *DELTA2**2-Y2DF2A*J2DF1A*Y1DF1B*J1B*SIGMA2*
       .  SIGMA1*DELTA2**2+Y2DF2A*J2DF1A*Y1DF1B*J1B*
       .  SIGMA2*DELTA2**2-Y2DF2A*J2DF1A*Y1B*J1DF1B*
       .  SIGMA2**2*SIGMA1*DELTA2**2+Y2DF2A*J2DF1A*Y1B*
       .  J1DF1B*SIGMA2**2*DELTA2**2+Y2DF2A*J2DF1A*Y1B*
       .  J1DF1B*SIGMA2*SIGMA1*DELTA2**2-Y2DF2A*J2DF1A*Y1B
       .  *J1DF1B*SIGMA2*DELTA2**2-Y2DF2A*J2DF1B*Y1DF1A
       .  *J1B*SIGMA2**2*SIGMA1*DELTA2**2+2.*Y2DF2A*J2DF1B
       .  *Y1DF1A*J1B*SIGMA2*SIGMA1*DELTA2**2-Y2DF2A*
       .  J2DF1B*Y1DF1A*J1B*SIGMA1*DELTA2**2+Y2DF2A*
       .  J2DF1B*Y1B*J1DF1A*SIGMA2**2*SIGMA1*DELTA2**2-2.*
       .  Y2DF2A*J2DF1B*Y1B*J1DF1A*SIGMA2*SIGMA1*DELTA2
       .  **2+Y2DF2A*J2DF1B*Y1B*J1DF1A*SIGMA1*DELTA2**2
       .  +Y2DF2A*J2B*Y1DF1A*J1DF1B*SIGMA2*SIGMA1**2*
       .  DELTA2*DELTA1-Y2DF2A*J2B*Y1DF1A*J1DF1B*SIGMA2
       .  *SIGMA1*DELTA2*DELTA1+ANS7
          ANS5=A*OMEGA*ANS6*(0.0,-1.0)
C
C
C       IMPEDANCE
C
        ZZ = ANS1/ANS5
C
C       REAL PART OF IMPEDANCE
C
        ZR = REAL(ZZ)
C
C
C       IMAGINARY PART OF IMPEDANCE
C
        ZI = AIMAG(ZZ)
C
C
C       MAGNITUDE OF IMPEDANCE
C
        Z = CABS(ZZ)
C
C
C       DB OF IMPEDANCE
C
        ZDB = 20.0*LOG10(Z)
        RETURN
        END
```
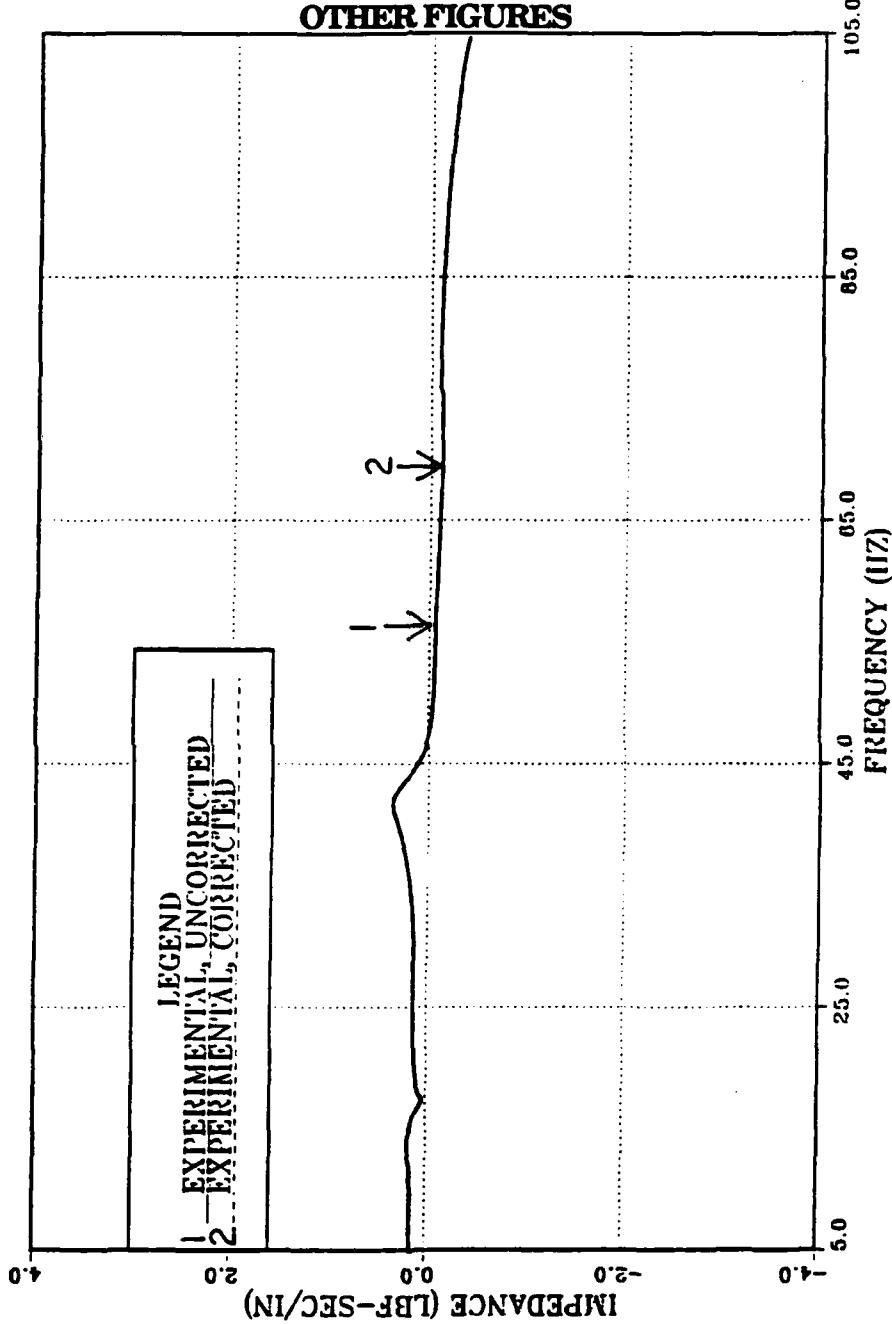
Figure 66. Experimental Real Part of the Driving Point Impedance of a 6 in Radius Elastic Plate, With and Without Shaker and Mount Correction, in the Frequency Range of 5 to 105 Hz.

130
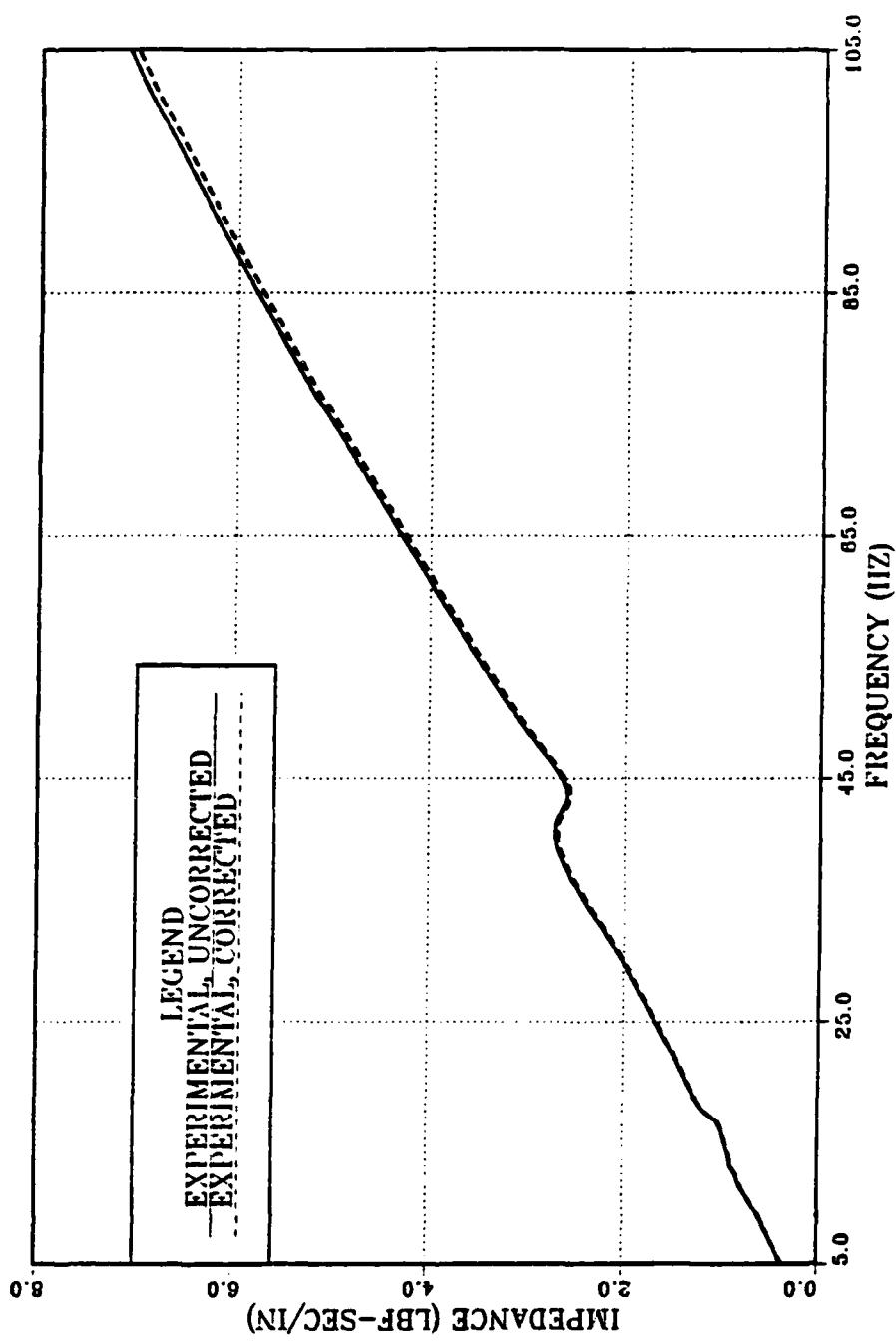
Figure 67. Experimental Imaginary Part of the Driving Point
Impedance of a 6 in Radius Elastic Plate, With and
Without Shaker and Mount Correction, in the Frequency
Range of 5 to 105 Hz.

131
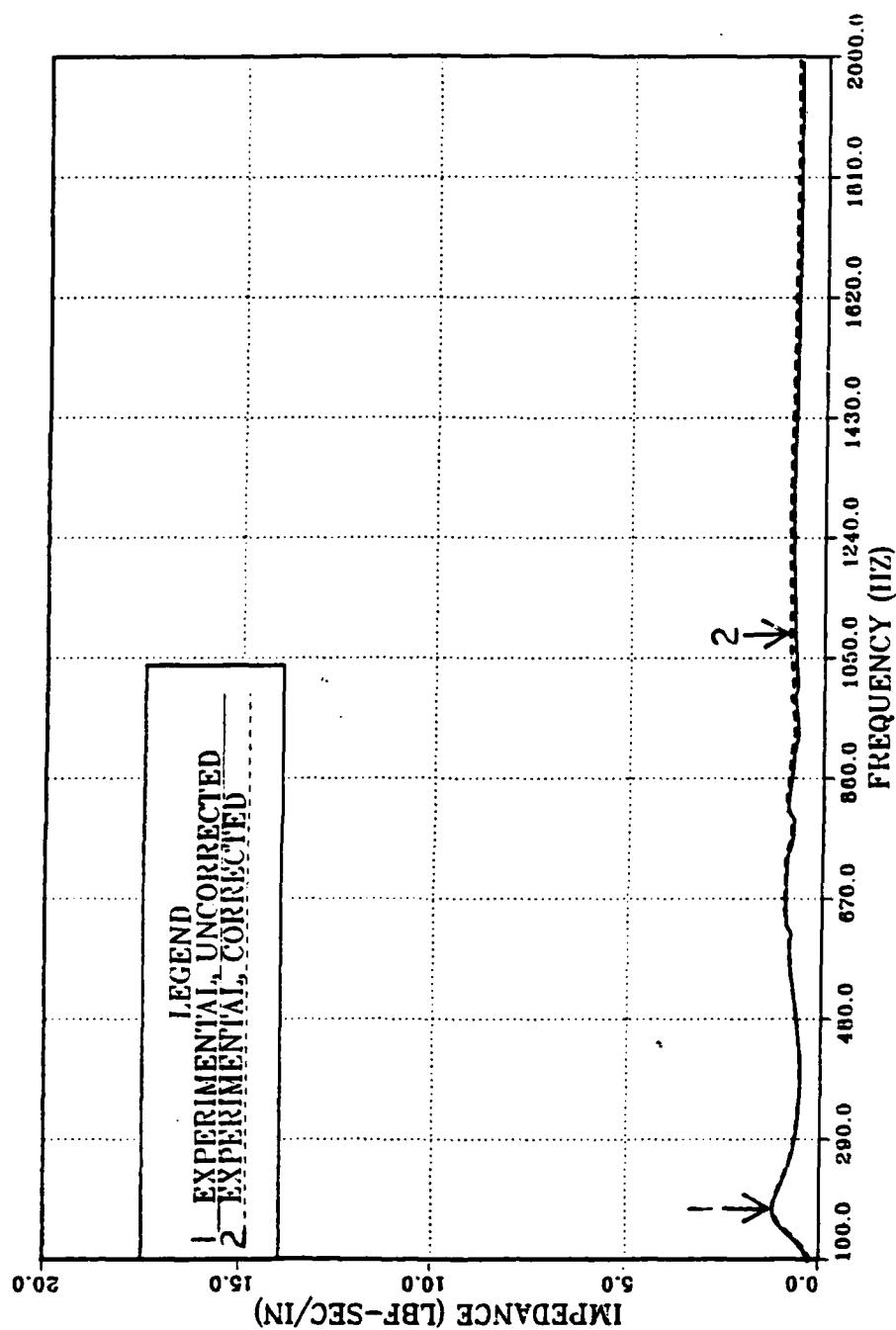
Figure 68. Experimental Real Part of the Driving Point Impedance of a 6 in Radius Viscoelastic Plate, With and Without Shaker and Mount Correction, in the Frequency Range of 100 to 2000 Hz at a Temperature of 100.5 Deg. F.
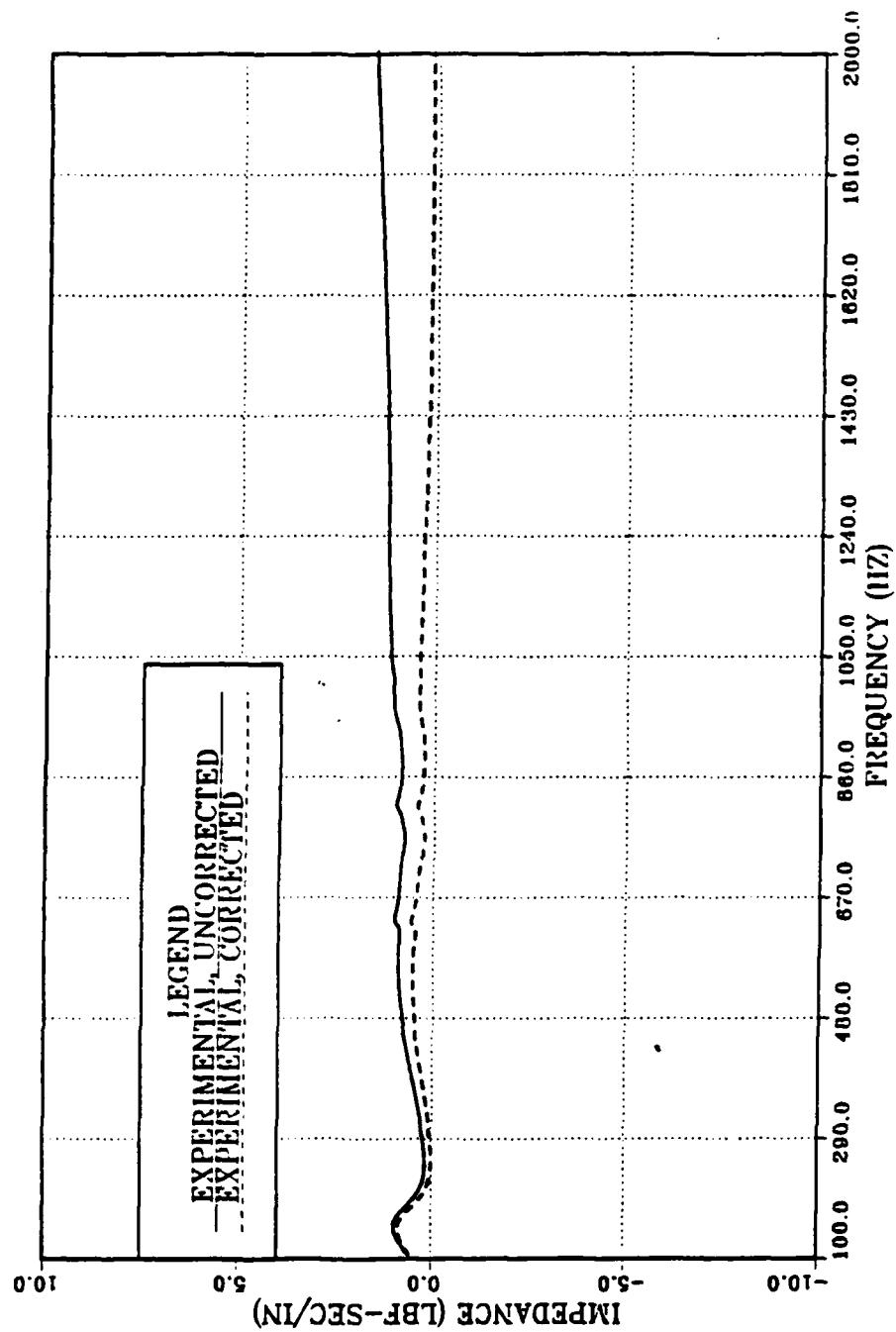
Figure 69. Experimental Imaginary Part of the Driving Point
Impedance of a 6 in Radius Viscoelastic Plate, With and
Without Shaker and Mount Correction, in the Frequency
Range of 100 to 2000 Hz at a Temperature of 100.5
Deg. F.

133
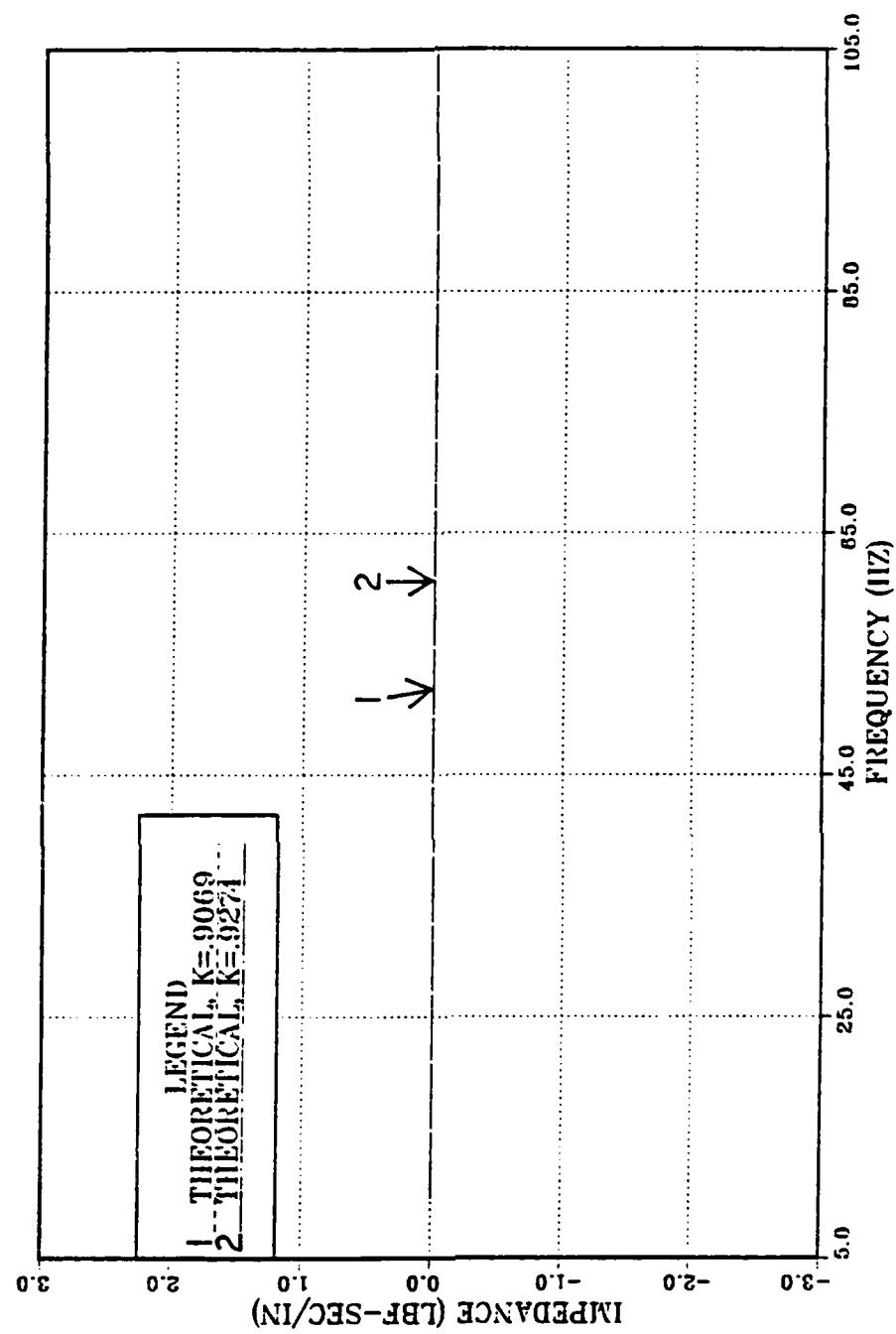
Figure 70. Effect of Shear Coefficient on the Theoretical Real Part of the Driving Point Impedance for a 5 in Radius Elastic Plate in the Frequency Range of 10 to 105 Hz.

134
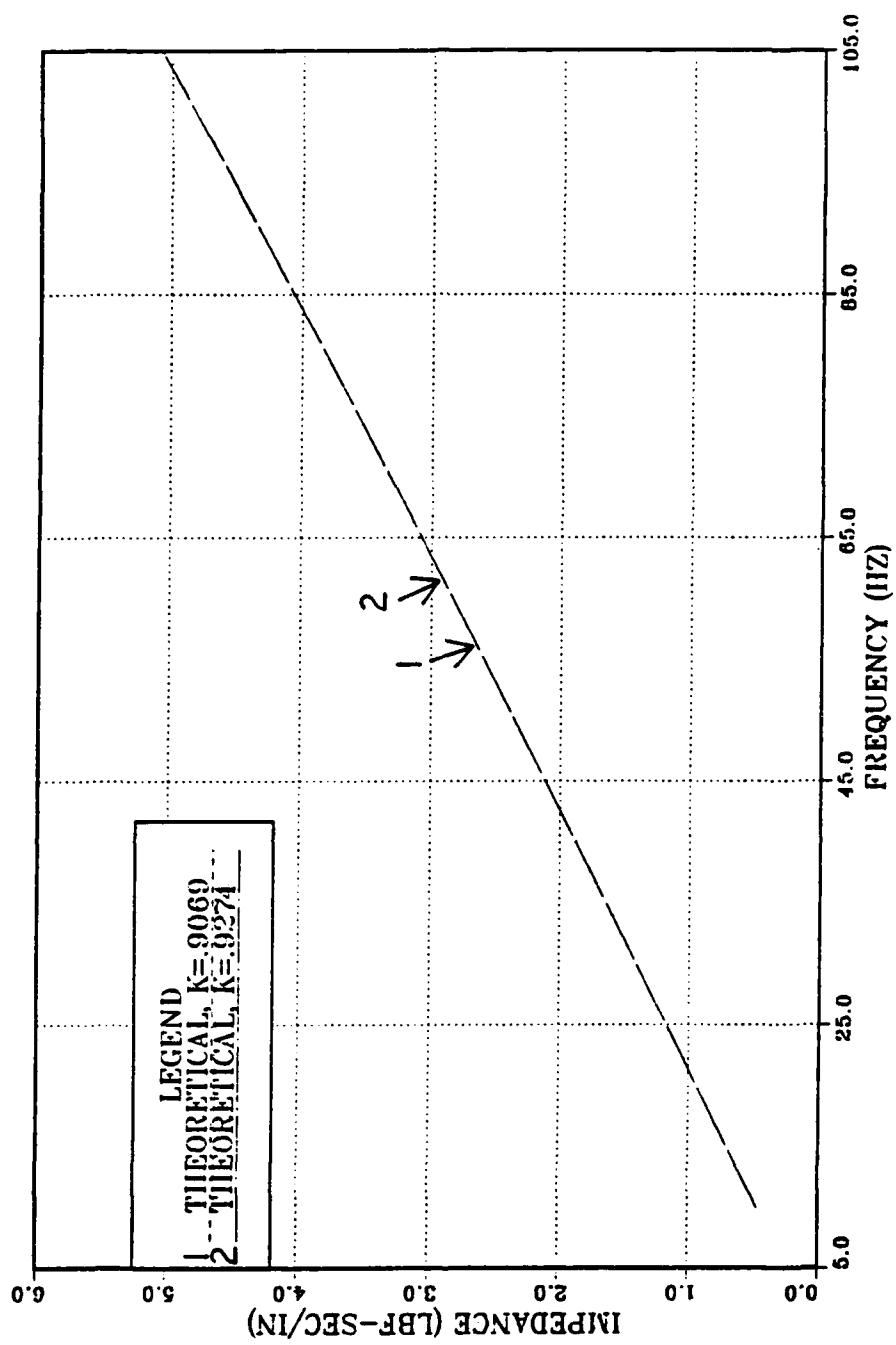
Figure 71. **Effect of Shear Coefficient on the Theoretical Imaginary Part of the Driving Point Impedance for a 5 in Radius Elastic Plate in the Frequency Range of 10 to 105 Hz.**

135
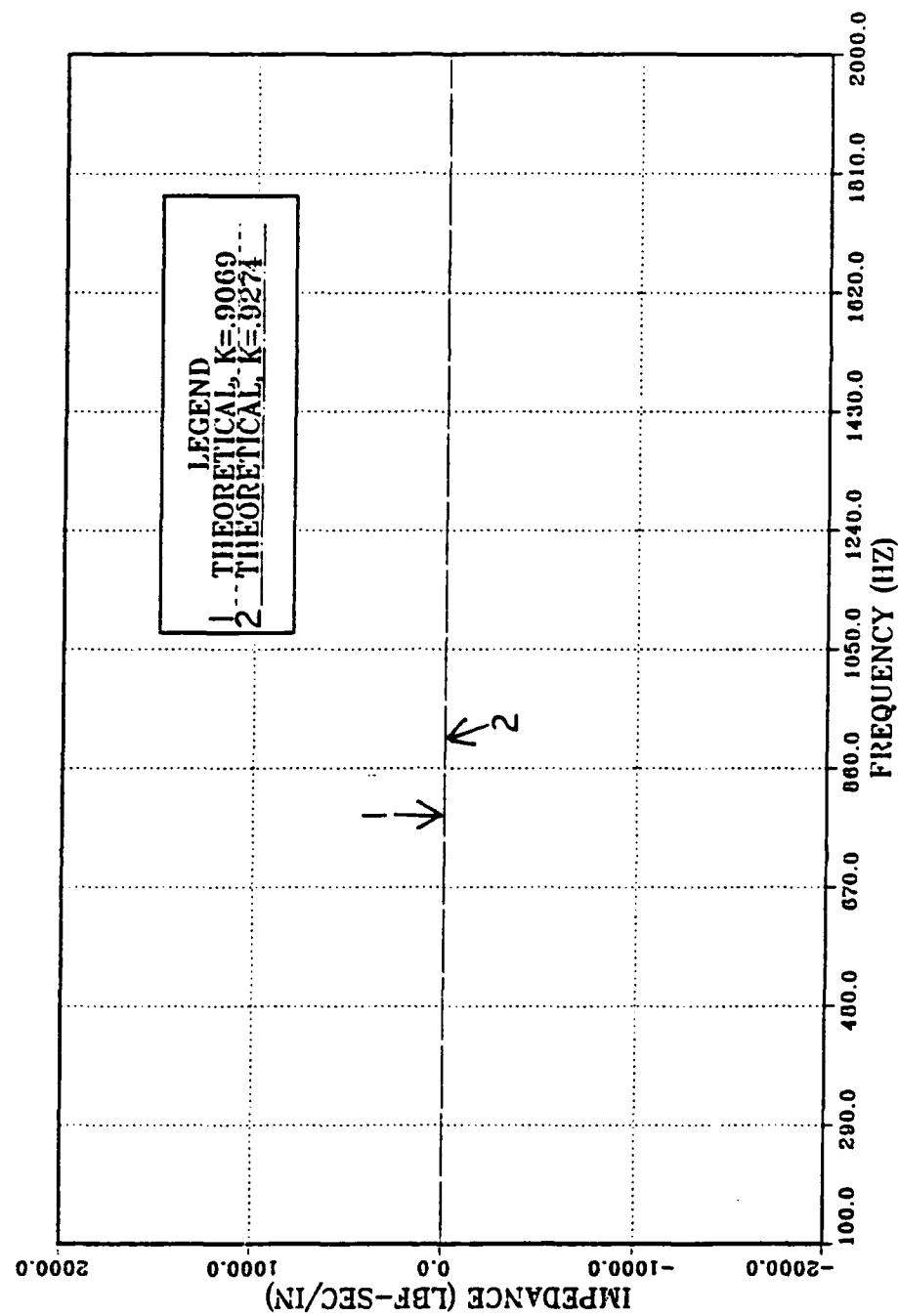
Figure 72. Effect of Shear Coefficient on the Theoretical Real Part of the Driving Point Impedance for a 5 in Radius Elastic Plate in the Frequency Range of 100 to 2000 Hz.

136
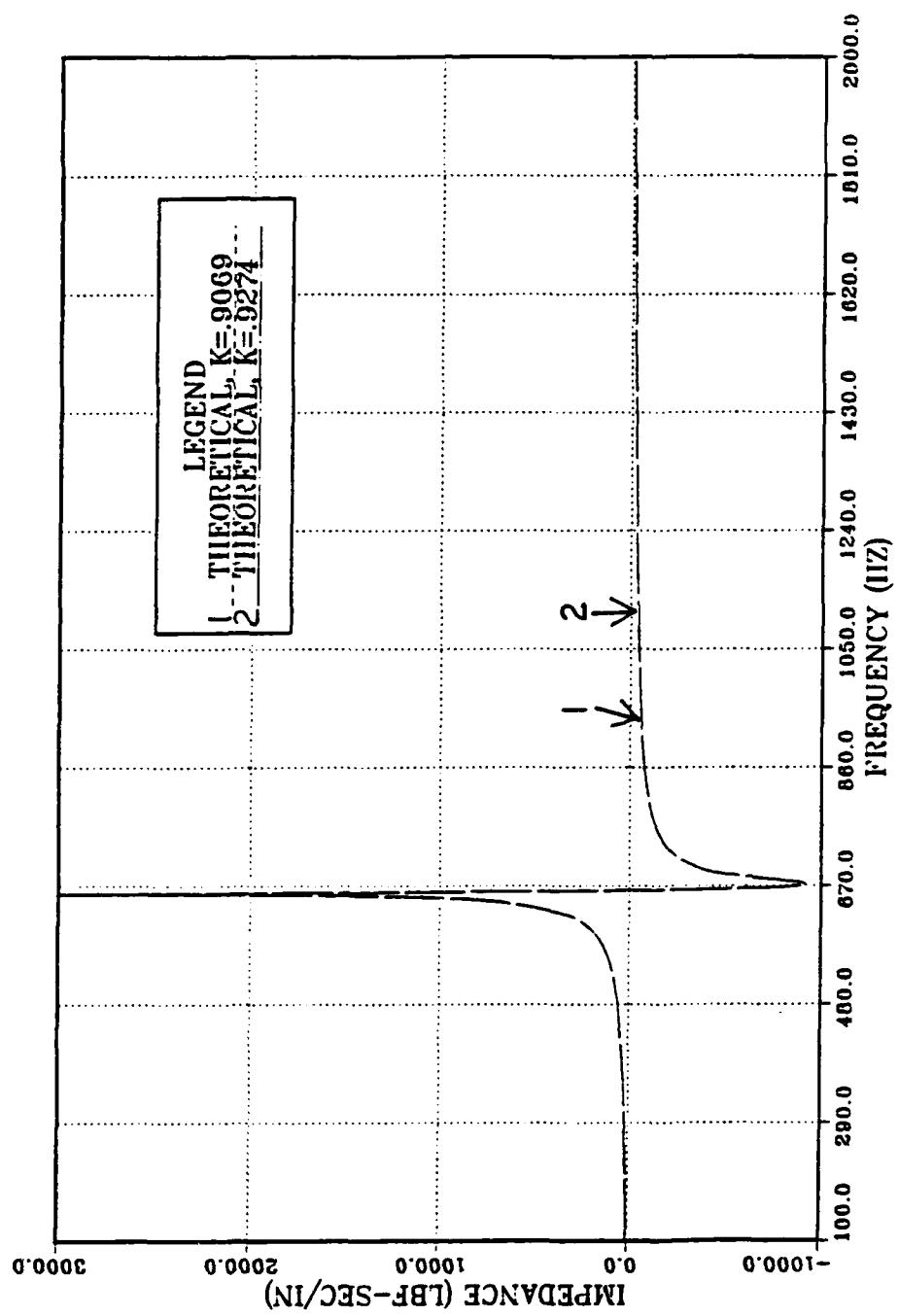
Figure 73. Effect of Shear Coefficient on the Theoretical Imaginary Part of the Driving Point Impedance for a 5 in Radius Elastic Plate in the Frequency Range of 100 to 2000 Hz.

137
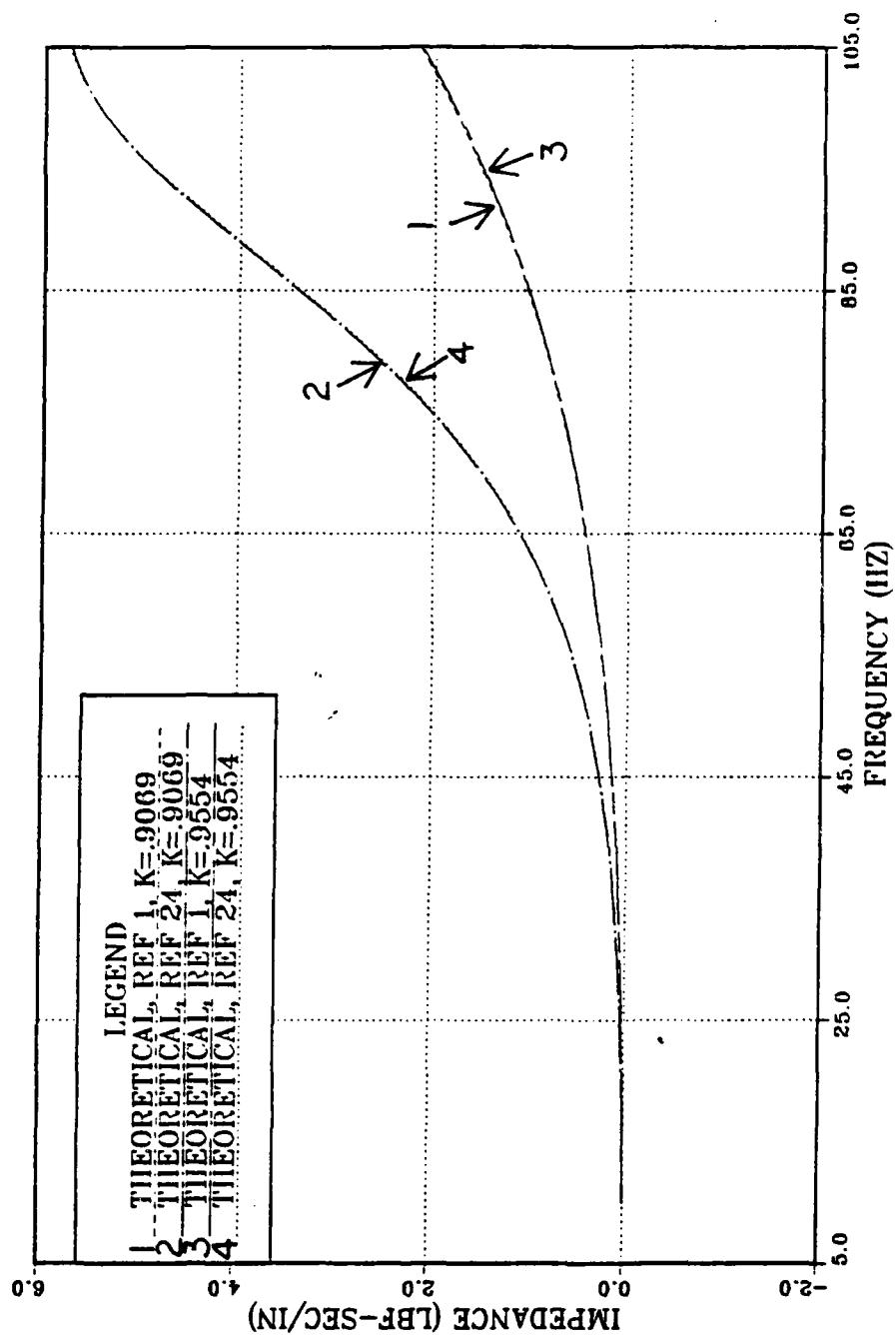
Figure 74. Effect of Shear Coefficient and Material Characteristics on
the Theoretical Real Part of the Driving Point Impedance
for a 5 in Radius Viscoelastic Plate in the Frequency
Range of 10 to 105 Hz at a Temperature of 80.0 Deg. F.

138
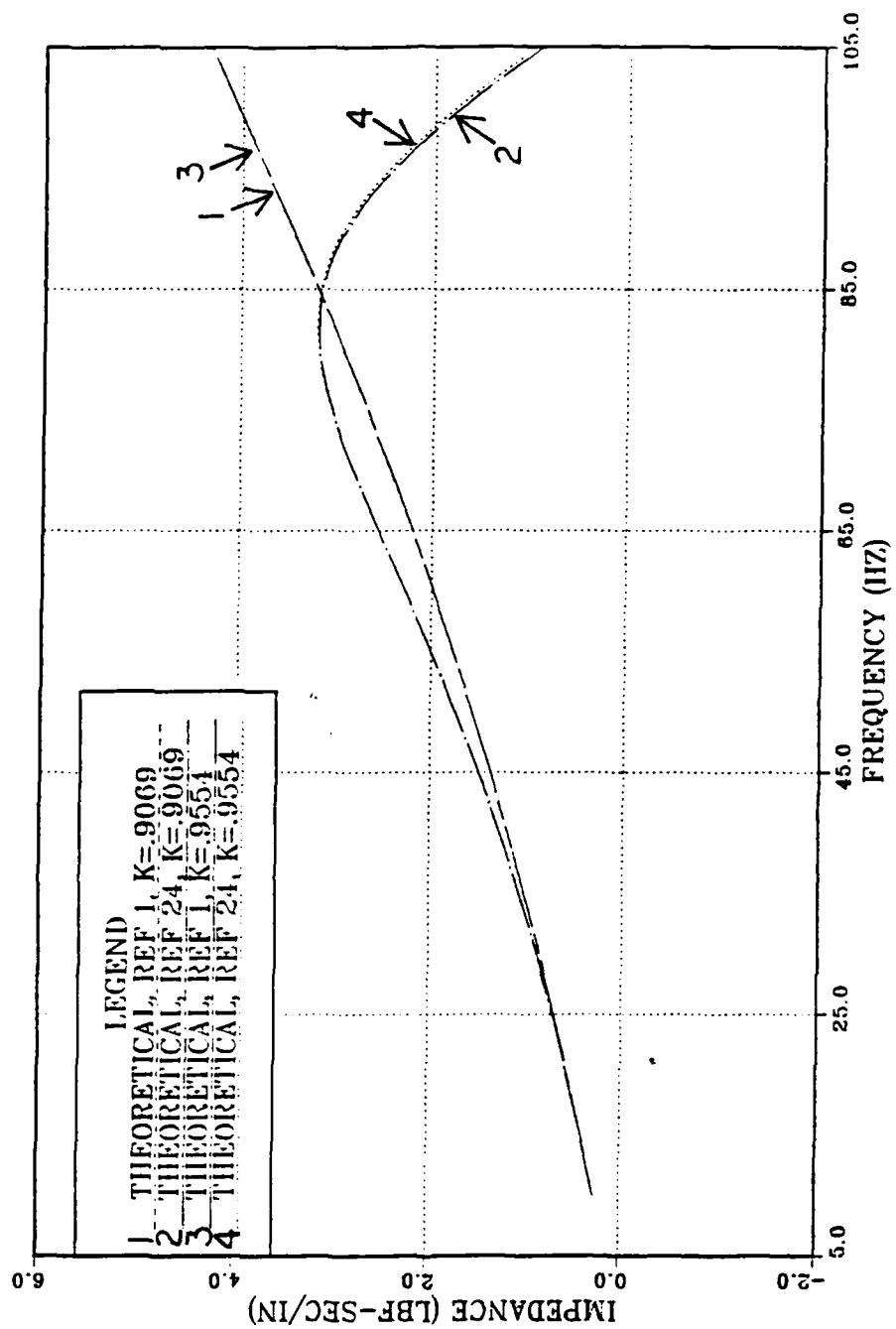
Figure 75. Effect of Shear Coefficient and Material Characteristics on the Theoretical Imaginary Part of the Driving Point Impedance for a 5 in Radius Viscoelastic Plate in the Frequency Range of 10 to 105 Hz at a Temperature of 80.0 Deg. F.

139
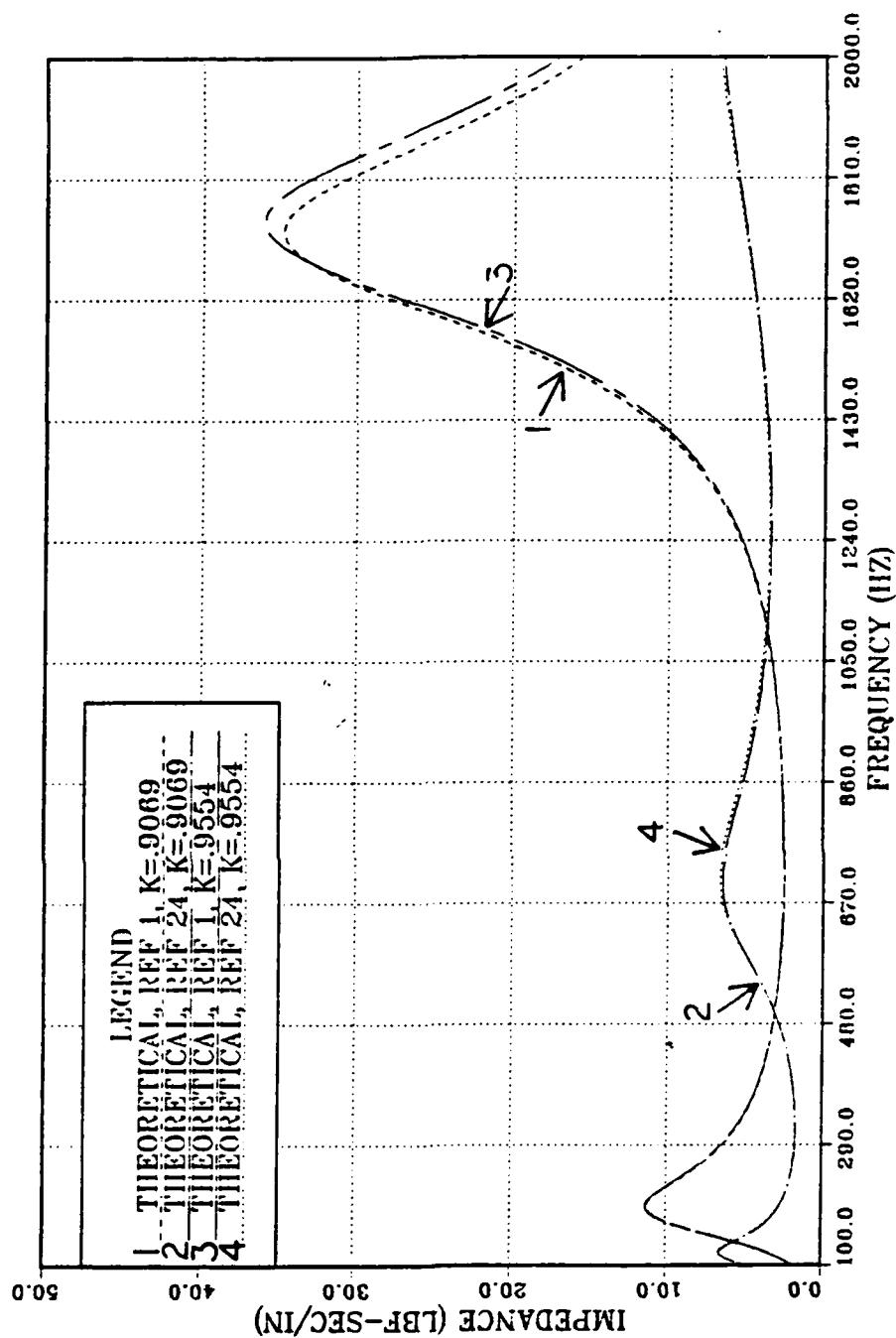
Figure 76. Effect of Shear Coefficient and Material Characteristics on the Theoretical Real Part of the Driving Point Impedance for a 5 in Radius Viscoelastic Plate in the Frequency Range of 100 to 2000 Hz at a Temperature of 77.3 Deg. F.

140
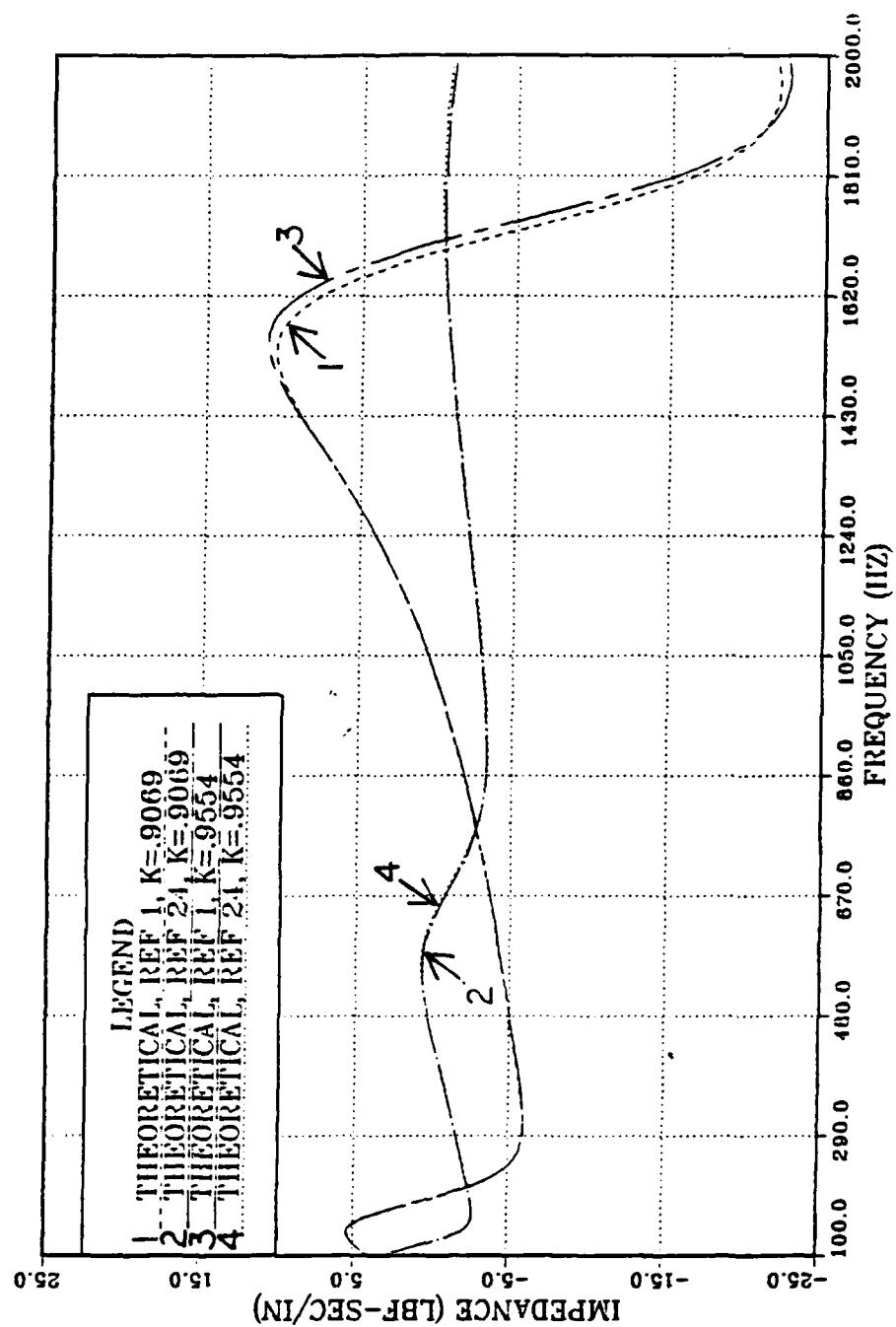
Figure 77. Effect of Shear Coefficient and Material Characteristics on the Theoretical Imaginary Part of the Driving Point Impedance for a 5 in Radius Viscoelastic Plate in the Frequency Range of 100 to 2000 Hz at a Temperature of 77.3 Deg. F.

141
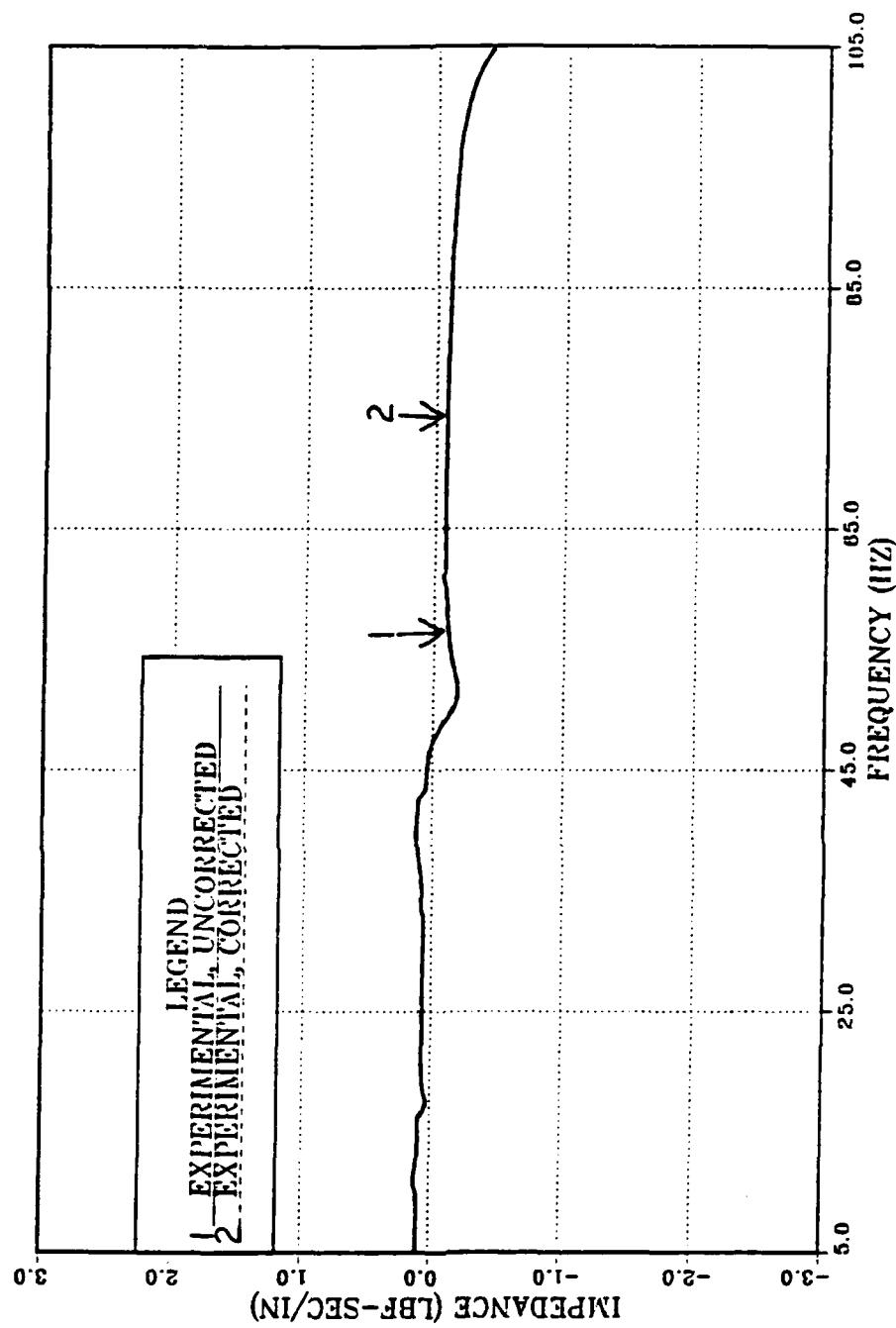
Figure 78. Experimental Real Part of the Driving Point Impedance of
a 5 in Radius Elastic Plate, With and Without Shaker and
Mount Correction, in the Frequency Range of 5 to 105 Hz.

142
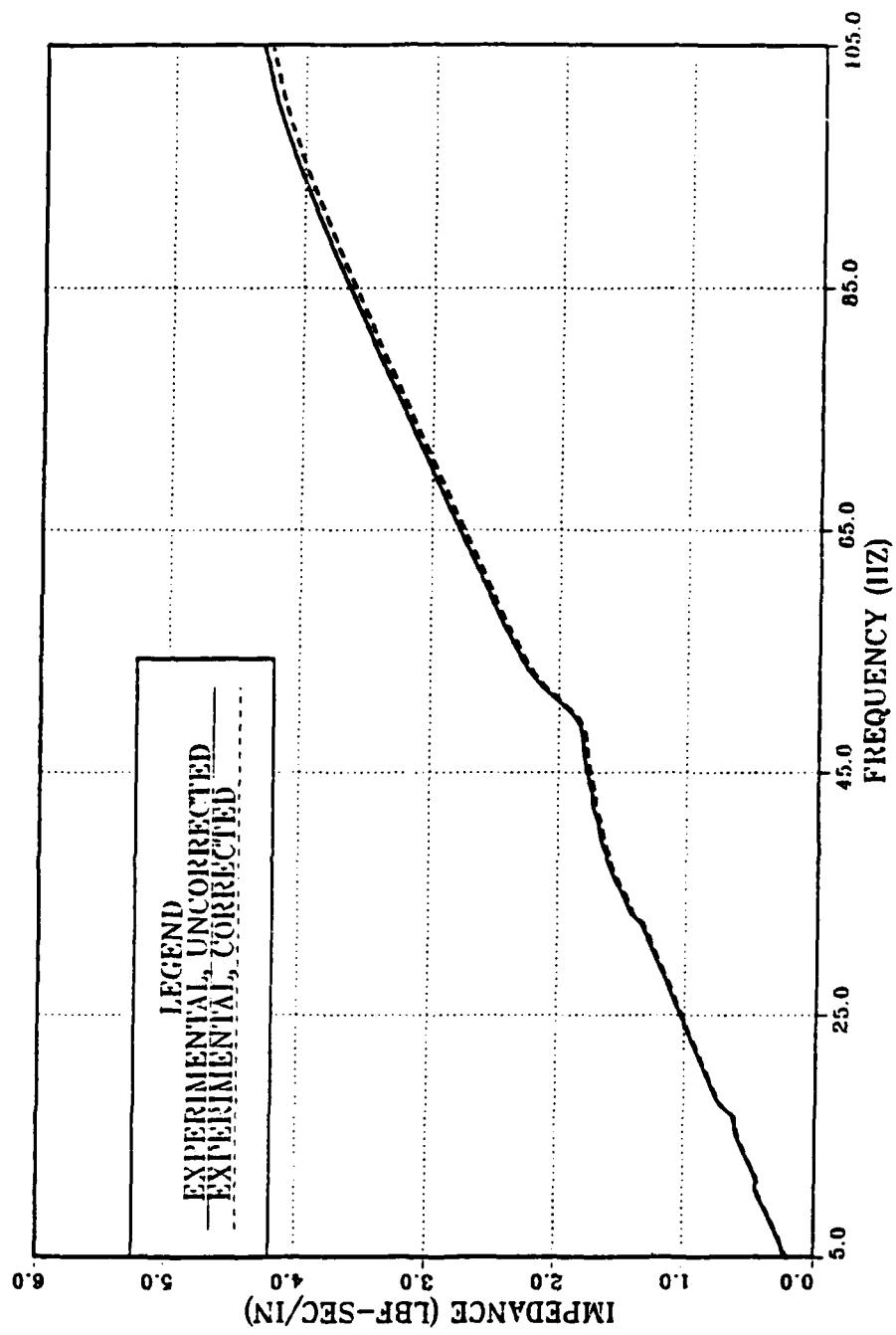
Figure 79. Experimental Imaginary Part of the Driving Point Impedance of a 5 in Radius Elastic Plate, With and Without Shaker and Mount Correction, in the Frequency Range of 5 to 105 Hz.
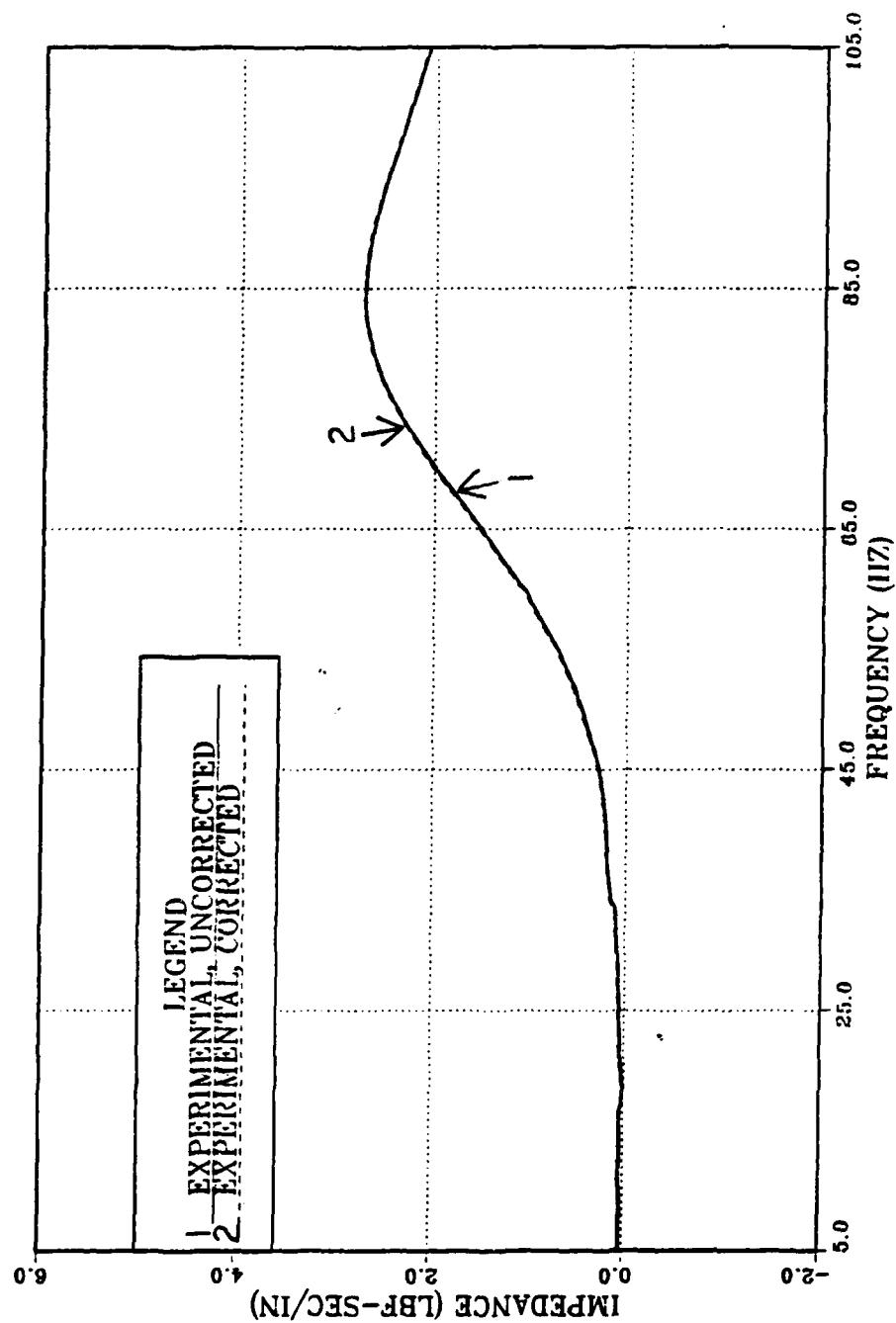
Figure 80. Experimental Real Part of the Driving Point Impedance of a 5 in Radius Viscoelastic Plate, With and Without Shaker and Mount Correction, in the Frequency Range of 5 to 105 Hz at a Temperature of 80.0 Deg. F.

144
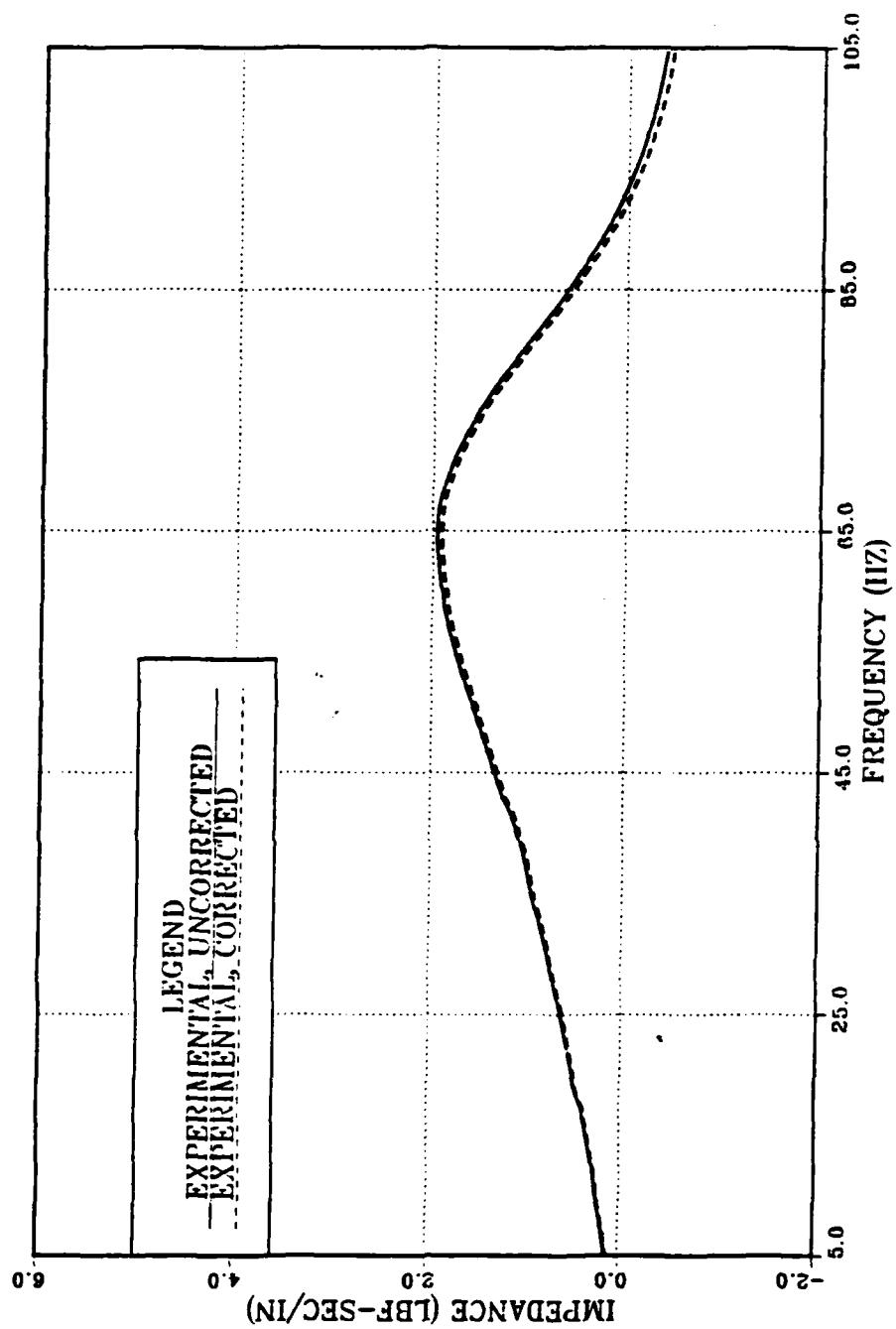
Figure 81. Experimental Imaginary Part of the Driving Point Impedance of a 5 in Radius Viscoelastic Plate, With and Without Shaker and Mount Correction, in the Frequency Range of 5 to 105 Hz at a Temperature of 80.0 Deg. F.

145
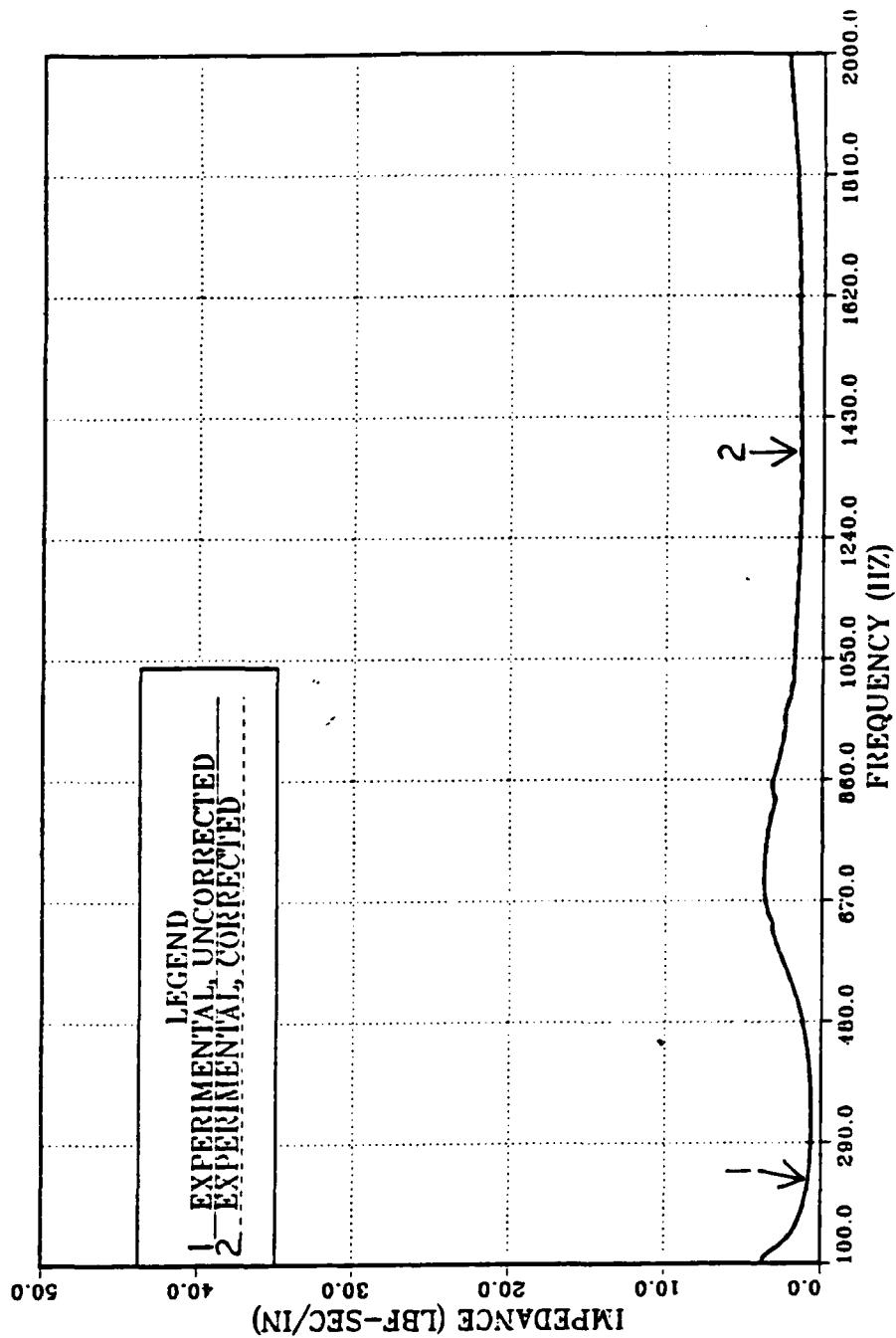
Figure 82. Experimental Real Part of the Driving Point Impedance of a 5 in Radius Viscoelastic Plate, With and Without Shaker and Mount Correction, in the Frequency Range of 100 to 2000 Hz at a Temperature of 77.3 Deg. F.

146
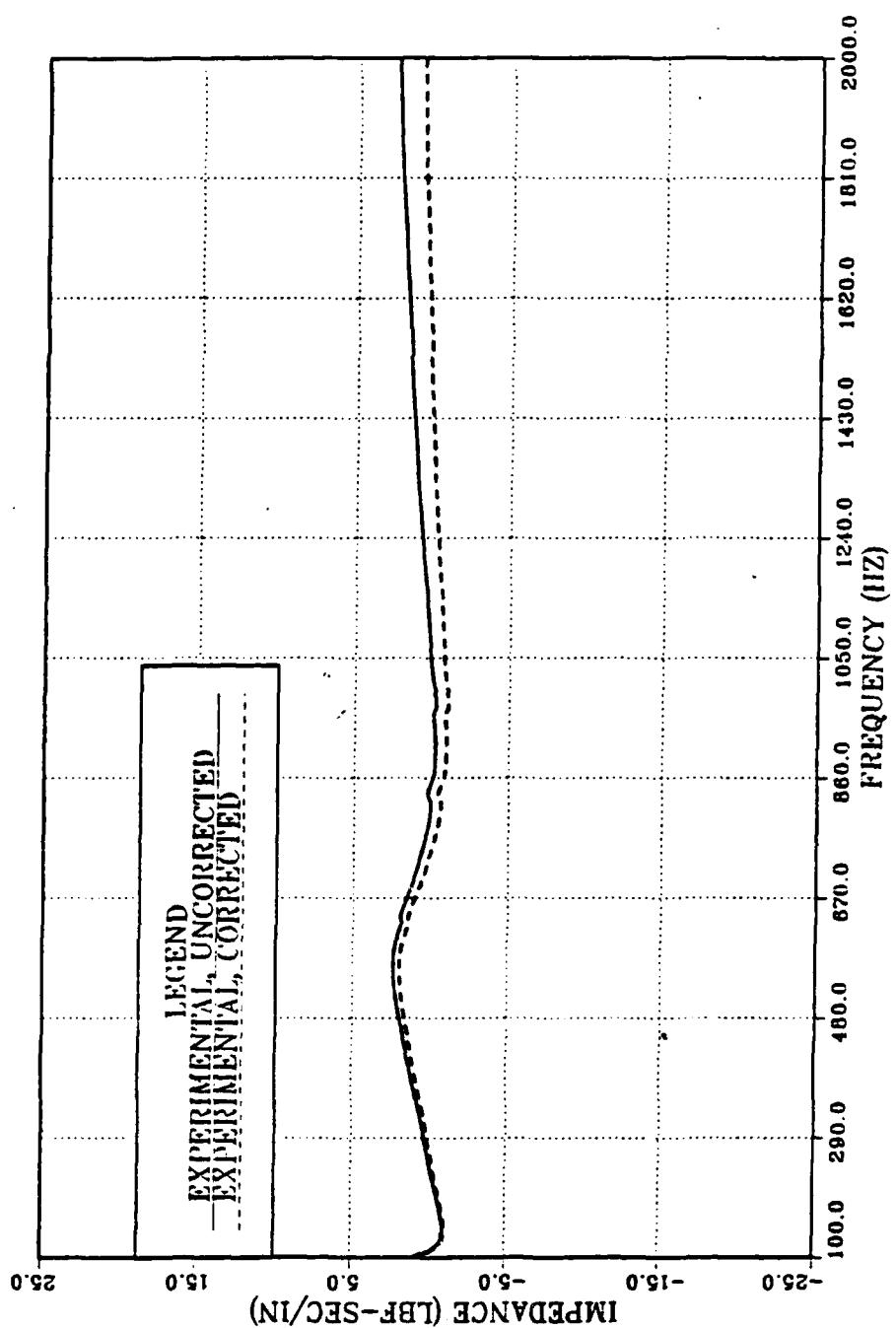
Figure 83. Experimental Imaginary Part of the Driving Point
Impedance of a 5 in Radius Viscoelastic Plate, With and
Without Shaker and Mount Correction, in the Frequency
Range of 100 to 2000 Hz at a Temperature of 77.3 Deg. F.

147
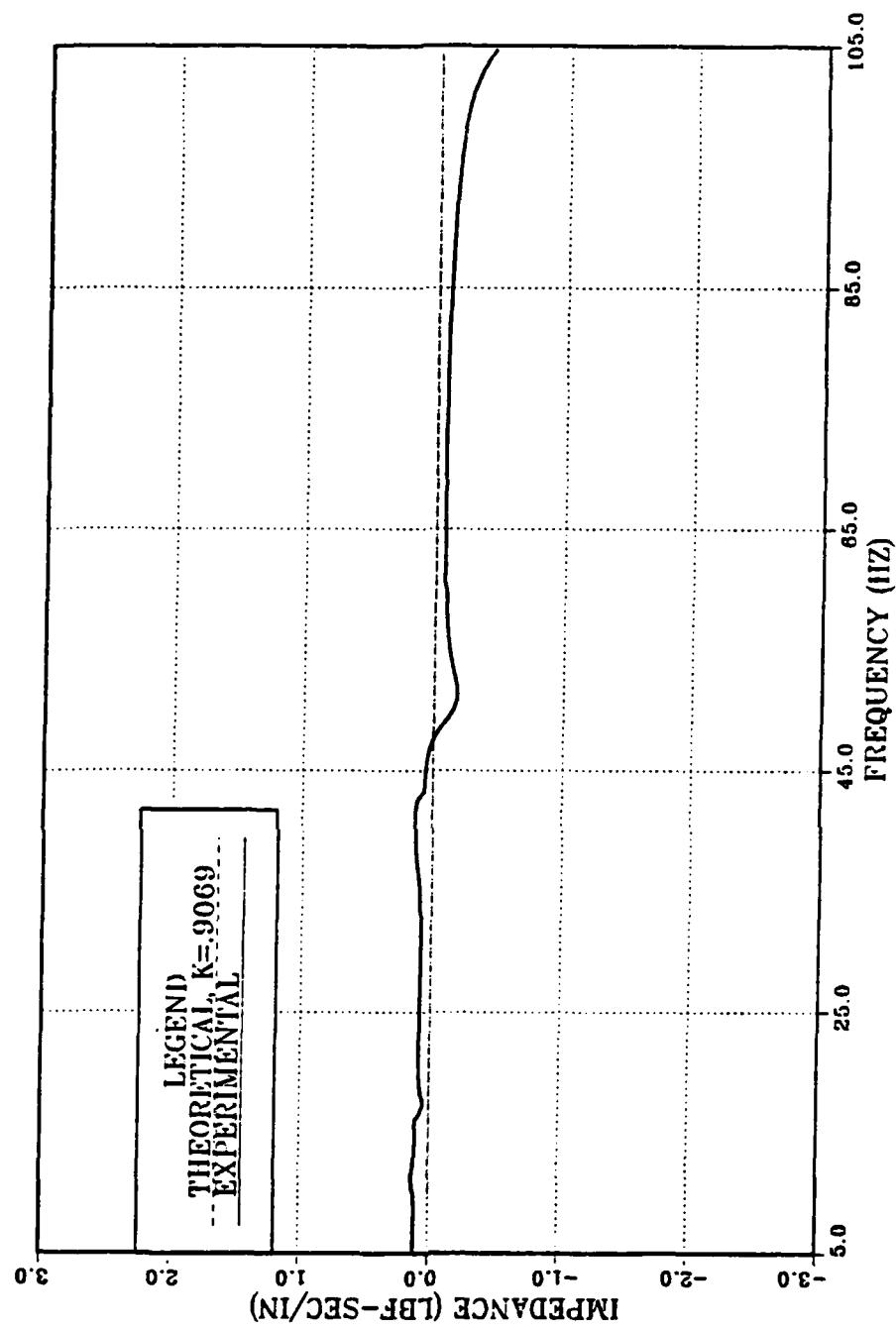
Figure 84. Theoretical and Experimental Comparison of the Real Part of the Driving Point Impedance for a 5 in Radius Elastic Plate in the Frequency Range of 5 to 105 Hz.

148
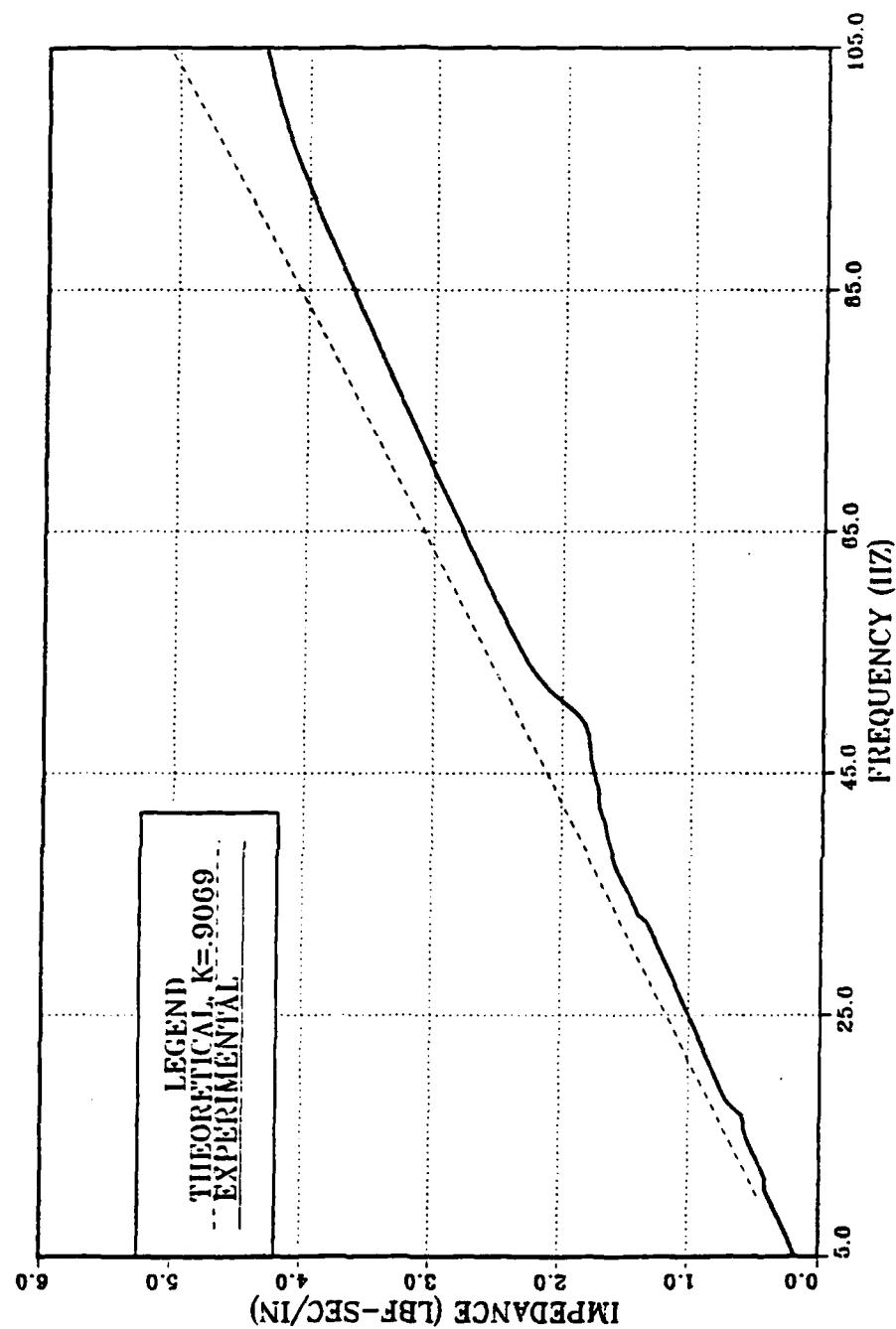
Figure 85. Theoretical and Experimental Comparison of the Imaginary Part of the Driving Point Impedance for a 5 in Radius Elastic Plate in the Frequency Range of 5 to 105 Hz.

149
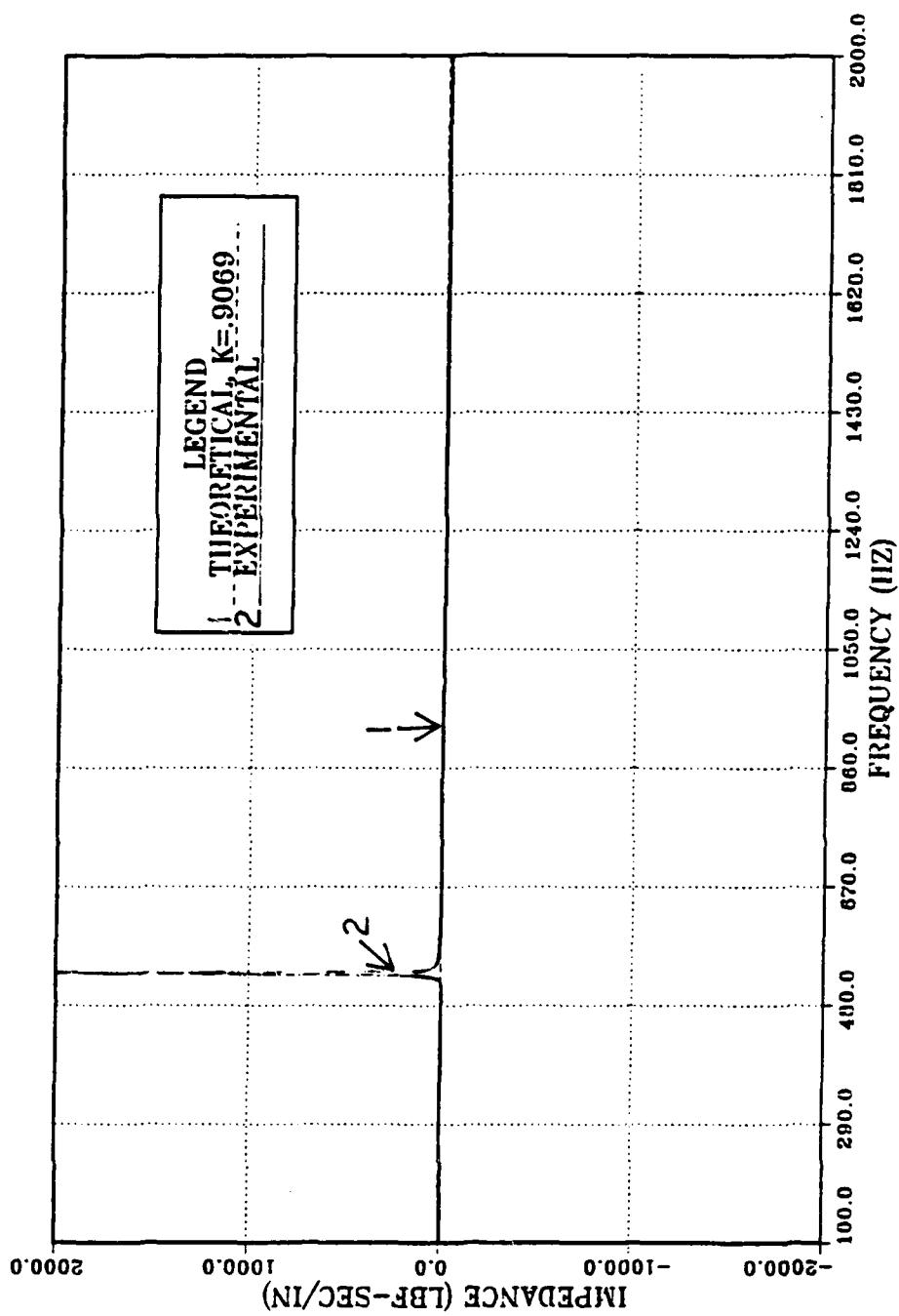
Figure 86. Theoretical and Experimental Comparison of the Real Part
of the Driving Point Impedance for a 5 in Radius Elastic
Plate in the Frequency Range of 100 to 2000 Hz.

150
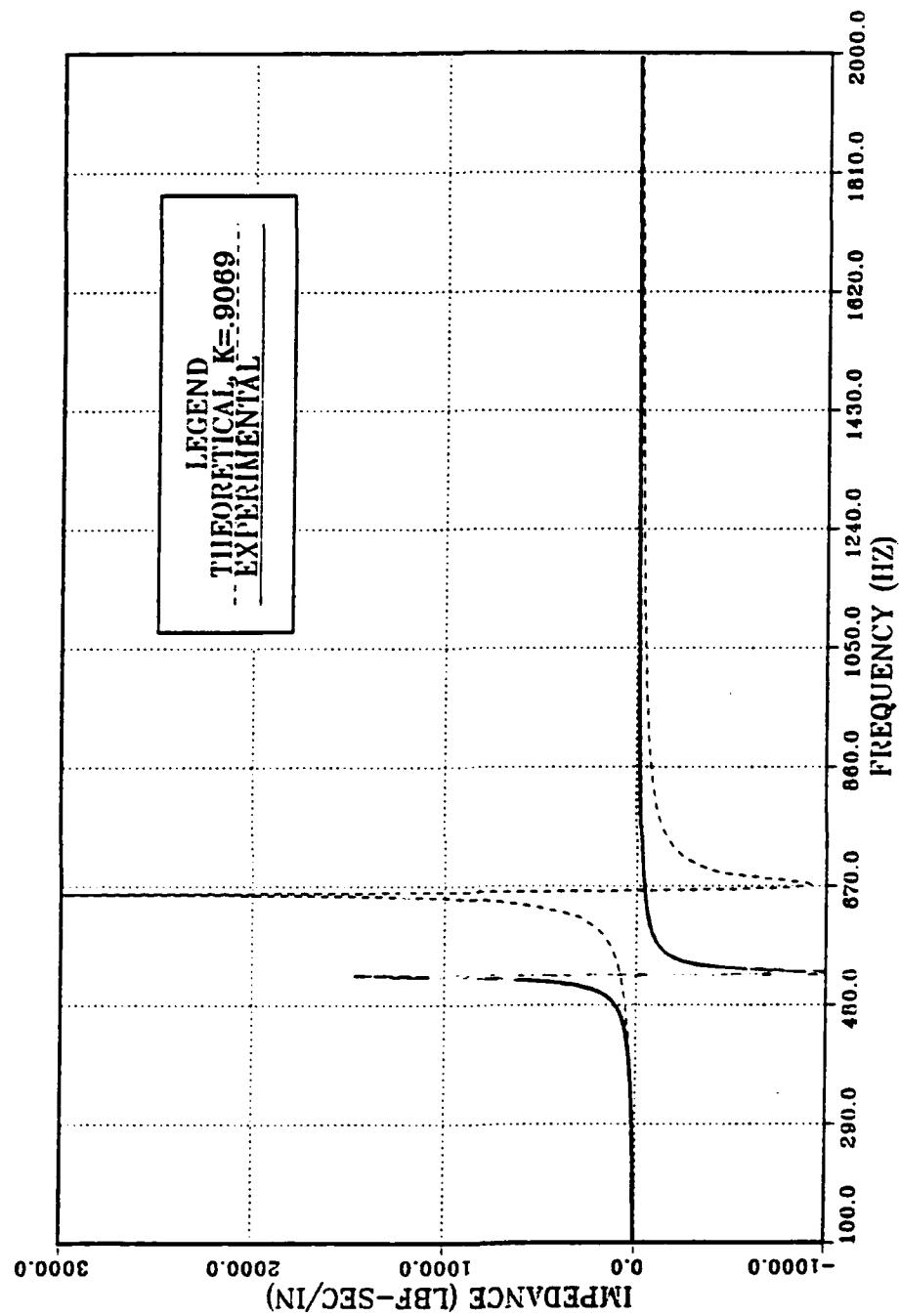
Figure 87. Theoretical and Experimental Comparison of the Imaginary Part of the Driving Point Impedance for a 5 in Radius Elastic Plate in the Frequency Range of 100 to 2000 Hz.

151
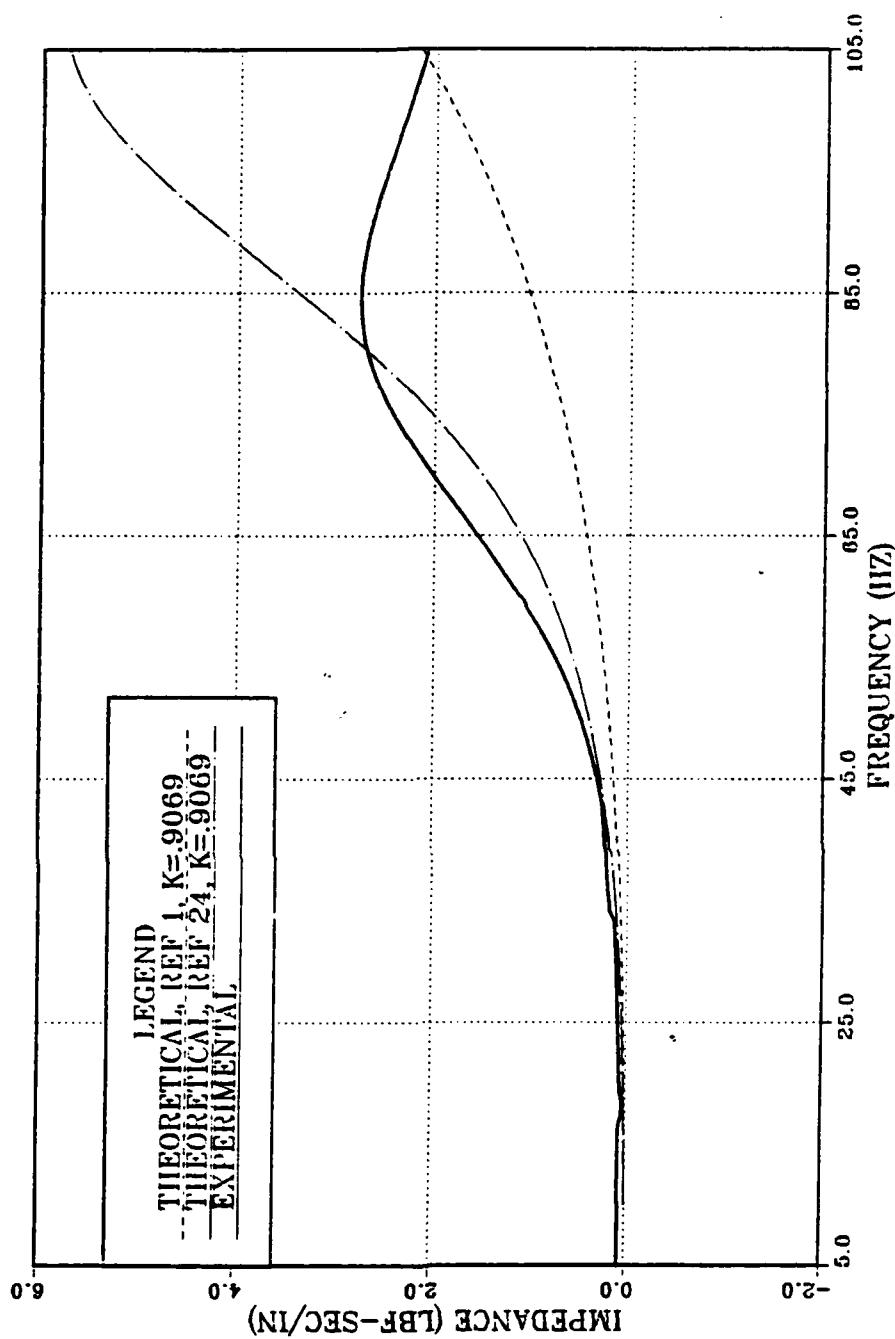
Figure 88. **Theoretical and Experimental Comparison of the Real Part of the Driving Point Impedance for a 5 in Radius Viscoelastic Plate in the Frequency Range of 5 to 105 Hz at a Temperature of 80.0 Deg. F.**
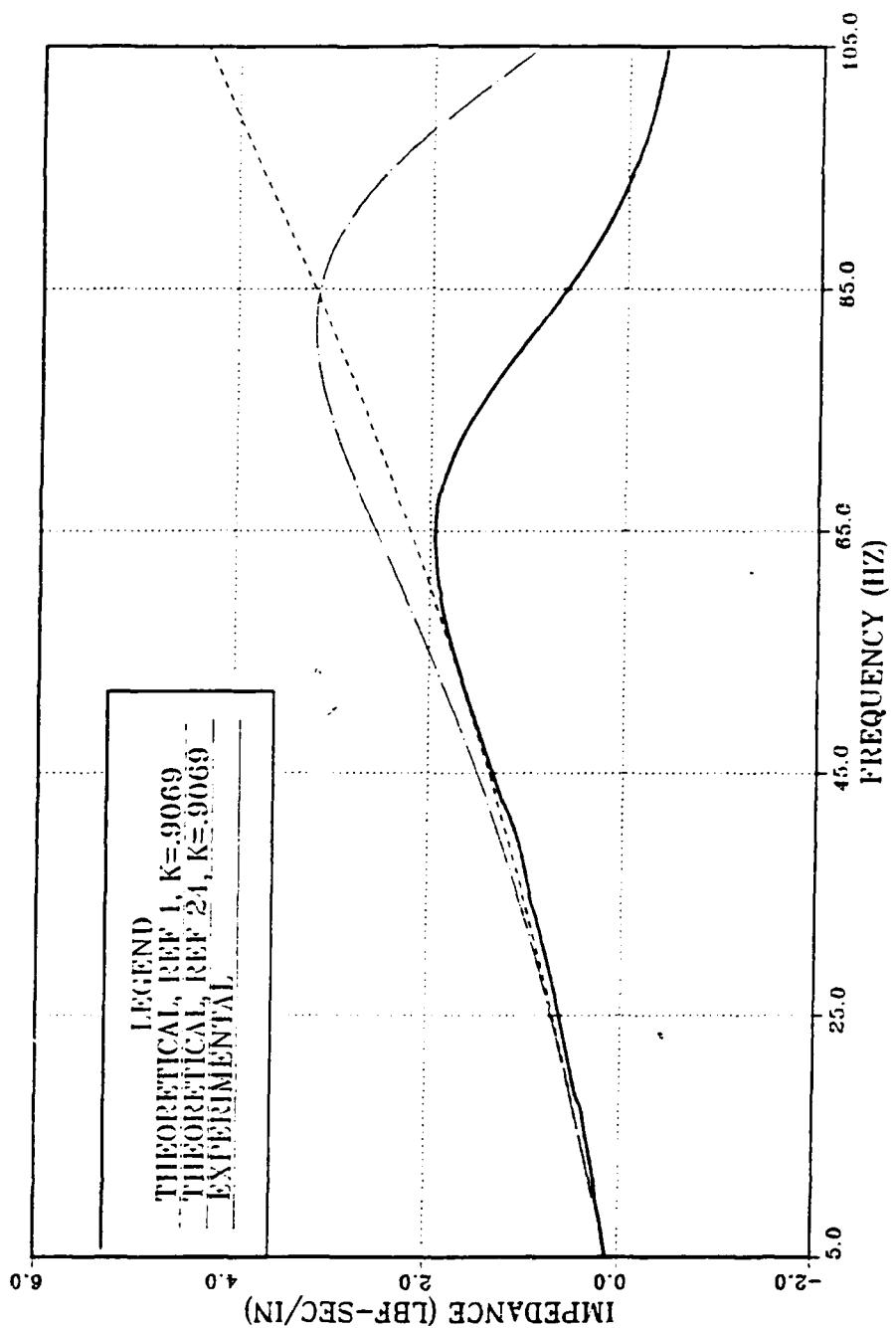
Figure 89. Theoretical and Experimental Comparison of the
Imaginary Part of the Driving Point Impedance for a 5 in
Radius Viscoelastic Plate in the Frequency Range of 5 to
105 Hz at a Temperature of 80.0 Deg. F.

153
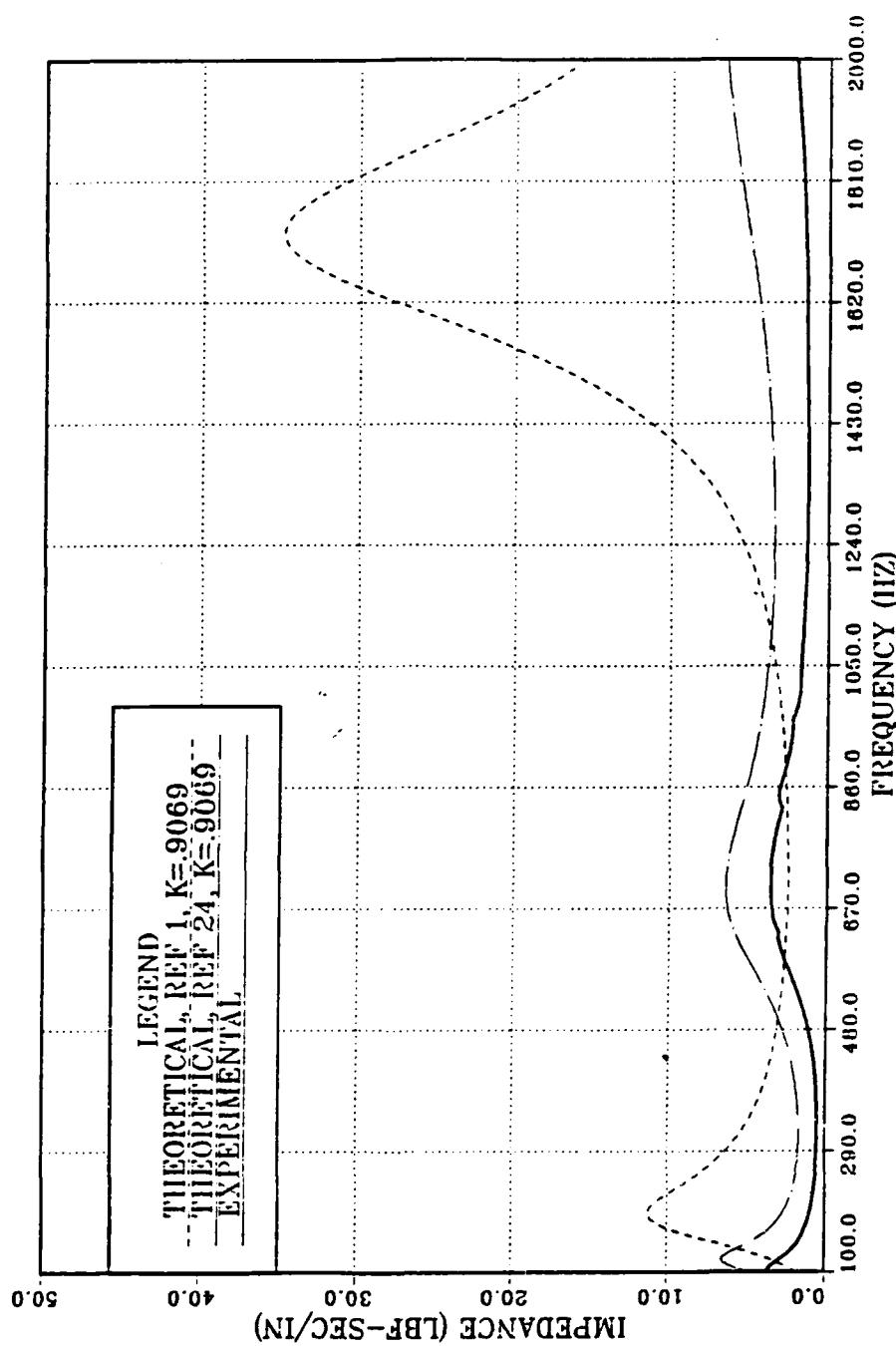
Figure 90. **Theoretical and Experimental Comparison of the Real Part of the Driving Point Impedance for a 5 in Radius Viscoelastic Plate in the Frequency Range of 100 to 2000 Hz at a Temperature of 77.3 Deg. F.**

154
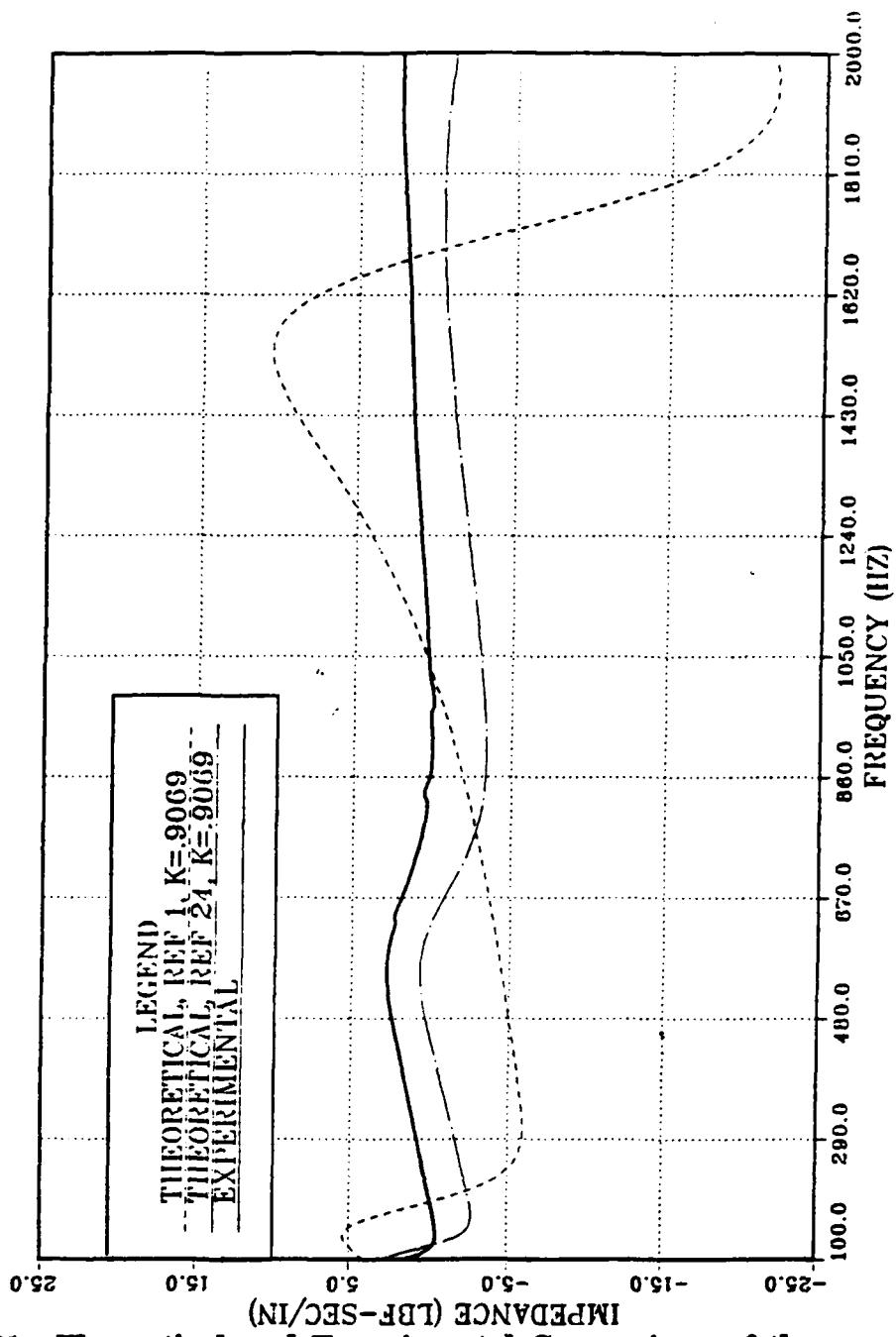
Figure 91. Theoretical and Experimental Comparison of the Imaginary Part of the Driving Point Impedance for a 5 in Radius Viscoelastic Plate in the Frequency Range of 100 to 2000 Hz at a Temperature of 77.3 Deg. F.

155
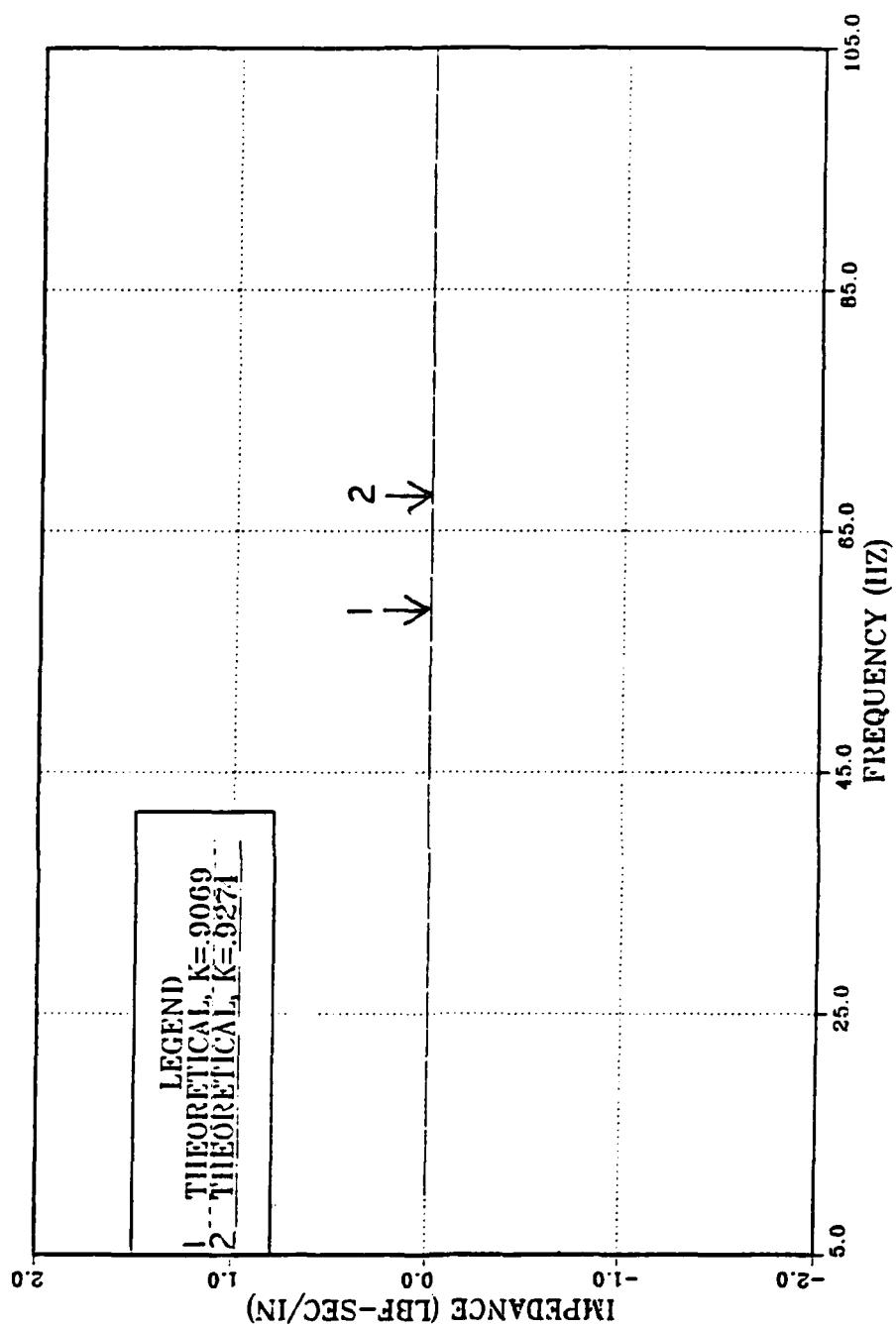
Figure 92. Effect of Shear Coefficient on the Theoretical Real Part of the Driving Point Impedance for a 4 in Radius Elastic Plate in the Frequency Range of 10 to 105 Hz.

156
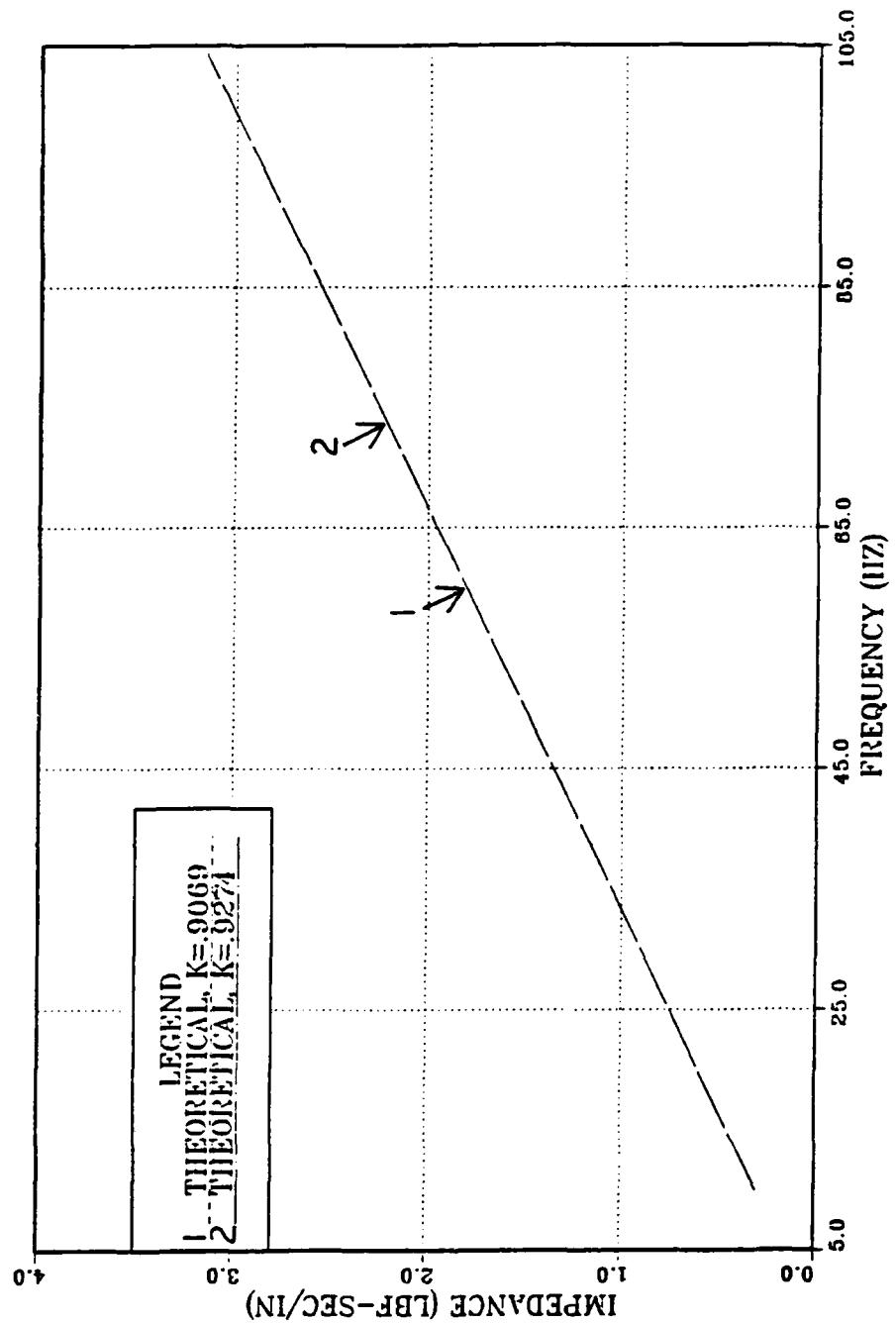
Figure 93. Effect of Shear Coefficient on the Theoretical Imaginary Part of the Driving Point Impedance for a 4 in Radius Elastic Plate in the Frequency Range of 10 to 105 Hz.

157
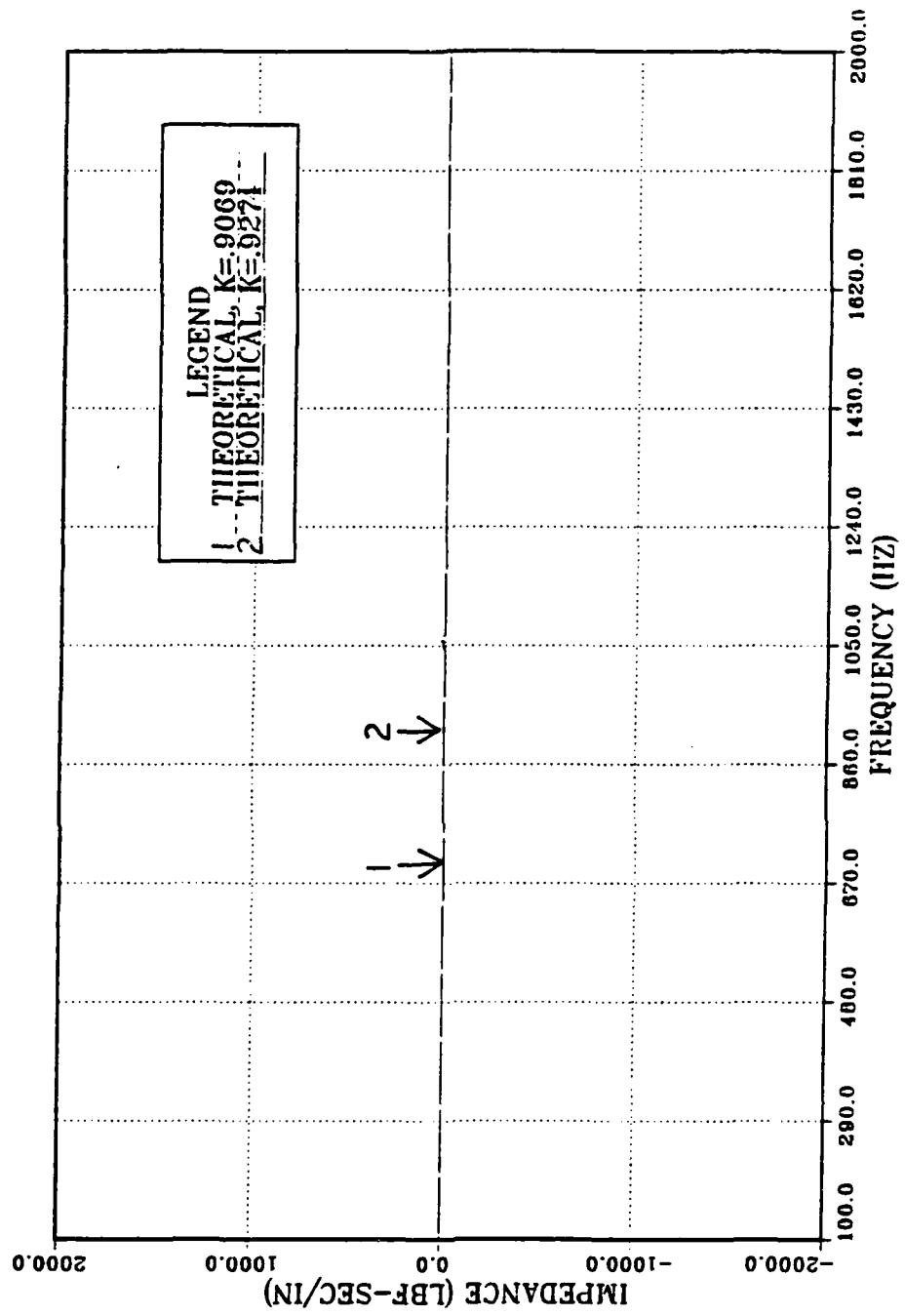
Figure 94. Effect of Shear Coefficient on the Theoretical Real Part of the Driving Point Impedance for a 4 in Radius Elastic Plate in the Frequency Range of 100 to 2000 Hz.

158
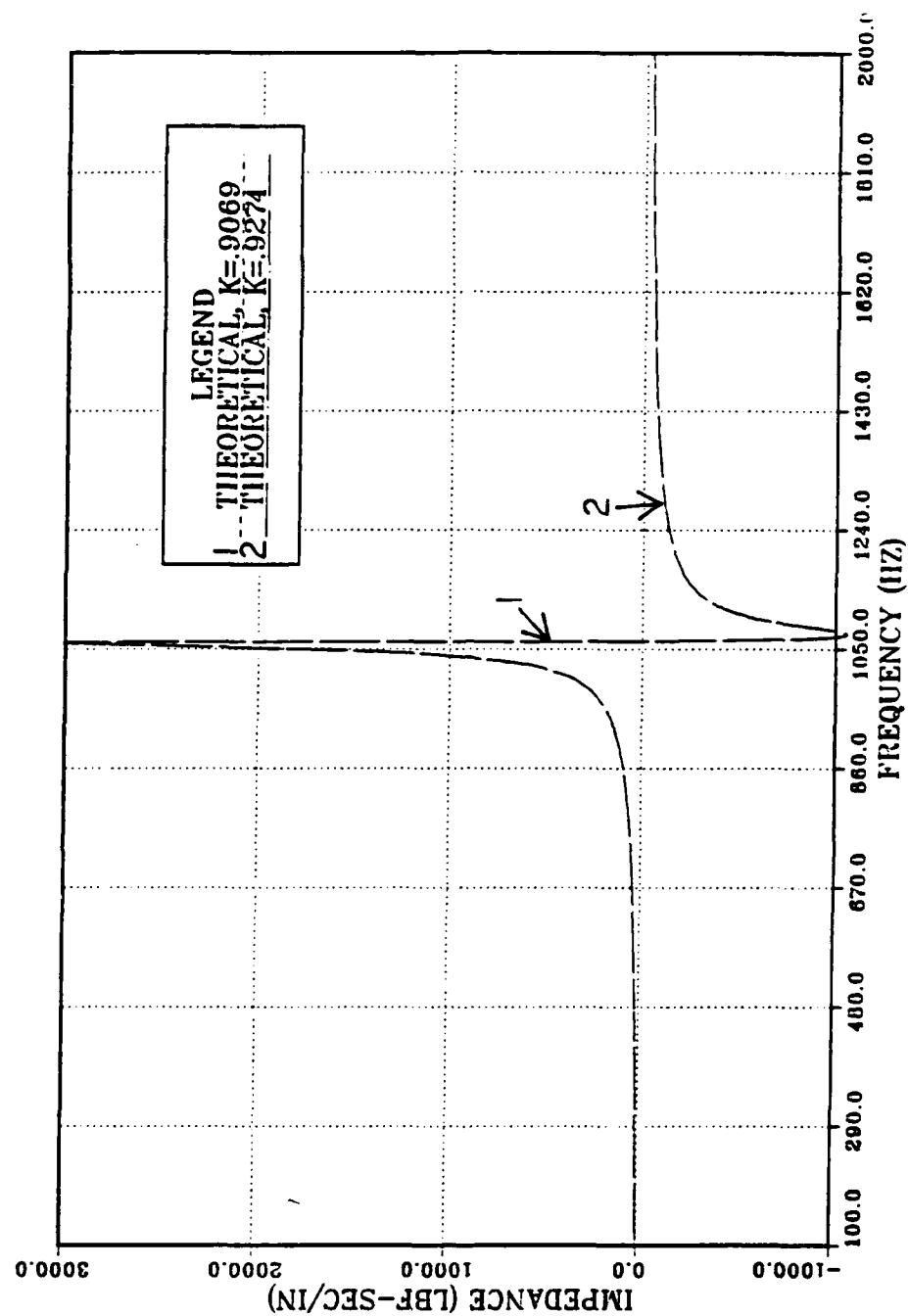
Figure 95. **Effect of Shear Coefficient on the Theoretical Imaginary Part of the Driving Point Impedance for a 4 in Radius Elastic Plate in the Frequency Range of 100 to 2000 Hz.**
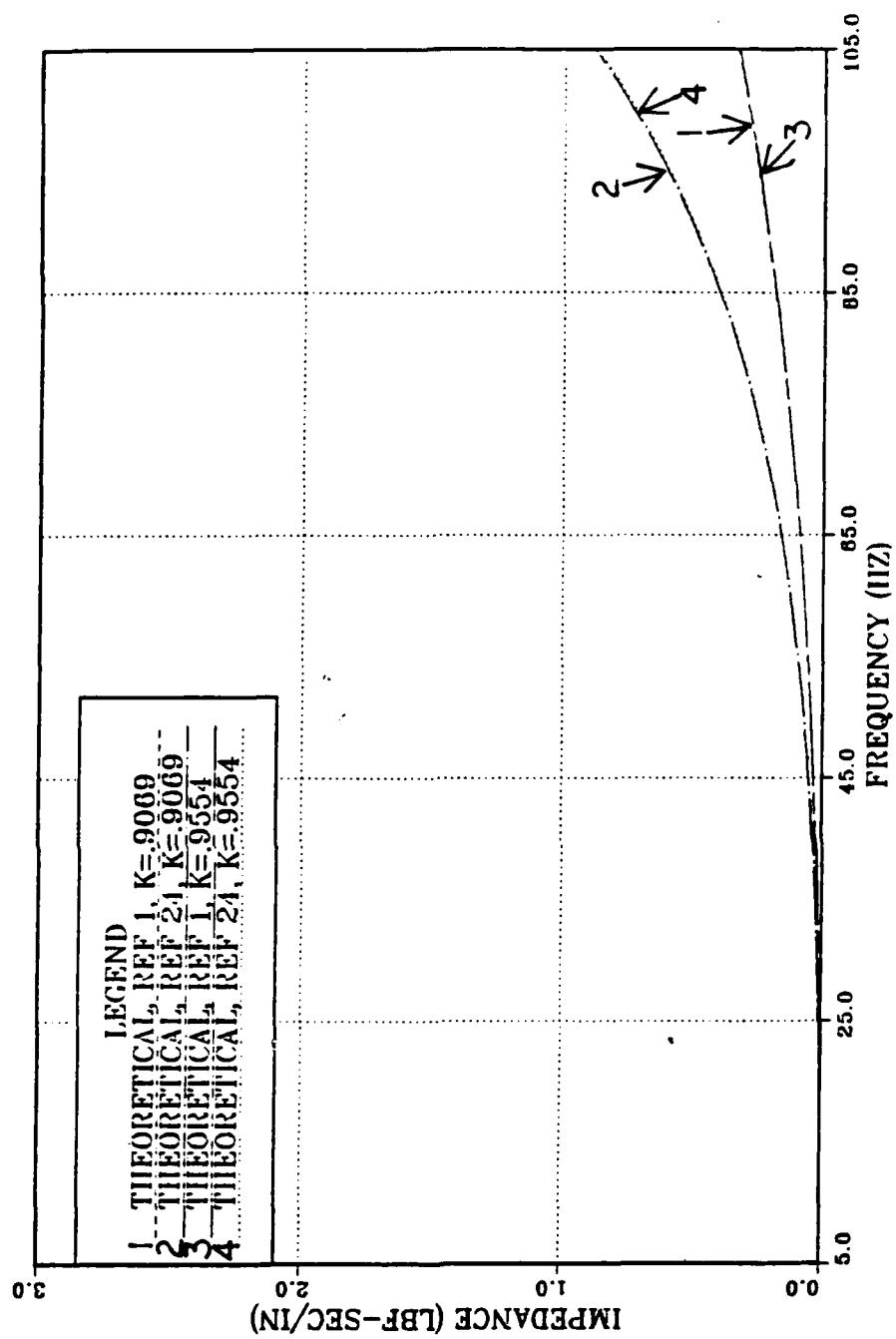
Figure 96. Effect of Shear Coefficient and Material Characteristics on the Theoretical Real Part of the Driving Point Impedance for a 4 in Radius Viscoelastic Plate in the Frequency Range of 10 to 105 Hz at a Temperature of 78.5 Deg. F.

160

Figure 97. Effect of Shear Coefficient and Material Characteristics on the Theoretical Imaginary Part of the Driving Point Impedance for a 4 in Radius Viscoelastic Plate in the Frequency Range of 10 to 105 Hz at a Temperature of 78.5 Deg. F.

161
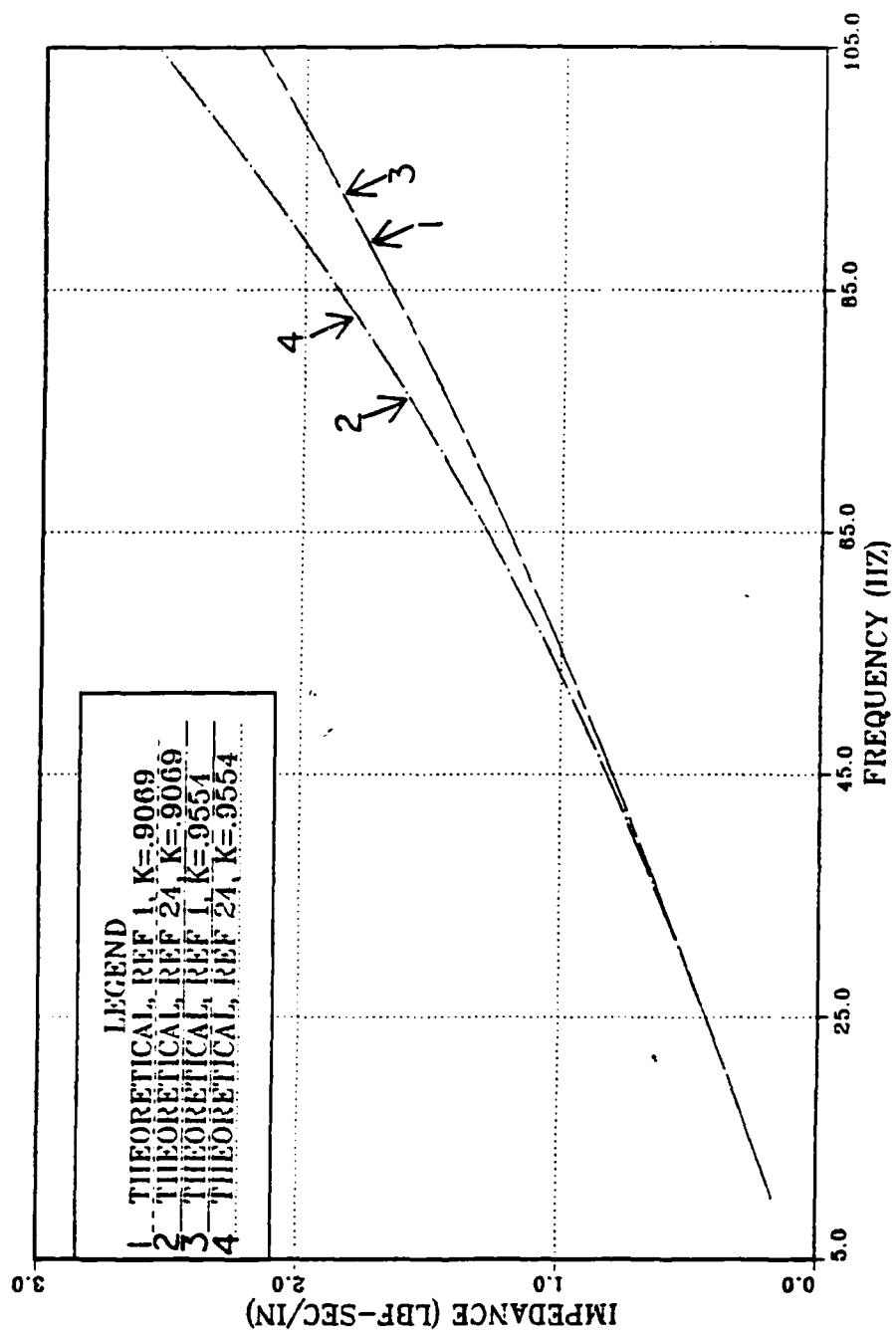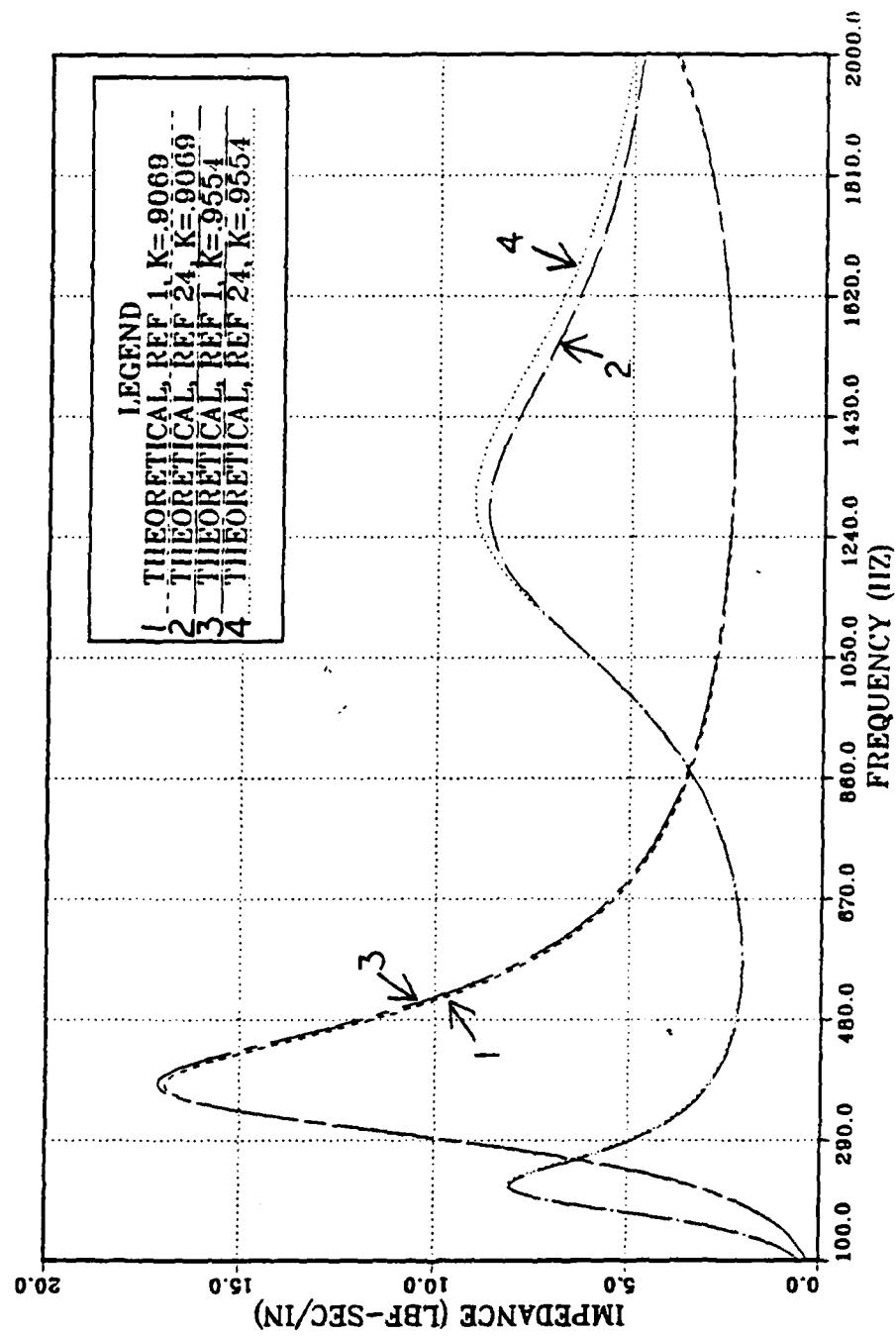
Figure 98. Effect of Shear Coefficient and Material Characteristics on the Theoretical Real Part of the Driving Point Impedance for a 4 in Radius Viscoelastic Plate in the Frequency Range of 100 to 2000 Hz at a Temperature of 74.5 Deg. F.

162
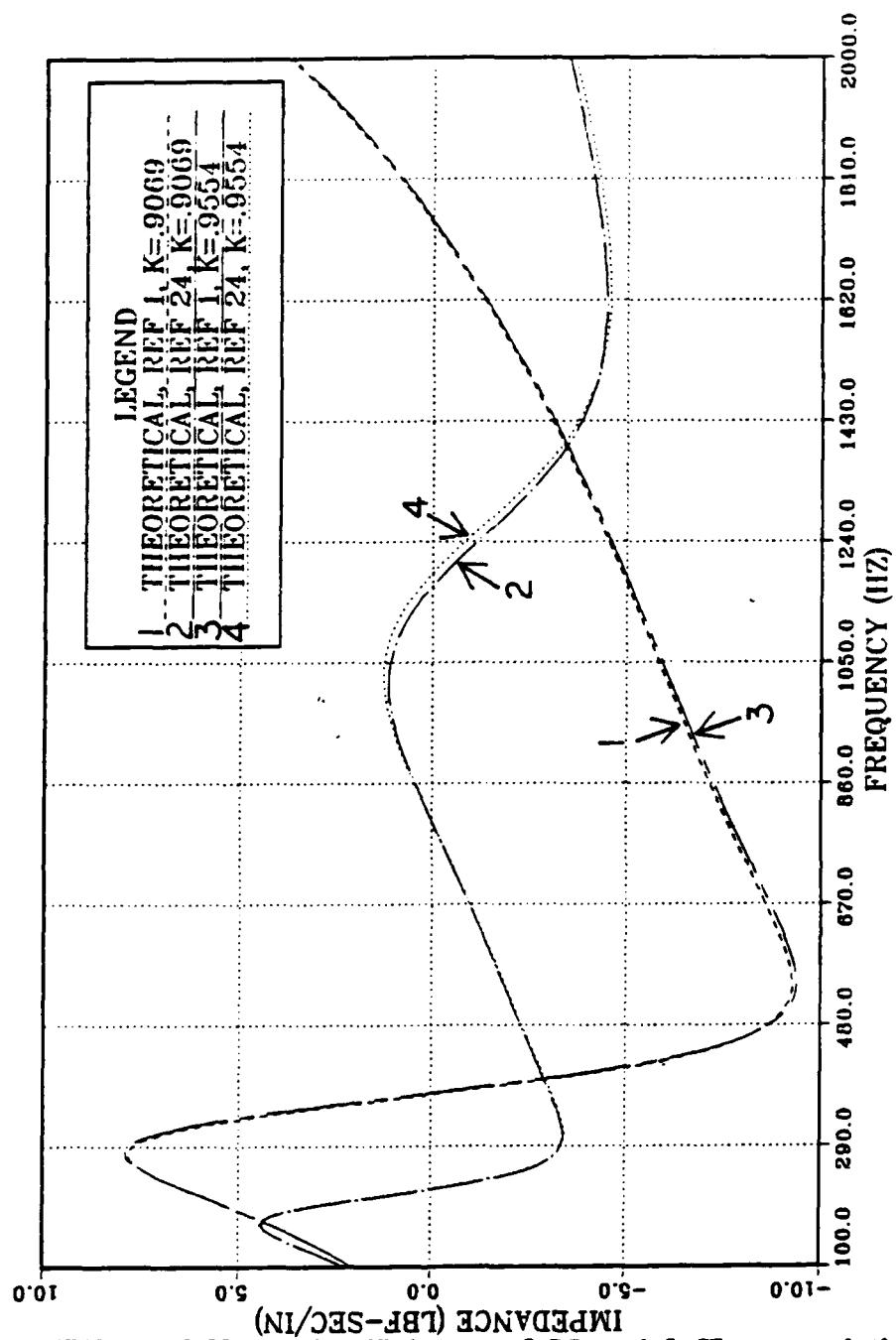
Figure 99. Effect of Shear Coefficient and Material Characteristics on the Theoretical Imaginary Part of the Driving Point Impedance for a 4 in Radius Viscoelastic Plate in the Frequency Range of 100 to 2000 Hz at a Temperature of 74.5 Deg. F.

163
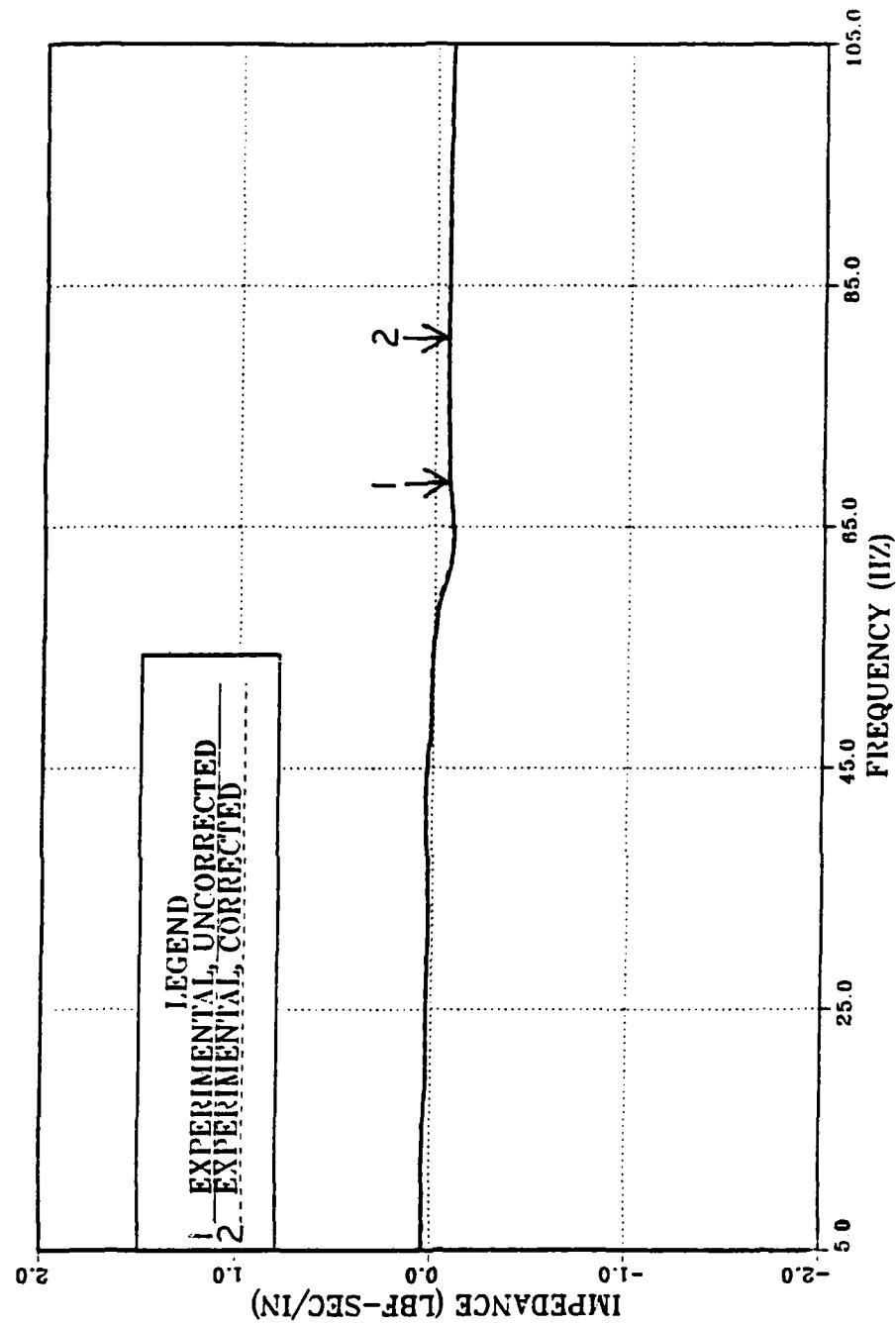
Figure 100. Experimental Real Part of the Driving Point Impedance of a 4 in Radius Elastic Plate, With and Without Shaker and Mount Correction, in the Frequency Range of 5 to 105 Hz.

164
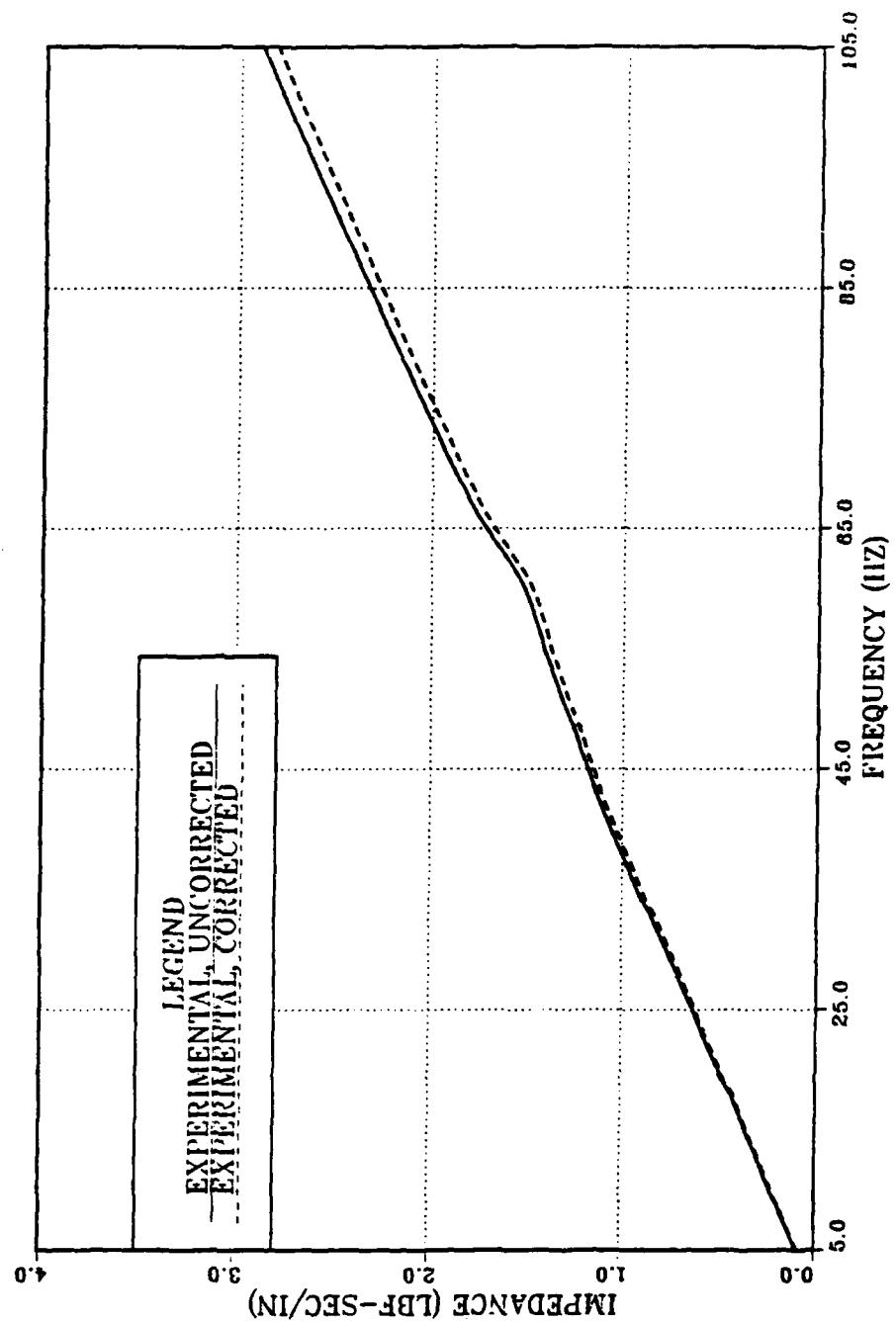
Figure 101. Experimental Imaginary Part of the Driving Point Impedance of a 4 in Radius Elastic Plate, With and Without Shaker and Mount Correction, in the Frequency Range of 5 to 105 Hz.

165
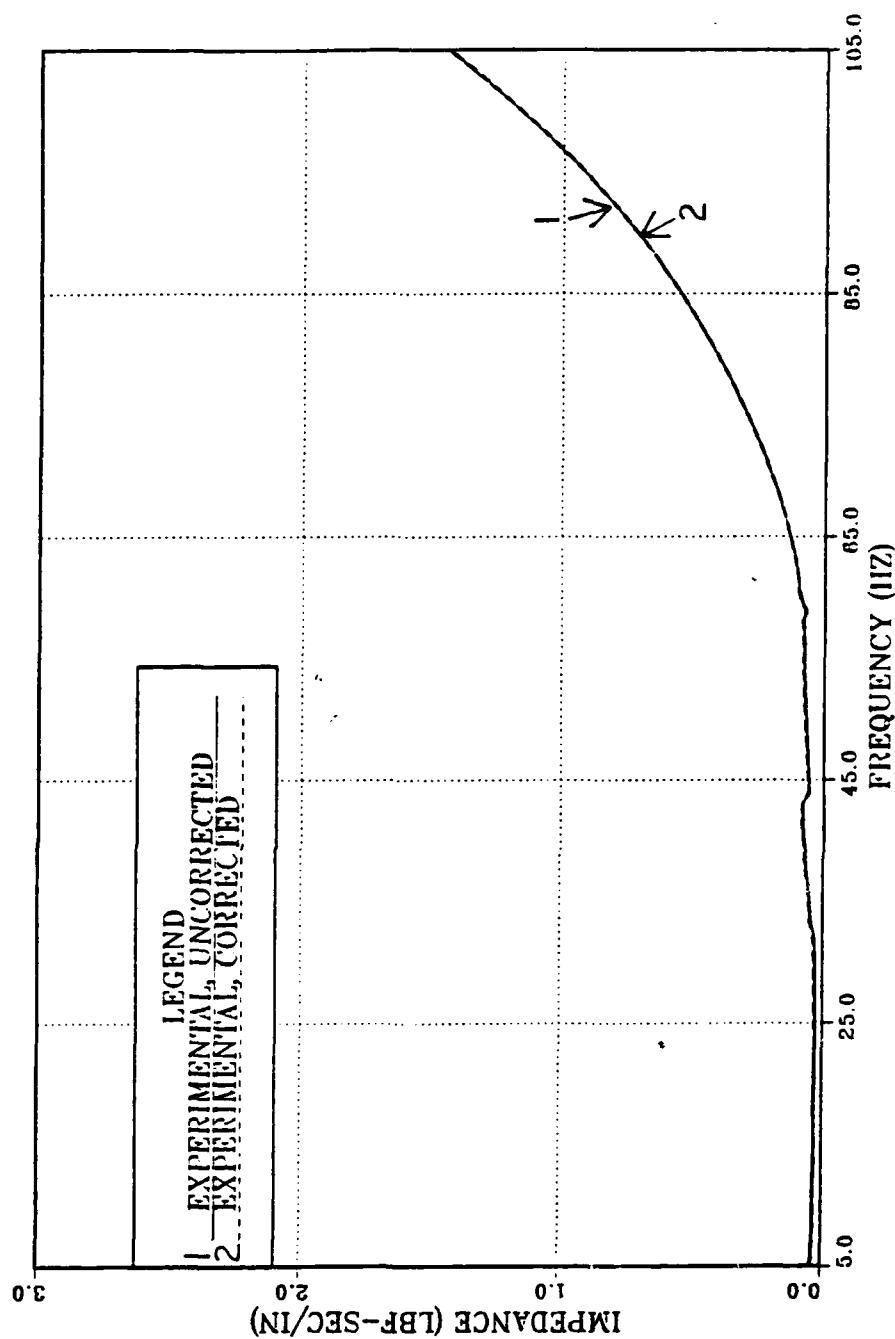
Figure 102. Experimental Real Part of the Driving Point Impedance of a 4 in Radius Viscoelastic Plate, With and Without Shaker and Mount Correction, in the Frequency Range of 5 to 105 Hz at a Temperature of 78.5 Deg. F.

166
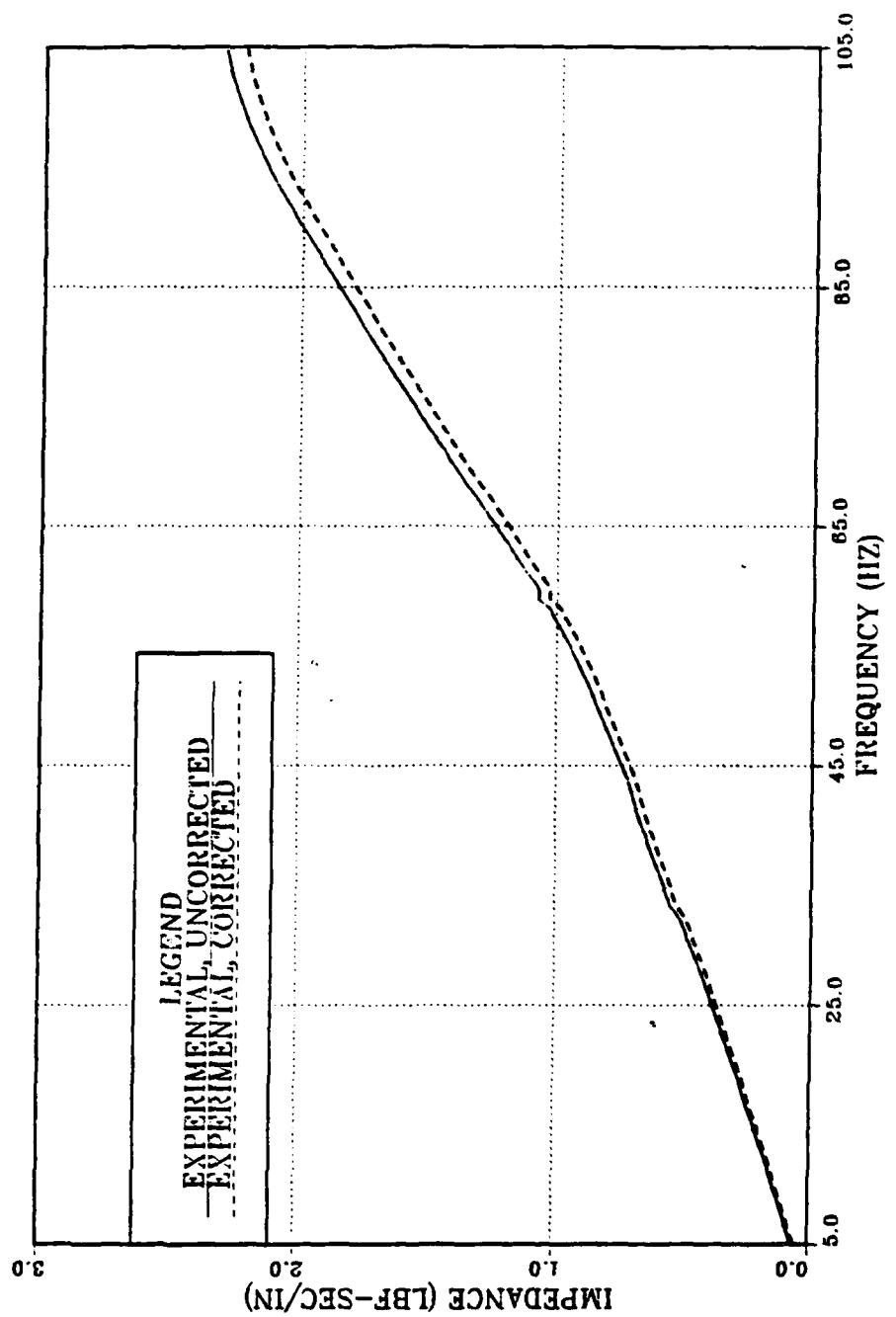
Figure 103. Experimental Imaginary Part of the Driving Point
Impedance of a 4 in Radius Viscoelastic Plate, With and
Without Shaker and Mount Correction, in the Frequency
Range of 5 to 105 Hz at a Temperature of 78.5 Deg. F.

167
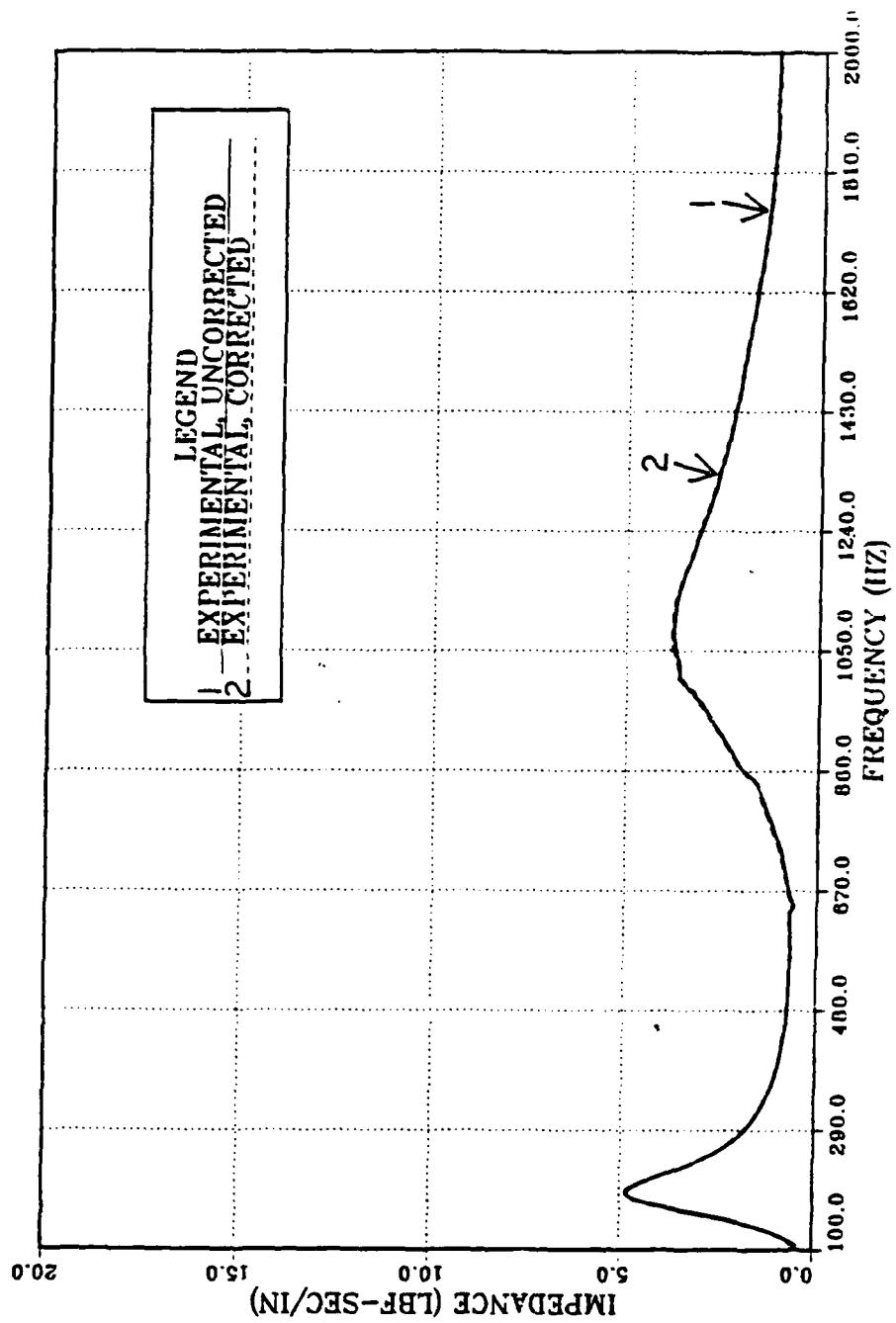
Figure 104. Experimental Real Part of the Driving Point Impedance of
a 4 in Radius Viscoelastic Plate, With and Without Shaker
and Mount Correction, in the Frequency Range of 100 to
2000 Hz at a Temperature of 74.5 Deg. F.

168
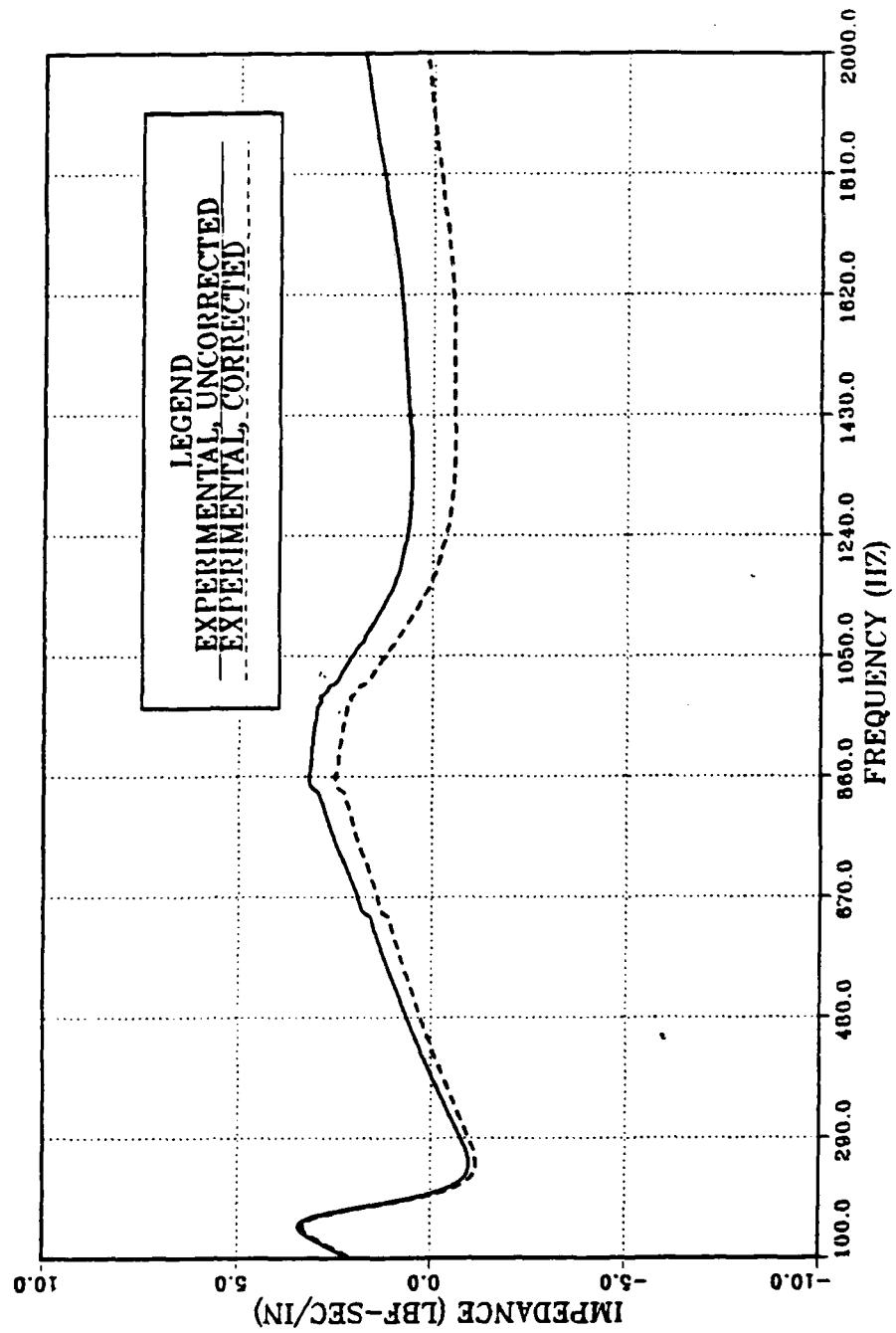
Figure 105. Experimental Imaginary Part of the Driving Point
Impedance of a 4 in Radius Viscoelastic Plate, With and
Without Shaker and Mount Correction, in the Frequency
Range of 100 to 2000 Hz at a Temperature of 74.5 Deg. F.

169
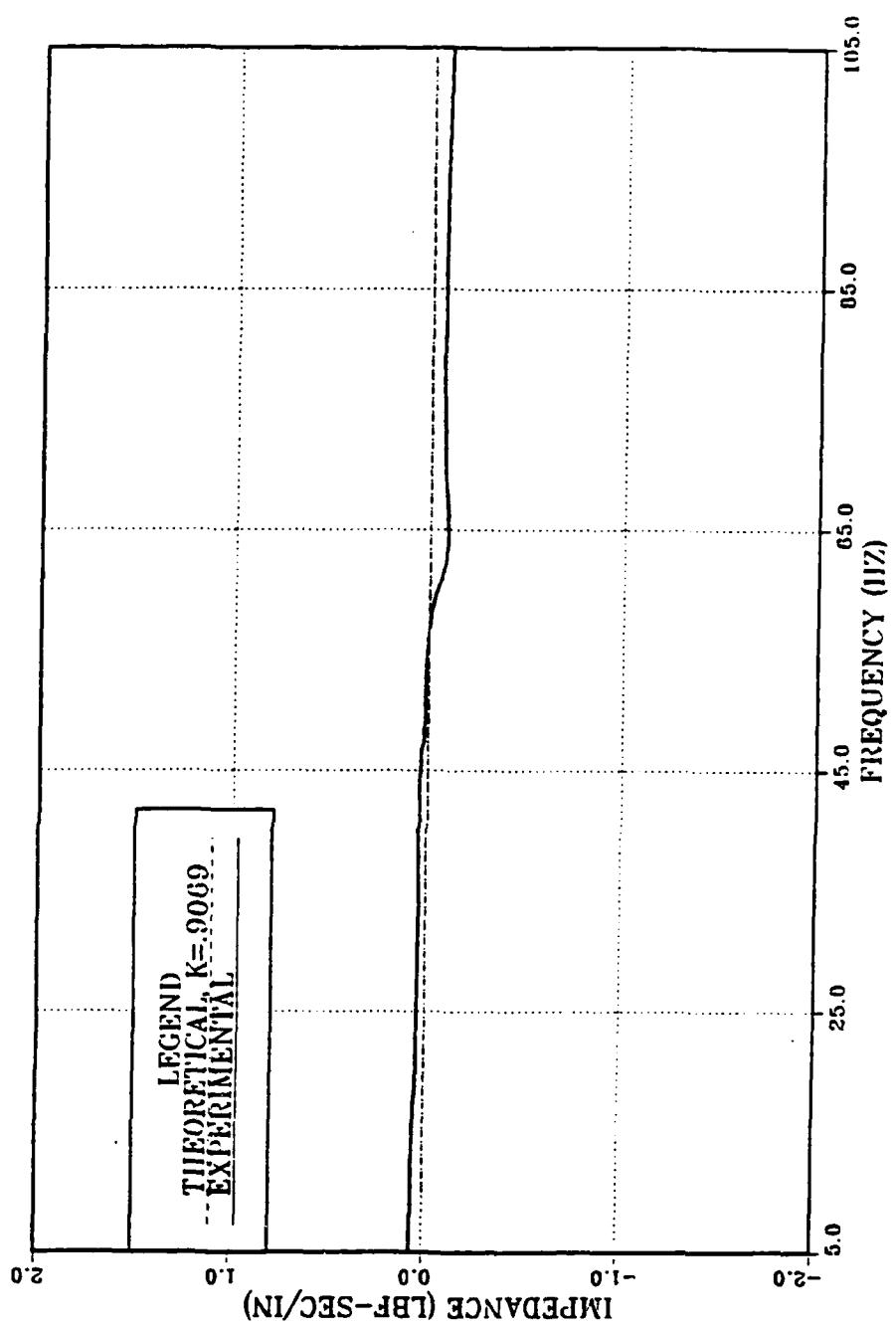
Figure 106. Theoretical and Experimental Comparison of the Real Part
of the Driving Point Impedance for a 4 in Radius Elastic
Plate in the Frequency Range of 5 to 105 Hz.

170
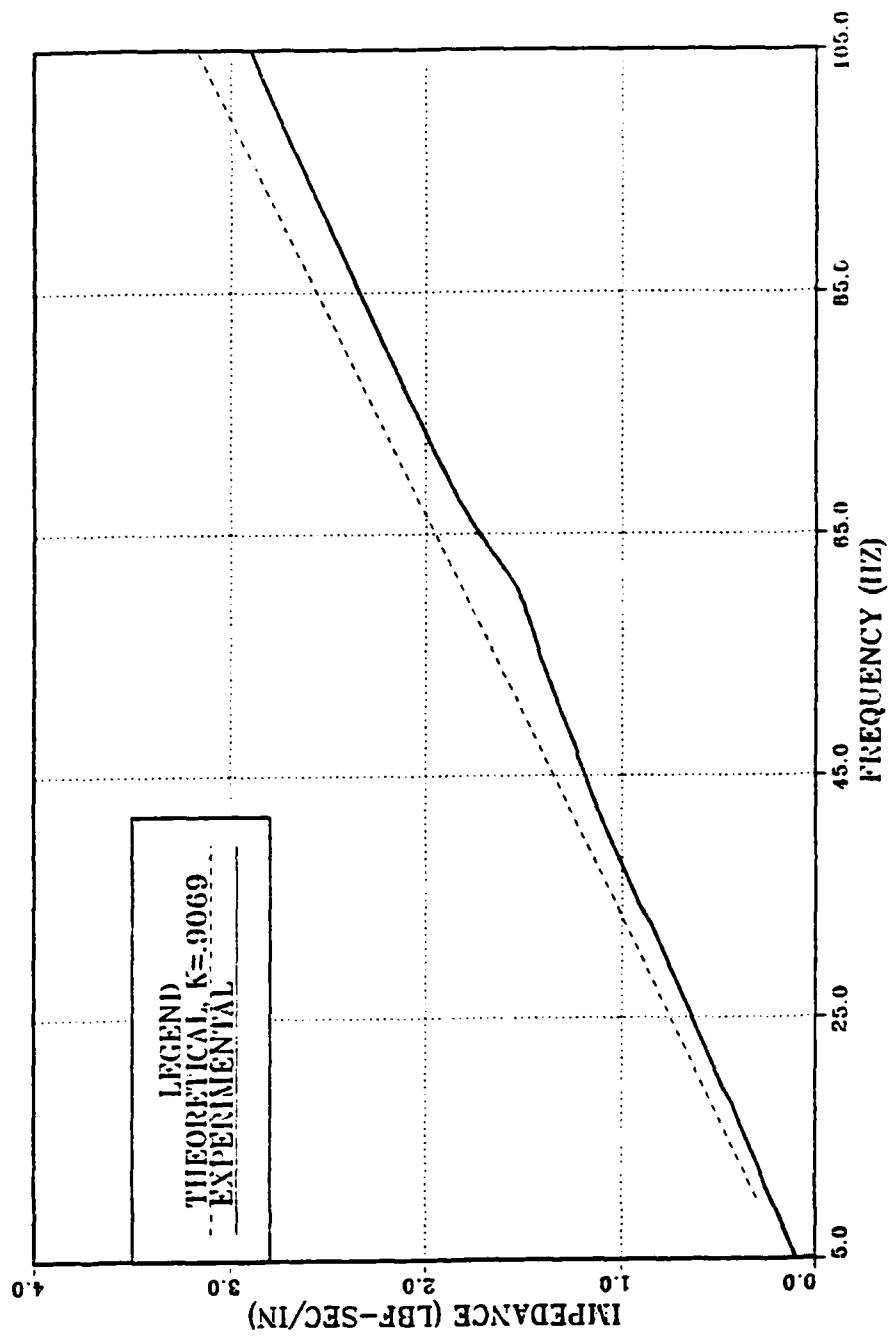
Figure 107. Theoretical and Experimental Comparison of the Imaginary Part of the Driving Point Impedance for a 4 in Radius Elastic Plate in the Frequency Range of 5 to 105 Hz.

171
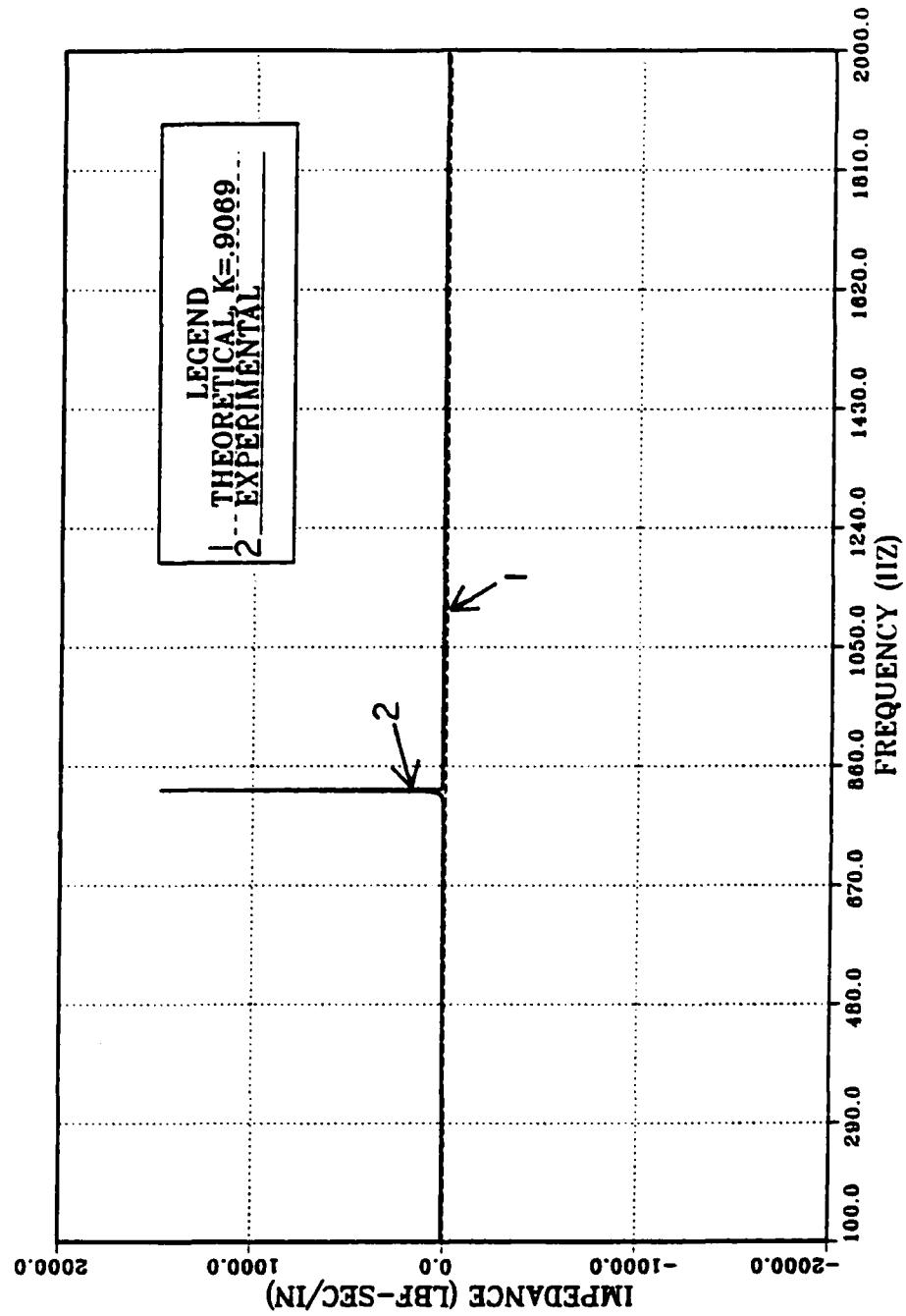
Figure 108. Theoretical and Experimental Comparison of the Real Part of the Driving Point Impedance for a 4 in Radius Elastic Plate in the Frequency Range of 100 to 2000 Hz.
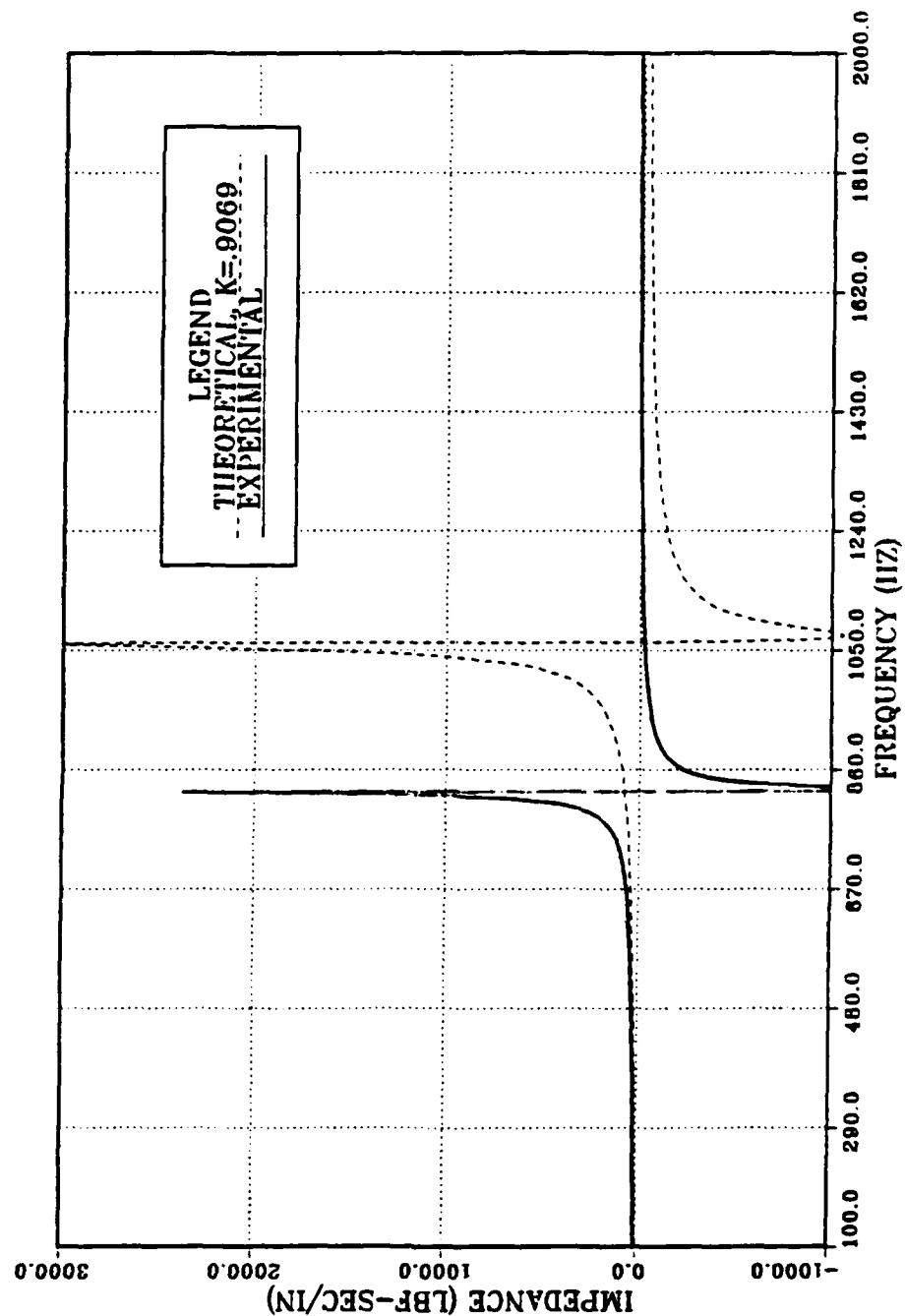
Figure 109. Theoretical and Experimental Comparison of the Imaginary Part of the Driving Point Impedance for a 4 in Radius Elastic Plate in the Frequency Range of 100 to 2000 Hz.

173
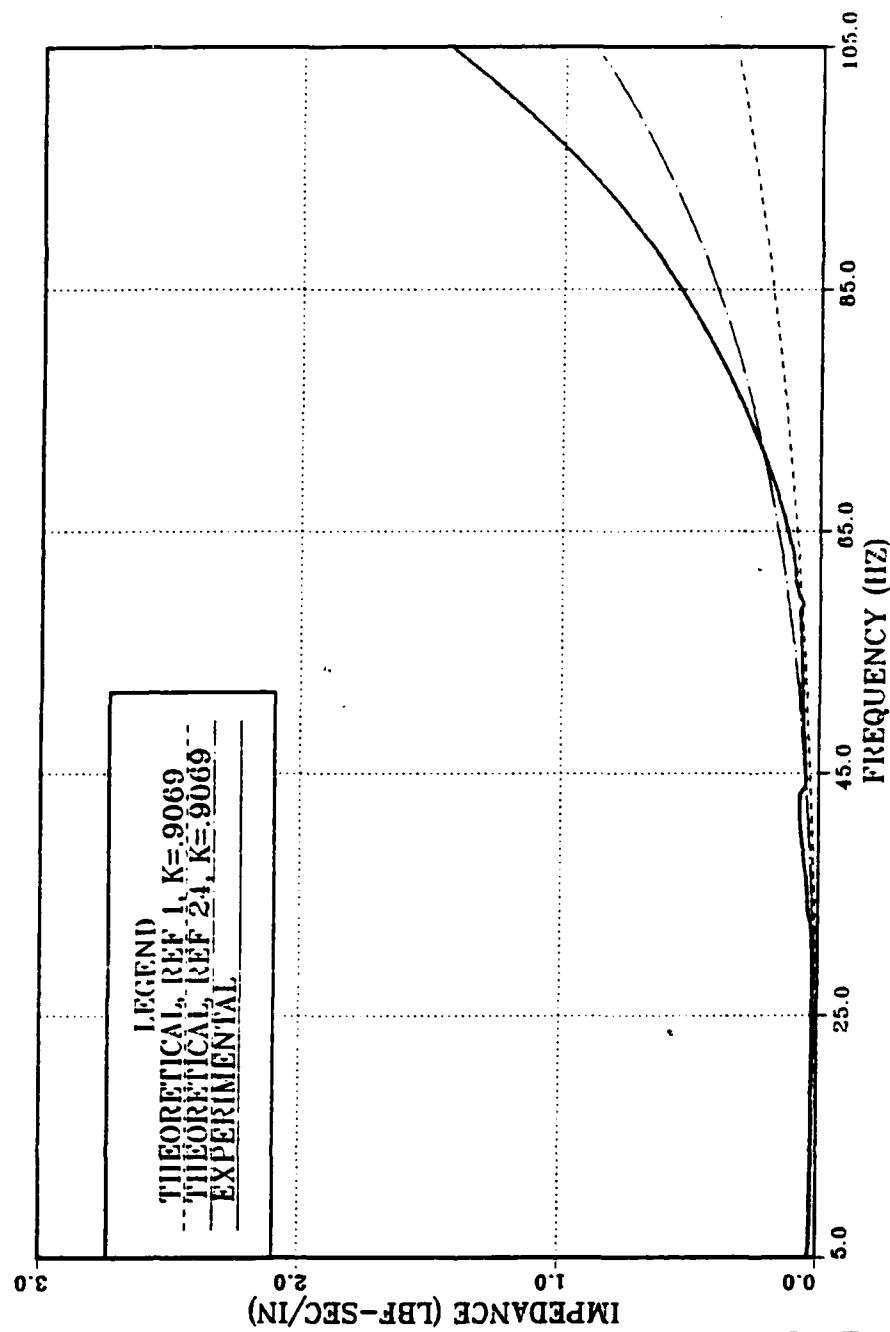
Figure 110. Theoretical and Experimental Comparison of the Real Part
of the Driving Point Impedance for a 4 in Radius
Viscoelastic Plate in the Frequency Range of 5 to 105 Hz at
a Temperature of 78.5 Deg. F.

174
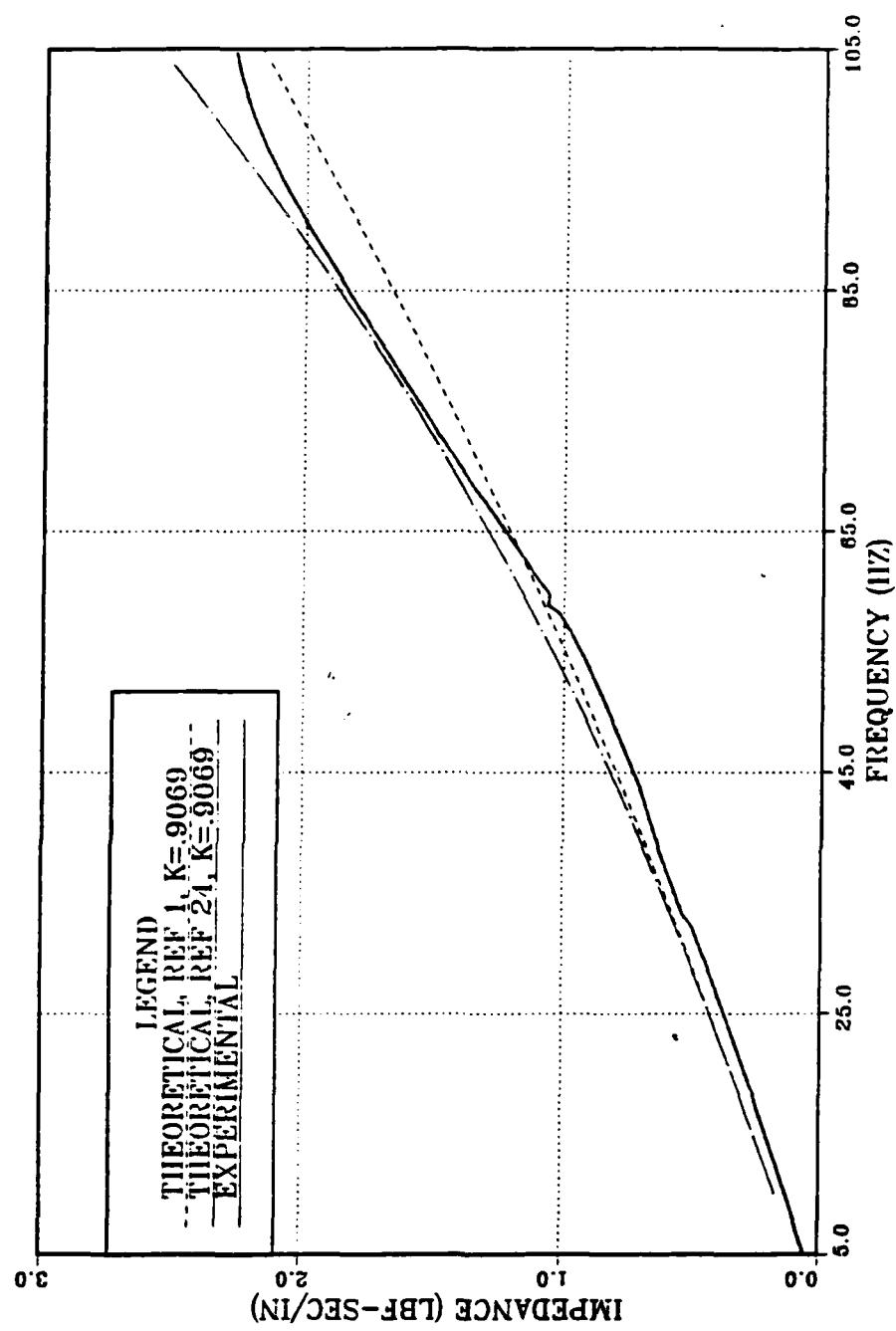
Figure 111. Theoretical and Experimental Comparison of the
Imaginary Part of the Driving Point Impedance for a 4 in
Radius Viscoelastic Plate in the Frequency Range of 5 to
105 Hz at a Temperature of 78.5 Deg. F.

175
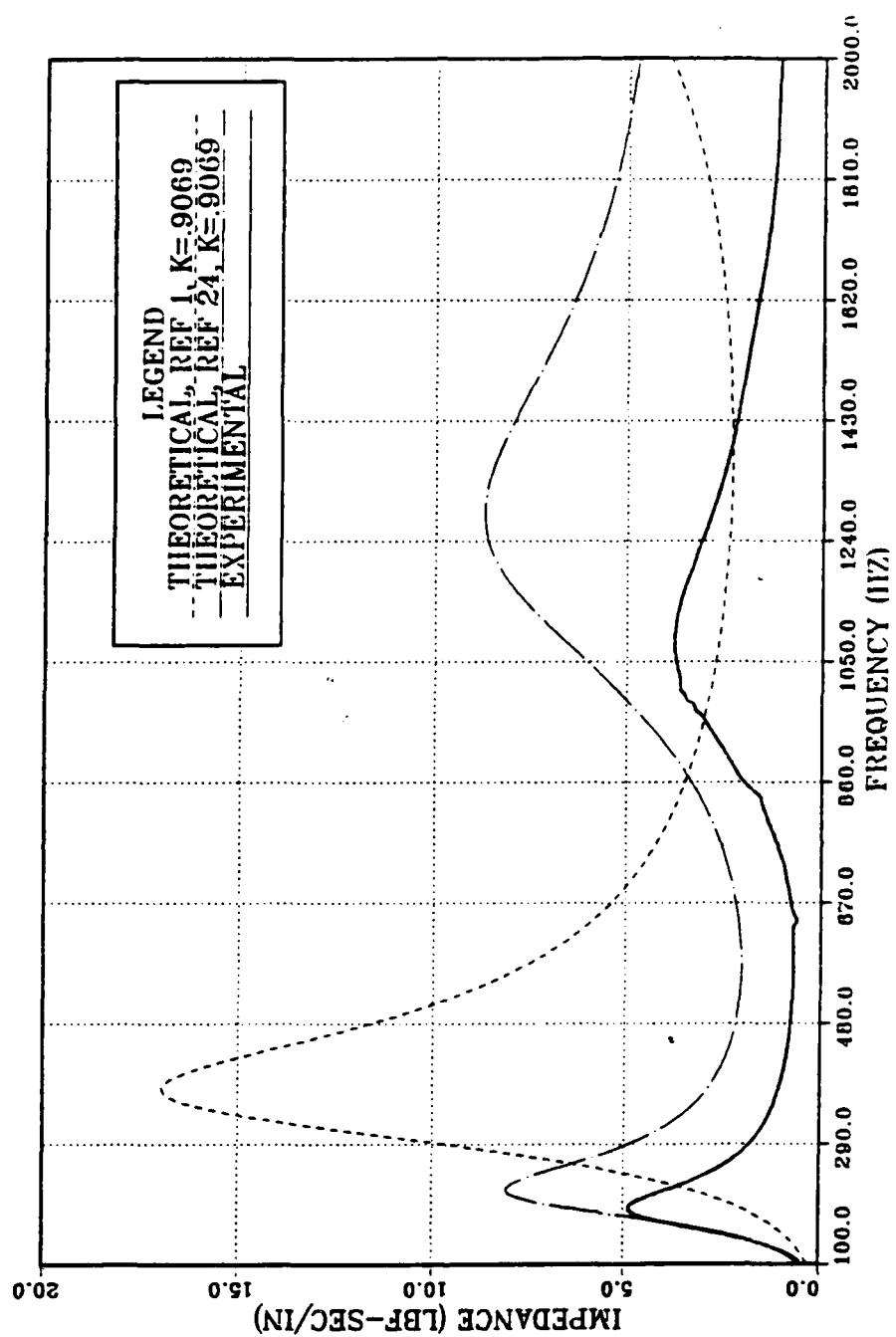
Figure 112. Theoretical and Experimental Comparison of the Real Part of the Driving Point Impedance for a 4 in Radius Viscoelastic Plate in the Frequency Range of 100 to 2000 Hz at a Temperature of 74.5 Deg. F.

176
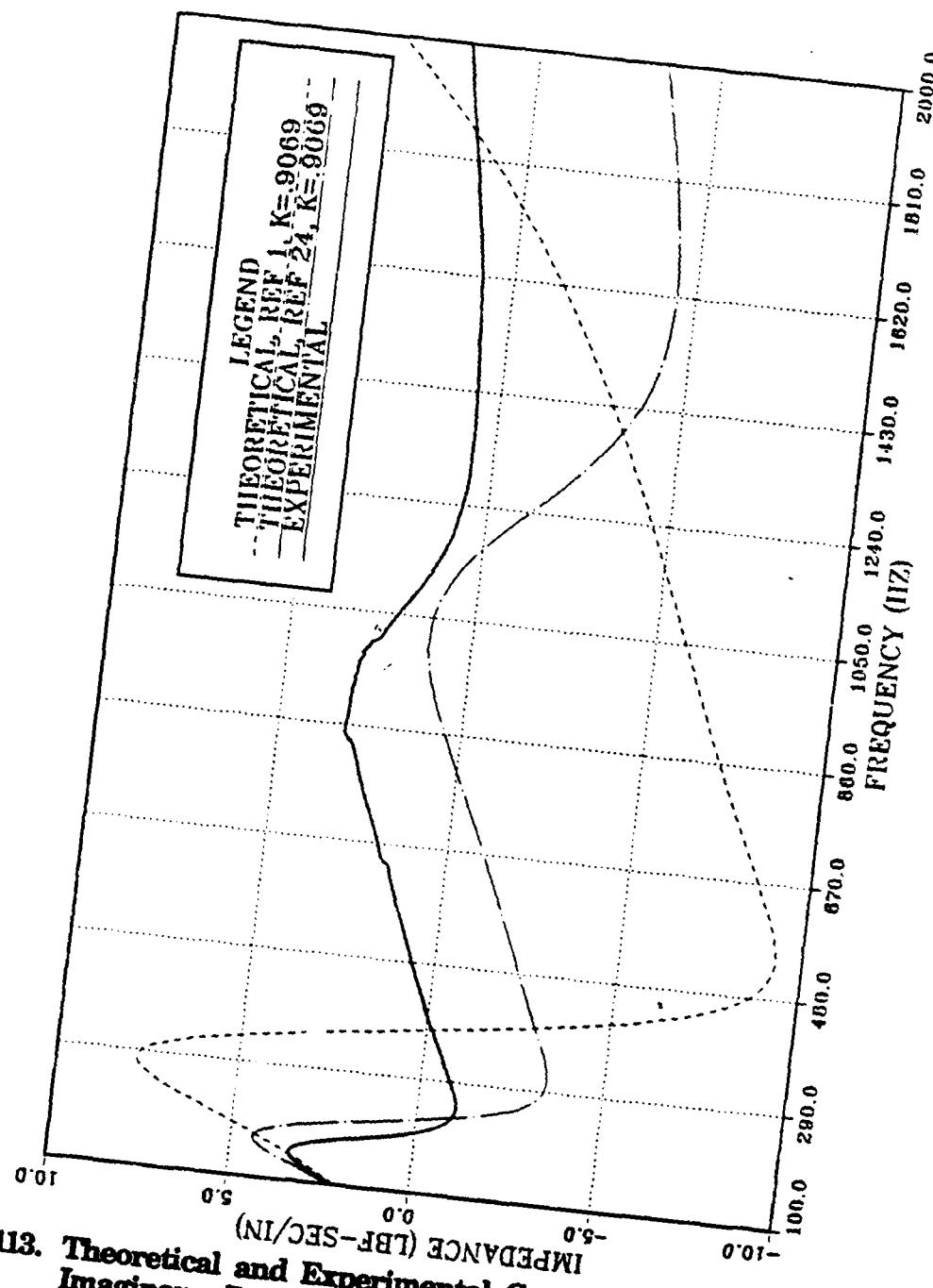
Figure 113. Theoretical and Experimental Comparison of the Imaginary Part of the Driving Point Impedance for a 4 in Radius Viscoelastic Plate in the Frequency Range of 100 to 2000 Hz at a Temperature of 74.5 Deg. F.

177

LIST OF REFERENCES

1.   Nashif, A.D., Jones, D.I.G., Henderson, J.P., Vibration Damping, John Wiley and Sons, Inc., 1985.

2.   Ungar, E.E. and Kurzweil, L.G., Structural Damping Potential of Waveguide Absorbers, in Vibrations Damping 1984 Workshop Proceedings, edited by Lynn Rogers, Air Force Wright Aeronautical Laboratories, AFWAL-TR-84-3064, pp. CC.1-CC.5, Nov. 1984.

3.   Flight Dynamics Laboratory, Air Force Wright Aeronautical Laboratories Report AFWAL-TR-83-3125, Preliminary Evaluation of Waveguide Vibration Absorbers, by Ungar, E.E. and Kurzweil, L.G., Jan. 1984.

4.   David Taylor Naval Ship Research and Development Center Report No. 6463, A Study to Guide the Development and Use of Waveguide Absorbers for Structural Damping, by Ungar, E.E. and Williams, B.F., Mar. 1987.

5.   Lee, G.G., Analytical and Experimental Studies of Beam Waveguide Absorbers for Structural Damping, Masters Thesis, Naval Postgraduate School, Monterey, CA, Mar. 1988.

6.   Bailey, P.B. and Chen, P.J., "Natural Modes of Vibration of Linear Viscoelastic Circular Plates with Free Edges", International Journal of Solids and Structures, Vol. 23, No. 6, pp. 785-795, 1987.

7.   Christensen, R.M., Theory of Viscoelasticity: An Introduction, pp. 16-20, Academic Press, 1971.

8. Budynas, R.G., _Advanced Strength and Applied Stress Analysis_, pp. 30-33, McGraw-Hill Book Company, 1977.

9. Ogata, K., _Modern Control Engineering_, pp. 20-51, Prentice-Hall, Inc., 1970.

10. Mindlin, R.D., "Influence of Rotatory Inertia and Shear on Flexural Motions of Isotropic, Elastic Plates", _Journal of Applied Mechanics_, Vol. 18, No. 1, pp. 31-38, Mar. 1951.

11. Mindlin, R.D. and Deresiewicz, H.,"Thickness-Shear and Flexural Vibrations of a Circular Disk", _Journal of Applied Physics_, Vol. 25, No. 10, pp. 1329-1332, Oct. 1954.

12. Irie, T., Yamada, G., and Aomura, S., "Natural Frequencies of Mindlin Circular Plates", _Journal of Applied Mechanics_, Vol. 47, No. 3, pp. 652-655, Sep. 1980.

13. Callahan, W.R., "On the Flexural Vibrations of Circular and Elliptical Plates", _Quarterly of Applied Mathematics_, Vol. 13, No. 4, pp. 371-380, Jan. 1956.

14. Kovach, L.D., _Boundary-Value Problems_, pp. 299-318, Addison-Wesley Publishing Company, 1984.

15. McLachlan, N.W., _Bessel Functions for Engineers_, Oxford University Press, 1961.

16. Meirovitch, L., _Analytical Methods in Vibrations_, pp. 179-189, The MacMillan Company, 1967.

17. Wang, C.T., Applied Elasticity, pp. 281-282, McGraw-Hill Book Company, Inc., 1953.

18. Reissner, H.J. and Friedrichs, K.O., "The Edge Effect in the Bending of Plates", Reissner Anniversary Volume, pp. 197-210, Edwards Bros., Inc., 1949.

19. Hearn, A.C., Reduce User's Manual, Rand Publication CP78, Apr. 1983.

20. Grossman, S.I., Multivariable Calculus, Linear Algebra, and Differential Equations, pp. 473-476, Acadmic Press, Inc., 1986.

21. Spiegel, M.R., Schaum's Outline Series-Mathematical Handbook of Formulas and Tables, pp. 136-145, McGraw-Hill Book Company, 1968.

22. Reismann, H. and Pawlik, P.S., Elasticity, Theory and Application, pp. 230-239, John Wiley and Sons, 1980.

23. Gere, J.M. and Timoshenko, S.P., Mechanics of Materials, pp. 742-747, PWS Publishers, 1984.

24. United McGill Corporation, Material Data Sheet MDS 47T, C-2204 Damping Material.

25. Vanderplaats, G.N., Numerical Optimization Techniques for Engineering Design, with Applications, pp. 30-32, McGraw-Hill Book Company, 1984.

26. Wilcoxon Research, Instruction Manual, Model F7/F4, pp. 1-8.

27. Bendat, J.S. and Piersol, A.G., <u>Engineering Applications of Correlation and Spectral Analysis</u>, pp. 78-120, John Wiley and Sons, 1980.

INITIAL DISTRIBUTION LIST

		No. Copies
1.	Defense Technical Information Center Cameron Station Alexandria, VA 22304-6145	2
2.	Library, Code 0142 Naval Postgraduate School Monterey, CA 93943-5002	2
3.	Dean of Science and Engineering, Code 06 Naval Postgraduate School Monterey, CA 93943-5000	2
4.	Research Administration Office, Code 012 Naval Postgraduate School Monterey, CA 93943-5000	1
5.	Department Chairman, Code 69 Naval Postgraduate School Monterey, CA 93943-5000	1
6.	Professor Young S. Shin, Code 69Sg Naval Postgraduate School Monterey, CA 93943-5000	4
7.	Professor David Salinas, Code 69Sa Naval Postgraduate School Monterey, CA 93943-5000	2
8.	Professor Kilsoo S. Kim, Code 69Ki Naval Postgraduate School Monterey, CA 93943-5000	1
9.	Dr. Arthur Kilcullen, Code 1962 David W. Taylor Naval Ship R&D Center Bethesda, MD 20084	5
10.	Mr. Maurice Sevik, Code 19 David W. Taylor Naval Ship R&D Center Bethesda, MD 20084	1

11. Mr. Gordon Eversteine, Code 1844   1
David W. Taylor Naval Ship R&D Center
Bethesda, MD 20084

12. Dr. Lawrence Maga, Code 196   1
David W. Taylor Naval Ship R&D Center
Bethesda, MD 20084

13. Dr. B. Whang, Code 1750.2   1
David W. Taylor Naval Ship R&D Center
Bethesda, MD 20084

14. Dr. Peter Doubleday   1
Underwater Sound Research Detachment
Naval Research Laboratory
P.O. Box 8337
Orlando, FL 32856

15. Mr. Bob Ting   1
Underwater Sound Research Detachment
Naval Research Laboratory
P.O. Box 8337
Orlando, FL 32856

16. Dr. Alfred Tucker   1
Office of Naval Research
800 North Quincy St.
Arlington, VA 22217

17. Mr. P. Majumdar, Code 55N   1
Naval Sea Systems Command Headquarters
Washington, DC 20362

18. Mr. Jerry Snyder, Code 55Y13   1
Naval Sea Systems Command Headquarters
Washington, DC 20362

19. Mr. Walter Madigosky   1
White Oak Laboratory
Naval Surface Weapons Center Detachment
10901 New Hampshire Ave.
Silver Spring, MD 20903

20. Dr. N. T. Tsai   1
Defense Nuclear Agency
SPSS
Washington, DC 20305-1000

21. Dr. Parviz Mahmoodi   1
    Building 201-BS-08
    3M Center
    St. Paul, MN 55144

22. Mr. A. Dwayne Nelson   1
    Building 230-1F-02
    3M Center
    St. Paul, MN 55144

23. LCDR Charles D. Hettema   2
    Code 330
    Pearl Harbor Naval Shipyard
    Pearl Harbor, HI 96860